**EUSKAL HERRIKO UNIBERTSITATEA / UNIVERSIDAD DEL**

**PAÍS VASCO**

**Facultad de Ciencia y Tecnología**

**Departamento de Química Inorgánica**

# "Strategies Towards Performance Enhancement in Lithium-Sulphur Batteries"

**A thesis presented for the degree of PhD to the University of the Basque Country in partial fulfilments of the requirements.**

By

## Marya Baloch

**2016**

Thesis Advisors:

**Dr. Devaraj Shanmukaraj**

**Prof. Teófilo Rojo**

*Dedicated to late. Mustaque Ali Baloch*

*“Read it with sorrow and you will feel hate.*

*Read it with anger and you will feel vengeful.*

*Read it with paranoia and you will feel confusion.*

*Read it with empathy and you will feel compassion.*

*Read it with love and you will feel flattery.*

*Read it with hope and you will feel positive.*

*Read it with humour and you will feel joy.*

*Read it with God and you will feel the truth.*

*Read it without bias and you will feel peace.*

*Don't read it at all and you will not feel a thing.”*

*— Shannon L. Alder*

*You see things; and you say, 'Why?' But I dream things that never were; and I say, 'Why not?'*

*— George Bernard Shaw.*

# *Acknowledgement*

I would like to express my deep gratitude to my supervisors Dr. Devaraj Shanmukaraj and Prof. Teófilo Rojo Aparicio, for their supervision and guidance during the period of my doctorate studies.

I also offer my regards to the other colleagues and staff in CIC EnergiGUNE, many thanks to the directors and management for their help. Special thanks to group leader of Li-based group Dr. Lide M. Rodríguez. I am grateful to Dr. Oleksandr Bondarchuk, for XPS measurements, for teaching me to manipulate XPS data and for nice discussion. Thanks to Chunmei and Emilie for their help. I would like to also thank Uxue for helping in translation of summary, eres la major y lo sabes, Itziar et. al. for great time. Also thanks to Nerea and Iñigo Lozano for proof-reading the Spanish summary version and all my friends from CIC.

Special thanks to Dr. Robert Dominko and Prof. Miran Gaberšček for his guidance and help in all aspects. I would like to thank my friends from NIC, Slovenia. Very special thanks to the pretty woman "Tanja" for really great time and all the love. Thanks to Alen and Špela for their help during working time, and their great friendship, also thanks to other lab mates: Urša and Maja, Matija, Gregor, Andraz, Jan, Klemen and Jože. Of course I can't forget Jerneja for all her help.

All my praises will always be to the Almighty God, for staying by my side and giving me strength when I needed. I would also like to show my great appreciation to my family by thanking them, for their real endurance and being with me always when I needed. Thanks to my mother Najam UN Nisa, my father Nazar Ali Baloch, for raising me and special thanks to put me in a school where I wanted to go. Thanks for letting me taking my own decisions and giving me all this confidence. After wards, I would like to thank my

brothers and sisters, first to Samina, for giving me extra love and care, my brother Dr. Aamir for adventures on his motor-bike and spoiling love, Tariq for his wit and advices throughout life, Memona for always taking my side, Dr. Saira for being my pride, you know you are the best, Mohsin, for being my little baby brother.

Extraordinary thanks to Vicky (Mushtaque) for believing in me and always telling me that I can achieve anything. He was also like a guiding light and I do not have words to explain what you mean in my life. Baba, Mummy, and you will always be with me, May you all rest in peace.

My sincere thanks goes to my awesome friends, of course Dr. Liana Annunziata, a friend, a sister, a mother and to be honest words are too few to explain my love and appreciation for you. Marivi Alvarez Atanes, Patricia Losada Nieto, for being my friends and family, living with you was the coolest thing that happened in my life. Thanks also to Eva Alvarez Atanes (my twin sister), Maider Zarrabeitia and Nuria Garcia for their friendship. Thanks to Dr. Elena Gonzalo for her non-stop help since I arrive to Vitoria. I also owe my thanks to Dr. Carmen M. López, for her guidance and encouragement.

Last but not the least my endless thanks to maitia, Yago Sanz Ortega, for never loosing hope in me. All this happened just because of you.

# Resumen

El trabajo de Tesis doctoral se ha llevado a cabo en el Centro de Investigación de Energía Cooperativa CICE (CIC energiGUNE) situado en el Parque Tecnológico de Alava, Miñano, España.

La Tesis se ha realizado bajo la dirección del Dr. Devaraj Shanmukaraj y el Prof. Teófilo Rojo. Además, se ha llevado a cabo una estancia de prácticas de doctorado de tres meses en el laboratorio de Instituto Nacional de Química (NIC) de Ljubljana, Eslovenia, bajo la supervisión del Prof. Miran Gaberšček.

La Tesis doctoral trata de explorar y dar soluciones a los principales problemas que presentan las baterías de litio-azufre (Li-S) actuales, tales como la reactividad del ánodo de litio metálico. Este proceso puede dar lugar a una reacción parasitaria de polisulfuros con el Li y a su vez a la formación de dendritas, junto con la disolución de las especies polisulfuro ($Li_2S_x$) en el electrolito.

A pesar de que se ha realizado un gran esfuerzo en el desarrollo de las mejoras en el sistema Li-S, la mayoría de ellos se han centrado en la parte catódica. Por ello, en esta Tesis, además de los materiales catódicos, se hace un enfoque especial a los ánodos de Li metálico, con el fin de superar los problemas mencionados anteriormente.

La Tesis se divide en 6 capítulos como se indica a continuación:

## Capítulo 1: Introducción

Se describe brevemente la cronología en el tiempo de las baterías, seguido de una breve reseña sobre las nuevas tecnologías emergentes más allá del sistema Li-ion, incluyendo

las baterías de Li-aire y Li-S. Se presenta un resumen general de diferentes componentes importantes en los sistemas Li-S y los principales problemas asociados a ellos. Asimismo, se describen los objetivos y motivos principales de la Tesis.

## Capítulo 2: Materiales y métodos

Se describen los métodos de preparación de los cátodos/materiales utilizados en esta Tesis, incluyendo la lista de productos químicos que se han empleado. Además, se proporciona una breve descripción sobre la preparación de la suspensión de cátodo, técnica de laminación y el conjunto de la celda electroquímica. Asimismo,, se describen las condiciones usadas para cada instrumentación/equipo empleados.

## Capítulo 3: Capas protectoras para ánodos en baterías de Li-S

Se ofrece una visión general sobre el tema de las capas protectoras para ánodos de Li metálico, incluyendo un resumen sobre la historia de dichas capas las cuales han sido utilizadas en las baterías recargables de Li. El principal objetivo de esta investigación, es conseguir una capa protectora eficaz para evitar el contacto directo del electrolito con el Li, inhibiendo así la deposición de las especies de polisulfuros reducidos en la superficie del ánodo de Li. Se han realizado numerosos experimentos para tratar de encontrar una capa protectora de nitruro de litio ($Li_3N$) más uniforme y efectiva, y poder así evitar el uso directo de Li metálico en el ánodo. Las capas protectoras antes y después del ciclado, se caracterizaron por Microscopia electrónica de barrido (SEM), Espectroscopia de fotoelectrones emitidos por rayos X (XPS) y difracción de Rayos-X (DRX). Con el fin de evaluar el rendimiento electroquímico de las celdas de Li-S, se llevaron a cabo mediciones galvanostáticas, voltametrías cíclicas y medidas de impedancias.

## Capítulo 4: Nuevo diseño de la arquitectura del ánodo híbrido

Se estudia el nuevo diseño de grafito/óxido de grafeno reducido, con el metal de litio como arquitectura híbrida para controlar las reacciones superficiales no deseadas en el ánodo. Se preparó una capa de grafito sobre una capa de litio como ánodo la cual fue testeada frente un cátodo de azufre. La capa de grafito juega un papel fundamental en la interfaz activa para controlar las reacciones electroquímicas parasitarias y reducir las reacciones nocivas, conduciendo a un mejor rendimiento de las baterías Li-S. La caracterización físico-química de las membranas de grafito se realizó utilizando medidas de difracción de RX "*in*-situ", SEM, y espectroscopia de Resonancia magnética nuclear (RMN) en estado sólido. La caracterización electroquímica se llevó a cabo utilizando voltametría cíclica y medidas de ciclado galvanostáticas en las celdas de Li-S.

## Capítulo 5: Líquidos iónicos poliméricos como "binder" en el cátodo de azufre

Se describe el nuevo método de impregnación de un electrolito polimérico a base de gel líquido iónico (poly (DDA) TFSI-PYR-14 TFSI LiTFSI) dentro del cátodo compuesto por carbono-azufre. Los cátodos se prepararon por impregnación de materiales compuestos CEcp600JD-S con un electrolito gel-polímero sin utilizar ningún aglutinante adicional. La caracterización electroquímica se realizó mediante ciclado galvanostático. La morfología del cátodo fue analizado mediante SEM. La superficie del ánodo de Li se ha analizado mediante la técnica SEM-FIB. Las medidas galvanostáticas se realizaron en una celda específica tipo bolsa de café (pouch-cell). Con el objeto de detectar la presencia de polisulfuros en las reacciones electroquímicas se han llevado a cabo medidas de espectroscopia UV/Visible "*in-Situ*". Este trabajo se ha realizado en el NIC (Instituto Nacional de Química Q), Ljubljana durante la estancia de tres meses.

# Capítulo 6: Polimeros organosulforados como cátodos en baterías Li-S

En este capítulo detallan dos nuevos tipos de materiales catódicos obtenidos a base de polímeros organosulfurados redox, que fueron sintetizados e investigados para el uso en baterías recargables de Li-S como un estudio de "prueba de concepto". Tanto la poliamina alifática como la polyazomethine conjugada fueron utilizadas como base para fijar las especies redox-activas. Se ha llevado a cabo el análisis de la actividad esperada de los enlaces S-S y/o de la estructura conjugada rígida, S-N, escisión / formación. Asimismo, se ha analizado el máximo voltaje que resulta de la unión al aceptor de electrones (N, C=N) con cinética rápida. Los polímeros sintetizados se caracterizaron utilizando un Espectrofotómetro infrarrojo de transformada de Fourier (FTIR), Calorimetría diferencial de barrido/ Análisis Termogravimétrico (DSC / TGA), DRX y espectroscopia Raman. El rendimiento de los procesos de descarga / carga para la viabilidad de estos cátodos en celdas basadas Li-S, se ha analizado mediante el estudio de medidas galvanostaticas.

# Conclusiones finales y perspectivas

Se presentan los logros generales de la Tesis, de acuerdo con los objetivos propuestos. Se describen las conclusiones más importantes obtenidas en el trabajo desarrollado en la Tesis y se describen los aspectos más importantes a desarrollar en posibles trabajos futuros.

# Summary

PhD thesis work has been carried out at Energy Cooperative Research Centre CICE (CIC EnergiGUNE) located at the Technological Park of Alava, Miñano, Spain.

The thesis work has been executed under the direction of Dr. Devaraj Shanmukaraj and Prof. Teofilo Rojo Aparicio. A PhD visiting internship of 3 months was performed in the Lab of NIC (National institute of chemistry) Ljubljana, Slovenia, under the direction of Prof. Miran Gaberšček.

This PhD thesis deals with exploring solutions to major problems occurring in Li-S (Lithium-Sulphur) battery such as reactivity of the lithium metal anode that could lead to parasitic reaction of polysulphides with Li and dendrite formation, along with dissolution of polysulphide species ($Li_2S_x$) in the electrolyte

Although vast efforts were undertaken for the development of the improvements in the Li-S system; most of them have been focused on the cathodes. Hence, this thesis, in addition to cathode materials, a special focus has also been made on Li metal anodes in order to overcome the issues related to metallic lithium.

This thesis is divided into 6 chapters as given below:

## Chapter 1: Introduction

Outlines briefly on the timeline of batteries followed by a short review on emerging new technologies beyond Li-ion, including Li-air and Li-S. Summary of the working principal and different important components of Li-S systems and major problems associated with the Li S systems have been presented. Main objectives and motives of this thesis have also been mentioned.

## Chapter 2: Materials and methods

This chapter demonstrates supporting information about preparation method for general cathodes/materials used in this thesis. List of chemical have been given. Furthermore, a description about slurry preparation, lamination technique, and electrochemical cell assembly are specified. Additionally, it embraces the explanation along with certain conditions used for instrumentation/equipment engaged in this thesis.

## Chapter 3: Protective layers for Li-anode in Li-S batteries

This chapter offers an overview on the subject of protective layers for metallic Li-anode, including summary about the history on Li-anode protective layers used in Li-rechargeable batteries. The major aim of this research i.e. to provide an effective protective layer to isolate lithium from any direct contact with electrolyte that inhibits deposition of reduced polysulphide species directly on the surface of Li-anode have been discussed. Numerous experiments have been performed to find an improved, uniform and effective $Li_3N$ protective layer technique; to avoid the direct use of metallic Li-anode. The protective layers before and after cycling were characterized by SEM (Scanning electron microscopy), XPS (X-ray photoelectron spectroscopy), and XRD (X-ray diffractometery). Galvanostatic measurements, CV (cyclic voltammetry) along with impedance analysis were performed to evaluate the electrochemical performance of the Li-S cells.

## Chapter 4: Novel design of hybrid anode architecture

This chapter revises the new design of graphite/reduced graphene oxide with lithium metal as hybrid anode architecture to control undesirable surface reactions on metallic Li-

anode. Graphite film is coupled with Li foil as an anode and tested against a sulphur cathode. The graphite film plays a role of an active interface layer to control the parasitic electrochemical reactions and reduce harmful side reactions, leading towards better performance of Li-S batteries. The graphite self-standing membranes were characterized using physico-chemical characterization techniques such as *in situ*-XRD, SEM and solid-state NMR spectroscopy. The electrochemical characterisations were performed using CV and galvanostatic cycling measurements in the Li-S cells.

## Chapter 5: Polymeric ionic liquids as binders in sulphur cathodes

This chapter defines the novel method of impregnating an ionic liquid based gel polymer electrolyte (poly (DDA) TFSI-$PYR_{14}$TFSI-LiTFSI) within carbon-sulphur composite cathode. Cathodes were prepared by impregnating CEcp600JD-S composites with a gel polymer electrolyte without using any additional binder or additional carbon additive. The cathodes were characterized by galavanostatic cycling measurements. The morphology of the cathodes, before and after cycling has been determined using SEM analysis. Li anode surface analysis has been carried out by SEM-FIB technique. Galvanostatic measurements were performed in a specific coffee bag cell in the Li-S cells. *In-situ* UV/Visible measurements were conducted to detect polysulphides in electrochemical reactions. This work has been carried out at NIC (National Institute of Chemistry), Ljubljana during the three months stay.

# Chapter 6: Organosulphur polymer as cathode in Li-S batteries.

This chapter reports two novel types of cathode materials based on redox organosulphur polymers, which were synthesized and investigated for rechargeable lithium batteries as a proof of concept study. Either an aliphatic polyamine or a conjugated polyazomethine had been used as the base to tether the redox-active species. The activity expected to come from either S-S bond or, made possible with the rigid conjugated backbone, S-N, cleavage/formation and higher voltage resulting from the attachment to electron-withdrawing group (N, C=N) with fast kinetics and diffusion have been analysed. The synthesized polymers were characterized by using FTIR (Fourier transform infrared spectroscopy), DSC/TGA (Differential Scanning Calorimetry / Thermogravimetry Analysis), XRD and Raman spectroscopy. Galvanostatic measurements were performed to evaluate the discharge/charge performance for the viability of these cathodes in Li-S based cells.

# Final conclusion and perspectives

It presents general achievements of the thesis, in agreement to the objectives and motives proposed in the light of state of the art. The brief outcome from each chapter has been discussed and remarks on future aspects and scopes have been mentioned.

*Chapter 1: Beyond Lithium-ion batteries: Lithium-Sulphur systems.*

1 Introduction ..... 1

**1.1 Batteries** ..... 2

1.1.1 Primary batteries ..... 4

1.1.2 Secondary batteries ..... 6

**1.2 Lithium rechargeable or Li-ion batteries** ..... 6

**1.3 Beyond Li-Ion** ..... 8

1.3.1 Lithium-Air ($O_2$) batteries ..... 10

1.3.2 Lithium-Sulphur batteries (Li-S) ..... 12

**1.4 Disadvantages/ problems of Li-S batteries** ..... 19

**1.5 Interests and objectives** ..... 20

**1.6 References** ..... 22

*Chapter 2: Materials and methods*

2 Introduction ..... 27

**2.1 List of chemicals: *Alphabetical order*** ..... 27

**2.2 Usage of chemicals** ..... 28

**2.3 Experimentation** ..... 28

2.3.1 *Cathode preparation* ..... 28

2.3.2 *Electrolyte preparation* ..... 30

*2.3.3 Anode preparation* ..... 33

*2.3.4 Battery configuration* ..... 34

**2.4 Characterization** ..... 37

*2.4.1 Electrochemical characterization techniques:* ..... 37

*2.4.2 Physico-chemical characterization/post-mortem techniques:* ..... 39

**2.5 References** ..... 50

*Chapter 3: Protective layers for lithium anode in Li-S batteries*

3 Introduction: Lithium Metal Anode ..... 52

**3.1 Protection of Li-anode** ..... 53

**3.2 Additives in liquid electrolytes for passivation layer:** ..... 54

**3.3 Solid protection layer: Modification of the Lithium Anode** ..... 56

**3.4 Experimentation** ..... 58

*3.4.1 $Li_3N$ layer -fabrication methods:* ..... 58

*3.4.2 Cathode preparation, cell assembly, physico-chemical and electrochemical characterization:* ..... 62

**3.5 Results and discussion:** ..... 62

*3.5.1 $Li_3N$ layer without binder:* 63
*3.5.2 $Li_3N$ layer with polymeric binder:* 66
*3.5.3 Rate capability:* 70
*3.5.4 CV and Impedance studies: with and without protective layer* 72
*3.5.5 Post-mortem analysis* 75
*3.5.6 $Li_3N$ layer formation by electrolyte additive:* 78
**3.6 Conclusion** 84
**3.7 References** 84
*Chapter4: Novel design of hybrid anode structure*
4 Introduction 90
**3.8 Experimentation** 96
*3.8.1 Preparation of Graphite films* 96
*3.8.2 Synthesis of reduced-Graphene oxide films* 96
*3.8.3 Preparation of rGO deposit* 97
*3.8.4 Cathode preparation, cell assembly, physico-chemical and electrochemical characterization:* 97
**3.9 Results and Discussion** 98
*3.9.1 Graphite* 98
*3.9.2 Graphene (rGO)* 110
**3.10 Conclusion** 114
**3.11 References** 116
*Chapter 5: Polymeric ionic liquids as binder in sulphur cathodes.*
5 Introduction 122
*5.1 Gel polymer electrolyte (GPE) ionic liquid as a binder* 124
**5.2 Experimentation** 125
*5.2.1 Introduction of GPE-PIL in C/S cathode* 125
*5.2.2 Mixing of sulphur/carbon (ECP600JD) composite with GPE-PIL* 125
*5.2.3 Optimization of cathode composites* 126
*5.2.4 Cell configuration:* 127
**5.3 Results and discussion** 128
*5.3.1 Physico-chemical characterization* 128
*5.3.2 In-Situ UV/Vis measurements:* 129
*5.3.3 Electrochemical characterizations* 131
**5.4 Conclusions** 138
**5.5 References** 139

6 Introduction ..... 143

**6.1 Synthesis** ..... 148

*6.1.1 Part 1: N-S bond cleavage/formation* ..... 148

*6.1.2 Part 2: S-S bond cleavage/formation* ..... 149

*6.1.3 Physico-chemical characterization* ..... 150

*6.1.4 Preparation of the carbon (Ckj-600) -organosulphur cathode:* ..... 150

*6.1.5 Electrochemical characterization* ..... 151

**6.2 Results and discussion** ..... 151

*6.2.1 Part 1: N-S bond cleavage/formation* ..... 151

*6.2.2 Part 2: S-S bond cleavage/formation* ..... 155

**6.3 Conclusion** ..... 161

**6.4 References** ..... 162

*Final Conclusions & perspectives* ..... 165

**7.1 Conclusions:** ..... 166

**7.2 Perspectives** ..... 167

*Appendix* ..... 169

Glossary ..... 170

Abbreviations ..... 174

List of Figures ..... 176

List of tables ..... 181

List of Publications ..... 182

Papers presented in national/international conferences ..... 183

# *Chapter 1: Beyond Lithium-ion batteries: Lithium-Sulphur systems.*

# 1 Introduction

For the demand of cleaner and greener energy, rechargeable batteries are promising for mobile applications such as electronic devices, electric vehicles, etc.[1]

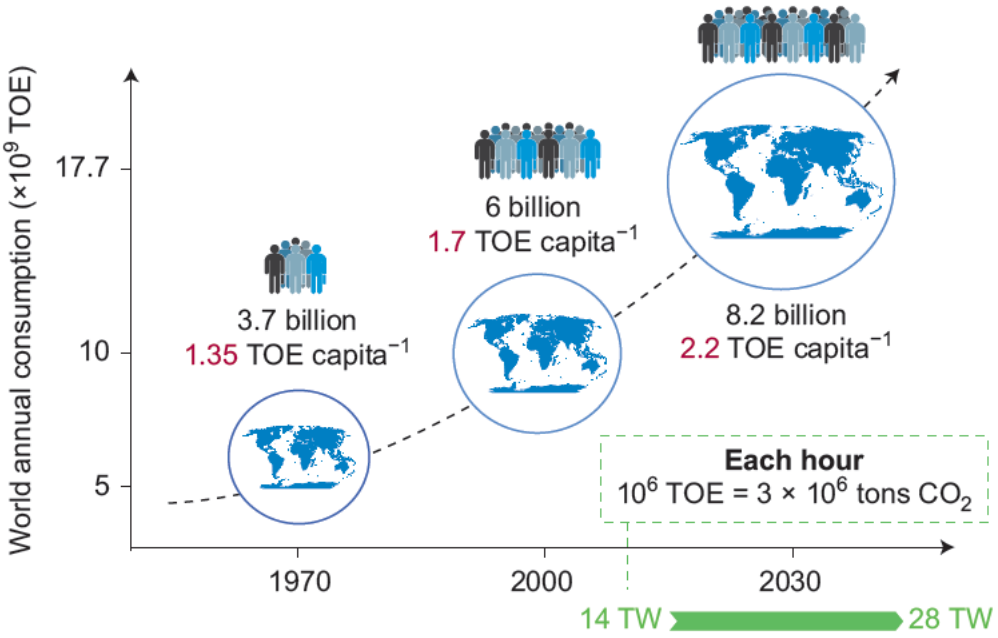


**Figure 1.1: Prognosis of the energy requirements up to year 2050 within whole world.** [2]

With changing lifestyle and world's energy demands (Figure 1.1), energy storage is significantly critical for the operative development of power-driven economy and implementation of renewable energy technologies as well as electricity generation (wind, wave, solar). By increasing number of residents with high-tech lifestyle desires, the energy will rise from 14 TW (2010) unto 28 TW (2050).[2]

The main source for technological revolution of past centuries has been mostly powered by mutation of combustion reaction, i.e. production of $CO_2$ polluting global environment and climatic concerns. This requires an immediate strategy to use energy for everyday errands, i.e. from barbecues to planes. In order to completely avoid toxic gas emission, we need low cost and ecological energy source. Hence batteries seem to be a solution

which could be used to store energy from sustainable sources (wind, wave and solar power).[2]

Therefore shifting our focus to battery science and technology will enable us to have efficient energy storage with low cost and longer lifetime. The material of choice for such changes should be an earth abundant material that can deliver huge redox capacities and able to reversibly react with cations i.e. lithium ion.[1]

## 1.1 Batteries

Nowadays, usage of batteries is quite common in devices such as mobile phones, portable computer and other electronics as well as in medical applications i.e. pace makers, surgical saws, drills, robotic inspection systems, and other medical devices. Necessity of batteries are deep-rooted in our everyday life.[3] thus, it's a call for cheaper and efficient battery technology.

Even though the battery term might have derived from Leyden jars of Benjamin Franklin 1760-1769 (Figure 1.2), the battery history begun with the letter of Alessandro Volta, Professor in University of Pavia, Italy to Royal Society of London on 20$^{th}$ March 1800. He reported his investigation upon "On the electricity excited by the mere contact of conducting substance of different kinds".[4] He defined an apparatus containing interchanging assembly of zinc (Zn) and silver (Ag)/copper (Cu) discs, aligned in pair with an absorbent like paper or leather soaked in electrolytic solution, i.e. aqueous sodium chloride or diluted sulphuric acid. Each Zn-$NaCl_{aq}$-Ag unit represents a single electrochemical cell. Stacking those units on each other represents battery which was called "Voltaic Pile" made of individual cells interconnected in series.

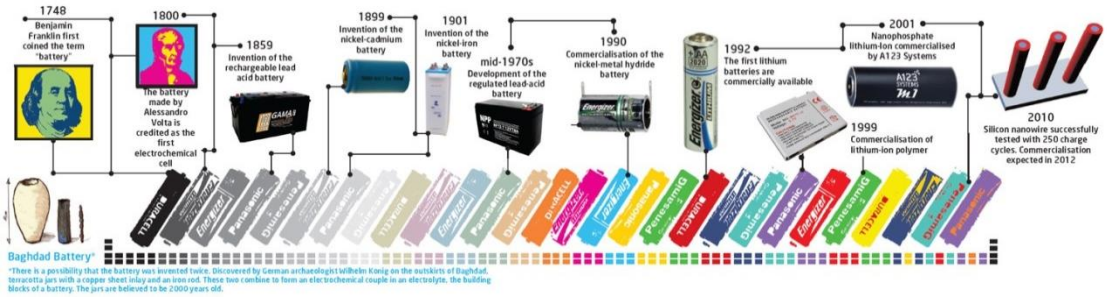


**Figure 1.2: Timeline of battery evolution, starting from 1748 when Benjamin Franklin first devised the word "Battery".**[5]

The initial battery known as "Voltaic Pile" opened a door for new research opportunities in the field of electric current and electrochemistry.

Restrictions of delivering currents for longer period in Voltaic pile was overcome by Daniell Cell, presented by John Frederich Daniel, a British researcher in 1820. The journey of battery evolution continued by Raymond Gaston Planté's lead-acid battery in 1859 following by the Nickel-Cadmium Battery from 1893-1909 of Jungner and Berg from Sweden.[6] The substitution of hydrogen-absorbing counter electrode by Cd-bases electrode is an extended version of the sealed nickel-cadmium batteries known as nickel-metal hydride batteries in1990 by Energizer Battery Manufacturing Inc.[7] In 1991, Sony commercialised the 1$^{st}$ cylindrical Li-ion battery,[8] further opening a door for the commercialisation of batteries such as Li-ion polymer battery, a pouch cell type battery and etc.

In principle, a battery typically holds negative electrode (an anode), which *oxidizes* during the electrochemical reaction and delivers electrons to the load (i.e. circuit, etc.). A positive electrode (cathode), which *reduces, and* an electrolyte, intermediate for electron transfer, and separators, placed in the middle of the cathode and anode for electrical insulation.[8,9]

In the process of battery, chemical free energy converts into electrical energy as stated by equation below:

*Equation 1:* $\Delta G = -nFE$ *G=Gibbs free energy*

*n= No. of electrons*

*F=Faraday's constant*

*E= Cell potential*

Numerous kinds of batteries (primary and secondary) have been developed on the basis of this (Equation 1) principle.[8]

### 1.1.1 Primary batteries

The batteries included in primary group are non-rechargeable cells. Owing to fixed amount of reacting compounds, the electrochemical reaction is irreversible. Generally, primary batteries give an advantage of high energy density via lower discharge rates and fair shelf life (Table 1.1).[8]

**Table 1.1: Different systems of primary batteries, denoting their major characteristics and applications.**[10]

| System | Characteristics | Applications |
|---|---|---|
| Zinc-carbon (Leclanché)<br>Zinc /$MnO_2$ | Usual, inexpensive battery, offered in a different sizes | Radios, children toys, lighting accessories |
| Magnesium ($Mg/MnO_2$) | Longer life with higher capacity | Transmitters (Military use), emergency transmitters (aeroplane) |
| Alkaline<br>(Zn/ alkaline /$MnO_2$) | General-use finest battery, performance at lower temperature, affordable | Several portable equipment |
| Silver / zinc ($Zn/Ag_2O$) | High-shelf life, High capacity (by weight), expensive | Hearing-aids, watches, photographic accessories, space |

| | | |
|---|---|---|
| | | and underwater assessment (large size batteries) |
| Lithium / soluble cathode | Better performance upon extensive temp. range, extraordinary energy density, longer life | All application withing the capacity range from 1-10,000 Ah |
| Lithium / solid cathode | Good rate capability, long life, higher energy density, modest cost, suitable for low-temp. | Alternative of conventional button and cylindrical cell type primary batteries |
| Lithium / solid electrolyte | Exceptional shelf life, lower power | Medical electrical devices |

Various anode-cathode arrangements have been used for primary systems, out of which merely a small number of them have attained practical accomplishment.

Different kinds of batteries are shown in Figure 1.3, which mostly contain single cylindrical cell and coin-type batteries or batteries based on several component cells.

Primary batteries are the most useful reservoir of power with lighter weight and used in portable electrical devices such as equipments for lighting, photography, radio-transistors, calculators, children toys, portable accesorries, watches and vice versa, providing freedom from electrical network. They are available in different sizes and shapes according to different application. [10]


**Figure 1.3: Commercially available different types of batteries .i.e. (right to left) CR2032 & LR44 coin cells, 9-Volt box battery, 23A, AAAA, AAA, AA, C, D, 4.5-volt.** [11]

### 1.1.2 Secondary batteries

Rechargeable batteries are based on reversible electrochemical reaction, which converts chemical energy to electric potential energy.[9] These batteries are generally assembled in their discharge state, and by applying an electric current, it reverses the chemical reactions for easy recharge.

Rechargeable batteries provide numerous advantages over primary batteries, such as 5x longer lifetime with a cycle life of more than 2000 cycles. Some of the characteristic are mentioned in Table 1.2.

**Table 1.2: Characteristics and applications of the secondary (rechargeable) battery systems.** [12]

| System | Characteristics | Applications |
|---|---|---|
| Ni-Cd | Well studied chemistry, long service life, high discharge currents and high temperatures. Enduring batteries that allow hyper-fast charging. | Medical equipment, aircrafts and UPS (uninterruptible power supply). |
| Ni-Metal Hydride | Alternative of NiCd, mild toxic metals, high specific energy. Available in $A^{++}$ and $A^{+++}$ cells | Medical instruments, industrial uses and hybrid cars |
| Pb-Acid | Economic price, low specific energy and cycle life. Toxicity of Lead toxic inhibits disposition in landfills | Wheelchairs, golf carts, emergency lighting, and UPS |
| Li-ion | Used instead of lead and nickel-systems, Li-ion requires security circuit, Expensive, higher cycle life and low maintenance compensate the price. | Computers, mobile phones, portable devices, etc. |

## 1.2 Lithium rechargeable or Li-ion batteries

Li-based rechargeable batteries are a potential and promising candidate to overcome the needs for stationary and EV application, due to their high specific energy density as can be seen in Figure 1.4. Also lithium is very reactive and light weight (density = 0.53 g/cm3)[13] element, which is another advantage for EV battery applications. Li-based batteries have wide cell voltage and operating temperature range.[14]

Lithium is found to be one of the best anode owing to its properties, but the reason that lithium metal reduces very fast and is highly electropositive (-3.045 V *vs.* SHE), only non-aqueous solvents can be a choice for the electrolytic solution, including many carbonate-based solvents i.e. ethylene carbonate (EC), propylene carbonate (PC), and dimethyl carbonate (DMC). However, these solvents have lower ionic conductivity. Besides, even in the most stable solvent, lithium metal will react to some extent.

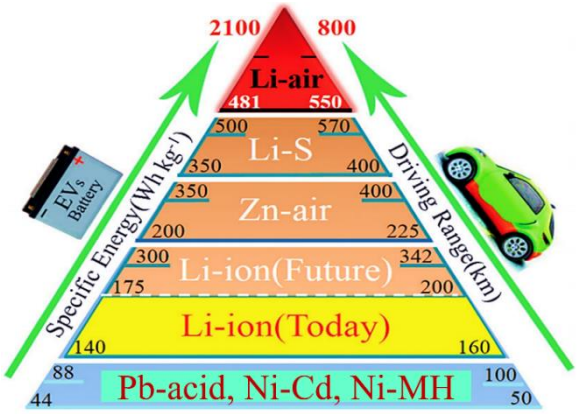


**Figure 1.4: Pyramid of different battery systems according to their energy densities (Wh $kg^{-1}$) and EV driving force (km).**[15]

In 1980s, layered oxide lithium cobalt oxide $LiCoO_2$ was studied by J. B. Goodenough,[16] supposing the best cathode material at that time. However, the dendritic growth during charging process made lithium batteries an unsafe device.[17] Figure 1.5 demonstrate schematic diagram of a typical battery operation mechanism.

Graphite was used as an anode by J.O. Besenhard in mid-1970s, in order to establish a way of intercalation of alkali metals into graphite.[18] Graphite displays a neat intercalation of lithium ions in stacks resulting in $LiC_6$ with electrode potential of 0.01 V vs. $Li/Li^+$, ideal anode material replacing metallic lithium. However, the specific capacity was much lower ~ 372 mAh $g^{-1}$, but the fact that there was no dendritic growth makes it a safer choice.

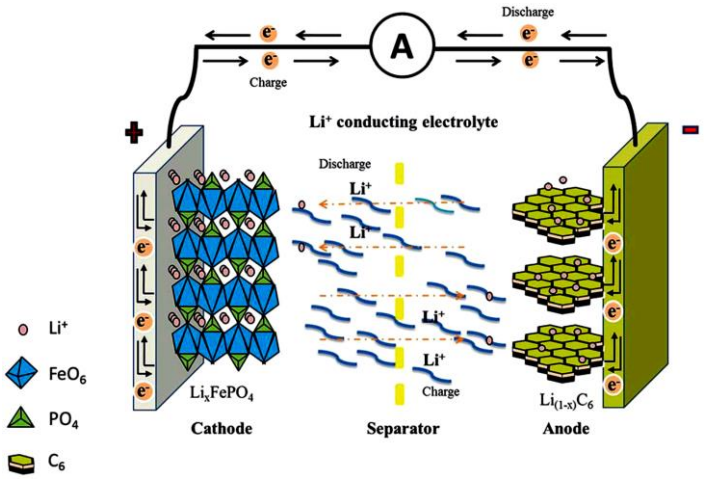


**Figure 1.5: Graphical drawing of a typical Li-ion battery with graphite anode and $Li_xFePO_4$ cathode immersed in $Li^+$ conducting organic electrolyte.**[19]

But, the specific capacity was not stable upon long cycling and later it was discovered that electrolyte decomposition plays a crucial role for cycle life.[20]

In general, graphite has been used widely as an anode, and chemical reactions taking place during cell cycling was based on intercalation of $Li^+$ ions, this is how the term lithium-ion batteries (LIB) was inferred.[21] Despite that, LIB was commercialized by Sony Co.® in 1991 which are universally used nowadays in consumer electronics[8], the research continues with a motive to achieve higher energy densities beside the fact that the cell chemistry and engineering of current LIB is quiet Similar as 25 years ago. Nonetheless there are still several obstacles including high cost, unsatisfactory cycle life, and low safety features[10], to be solved before scaling up for energy application.

## 1.3 Beyond Li-Ion

"Beyond lithium ion" concept is not yet clear, due to uncertainty of any advanced system that offers a commercial success.

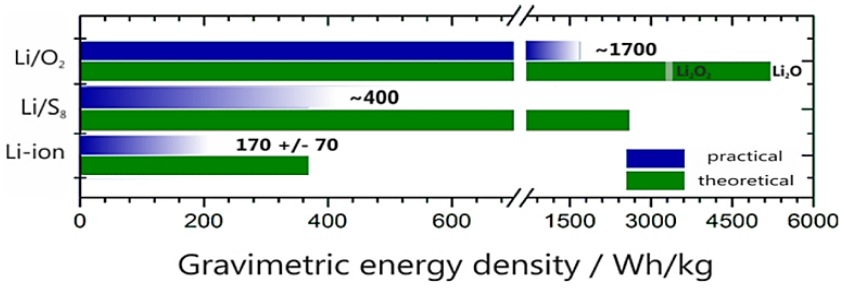


**Figure 1.6: Theoretical and experimental gravimetric energy density (Wh $kg^{-1}$) of Li-based systems. Practical estimated values denote to the cell level.**[22]

Vast investigations have been done within Li-based systems (Figure 1.6); however the focus is pointed to explore materials for futuristic LIBs, which is supposed to replace conventional materials.

***Table 1.3: Demonstration shows theoretical voltages and capacities of few lithium based batteries. Values mentioned are denoted to the cathode and anode.***[23]

| **Battery** | **Configuration** | | | **Theoretical Values** | |
|---|---|---|---|---|---|
| **System** | **Anode** | **Cathode** | **Reaction Mechanism** | **V** | **mAh/g** |
| $Li/FeS_2$ | Li | $FeS_2$ | $4Li+FeS_2 \leftrightarrow 2Li_2S+Fe$ | 1.8 | 726 |
| $Li\text{-}MnO_2$ | Li | $MnO_2$ | $Li+MnO_2 \leftrightarrow MnO_2(Li^+)$ | 3.5 | 286 |
| $Li/I_2$ | Li | $I_2$ | $Li+1/2I \leftrightarrow 2\ LiI$ | 2.8 | 200 |
| $Li\text{-}O_2$ | Li | $O_2$ | $2\ Li + 1/2\ O_2 \leftrightarrow Li_2O$, $2Li + O_2 \leftrightarrow Li_2O_2$ | 2.91, 2.96 | 1794, 1168 |
| Li-S | Li | S | $2Li+S \leftrightarrow Li_2S$ | 2.53 | 1675 |

Considering new chemistries of LIB to accomplish higher energy, research found the material that can reversibly intercalate or intercalate two lithium ions simultaneously; proposing the ability to achieve double specific capacity.[24]

Based on the gravimetric energy densities, new chemistries such as Li–$O_2$ (Air) and Li–S (Sulphur) batteries could fulfil the needs of higher energy density (Figure 1.6) as compared to classical Li-ion systems.[25]

### 1.3.1 Lithium-Air ($O_2$) batteries

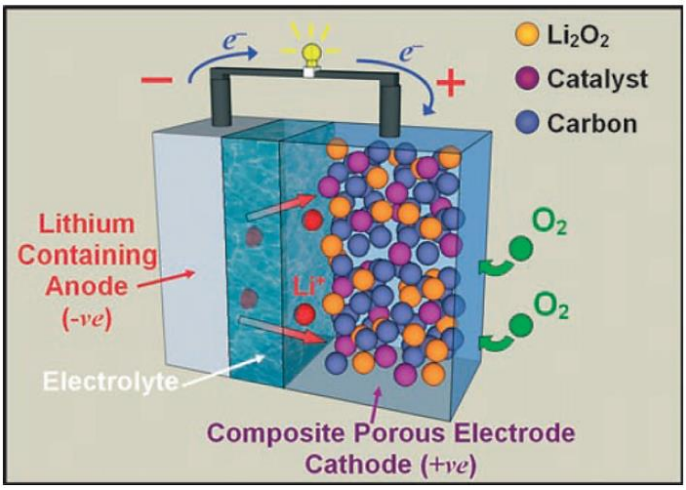


**Figure 1.7: Diagram of a classic Li-air system using Li-based anode and porous carbon as cathode with organic $Li^+$ conducting electrolyte.[26]**

Li-air is one of the promising technologies among several different energy storage electrochemical systems. It provides 10x higher theoretical energy density than typical Li-ion battery.[27–29] The reason behind such high capacity is due to the employment of a metallic lithium instead of a graphitic anode along with porous air cathode (Figure 1.7). Blockage of porous carbonaceous structure by precipitated reaction compound ($Li_2O_2$) alters the trail of oxygen pathway leading to capacity fade. Hence, designing a finest air cathode comprised of μm sized pores for fast oxygen diffusion is crucial. Meanwhile, need of nano-porosity (2-50 nm) to catalyse Li-$O_2$ reactions is critical too. $Li^+$ ions travel towards carbon cathode during the discharge and reacts with the oxygen entering through the porous structure of carbon. The discharge product $Li_2O_2$ forms thin films of nm size. The slight deviations $U_{dis}$ (discharge potential) features a steep descent in voltage at the

end of the discharge cycle known as 'sudden death'. Upon charging, the electrolyte degradation causes the incompetence. There are two main electrochemical paths during discharge, processes occurring at 1) surface 2) solution.

On charging, $Li_2O_2$ oxidises, to let free $Li^+$ ions diffuse and lodge back to Li-anode. The electrochemical reactions[27] that takes place at the cathode and Li-anode during cycling of Li-air battery are given below:

*Equation 2a:* $Li \rightarrow Li^+ + e^-$ *Anode*

*Equation 2b:* $2Li^+ + 2e^- + O_2 \rightarrow Li_2O_2$ *Cathode*

Li-air system are very promising candidates for futuristic applications, although their development is still at an early laboratory stage. In order to attain a high discharge capacity and rechargeability, issues of cathode stability, electrolyte degradation, and dendrite growth at Li-anode, has to be dealt with.[30]

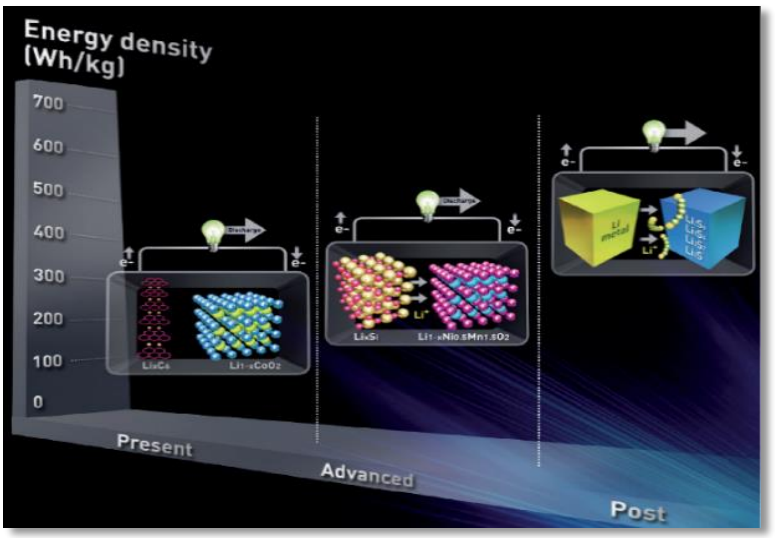


**Figure 1.8: schematic diagram showing evolution of energy density in Li-based batteries.**[1]

Even though the research of post Li-ion extends in different directions, we decided to take into consideration the challenges and progresses on lithium–sulphur (Li–S) batteries since the need of doubled energy density and specific capacity could be fulfilled by redox driven phase-transformation chemistry that includes sulphur as positive electrode. Li-S

battery technology is an alternative and better candidate to enhance the range and power of EVs due to their higher specific capacity and initial charging capacity of 5-7x advanced than traditional Li-ion systems.[31]

Li-S batteries displays a theoretical gravimetric energy density of 2500 Wh $kg^{-1}$, volumetric energy density of 2800 Wh $L^{-1}$ and specific capacity of 1675 mAh·$g^{-1}$.[32] It could be an interesting and promising candidate, basically because of low cost and abundance of sulphur which is non-toxic and environment friendly in nature. Li-S batteries can be operated at wide temperature ranges and provides intrinsic protection mechanism from over charging which assures battery safety, as well as probability of long cycling.[33]

### 1.3.2 Lithium-Sulphur batteries (Li-S)

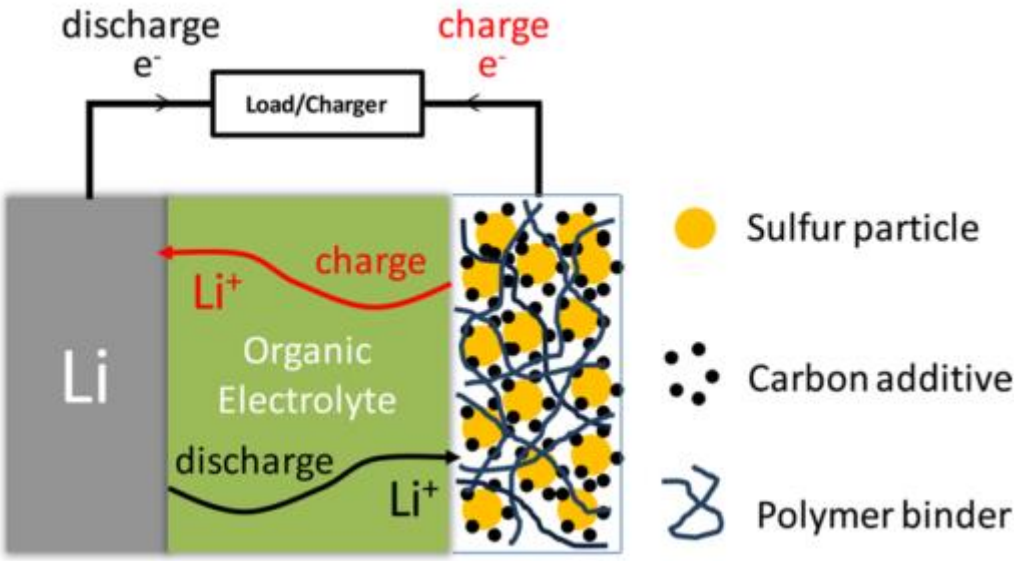


**Figure 1.9: Schematic diagram of a Li−S cell with its charge/discharge operations.**

Sulphur is promising as cathode material due to its capability of intercalating two electrons simultaneously in addition to its low cost and natural abundance. The sulphur molecule ($S_8$) can be found as eight sulphur atoms in a rucked up ring, with stable conformation at standard temperature and pressure (STP).

A schematic diagram (Figure 1.9) of the components in a single Li−S cell and its operation (charge and discharge) with a Li metal anode and a $Li^+$ ion conducting organic electrolyte (liquid/solid).[34]

The overall reduction-oxidation reaction of Li-S system is mentioned below:[35]

*Equation 3* $S_8 + 16Li + 16e^- \leftrightarrow 8Li_2S$ *2.15 V vs. Li/Li*$^+$

Sulphur cathode due to its insulating nature requires a supporting electronically conductive additive (e.g., carbon black). A prominent challenge to the LSB chemistry is related to the multi-step process from $S_8$ to $Li_2S$. Compared to the simple intercalation reaction of LIBs, sulphur undergoes a series of electrochemical reactions[36], as can be seen Equation 4a-e:

Equation 4a $2Li^+ + S_8 + 2e^- \leftrightarrow 2Li_2S_8$

Equation 4b $2Li^+ + Li_2S_8 + 2e^- \leftrightarrow 2Li_2S_6$

Equation 4c $2Li^+ + Li_2S_6 + 2e^- \leftrightarrow 2Li_2S_4$

Equation 4d $2Li^+ + Li_2S_4 + 2e^- \leftrightarrow 2Li_2S_2$

Equation 4e $2Li^+ + Li_2S_2 + 2e^- \leftrightarrow 2Li_2S$

The operation of Li-S batteries depends on the successful evolution of each of these reactions. Furthermore, the physical properties of each of the species diverge greatly. For example, while $S_8$ and $Li_2S$ are solid and insoluble in common electrolytes, each of the intermediate polysulphide reduction species are soluble in organic solvents as well as ionic liquids and polymers. During cycling, the sulphides are sequentially produced and consumed as shown in Figure 1.10.

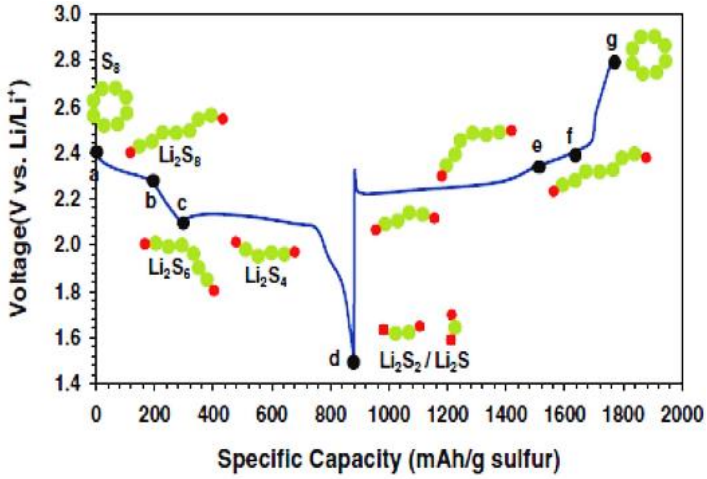


**Figure 1.10: A typical voltage vs. capacity plot for a Li-S cell explaining the evolutions of polysulphide species.**[37]

Thus, as each species is formed, it can diffuse from the cathode to the electrolyte, reducing the overall quantity of active cathode material, which results in decreased battery capacity. Moreover, it is possible for the species to migrate through the electrolyte towards the lithium anode; at that point they can be further reduced to a shorter polysulphide chain resulting in polysulphide shuttle. It can be seen as parasitic reduction of useful energy as the species migrate and react at each electrode, and is deliberated as one of the greatest challenges associated with Li-S batteries.[36] When polysulphide species undergo migration, they will precipitate as solid $Li_2S$ once fully reduced. This species is completely insoluble and is potentially impossible to regain use of those molecules.

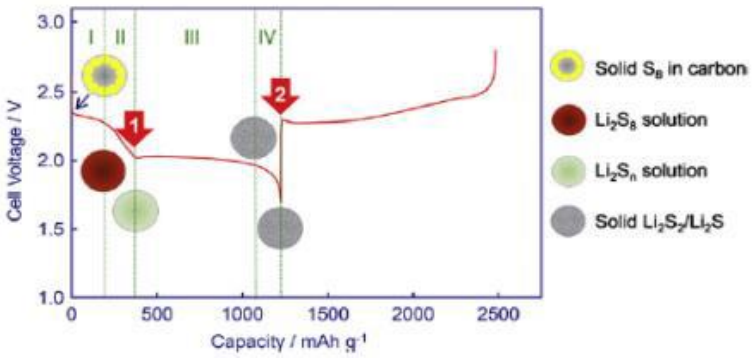


**Figure 1.11: Discharge/charge voltage vs. capacity profile of a typical Li-S battery.**[38]

Generally, discharge shows two distinct plateaus at 2.4 V and 2.1 V indicating the mechanism of sulphur transformation into polysulphides and precipitation of $Li_2S$ respectively.[38] In Figure 1.11; the 1st arrow represents viscous electrolytic solution concentrated by polysulphides. Meanwhile, the 2nd arrow shows a decreased polarization resulting phase transition from the solid $Li_2S_2$ and $Li_2S$ to the dissolved polysulphides. During charge, $Li_2S_2$ and $Li_2S$ oxidized into the solubilized polysulphides in the electrolyte resulting in reduced polarization.[39]

Discharge process initiates by opening of $S_8$ ring while reduction, leading the formation of long chain polysulphides (Region I= $Li_2S_{8\ or\ 6}$) seen by plateau at 2.3V vs. $Li/Li^+$. The long chain polysulphides further reduced to intermediate and lower chain polysulphides (Region II= $Li_2S_{4\ or\ 2}$ and $Li_2S$) giving plateau at 2.1V vs. $Li/Li^+$.

In order to take part in the race for best battery for the EVs application, Li-S, due to its high theoretical capacity could be an aspiring system. However, the development of these batteries is still challenging within upcoming years. Manipulating the physico-chemical properties of battery components such as cathode, anode, electrolyte, and the separator could be a solution to achieve these goals. Following this phenomenon, below a brief introduction of major component in Li-S batteries has been given.

#### *1.3.2.1 Sulphur cathode*

Although sulphur cathode enriches the battery with higher energy density, it still faces serious problems as being the most fundamental element of the Li-S batteries. Insulating behaviour of sulphur could inhibit the straight use in Li-S batteries as a cathode material.[33,40–43]

Therefore, sulphur is usually mixed with an electronic conductive additive (i.e. carbon). Optimisation of sulphur cathodes fall into two main categories, modifying the structure

and mixing techniques of conductive additives and cathodes starting from their polysulphides.

In order to avoid blockage in the pathway of $Li^+$ ions and for the sake of good electrical connection to ease electron transport, enduring the structural reliability of cathode among cell progression becomes a very important factor especially to achieve highly porous and homogeneous dispersion of sulphur.

Mesoporous (CMK-3) carbon addition in sulphur gives reversible capacity with initial discharge capacity of 1320 Ah/kg and remarkable life cycle. Nazar et al[40] reported linkage polyethylene glycol (PEG) on carbon surface to trap polysulphides (Figure 1.12).

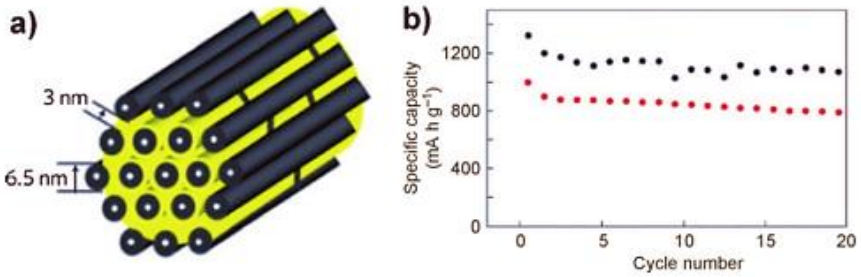


**Figure 1.12. a) CMK-3, a channel of mesoporous carbon with sulphur encapsulation using vapour phase infusion. b) Comparison of CMK-3/S with PEG (black) vs. CMK-3/S without PEG (red).** [40]

A porous hollow sulphur carbon composite was prepared by sulphur encapsulation in porous channels using vapour phase infusion, with a total sulphur content of 64.8% (70% : 30%, S:C). This composite displayed a high rate capability and 1071 $mAhg^{-1}$ discharge capacity with 91% of capacity retention at 0.5 C after cycling for 100 cycles.[44]

Recently, Lithium sulphide ($Li_2S$) has been shown as viable materials for cathode with a high theoretical capacity ~ 1166 mAh $g^{-1}$ in Li-S batteries. $Li_2S$ have low electronic and ionic conductivity, as well as it faces the problems of polysulphide shuttle during cycling leading to poor cycling life and rate capability. The carbon precursor (polystyrene) has been used to achieve the porous carbon-coated $Li_2S$ ($Li_2S$@C) composites. Reversible

specific capacity of 676 mAh $g^{-1}$ (equal to 971 mAh $g^{-1}$ sulphur) after 3 cycles at the current density of 0.1 A $g^{-1}$ has been obtained.[45]

#### *1.3.2.2 Lithium anode*

Li-anode is a key element of Li-S batteries, but yet it hasn't been widely studied since 1970s to 1980s.[46–50] Major problem of Li-anode is the high reactivity towards electrolyte and the soluble polysulphides. For Li-S batteries, Li metal proves to be the best candidate as an anode; however, critical issues such as dendritic growth, insolubility of $Li_2S_2$ and $Li_2S$ and reactions taking place on the surface of Li-foil favouring deleterious reactions of polysulphides, inhibits the use of Li metal. Protecting the surface of the Li-anode is not an easy chore, when it comes to retaining higher capacity and ample rate capability simultaneously. Therefore efforts were focussed on forming an isolating/ passivating layer called as "solid electrolyte interphase" (SEI) layer that not only provides protection of Li-anode, but also enable $Li^+$ diffusion. The passivation layer could be introduced pre-formed (ex-situ) by modifying surface of metallic Li-anode before assembling the battery; or in-situ by addition of suitable additive, that leads to the formation of passivation layer during cycling. Studies found that the sulphur compounds ($Li_2S$ and $Li_2S_x$) deposition on protected Li-surface is lower than unprotected surface of Li-anode.[35]

#### *1.3.2.3 Electrolyte*

Organic electrolyte used for LIBs are not valid for Li-S batteries system, due to the high polysulphide solubility in the electrolyte. Normally, the basic requirement of electrolyte for Li-S battery is high ionic conductivity, high electrochemical stability towards polysulphides and low viscosity. Numerous studies have been conducted on the influence of electrolyte constituent, such as tetrahydrofuran (THF), 1, 2-dimethoxyethane (DME), 1, 3-DIOXolane (DOX), tetra (ethylene glycol) dimethyl ether (TEGDME)[51–70]

Usually for Li-S batteries, a mixture of solvents (binary or ternary) and additives are being used as an electrolyte optimized on the basis of low /high solubility of polysulphides while maintaining good electrochemical stability and conductivity. Owing to an outstanding capacity of ~1200 mAh $g^{-1}$ upon 1$^{st}$ discharge, Tetra (ethylene glycol) dimethyl ether (TEGDME) / 1, 3-DIOXolane (DIOX) and Diethylene glycol dimethyl ether (Diglyme)/1, 3-DIOXolane (DOX) are striking organic solvent mixture for sulphur cathode.[67] 1, 2-dimethoxyethane (DME) and 1,3-DIOXolane (DIOX) combination has also been documented as good electrolyte with LiTFSI salt to improve the inclusive performance of Li-S battery.[71,72] The DME controls sulphur solubility and the electrochemical reaction of polysulphide (Figure 1.13), while DIOX acts as a stabilizer of polysulphides in the electrolyte against lithium metal.[57] Interconnected with the aforesaid challenges for Li-S system is the issue of anode stability. As with all lithium metal anode battery designs, there is a significant concern linked to dendrite growth during cycling. An additional problem of $Li_2S$ insulating layer in Li-S batteries suggests that greater attention should be devoted to stabilize the integrity of the anode.

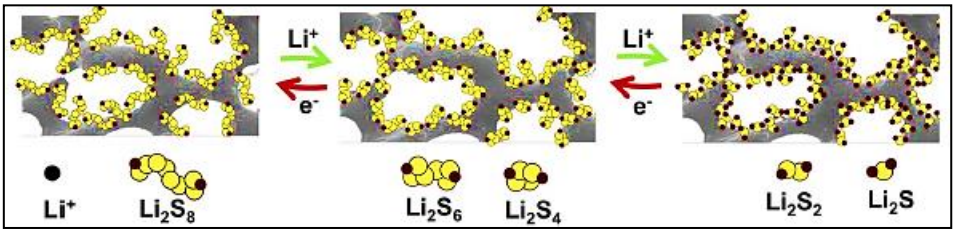


**Figure 1.13: Representation of electrochemical reaction of polysulphides within the organic electrolyte.**[73]

Recent work has suggested several routes to achieve that; in this dissertation we will follow an option to use protective layers, in order to save the surface of Lithium metal from direct exposure to electrolyte. The idea is to create a passivation of the lithium anode, preventing parasitic reduction of polysulphides and lessening the effect of the polysulphide shuttle. It is crucial to use layers that conduct only lithium ions; however,

this approach has its own inherent complexities, such as the stabilization against lithium metal and against polysulphides.

## 1.4 Disadvantages/ problems of Li-S batteries

LIBs with cathodes (such as $LiCoO_2$, $LiMn_2O_4$, $LiFePO_4$) have inherent limitation of theoretical capacity with a practical specific capacity summing up to only 210 mAh $g^{-1}$.[58,74–77]

Besides lower theoretical capacity, transition metals (like Cu, Ag, Cr, Ni, Co, etc.) consumed within these cathodes are not only expensive, but also toxic. In this regard; abundant elemental sulphur ($S_8$) is a desirable choice owing to its low cost, non-toxicity, and high theoretical capacity of 1675 mAh $g^{-1}$,[78] to expand possibility for an application for the electric vehicles (EVs) or large energy storage systems.

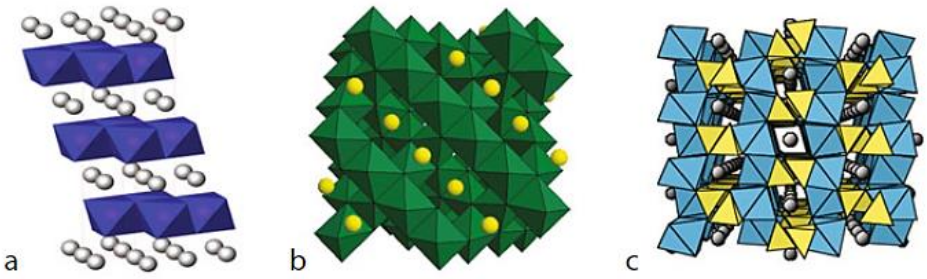


**Figure 1.14: Commonly used cathode in LIBs. a) Layered pattern of $LiCoO_2$, Theoretical capacity: 140 mAh $g^{-1}$(b) Cubic $LiMn_2O_4$ (LMO) spinel, Theoretical capacity: 100-120 mAh $g^{-1}$ (c) $LiFePO_4$ (LFP) with olivine structure, Theoretical capacity: 150-170 mAh $g^{-1}$.**[79]

Further to demonstrating that $S_8$ cathode could be most capable cathode for the next generation of high-energy rechargeable battery,[80] several problems beside the insulating nature of sulphur has been reported. Such as reactivity of the lithium metal anode which could lead to parasitic reaction of polysulphides with Li and dendrite formation, along with dissolution of polysulphide species ($Li_2S_x$) in the electrolyte which might lead to loss of active mass resulting grave capacity decay upon cycling i.e. poor cycling life.[41,43,81,82]

Immense efforts has been aimed for the development of improvement in sulphur cathodes in the Li-S system; i.e. by using different sorts of conductive carbons [43,81–85], which allowed for partially overcoming the insulating problem. Although it's astonishing that mostly those approaches endeavoured up to now in the Li-S battery have been focused on the cathode difficulties, ignoring those related to the anode or electrolyte.

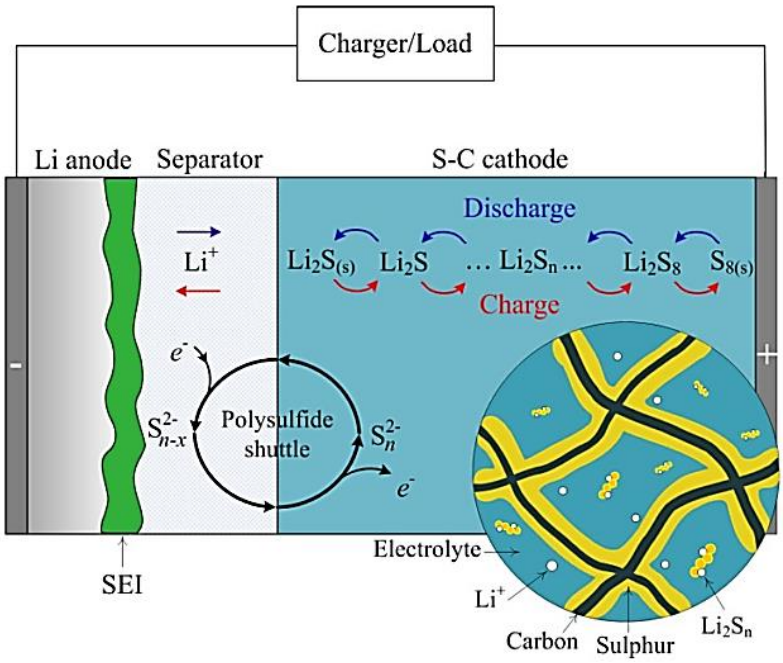


**Figure 1.15: Summary of the effects of polysulphide dissolution, Shuttle phenomenon, effect on the cathode, insoluble products upon charge and discharge.**[86]

## 1.5 Interests and objectives

This thesis deals with the major issues in Li-S batteries and possible solutions for it.

1. Li-anode protection via applying Li-conducting protective layer i.e. $Li_3N$. The $Li^+$ ion conductive protective layer has been employed by different coating techniques to achieve efficient coating with low interfacial resistance.

2. Graphite/rGO and lithium metal hybrid structured anode to control the undesirable surface reactions on lithium during cycling. By lithiating the graphite/rGO protective layer via contact with metallic Li-anode, it functions as self-regulated SEI layer to provide continuous $Li^+$ ions. Also, it provides the protection over Li-anode to reduce deleterious side reactions leading to improved performance.
3. The embedded cathodes of the sulfur/carbon composite are fabricated by using GPE-PIL coating without using any additional binder or carbon additive for enhanced performance and trapping of polysulphides species.
4. Alternative redox organosulphur polymer cathode has been used to control the problems related to polysulphide shuttle by inhibiting them within the cathode. Due to presence of N-S bond within the backbone of compound moiety provides high voltage advantage.

## 1.6 References


(1) Choi, N.-S.; Chen, Z.; Freunberger, S. a; Ji, X.; Sun, Y.-K.; Amine, K.; Yushin, G.; Nazar, L. F.; Cho, J.; Bruce, P. G. Challenges Facing Lithium Batteries and Electrical Double-Layer Capacitors. *Angew. Chem. Int. Ed. Engl.* **2012**, *51*, 9994–10024.

(2) Larcher, D.; Tarascon, J.-M. Towards Greener and More Sustainable Batteries for Electrical Energy Storage. *Nat. Chem.* **2014**, *7*, 19–29.

(3) Rastler, D. New Demand for Energy Storage. *EEI Electr. Perspect.* **2008**, 30–47.

(4) Hadjipaschalis, I.; Poullikkas, A.; Efthimiou, V. Overview of Current and Future Energy Storage Technologies for Electric Power Applications. *Renew. Sustain. Energy Rev.* **2009**, *13*, 1513–1522.

(5) UPS Battery Center. History Of Batteries: A Timeline, 2014.

(6) History of battery invention and development.

(7) Energizer. Nickel Metal Hydride ( NiMH ). *Handb. Appl. Man.* **2010**, *7323*, 1–16.

(8) J.O. Besenhard. Handbook of Battery Materials. *J. Chem. Inf. Model.* **2013**, *53*, 1689–1699.

(9) Robert Routledge. A Popular History of Science. *Igarss 2014* **2014**, 1–5.

(10) Ehrlich, G. M. *Lithium-Ion Batteries in D. Linden, T. B. Reddy (Eds.) Handbook of Batteries, McGraw-Hill Professional, New York, 2001, pp.165*; 2002.

(11) List of Battery Sizes - Wikipedia, the Free Encyclopedia.

(12) Buchmann, I. Secondary (Rechargeable) Batteries – Battery University, 2013.

(13) Tarascon, J. M.; Armand, M. Issues and Challenges Facing Rechargeable Lithium Batteries. *Nature* **2001**, *414*, 359–367.

(14) Brodd, R. J. 75th Anniversary Review Series Primary Batteries 1951-1976. **1978**.

(15) Zhao, N.; Li, C.; Guo, X. Review of Methods for Improving the Cyclic Stability of Li–Air Batteries by Controlling Cathode Reactions. *Energy Technol.* **2014**, *2*, 317–324.

(16) Mizushima, K.; Jones, P. C.; Wiseman, P. J.; Goodenough, J. B. LixCoO2 (0<x□1): A New Cathode Material for Batteries of High Energy Density. *Solid State Ionics* **1981**, *3-4*, 171–174.

(17) Takehara, Z. Future Prospects of the Lithium Metal Anode. *J. Power Sources* **1997**, *68*, 82–86.

(18) Besenhard, J. O. The Electrochemical Preparation and Properties of Ionic Alkali Metal-and NR4-Graphite Intercalation Compounds in Organic Electrolytes. *Carbon N. Y.* **1976**, *14*, 111–115.

(19) Lee, H.; Yanilmaz, M.; Toprakci, O.; Fu, K.; Zhang, X. A Review of Recent Developments in Membrane Separators for Rechargeable Lithium-Ion Batteries. *Energy Environ. Sci.* **2014**, *7*, 3857–3886.

(20) Flandrois, S.; Simon, B. Carbon Materials for Lithium-Ion Rechargeable Batteries. *Carbon N. Y.* **1999**, *37*, 165–180.

(21) Winter, M.; Besenhard, J. O.; Spahr, M. E.; Novák, P. Insertion Electrode Materials for Rechargeable Lithium Batteries. *Adv. Mater.* **1998**, *10*, 725–763.

(22) Adelhelm, P.; Hartmann, P.; Bender, C. L.; Busche, M.; Eufinger, C.; Janek, J. From Lithium to Sodium: Cell Chemistry of Room Temperature Sodium–air and Sodium–sulfur Batteries. *Beilstein J. Nanotechnol.* **2015**, *6*, 1016–1055.

(23) Kolosnitsyn, V. S.; Karaseva, E. V. 005 Lithium-Sulfur Batteries: Problems and Solutions. *Russ. J. Electrochem.* **2008**, *44*, 506–509.

(24) Sapunkov, O.; Pande, V.; Khetan, A.; Choomwattana, C.; Viswanathan, V. Quantifying the Promise of 'beyond' Li–ion Batteries. *Transl. Mater. Res.* **2015**, *2*, 045002.

(25) Bruce, P. G.; Freunberger, S. A.; Hardwick, L. J.; Tarascon, J.-M. Li–O2 and Li–S Batteries with High Energy Storage. *Nat. Mater.* **2011**, *11*, 19–29.

(26) Song, M. K.; Park, S.; Alamgir, F. M.; Cho, J.; Liu, M. Nanostructured Electrodes for Lithium-Ion and Lithium-Air Batteries: The Latest Developments, Challenges, and Perspectives. *Mater. Sci. Eng. R Reports*

**2011**, *72*, 203–252.

(27) Abraham, K. M.; Jiang, Z. A Polymer Electrolyte-Based Rechargeable Lithium/oxygen Battery. *J. Electrochem. Soc* **1996**, *143*, 1–5.

(28) Lu, Y. C.; Gasteiger, H. A.; Parent, M. C.; Chiloyan, V.; Horn, S., Y. The Influence of Catalysts on Discharge and Charge Voltages of Rechargeable Li-Oxygen Batteries. *Electrochem. Solid State Lett.* **2010**, *13*, A69–A72.

(29) Zheng, J. P.; Liang, R. Y.; Hendrickson, M.; Plichta, E. J. Theoretical Energy Density of Li-Air Batteries. *J. Electrochem. Soc* **2008**, *155*, A432–A437.

(30) Christensen, J.; Albertus, P.; Sanchez-Carrera, R. S.; Lohmann, T.; Kozinsky, B.; Liedtke, R.; Ahmed, J.; Kojic, A. A Critical Review of Li/Air Batteries. *J. Electrochem. Soc.* **2012**, *159*, R1.

(31) Manthiram, A.; Fu, Y.; Chung, S.; Zu, C.; Su, Y.; Table, S.; Page, S.; Page, S.; Page, S.; Page, S.; *et al.* Supporting Information Rechargeable Lithium-Sulfur Batteries Table of Contents S-Microporous Carbon S-Mesoporous Carbon. 1–13.

(32) Evers, S.; Nazar, L. F. New Approaches for High Energy Density Lithium-Sulfur Battery Cathodes. *Acc. Chem. Res.* **2013**, *46*, 1135–1143.

(33) Ji, X.; Nazar, L. F. Advances in Li–S Batteries. *J. Mater. Chem.* **2010**, *20*, 9821.

(34) Winter, M.; Brodd, R. J. What Are Batteries, Fuel Cells, and Supercapacitors? *Chem. Rev.* **2004**, *104*, 4245–4269.

(35) Mikhaylik, Y. V.; Akridge, J. R. Polysulfide Shuttle Study in the Li/S Battery System. *J. Electrochem. Soc.* **2004**, *151*, A1969–A1976.

(36) Dominko, R.; Patel, M. U. M.; Lapornik, V.; Vizintin, A.; Koželj, M.; N. Tušar, N.; Arčon, I.; Stievano, L.; Aquilanti, G.; Stievano, L.; *et al.* Analytical Detection of Polysulfides in the Presence of Adsorption Additives by Operando X-Ray Absorption Spectroscopy. *J. Phys. Chem. C* **2015**, *119*, 19001–19010.

(37) Angulakshmi, N.; Stephan, A. M. Efficient Electrolytes for Lithium-Sulfur Batteries. *Front. Energy Res.* **2015**, *3*, 1–8.

(38) Zhang, S. S. Liquid Electrolyte Lithium/sulfur Battery: Fundamental Chemistry, Problems, and Solutions. *J. Power Sources* **2013**, *231*, 153–162.

(39) Evers, S.; Nazar, L. F. New Approaches for High Energy Density Lithium-Sulfur Battery Cathodes. *Acc. Chem. Res.* **2013**, *46*, 1135–1143.

(40) Ji, X.; Lee, K. T.; Nazar, L. F. A Highly Ordered Nanostructured Carbon–sulphur Cathode for Lithium–sulphur Batteries. *Nat. Mater.* **2009**, *8*, 500–506.

(41) Manthiram, A.; Fu, Y.; Su, Y.-S. Challenges and Prospects of Lithium-Sulfur Batteries. *Acc. Chem. Res.* **2013**, *46*, 1125–1134.

(42) Ellis, B. L.; Lee, K. T.; Nazar, L. F. Positive Electrode Materials for Li-Ion and Li-Batteries. *Chem. Mater.* **2010**, *22*, 691–714.

(43) Jayaprakash, N.; Shen, J.; Moganty, S. S.; Corona, A.; Archer, L. A. Porous Hollow Carbon@sulfur Composites for High-Power Lithium-Sulfur Batteries. *Angew. Chemie - Int. Ed.* **2011**, *50*, 5904–5908.

(44) Wang, Y.-X.; Huang, L.; Sun, L.-C.; Xie, S.-Y.; Xu, G.-L.; Chen, S.-R.; Xu, Y.-F.; Li, J.-T.; Chou, S.-L.; Dou, S.-X.; *et al.* Facile Synthesis of a Interleaved Expanded Graphite-Embedded Sulphur Nanocomposite as Cathode of Li–S Batteries with Excellent Lithium Storage Performance. *J. Mater. Chem.* **2012**, *22*, 4744.

(45) Peled, E.; Sternberg, Y.; Gorenshtein, A.; Lavi, Y. Lithium-Sulfur Battery : Evaluation of Dioxolane-Based Electrolytes. *J. Electrochem. Soc.* **1989**, *136*, 2–6.

(46) Xu, K. Nonaqueous Liquid Electrolytes for Lithium-Based Rechargeable Batteries. *Chem. Rev.* **2004**, *104*, 4303–4417.

(47) Rauh, R. D.; Abraham, K. M.; Pearson, G. F.; Surprenant, J. K.; Brummer, S. B.; Corporation, E. I. C. A Lithium/Dissolved Sulfur Battery with an Organic Electrolyte. *J. Electrochem. Soc.* **1979**, *126*, 523.

(48) Peled, E. The Electrochemical-Behavior of Alkali and Alkaline-Earth Metals in Non-Aqueous Battery Systems - the Solid Electrolyte Interphase Model. *J. Electrochem. Soc.* **1979**, *126*, 2047–2051.

(49) Aurbach, D.; Gofer, Y.; Langzam, J. The Correlation between Surface-Chemistry, Surface-Morphology, and

Cycling Efficiency of Lithium Electrodes in a Few Polar Aprotic Systems. *J. Electrochem. Soc.* **1989**, *136*, 3198–3205.

(50) Demir-Cakan, R.; Morcrette, M.; Guéguen, A.; Dedryvère, R.; Tarascon, J.-M. Li–S Batteries: Simple Approaches for Superior Performance. *Energy Environ. Sci.* **2013**, *6*, 176.

(51) Ryu, H. S.; Ahn, H. J.; Kim, K. W.; Ahn, J. H.; Cho, K. K.; Nam, T. H. Self-Discharge Characteristics of Lithium/sulfur Batteries Using TEGDME Liquid Electrolyte. *Electrochim. Acta* **2006**, *52*, 1563–1566.

(52) Chang, D. R.; Lee, S. H.; Kim, S. W.; Kim, H. T. Binary Electrolyte Based on Tetra(ethylene Glycol) Dimethyl Ether and 1,3-Dioxolane for Lithium-Sulfur Battery. *J. Power Sources* **2002**, *112*, 452–460.

(53) Smart, M. C.; Ratnakumar, B. V.; Surampudi, S. Use of Organic Esters as Cosolvents in Electrolytes for Lithium-Ion Batteries with Improved Low Temperature Performance. *J. Electrochem. Soc.* **2002**, *149*, A361.

(54) Kolosnitsyn, V. S.; Karaseva, E. V; Amineva, N. A.; Batyrshina, G. A. Cycling Lithium – Sulfur Batteries. *Russ. J. Electrochem.* **2002**, *38*, 329–331.

(55) Gretfswald, E.--arndt-universitat. Effect of Polysulfide-Containing Electrolyte on the Film Formation of the Negative Electrode. *J. Power Sources* **1997**, *68*, 328–332.

(56) Kim, S.; Jung, Y.; Lim, H. S. The Effect of Solvent Component on the Discharge Performance of Lithium-Sulfur Cell Containing Various Organic Electrolytes. *Electrochim. Acta* **2004**, *50*, 889–892.

(57) Zhu, X.; Wen, Z.; Gu, Z.; Lin, Z. Electrochemical Characterization and Performance Improvement of Lithium/sulfur Polymer Batteries. *J. Power Sources* **2005**, *139*, 269–273.

(58) Marmorstein, D.; Yu, T. H.; Striebel, K. A.; McLarnon, F. R.; Hou, J.; Cairns, E. J. Electrochemical Performance of Lithium/sulfur Cells with Three Different Polymer Electrolytes. *J. Power Sources* **2000**, *89*, 219–226.

(59) Shin, J. H.; Kim, K. W.; Ahn, H. J.; Ahn, J. H. Electrochemical Properties and Interfacial Stability of (PEO)(10)LiCF3SO3-TinO2n-1 Composite Polymer Electrolytes for Lithium/sulfur Battery. *Mater. Sci. Eng. B-Solid State Mater. Adv. Technol.* **2002**, *95*, 148–156.

(60) Aurbach, D.; Youngman, O.; Gofer, Y.; Meitav, A.; Dan, P. The Electrochemical Behavior of 1,3-Dioxolane-LiClO4 Solutions - I. Uncontaminated Solutions. *Electrochim. Acta* **1990**, *35*, 625–638.

(61) Kolosnitsyn, V. S.; Karaseva, E. V.; Ivanov, a. L. Electrochemistry of a Lithium Electrode in Lithium Polysulfide Solutions. *Russ. J. Electrochem.* **2008**, *44*, 564–569.

(62) Yuan, L. X.; Feng, J. K.; Ai, X. P.; Cao, Y. L.; Chen, S. L.; Yang, H. X. Improved Dischargeability and Reversibility of Sulfur Cathode in a Novel Ionic Liquid Electrolyte. *Electrochem. commun.* **2006**, *8*, 610–614.

(63) Choi, Y. J.; Kim, K. W.; Ahn, H. J.; Ahn, J. H. Improvement of Cycle Property of Sulfur Electrode for Lithium/sulfur Battery. *J. Alloys Compd.* **2008**, *449*, 313–316.

(64) Ryu, H. S.; Guo, Z.; Ahn, H. J.; Cho, G. B.; Liu, H. Investigation of Discharge Reaction Mechanism of Lithium|liquid Electrolyte|sulfur Battery. *J. Power Sources* **2009**, *189*, 1179–1183.

(65) Yamin, H.; Gorenshtein, A.; Penciner, J.; Sternberg, Y.; Peled, E. Lithium Sulfur Battery. **1988**, 11–14.

(66) Shin, J. H.; Cairns, E. J. N-Methyl-(N-Butyl)pyrrolidinium Bis(trifluoromethanesulfonyl)imide-LiTFSI-Poly(ethylene Glycol) Dimethyl Ether Mixture as a Li/S Cell Electrolyte. *J. Power Sources* **2008**, *177*, 537–545.

(67) Trofimov, B. A.; Markova, M. V.; Morozova, L. V.; Prozorova, G. F.; Korzhova, S. A.; Cho, M. D.; Annenkov, V. V.; Mikhaleva, A. I. Protected Bis(hydroxyorganyl) Polysulfides as Modifiers of Li/S Battery Electrolyte. *Electrochim. Acta* **2011**, *56*, 2458–2463.

(68) Choi, J. W.; Cheruvally, G.; Kim, D. S.; Ahn, J. H.; Kim, K. W.; Ahn, H. J. Rechargeable Lithium/sulfur Battery with Liquid Electrolytes Containing Toluene as Additive. *J. Power Sources* **2008**, *183*, 441–445.

(69) Choi, J. W.; Kim, J. K.; Cheruvally, G.; Ahn, J. H.; Ahn, H. J.; Kim, K. W. Rechargeable Lithium/sulfur Battery with Suitable Mixed Liquid Electrolytes. *Electrochim. Acta* **2007**, *52*, 2075–2082.

(70) Wang, J. L.; Yang, J.; Xie, J. Y.; Xu, N. X.; Li, Y. Sulfur-Carbon Nano-Composite as Cathode for Rechargeable Lithium Battery Based on Gel Electrolyte. *Electrochem. commun.* **2002**, *4*, 499–502.

(71) Wu, F.; Wu, S. X.; Chen, R. J.; Chen, S.; Wang, G. Q. Electrochemical Performance of Sulfur Composite Cathode Materials for Rechargeable Lithium Batteries. *Chinese Chem. Lett.* **2009**, *20*, 1255–1258.

(72) Whittingham, M. S. Lithium Batteries and Cathode Materials. *Chem. Rev.* **2004**, *104*, 4271–4301.

(73) Babu, G.; Ababtain, K.; Ng, K. Y. S.; Arava, L. M. R. Electrocatalysis of Lithium Polysulfides: Current Collectors as Electrodes in Li/S Battery Configuration. *Sci. Rep.* **2015**, *5*, 8763.

(74) Ji, X.; Lee, K. T.; Nazar, L. F. A Highly Ordered Nanostructured Carbon-Sulphur Cathode for Lithium-Sulphur Batteries. *Nat. Mater.* **2009**, *8*, 500–506.

(75) Sun, Y.-K.; Myung, S.-T.; Park, B.-C.; Prakash, J.; Belharouak, I.; Amine, K. High-Energy Cathode Material for Long-Life and Safe Lithium Batteries. *Nat. Mater.* **2009**, *8*, 320–324.

(76) Yang, Y.; McDowell, M. T.; Jackson, A.; Cha, J. J.; Hong, S. S.; Cui, Y. New Nanostructured Li2S/Silicon Rechargeable Battery with High Specific Energy. *Nano Lett.* **2010**, *10*, 1486–1491.

(77) The Sulphur Electrode . Fused Salts and Solid Electrolytes . R . P . Tischer. **1985**, *182*, 1985.

(78) Kumaresan, K.; Mikhaylik, Y.; White, R. E. A Mathematical Model for a Lithium–Sulfur Cell. *J. Electrochem. Soc.* **2008**, *155*, A576.

(79) Meyers, R. A. *Encyclopedia of Sustainability Science and Technology*; 2012.

(80) Yang, Y.; Zheng, G.; Cui, Y. Nanostructured Sulfur Cathodes. *Chem. Soc. Rev.* **2013**, *42*, 3018–3032.

(81) Zhang, B.; Qin, X.; Li, G. R.; Gao, X. P. Enhancement of Long Stability of Sulfur Cathode by Encapsulating Sulfur into Micropores of Carbon Spheres. *Energy Environ. Sci.* **2010**, *3*, 1531.

(82) Schuster, J.; He, G.; Mandlmeier, B.; Yim, T.; Lee, K. T.; Bein, T.; Nazar, L. F. Spherical Ordered Mesoporous Carbon Nanoparticles with High Porosity for Lithium-Sulfur Batteries. *Angew. Chemie - Int. Ed.* **2012**, *51*, 3591–3595.

(83) Cells, L. S.; Ji, L.; Rao, M.; Zheng, H.; Zhang, L.; Li, O. Y.; Duan, W. Graphene Oxide as a Sulfur Immobilizer in High Performance. **2011**, 18522–18525.

(84) Ji, L.; Rao, M.; Aloni, S.; Wang, L.; Cairns, E. J.; Zhang, Y. Porous Carbon Nanofiber–sulfur Composite Electrodes for Lithium/sulfur Cells. *Energy Environ. Sci.* **2011**, *4*, 5053.

(85) Zheng, G. Y.; Yang, Y.; Cha, J. J.; Hong, S. S.; Cui, Y. Hollow Carbon Nanofiber-Encapsulated Sulfur Cathodes for High Specific Capacity Rechargeable Lithium Batteries. *Nano Lett.* **2011**, *11*, 4462–4467.

(86) Wild, M.; O'Neill, L.; Zhang, T.; Purkayastha, R.; Minton, G.; Marinescu, M.; Offer, G. J. Lithium Sulfur Batteries, a Mechanistic Review. *Energy Environ. Sci.* **2015**, *8*, 3477–3494.

# *Chapter 2: Materials and methods*

# 2 Introduction

This chapter is a demonstration of supportive information about general procedures of cathodes/materials preparation, cell assembly, etc., employed in the whole thesis. Additionally, description about certain conditions used for instrumentation/equipment engaged in this thesis is presented.

## 2.1 List of chemicals: *Alphabetical order*

| Chemical abb. | Classification | Company |
|---|---|---|
| ACN | Acetonitrile ≥99.93%, 75-05-8 | Sigma-Aldrich |
| Acetone | ≥99.9% 67-64-1 | Sigma-Aldrich |
| Celgard2400 | Polypropylene membrane | Celgard® |
| C-$KJ_{600}$ /$ECP_{600}$JD | Carbon ketjenblack 600 powder,1333-86-4 | Azko Nobel/imerys |
| $C_{SP}$ | Carbon Black Super P®1333-86-4 | TIMCAL TIMREX® |
| $CS_2$ | Carbon disulphide ≥99.9%, 75-15-0 | Sigma-Aldrich |
| DMSO | Dimethyl sulphoxide ≥99.9%, 67-68-5 | Sigma-Aldrich |
| DIOX | 1, 3- Dioxolane anhydrous 99.8%, 646-06-0 | Sigma-Aldrich |
| DME | 1,2-Dimethoxyethane anhydrous 99.5%,110-71-4 | Sigma-Aldrich |
| $Et_2N$ | Diethyl amine-Synthesised | CIC |
| EPDM | Ethylene-Propylene-Diene Monomer | Sigma-Aldrich |
| EM005/ $PYR_{14}$TFSI | *N*-methyl-*n*-butyl-pyrrolidinium-bis(trifluoromethylsulphonyl)imide, 99.9% , Pyr0408a | Solvionic |
| GF | Glass fiber, *Z242063* | Whatmann® |
| Gr/$SFG_6$ | Graphite, 7782-42-5 | TIMCAL TIMREX® |
| GO/rGO | Graphene oxide/reduced Graphene oxide | CIC/graphene-A |
| $H_2O$ | Distilled water | CIC |
| Li-foil | Lithium metal, battery grade 7439-93-2 | Rockwood |
| $Li_3N$ | Lithium nitride ≥99.5%, 26134-62-3 | Sigma-Aldrich |
| $LiNO_3$ | Lithium Nitrate 99.9%, 7790-69-4 | Sigma-Aldrich |

| | | |
|---|---|---|
| LiTFSI | Lithium bis(trifluoromethylsulphonyl)imide, 99+%, S001 | Solvionic |
| MeOH($CH_3OH$) | Methanol, 99.8%, 67-56-1 | Sigma-Aldrich |
| MeTHF | Methyl tetrahydrofuran anhydrous ≥ 99%, 96-47-9 | Sigma-Aldrich |
| NMP | N-Methyl-2-pyrrolidone 99.5%, 872-50-4 | Sigma-Aldrich |
| PEOX | Poly(2-ethyl-2-oxazoline) $M_w$ ~ 50,000, 25805-17-8 | Sigma-Aldrich |
| PVdF | Poly(vinylidene fluoride), 24937-79-9 | Solef® |
| PEO | Poly(ethylene oxide) Mw~ 50,000, 25322-68-3 | Sigma-Aldrich |
| $S_8$ | Sulphur powder, purum ≥99.5%, 7704-34-9 | Sigma-Aldrich |
| Sulpholane | Tetramethylene sulphone 99%, 126-33-0 | Sigma-Aldrich |
| TEGDME | Tetra (ethylene glycol) dimethyl ether, 99%, 112-49-2 | Sigma-Aldrich |
| THF | Tetrahydrofuran, ≥99.9%, 109-99-9 | Sigma-Aldrich |

## 2.2 Usage of chemicals

The solvents used were anhydrous and were dried with molecular sieves (4A$^o$) inside the glove box for at least 48 hrs. Chemicals were dried in Büchi oven under vacuum at temperature according to their properties for 24 h and were stored inside the glovebox.

## 2.3 Experimentation

### 2.3.1 *Cathode preparation*

#### 2.3.1.1 DMSO technique for S/Ckj600 composite:

Sulphur/carbon composites were prepared using DMSO solvent technique.[1] Sulphur and Carbon ketjen $black_{600}$ was taken in a wt. % of 70:30 for preparation of the composite. The mixture was hand milled for 10 minutes and then transferred into a tightly closed flask with ~100-150mL of DMSO. The oil bath was heated until 155 °C. The composite mixture was kept in hot oil bath over stirring for 4 h.

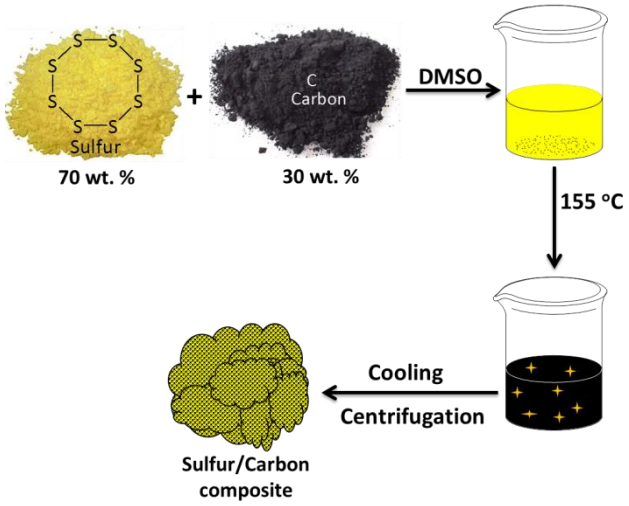


**Figure 2.1: schematic diagram of the composite mixing by using DMSO solvent technique.**

The mixture was then cooled down to room temperature upon stirring, followed by centrifugation at 4000 rpm for 45min. The homogenous S/C composite powder was dried under vacuum overnight at 60 °C.[2]

### 2.3.1.2 S/Ckj600 composite cathode:

1. *Powder cathode:*

The composite powder of S/C, prepared by DMSO technique was used for cycling of Li-S batteries, in order to accumulate and understand the properties and performance of sulphur cathode without/with any binder.

2. *Laminated cathode:*

The composite mixture of (70:30 wt. %) of sulphur and carbon ketjen black$_{600}$ ($C_{ECP600JD}$) was wet-ball milled with polymeric binder PVdF or PIL/PEO with a wt. % of (90:10 or 50:50) in NMP/ACN. No additional carbon was added. Wet ball milling was done for 30 minutes at 8000 rpm on 8000M mixer/mill (© SPEX SamplePrep). The mixture was laminated on a carbon coated Al-current collector by using Dr. Blade with a wet thickness 300 µm. The laminate were allowed to settle down at room temperature and then dried under vacuum for overnight at 60$^{o}$C.

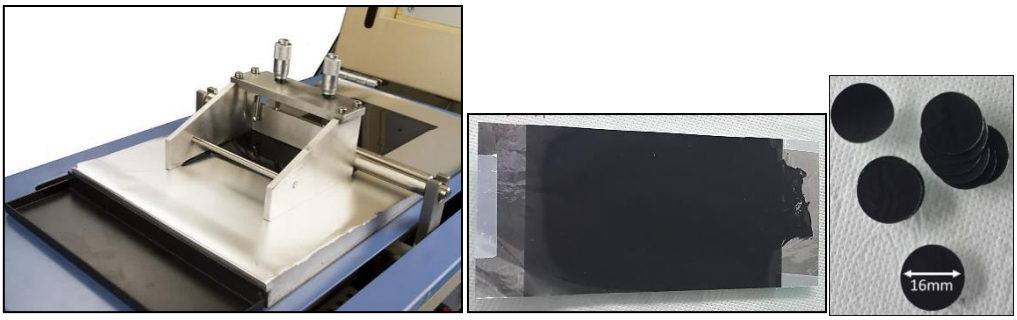


**Figure 2.2: Showing casting on current collector by using Dr. Blade technique; prepared laminate and the punched spherical disc cathodes.**

Spherical disc (Ø =12mm for coin cell and Ø =16mm for pouch cell) were punched with the sulphur loading ~1.5-2 mg $cm^{-2}$. The disc was dried prior to storing *inside the glovebox ($O_2$ and $H_2O$ < 1 ppm).*

## 2.3.2 *Electrolyte preparation*

### 2.3.2.1 Liquid Electrolyte:

1. *<u>1M LiTFSI in DME: DIOX (1:1 vol. %)</u>*

Lithium Bis (Trifluoromethanesulphonyl) Imide (LiTFSI) was dried overnight under vacuum at 110$^oC$ while solvents DME and DIOX (mixture of 1:1 vol. %) were dried by using molecular sieves (4$^oA$) overnight in a glovebox with $H_2O$ and $O_2$ level of <1ppm.

Dried LiTFSI powders were dissolved at a concentration of 1M in the 1:1 vol. % mixture of DME and DIOX, stirred overnight and used as $Li^+$ ion conductive electrolyte. The water ppm has been checked by using Karl fischer titration (METLER TOLEDO).

2. *<u>1M LiTFSI in TEGDME: DIOX (1:1 vol. %)</u>*

1M LiTFSI in 1:1, vol. % mixture of TEGDME and DIOX were received from Solvionic under the project of EuroLIS in NIC, Slovenia. The electrolyte was used as received.

3. *1M LiTFSI in MeTHF*

It was noted that upon contact with DME: DIOX based electrolyte, PEO binder swells and partially gets dissolved in electrolyte losing the shape and integrity of the cathode. The dried LiTFSI (1 M concentration) were dissolved in MeTHF stirred overnight and used as $Li^+$ ion conductive electrolyte. To avoid solubility, MeTHF solvent was used for batteries with PEO binder included.

### 2.3.2.2 Solid Electrolyte:

1. *PEO: LiTFSI (1:20)*

Homogenous PEO : LiTFSI (EO/$Li^+$ : 20:1) has been prepared by solvent casting method [3]. Due to hygroscopic nature of LiTFSI, it has been dissolved in dry acetonitrile inside the glovebox ($O_2$ and $H_2O$ < 1 ppm).

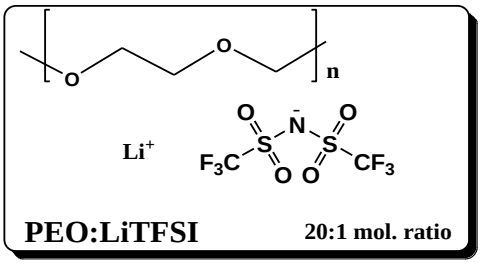


**Figure 2.3: The homogenous slurry of PEO: LiTFSI in dry acetonitrile after stirring for 24hrs and the structural diagram of PEO: LiTFSI.**

Then the PEO polymer was added slowly to the mixture over stirring in a closed vial at a moderate speed to avoid lumps. The ratio of PEO to the solvent was 1:50 to have homogenous dispersion and no agglomeration. Once the consistency of the slurry is viscous, the casting process was performed.

Casting:

The material with lower adhesive property such as low density teflon (polytetrafluoroethylene) disk has been chosen for casting the thick slurry of PEO: LiTFSI polymeric mixture. Once the polymeric suspension settles down upon Teflon dish, it was placed in a desiccator for slow evaporation under inert atmosphere.

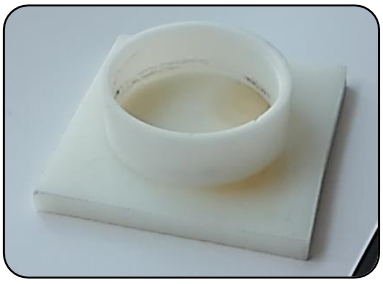

**Figure 2.4: PTFE disc for casting of PEO: LiTFSI mixture.**

Once dried, hot pressing at 60ºC were carried out, following the punching of membranes (Ø = 16 mm). The membranes were dried in vacuum oven at 45ºC overnight and then transferred to the glovebox ($O_2$ and $H_2O$ < 1 ppm).

2. *PIL (EM005)*

The Gel polymer electrolyte poly (DDA) TFSI-$PYR_{14}$TFSI-LiTFSI (EM005) was acquired from Solvionic with following composition: Lithium bis(trifluoromethanesulphonyl)imide (LiTFSI) : *N*-butyl-*N*-methylpyrplidinium bis(trifluoromethanesulphonyl)imide ($PYR_{14}$TFSI) (1:9 mol ratio) and 58 wt.% poly (diallyldimethylammonium) bis (trifluoromethanesulphonyl)imide (poly (DDA) TFSI) in acetone.

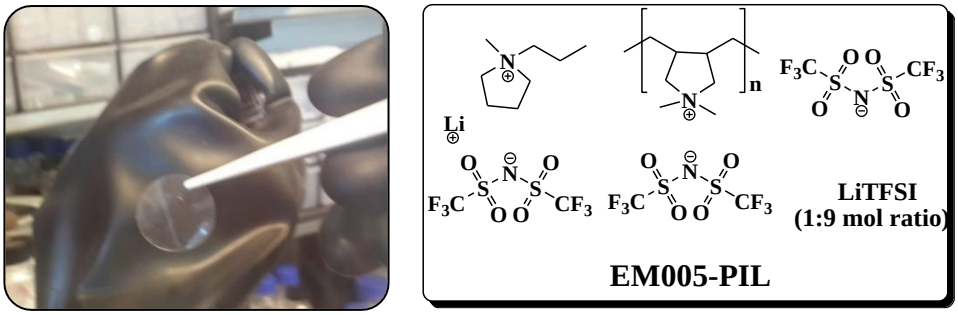


**Figure 2.5: Casted and punched membrane of PIL-EM005 (200um) and structure of EM005-PIL comprised of 3 cations ($PIL^+$, $IL^+$, $Li^+$) and 1 anion ($TFSI^-$).**

Casting:

*M*embranes were casted inside the glove box on the Mylar film support using drop coating technique. The membrane was dried over 24hrs at room temperature. Once dried, a homogenous membrane of 200 µm thickness was peeled and punched (Ø = 20 mm) into desired shape.

## *2.3.3 Anode preparation*

### 2.3.3.1 Li-metal

Li- foil was used as anode for Li-S battery in the present work. Metallic Li-foils, stored in the glove box to avoid any adverse reactions with air were punched into small circular discs.

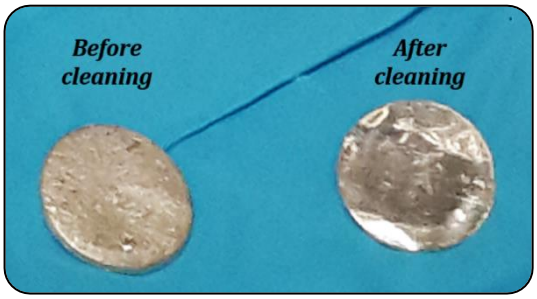


**Figure 2.6: Image of metallic Li before and after cleaning for battery testing.**

The oxidized surface was cleaned to obtain best battery performance. To clean off the oxide layer, the surface was scraped with a brush. Once the surface is scraped, the Li-foil was rolled out in order to smoothen the surface until it becomes shiny.

Processed Li-foils were punched into different sizes (Ø = 16, 14, 12, 10 mm) with

suitable puncher.

## 2.3.4 Battery configuration

### 2.3.4.1 Coin-cell assembly

For Li-based batteries exploration, coin type cells are commonly known as standard testing platform. Components of coin cells and the equipment to assemble them are commercially available. The use of coin cells are now a days widespread and well established in the battery society.[4]

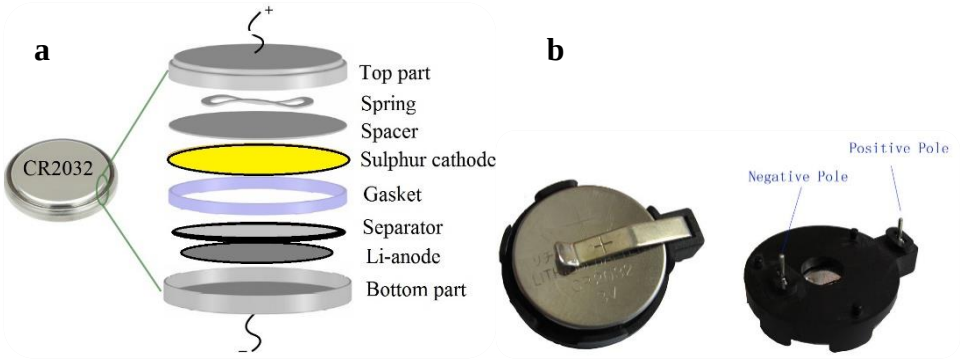


**Figure 2.7: a) schematic diagram of CR2032 coin type cell configuration. b) Photograph of coin cell within the holder.**

Galvanostatic cycling was performed in CR2032 coin cells, with S/C composite (powdered or laminated) cathode separated from Li-anode by using glassfiber separator wetted with 1M LiTFSI in DME: DIOX (1:1 vol. %) at room temperature. The amount of electrolyte was standardised to 60 µL $mg^{-1}$ of sulphur. The cells were mounted in a glove box with lower oxygen and water contents (< 1ppm). The galvanostatic testing of batteries were carried out using Maccor 4200 galvanostat/potentiostat with voltage range of 1-3V at different current densitites.

### 2.3.4.2 Coffee-bag cell assembly

In a coffee bag type cell, S/C composite laminated cathode (Ø = 16mm) was separated from the Li-anode (Ø = 16mm) by Celgard 2400 (Ø = 20mm) wetted with 1M LiTFSI in

TEGDME: DIOX (1:1, vol. %). The amount of electrolyte was standardised to 60 µL $mg^{-1}$ of sulphur and the batteries were assembled inside the glove box by using coffee bag cell sealer.


**Figure 2.8: a) Photograph of a Li-S coffee bag cell. b) Schematic presentation of the liquid Li-S battery configuration.**

The galvanostatic testing of batteries were carried out using Maccor 4200 galvanostat/potentiostat with voltage range of 1-3V at C/20.

### 2.3.4.3 Coffee-bag cell for in-situ UV/Vis measurement

Cell assembly was similar to typical coffee bag cell, S/C composite laminated cathode (Ø = 16mm) was separated from the Li-anode (Ø = 20mm) by using glassfiber (Ø = 20mm) wetted with 1M LiTFSI in TEGDME: DIOX (1:1, vol. %). The amount of electrolyte was standardised to 60 µL $mg^{-1}$ of sulphur. The Li-foil contains a hole, half of the size of cathode to avoid any interference during in-situ measurement and the batteries were assembled inside the glove box (Figure 2.9).

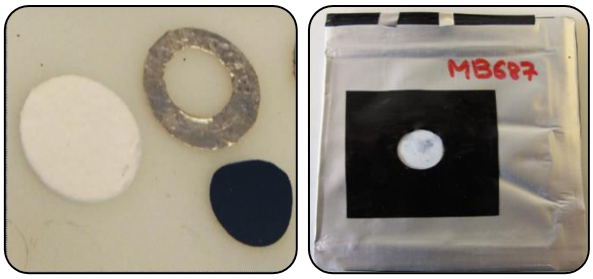


**Figure 2.9: Image of battery component to be tested in *in-situ* experiment before assembly, and assembled coffee bag cell with a glass window for the in-situ UV/Visible measurements.**

A hole was punched in the coffee bag cell casing and covered by a glass window to obtain UV/Vis spectra from the cathode without any interference. This configuration allows the exposure of polysulphides in the separator. For in-situ measurements, the coffee bag cell was attached to a UV/Vis spectrometer. This allows the direct focus of UV light towards the glass window.

### 2.3.4.4 Cell for in-situ XRD measurement

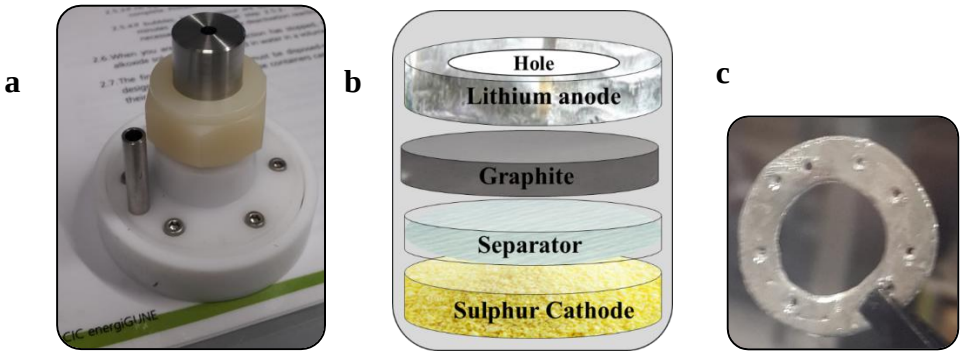


**Figure 2.10: a) Image of in-situ XRD cell with beryllium window and PTFE body, b) Schematic diagram of the configuration of cell, c) The perforated Li-anode, with 10mm hole used for in-situ measurements.**

The cell was fabricated as shown in figure above (Figure 2.10). The cell contains a beryllium window as a cathode/anode current collector for enabling diffraction studies on the cathode/anode materials during in-situ measurements. Composition of cell follow conventional battery assembly of S/C cathode (30:70 wt. %) separated from graphite/Li hybrid anode by using 18mm of glassfiber separator wet with 1M LiTFSI in DME: DIOX

(1:1 vol. %). The Lithium has been perforated (Figure 2.10c) in order to clearly measure the electrochemical changes occurring at graphite surface beneath the Li foil.

## 2.4 Characterization

### *2.4.1 Electrochemical characterization techniques:*

Measurements for evaluating the electrochemical performance of Li-ion batteries including cyclic voltammetry (CV), galvanostatic charge-discharge testing, and electrochemical impedance spectroscopy studies are explained below:

#### 2.4.1.1 Cyclic Voltammetry (CV)

CV is a commonly used technique for obtaining qualitative data of electrochemical reactions of the batteries. It proposes a fast site of redox potentials of the electrode/electrolyte species. A series of voltage is applied to the battery *vs.* time at a constant rate (scan rate =mV $s^{-1}$) and fixed voltage range (1-3V). During scan, voltage sweeps back and forth between the voltage range applied, and corresponding currents are obtained. The monitored current is plotted as a function of voltage. The potential is applied with respect to a reference electrode ($R_E$) and the current is measured between the working electrode ($W_E$) and the counter electrode ($C_E$).

CV scan starts with current at zero flow, during the sweep scan the analytes that can reduce (oxidise, depending on sweep direction) will produced a current over the range of potential. The current flow will ultimately reaches a peak and falls, the peak area specifies high electron transfer rate in contrast with the voltage scan rate. Slow sweep scan give extra time for the high mass diffusion layer when compared to high sweep scan. Owing to faster electron transfer kinetics (reversible), the electrode reaction delivers characteristic current peaks. Thus, this principle can be employed to investigate the potentials of the electrochemical reaction. [5]

**Sample preparation**

Full-cell and symmetric configuration coin cells CR2032 has been used for CV measurements, the cell assembly can be seen in section: Battery configurations.

**Instrument used:**

Biologic - 6 X Biologic VMP3 using EC-Lab software.

### 2.4.1.2 Galvanostatic cycling (Discharge and Charge) GCPL

In order to determine the practical capacity of an electrode material, Galvanostatic Cycling with Potential Limitation (GCPL) technique is used. The capacity is generally derived from the current (A or mA) and the time (h) and the unit of capacity is Ah or mAh. GCPL measurements are normally conducted by applying a constant current density defined as C-rate. The charge/discharge capacity can be calculated by the equation given below where 'I' is the current density and 't' is the time of completion of one cycle.[5]

$$Q = I \times t$$

**Sample preparation**

Full-cell configuration coin cells CR2032 has been used for GCPL cycling measurements, the cell assembly can be seen in section: Battery configurations.

**Instrument used**

MACCOR Battery Tester and Biologic-6 X Biologic Vmp3 using EC-Lab software.

### 2.4.1.3 Electrochemical Impedance Spectroscopy (EIS)

EIS is the measurement of dielectric properties of a system as a function of frequency with a small applied perturbation (AC signal). It delivers information regarding the mechanism of an electrochemical reaction process.

A range of frequencies can be used for EIS technique to measures the impedance, and

the data about a system is presented graphically as Nyquist or Bode plot.[5,6]

**Sample preparation**

EIS measurements have been carried out on Full-cell and symmetric cell configuration using a CR2032 coin cell before and after cycling. The cell resistance with and without protective layers have been measured over a frequency range from 0.1 Hz to 1.0 MHz with a signal amplitude of 10 mV. The cell assembly can be seen in section: Battery configurations.

**Instrument used**

Biologic-6 X Biologic Vmp3 using EC-Lab software.

## *2.4.2 Physico-chemical characterization/post-mortem techniques:*

### 2.4.2.1 Scanning Electron Microscopy (SEM)

**a** **b**

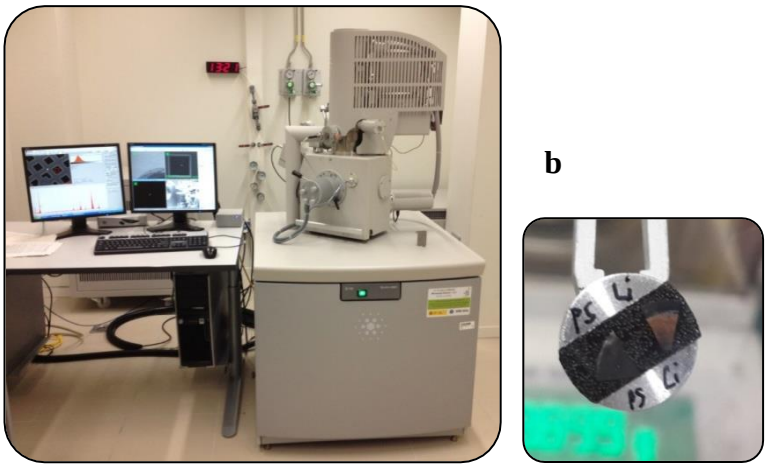


***Figure 2.11: a) SEM equipment used for SEM measurements, b) Sample holder showing the preparation of samples by adhesion on carbon tape.***

The Scanning Electron Microscope (SEM) uses a focused beam of high-energy electrons to generate a variety of signals at the surface of solid specimens. Signals that derive from electron-sample interactions reveal information about the sample including external

morphology (texture), chemical composition, crystalline structure and orientation of materials.

Resolution of the SEM image is directly dependent on the diameter of electron beam. SEM equipment includes Energy-dispersive X-ray spectroscopy (EDS) to evaluate the qualitative and semi quantitative elemental analysis defined as elemental maps, which are accurate representation of the elemental distribution within the sample.

**Sample Preparation for SEM**

The samples for SEM have been prepared inside the glovebox ($O_2$ and $H_2O$ < 1 ppm) using carbon tape for adhesion of samples on the SEM mount support for investigating the morphology, thickness and surface changes.

**Instrument used**

Quanta 200 FEG (FEI) scanning electron microscope (SEM) in CIC, Miñano, Spain, and field-emission scanning electron microscope (FE SEM) Supra 35 VP (Zeiss, Germany), in NIC, KI, Slovenia.

### 2.4.2.2 X-ray photoelectron spectroscopy (XPS)

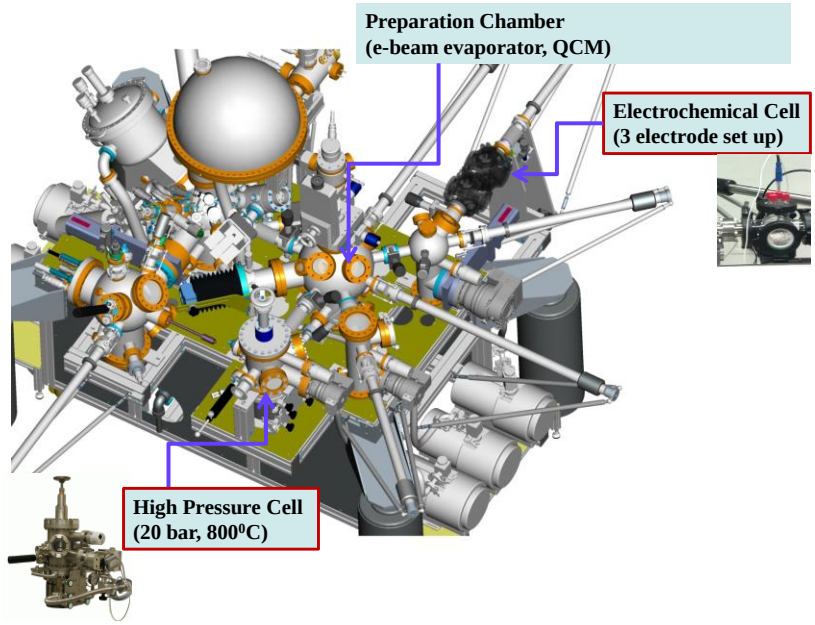


***Figure 2.12: Schematics of the XPS equipment used for sample measurements.***[7]

XPS is a surface analysis technique based on photoemission. Samples can be measured by penetration depth up to few nanometres. The experiments usually are conducted in high-vacuum (HV, P ~ $10^{-8}$ millibar) or ultra-high vacuum (UHV, P < $10^{-9}$ millibar) settings, where the sample is irradiated by monoenergetic soft X-ray from an Al $K_\alpha$ source with an energy of hν = 1486.6 eV. Upon penetration with X-ray photon, the electron is ejected from core level of energy hν. Electron spectrometer scrutinises the energy of emitted photoelectrons. Simultaneously the kinetic energy (binding energy) and ejected electrons from 0 to 10 nm of the material are analysed. [8,9]

#### Sample Preparation for XPS

The samples prepared inside the glovebox ($O_2$ and $H_2O$ < 1 ppm) were fixed on the molybdenum sample holder by using adhesive carbon tape and placed in an air-tight wobble stick specialized for air-sensitive samples for XPS measurements. The Li-sample were cleaned using Ar gun before measurements.

**Instrument used**

Specs Multi Technique Surface Analysis System for High Resolution XPS Kratos Axis Ultra spectrometer. Each photoemission spectrum was recorded with constant pass energy of 20 eV. The photoemission peaks were calibrated using the hydrocarbon contamination peak at 285 eV in the C 1*s* spectra.

### 2.4.2.3 Attenuated total reflectance Fourier-transform infrared spectroscopy (ATR-FTIR)

ATR is a quantitative and qualitative sampling technique[10] used in combination with IR spectroscopy enabling the direct examination of the sample (liquid or solid). The ATR uses the total internal reflectance of IR beam upon contact with the sample.

**Sample Preparation for FTIR**

The preparation for non-air sensitive samples was carried out by using KBr pellets, and for air-sensitive FTIR-ATR was used, which allow direct placement of sample on the germanium crystal.

**Instrument used**

Nexus Thermo FTIR-ATR spectrometer (4 $cm^{-1}$ resolution, 32 scans).

### 2.4.2.4 Raman Spectroscopy:

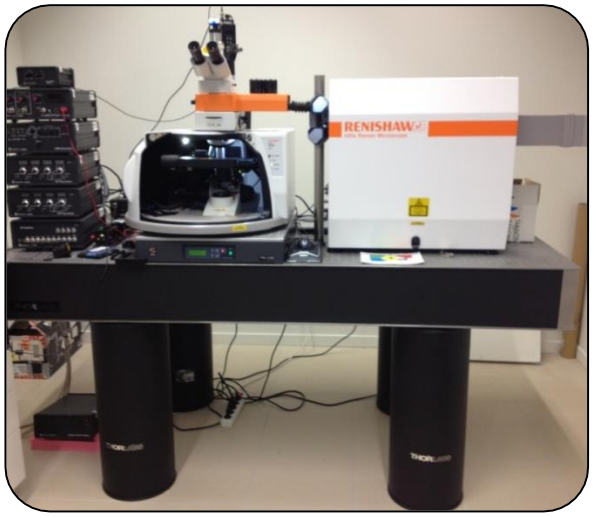


**Figure 2.13: Raman spectrometer used to collect data.**

Raman spectrometer is used to evaluate the vibrational, rotational or any other lower frequency modes in a sample. It is commonly known for providing fingerprint details of molecules for identification.

Raman spectrometer use the principle of scattering of monochromatic light by a laser in the range of visible, near IR, or near UV. Laser interacts with molecular vibrations, phonons or other excitation, which are responsible for the shifting of energy of the laser photons up or down. The shift of energy cause by the irradiation of the sample by laser beam is collected via lens and sent to monochromator. [11–14]

**Sample Preparation for Raman spectroscopy**

Powder samples were dried for 16h under vacumm before measurement.

**Instrument used**

NANONICS & RENISHAW - Nanonics Multiview 2000 TERS with Raman Spectrometer

### 2.4.2.5 X-Ray Diffraction (XRD)

**a** **b**

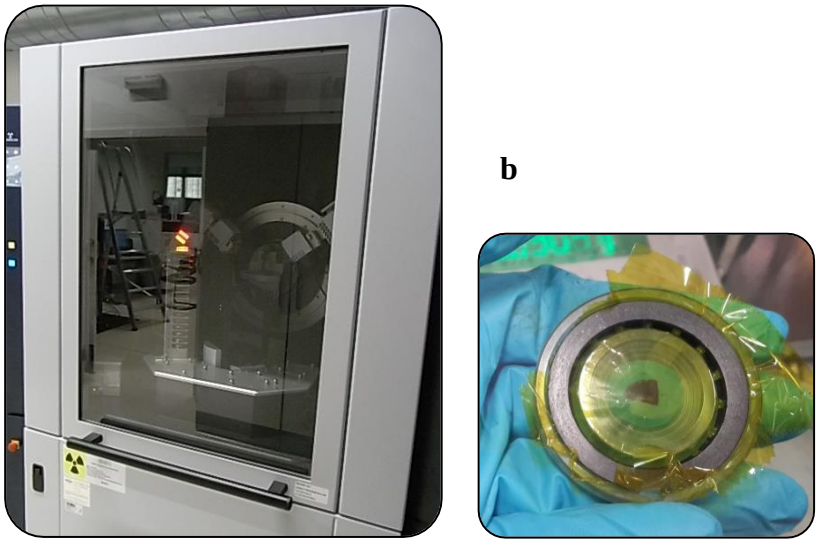

**Figure 2.14: a) Bruker advance D8 diffractometer used for testing samples, b) sample holder cover with capton for air-sensitive samples.**

XRD is an analytical technique mostly used for phase identification of the crystalline samples, and provides information regarding unit cell dimensions, atomic spacing, and crystal structures.

Monochromatic radiation is based on the filtered X-rays produced by a cathode ray tube. XRD is dependent on constructive interference of monochromatic X-rays and a crystalline sample. The contact of the incident rays with the sample generates a diffracted ray and constructive interfering medium, which satisfy the Bragg's Law ($n\lambda=2d \sin \theta$). The Law relates the diffraction angle and the lattice spacing in a crystalline sample to the wavelength of electromagnetic radiation (EMR). The diffracted X-rays are monitored, detected, processed and counted.

**Sample Preparation for XRD**

The non-air sensitive homogenized fine powder was firmly packed in the sample holder, slightly pressed uniformly with glass slide, assuring a flat surface. Air-sensitive samples were packed inside the glovebox ($O_2$ and $H_2O$ < 1 ppm) by protecting with capton. The

transfer from GB to the instrument was done quickly in a sealed bag. The films were keep intact by placing very little amount of clay. The standard measurement were run for 1 h in a 2θ range of 15-80.

**Instrument used**

Bruker D8 Advance diffractometer, the radiation frequency used was the Kα1 line from Cu (1.5406 Å), with a power supply of 40 kV and 40 mA. The crystallite size along the c-axis (Lc) was obtained from the (002) reflection of the XRD patterns, which were recorded at steps of 0.01º and at intervals of 6 s per step.

### 2.4.2.6 In situ X-Ray Diffraction (in-situ XRD)

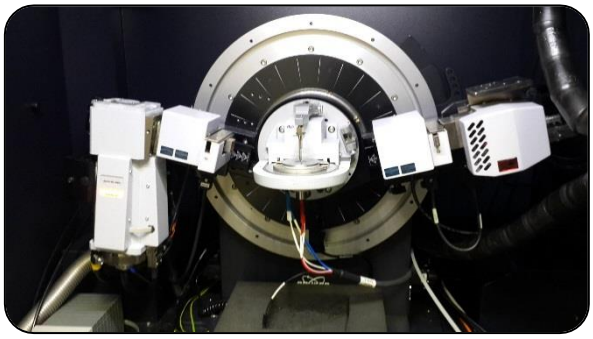

**Figure 2.15: The image of Bruker instrument for in-situ XRD.**

The working principle of the *in-situ* XRD has been mentioned earlier in section 2.4.2.5.

***Sample Preparation for in-situ XRD***

The cell assembly for in-situ measurements is given in the section; Battery configurations. The measurement was started when the battery was at the state of rest, the XRD spectra were recorded each 30 min in the range of 15-45 ° for one cycle at C/10.

***Instrument used***

In-situ X-ray diffraction analysis of the samples has been measured by a BRUKER - D8 ADVANCE X-ray diffractometer with copper radiation (Cu Kα, λ=1.5418 Å). Galvanostatic cycling was carried out on VMP3 Biologic by using EC-Lab software.

### 2.4.2.7 Solid-state Nuclear Magnetic Resonance spectroscopy (SS-NMR)

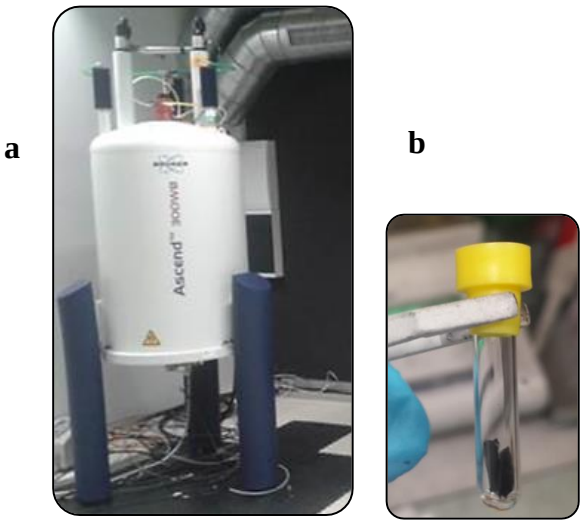


**Figure 2.16: Solid state NMR 500 MHz instrument used for analysis of NMR and the Image of sample holder prepared inside the glovebox under argon atmosphere.**

SS-NMR is usually used for measuring the isotopes with an intrinsic magnetic moment; it means that the nuclei of nonzero spin are active in a magnetic field. In the magnetic field with nuclei of different spin, the energy and resonance show the difference, which is called chemical shift with a unit of ppm. The molecular structure can be concluded by the position of chemical shift.

**Sample Preparation for SS-NMR**

The samples were packed in a NMR tube (Figure 2.16b), inside the glovebox ($O_2$ and $H_2O$ < 1 ppm) and were transferred for measurements in an air-tight holder.

**Instrument used**

SS-NMR spectra are recorded with a Bruker Advance III 500 spectrometer, at a frequency $\nu_o$= 500.24 MHz for $^7$Li. $^7$Li NMR experiments were conducted using single pulses $\pi/2$ of 2.5 μs.

### 2.4.2.8 In-situ Ultra Violet/Visible measurements (in-situ UV/Vis)

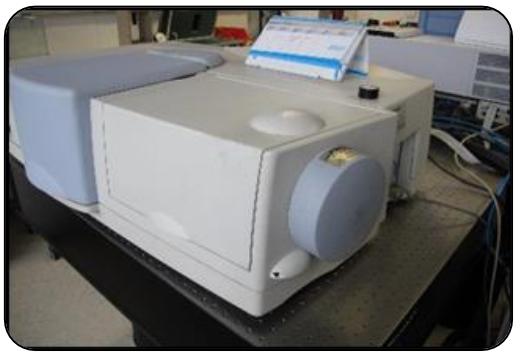

**Figure 2.17: UV/Visible equipment used for in-situ measurements.**

UV/Vis spectroscopy is a common analytical technique, it's based on absorbance/reflectance of the sample in the UV/Vis region, i.e. UV region is 200-400nm, and visible region is 400-800nm. The obtained UV/Vis spectra peaks are the results of excitation of π or n electrons upon irradiation, they absorb the energy and shift from HOMO to the LUMO orbitals.[15] UV/Vis absorption spectra is collected by distribution of light of a known intensity via the sample and record the decrease in intensity as a function of wavelength.

**Sample Preparation for in-situ UV/Vis measurements**

The main experiment was carried out to evaluate the polysulphide species in the electrolyte in the light of UV/Visible. The battery assembly was performed in an argon filled glove box, for further details section: Battery configurations. The cell was attached fixed to UV/Vis spectrometer and the measurements were started by initiating the cycling of battery via Biologic SP-200 galvanostat/potentiostat at C/20. During cycling,

the UV/Vis spectra was recorded each 15 min in the range of 800-250 nm.

**Instrument used:**

Perkin-Elmar Lambda 950 UV/Vis spectrometer

### *2.4.2.9* Simultaneously Thermogravimetric analysis /Differential scanning calorimetry (STA/TG-DSC)

***Figure 2.18: The TG-DSC instrument used for measurements.***

The TG-DSC method is widely used over a large range of temperatures, even at very high temperatures. Inorganic products (minerals, raw materials) are often investigated using such a method. DSC defines heat flow and temperature linked with material transitions as a function of time/temperature. It can also give information about quantitative and qualitative measurements of the endothermic and exothermic processes of the sample during physical transitions due to melting, crystallization, glass transitions, oxidation, phase changes, etc. Glass transition temperature (Tg), usually depends on the treating of the sample, and natural characteristics i.e. molecular weight, bonding and structure. On a DSC curve, Tg is an endothermic process, since it's recorded by breaking the bonds of the sample by using energy.

**Sample Preparation for TG/DSC**

Powder samples were dried prior to TG/DSC experiment, the small quanity of sample (6-8mg) has been weighed in Al crucibles. The measurements were carried out under continuos flow of argon (60 mL $min^{-1}$) in the range of 25ºC-500ºC with a heating rate of 10 ºC $min^{-1}$.

**Instrument used**

Sta 449 F3 System Connected To Qms 403 Aëolos (Netzsch).

## 2.5 References


(1) Li, K.; Wang, B.; Su, D.; Park, J.; Ahn, H.; Wang, G. Enhance Electrochemical Performance of Lithium Sulfur Battery through a Solution-Based Processing Technique. *J. Power Sources* **2012**, *202*, 389–393.

(2) Wang, D.-W.; Zeng, Q.; Zhou, G.; Yin, L.; Li, F.; Cheng, H.-M.; Gentle, I. R.; Lu, G. Q. M. Carbon-Sulfur Composites for Li-S Batteries: Status and Prospects. *J. Mater. Chem. A* **2013**, *1*, 9382–9394.

(3) Stephan, A. M. Review on Gel Polymer Electrolytes for Lithium Batteries. *Eur. Polym. J.* **2006**, *42*, 21–42.

(4) Stoller, M. D.; Stoller, S. A.; Quarles, N.; Suk, J. W.; Murali, S.; Zhu, Y.; Zhu, X.; Ruoff, R. S. Using Coin Cells for Ultracapacitor Electrode Material Testing. *J. Appl. Electrochem.* **2011**, *41*, 681–686.

(5) Bard, A. J.; Faulkner, L. R. ELECTROCHEMICAL METHODS Fundamentals and Applications-2nd Ed. *JOHN WILEY SONS, INC.* **2001**, 3–7.

(6) Kremer, F.; Schönhals, A. Broadband Dielectric Spectroscopy. **2003**, 64.

(7) Bondarchuk, O.; Morel, A.; Bélanger, D.; Goikolea, E.; Brousse, T.; Mysyk, R. Thin Films of Pure Vanadium Nitride: Evidence for Anomalous Non-Faradaic Capacitance. *J. Power Sources* **2016**, *324*, 439–446.

(8) Lee, J. T.; Nitta, N.; Benson, J.; Magasinski, A.; Fuller, T. F.; Yushin, G. Comparative Study of the Solid Electrolyte Interphase on Graphite in Full Li-Ion Battery Cells Using X-Ray Photoelectron Spectroscopy, Secondary Ion Mass Spectrometry, and Electron Microscopy. *Carbon N. Y.* **2013**, *52*, 388–397.

(9) John F. Moulder, William F. Stickle, Peter E. Sobol, K. D. B. Handbook of X-Ray Photoelectron Spectroscopy. **1992**, 1–261.

(10) Pike Technologies. APPLICATION NOTE ATR – Theory and Applications. *Pike Technol.* **2014**, 1–3.

(11) Gardiner, D. J.; Graves, P. R.; Bowley, H. J. Practical Raman Spectroscopy. **1989**, 157.

(12) Ru, E. C. Le; Etchegoin, P. G. Principles of Surface-Enhanced Raman Spectroscopy and Related Plasmonic Effects. *Elsevier Ltd* **2009**, 1–656.

(13) Lombardi, J. R.; Birke, R. L.; Lu, T.; Xu, J. Charge-Transfer Theory of Surface Enhanced Raman Spectroscopy: Herzberg–Teller Contributions. *J. Chem. Phys.* **1986**, *84*, 4174–4180.

(14) Keresztury, G. Raman Spectroscopy : Theory. *Handb. Vib. Spectrosc.* **2006**, 71–87.

(15) Patel, M. U. M.; Dominko, R. Application of in Operando UV/Vis Spectroscopy in Lithium-Sulfur Batteries. *ChemSusChem* **2014**, *7*, 2167–2175.

# *Chapter 3: Protective layers for lithium anode in Li-S batteries.*

# 3 Introduction: Lithium Metal Anode

Li metal anodes has always been a subject of interest owing to its high specific capacity of 3862 mAh $g^{-1}$ and lowest electrochemical potential (-3.04V vs SHE) compared to other Li-based anodes.[1] High reactivity and formation of dendrites during cycling leading to a main concern for safety. Major problems with Li-anode are linked to the reactivity by both electrolyte solution and the soluble polysulphides. There have been several efforts to overcome the drawbacks by encapsulation of the sulphur particles within carbon nanomaterials, using different electrolytic solvents.[2,3] Although slight improvements were observed, the capacity fades due to active material utilisation and passivated Li gives a solemn problem. The effective solution to avoid such complications is isolation between highly reactive metallic Li-anode from organic liquid electrolyte and dissolved polysulphides species. Solid electrolyte interphase (SEI) layer could play a role of adequate passivation layer between the Li-foil surface and electrolyte which could inhibit the dendrite growth.[4]

Widespread research suggested that the performance of a battery including cyclability, safety and exfoliation of the scruffy lithium are completely reliant on the features of the SEI layer.[5–8] The passivation effects are dependent of the homogeneity of SEI.[1] Dendrite formation arise from instability of the passivation layer (SEI layer) on the metallic lithium anode.[1,9] The unstable SEI cannot accommodate the shape and volume changes of the lithium electrode during cycling, leading to non-uniform lithium deposition and dissolution, resulting in formation of lithium dendrites.[1] Moreover, the breakdown of the SEI layer could result in the exposure of the fresh Li-anode surface to the electrolyte and parasitic reactions to form a new SEI layer, which decrease the lithium cycling efficiency.[1] Consequently, conservation of a stable passivation layer is quite difficult,

however the degradation of the metallic lithium anode is even worse in Li−S batteries.[10–12] During shuttle effect, polysulphide travel through the separator within electrolyte towards Li-anode resulting $Li_2S_2$/$Li_2S$ deposition on Li-anode surface.[13,14] The deposit of $Li_2S_2$/$Li_2S$ is of insulating nature, which complicate the reversible reaction of Li-polysulphides ($Li_2S_x$) resulting in subsequent loss of active mass.[15] Additionally, $Li_2S_2$/$Li_2S$ insulating deposit hinder the fast diffusion of $Li^+$ followed by poor rate capability and cycling performance.[10]

## 3.1 Protection of Li-anode

The morphology and chemical composition of the passivation layer on the lithium surface are greatly influenced by the electrolyte solvents and lithium salts.[16] For example, 1,4-Dioxane (Diox) is one of the most regularly used electrolyte solvents in Li−S batteries.[17] During the discharge/charge electrochemical process, Diox is reduced to several ROLi (R refers to alkyl) species and oligomers with −OLi edge groups, enhancing the flexibility of the passivation layer on the lithium surface, which assists the passivation layer's ability to accommodate lithium morphological changes upon cycling.[16]

Recently, Ionic Liquids (ILs) as a favourable new class of electrolyte solvents for Li−S batteries have been considered. An IL-enhanced passivation layer on the lithium surface is found to exhibit a smoother morphology and less complicated surface chemistry compared to that formed with the conventional organic electrolytes.[18] Lithium metal was reported to be protected from the continuous attack of polysulphides with an N-methyl-N-butylpyrrolidinium bis- ((trifluoromethyl)sulphonyl)imide ($Py_{14}$TFSI)-modified passivation layer, leading to improved Coulombic efficiency and cycling stability.[18] In terms of lithium salts, lithium trifluoromethanesulphonate ($LiCF_3SO_3$) and LiTFSI used in Li−S batteries have high dissociation constants, high oxidation and temperature

stability, nontoxicity, and insensitivity to moisture. Unfortunately, they seem to have no obvious positive effect on the passivation layer that forms on the lithium metal surface.[1]

## 3.2 Additives in liquid electrolytes for passivation layer:

Numerous attempts have been taken to improve the homogeneity of the SEI, including fabrication of protective films via additives in electrolyte,[1] i.e. $LiNO_3$,[19–22] carbonate,[23,24] etc. Mikhaylik[25,26] patented an oxidizing additive named lithium nitrite ($LiNO_3$), it has been introduced in the electrolytes to form an in situ protective layer on the Li-anode surface to stabilize the Li-anode.[26] Aurbach et al.[11] thoroughly studied the effect of $LiNO_3$ on the Li surface through electrochemical characterization, Fourier transform infrared (FTIR) spectroscopy and XPS analyses. $LiNO_3$ was identified to suppress polysulphide shuttling because of its direct reduction by lithium to $Li_xNO_y$ species and its oxidation of sulphur species to $Li_xSO_y$ moieties, passivating the lithium anode surface and alleviating parasitic reactions between lithium and sulphur species.[11] Nonetheless, it was concluded that achievement of homogenous passivation between Li-anode and electrolyte is quite difficult.[16,27,28]

Zhang, recently explained the function of $LiNO_3$ on the sulphur cathode by addition of insoluble Mg $(NO_3)_2 6H_2O$ as cathode additive in Li-S batteries. Further to confirmation of supressing effects of $LiNO_3$ towards redox shuttle, $NO_3^-$ anions are skilled of catalysing the reversible reaction of solubilised polysulphides ($Li_2Sx$) to insoluble elemental sulphur ($S_8$). Soluble nitrate within the electrolyte and insoluble nitrate in cathode combination directs the synergetic enhancement on the cycling of the Li-S batteries. Electrochemical studies in Li-S batteries with electrolyte containing $LiNO_3$, proposed involvement of $NO_3$ radical catalysis that instantaneously oxidize the dissolved $Li_2Sx$ species in electrolyte in to insoluble $S_8$.[21]

However, it is worth mentioning that $LiNO_3$ is progressively consumed with the development of new lithium dendrites and the formation of a new passivation layer during Li−S cell operation, which limits its ability to stabilize the lithium surface for long-term cycling or in a polysulphide-rich environment. Additionally, $LiNO_3$ reduce at potential lower than 1.6V at the cathode, which negatively impacts the cycle stability of Li−S batteries.[19,29]

An alternative to $LiNO_3$, lithium bisoxalatoborate (LiBOB), was identified to modify the passivation layer on the lithium surface in Li−S batteries.[30] Higher discharge capacity and smoother lithium surface morphology were obtained in the presence of LiBOB in the electrolyte.[30–32] Finally, phosphorus pentasulphide ($P_2S_5$) disclosed by Lin et al.[33] facilitates formation of highly $Li^+$ conductive level and thick passivating layer on the Li-anode, avoiding the deposition of insoluble $Li_2S_2/Li_2S$.[33] The deposition is avoided due to the fact that $P_2S_5$ reacts with polysulphides ($1<x<8$). The formation of soluble complexes occurs which transforms the least soluble $Li_2S_2/Li_2S$ species in to most soluble complexes.[33]

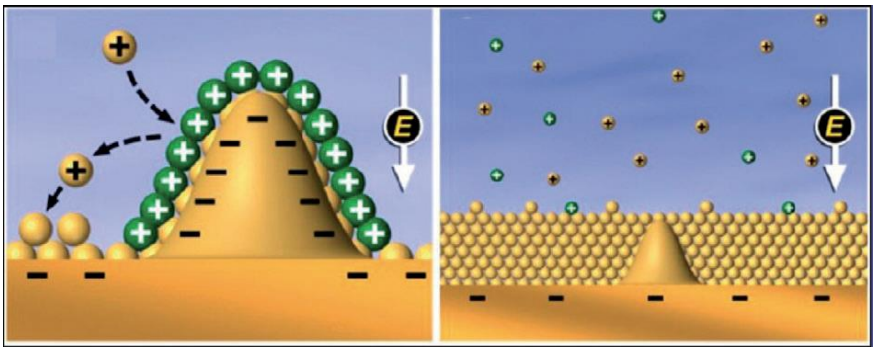


**Figure 3.1: Schematic explanation of the self-healing electrostatic shield mechanism of the Li deposition process. [34]**

Zhang et al. projected that by introducing the certain cations (i.e. $Ce^+$ or $Ru^+$) with lower reduction potential than of $Li^+$ in the electrolytes, the morphology of Li deposition can be tuned from needle like dendrites to mirror-like films (Figure 3.1). The phenomenon is

called as self-healing electrostatic shield mechanism for controlling the Li dendrites growth behaviour.[34]

## 3.3 Solid protection layer: Modification of the Lithium Anode

Solid polymer electrolytes have been used as protection for Li-anode due to their high $Li^+$ conductivity. The protective layer has been fabricated by cross-linking of the PEG-DMA (poly (ethylene glycol) dimethacrylate) in liquid electrolyte ($LiClO_4$ in TEGDME) and MBF (methylbenzoylformate) photoinitiator. Improvements have been observed with this protective layer when compared to non-protected Li-anode. The Li-anode with protection displayed a slicker and denser surface morphology after $50^{th}$ cycle [35]. As an alternative method, sulphur powder has been casted on Li-anode for the purpose of protection.[36] Surprisingly, the lower amount of polysulphides ($Li_2S_x$) and $Li_2S$ on the surface of Li-anode were observed with improved properties as compared to non-protected one.[36]

The reliability of the lithium metal anode depends significantly on the stability of its passivation layer, which could be improved by changing the electrolyte solvents and introducing additives. Despite the vast advances accumulated for metallic Li-anode protection; especially in Li−S batteries, ample control including stability, robustness of Li-anode surface upon cycling has not been achieved yet which hinders the Li−S batteries commercialization.

Discovering the appropriate and best surface protection for the Li-anode is proved to be difficult, particularly when the requirements are high rate capability and capacity, simultaneously. Therefore, another approach is to introduce a pre-formed Li-ion conductive layer on anode. This layer will provide the protection of Li-anode, as well as due to permeability for $Li^+$; it permits fast transmission of $Li^+$ in the electrical field. The protection layer could be employed on Li-anode pre-formed by using materials with high

$Li^+$ conductivity i.e. lithium-nitrogenous compound, before assembling the batteries or in situ during the operation of the batteries, through modifying the Li-anode.

Hence, in this chapter the lithium nitride ($Li_3N$) as the protective layer for Li-anode has been proposed to overcome problems of metallic Li-anode in Li-S systems. $Li_3N$ was mainly studied as a solid electrolyte in Li-ion batteries.[37–39] $Li_3N$ has exceptionally fast ionic conduction, but its decomposition voltage is very low (0.44 V). Therefore, it cannot be used as anode material directly.[40] Owing to its high ionic conductivity (~ $10^{-3}$ S $cm^{-1}$) that doesn't hinder the migration of $Li^+$ ions,[41,42] as well as prevents the parasitic side reaction between Li-anode and electrolyte, by providing a stable SEI layer.[43] Thus, not only any connection among Li-polysulphides (i.e. $Li_2S_x$, $3 \leq x \leq 8$) and the metallic Li-anode will be stopped suppressing unsought corrosive reaction, but also Li-polysulphides can migrate back towards cathode and their reutilization are possible as shown in schematic Figure 3.2.

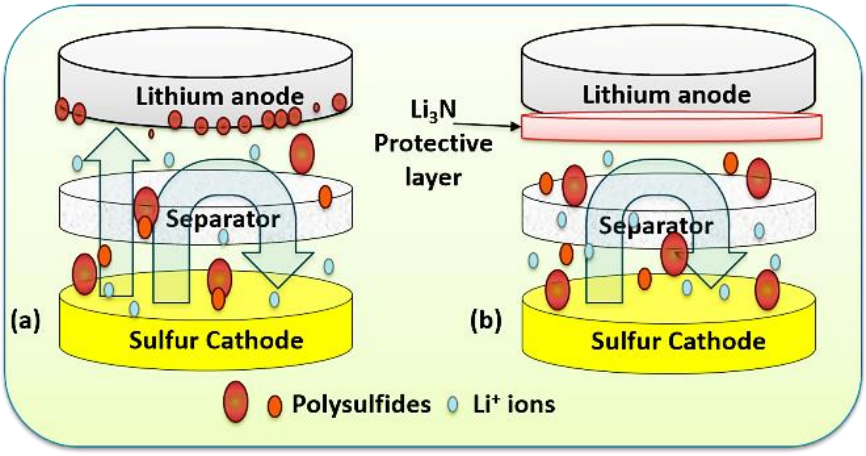


**Figure 3.2: Schemtaic diagram of Li-S cell (a) without the protective layer (b) with $Li_3N$ protective layer.**

This approach additionally inhibits the capacity fading and the improved cycling performance is therefore realized. Furthermore, the growth of Li dendrites because of non-uniform Li can be blocked by $Li_3N$ layer, assuring the safety of the battery.[26,33,34,41,44]

$Li_3N$ layer was employed by different approaches including preformed layers with and without binder and likewise by addition of an additive in the electrolyte to achieve *in-situ* formation of $Li_3N$ layer.

As the schematic of the cell configuration depicts the aim of this work, to know the effect of using $Li_3N$ as a protective layer for Li metal anodes in Li sulphur batteries without using any additional film forming additives like $LiNO_3$. The powder composite cathodes have been used throughout the study, in order to isolate the role of $Li_3N$ as a protective layer in these battery systems and avoid any additional binder effect.

## 3.4 Experimentation

### *3.4.1 $Li_3N$ layer -fabrication methods:*

The Lithium nitride layer to be used as a physical barrier or protective layer on the surface of the Li-foil was fabricated using ex-situ and in-situ techniques. The different ex and *in-situ* techniques employed were:

### 3.4.1.1 $Li_3N$ layer without binder:

- $Li_3N$ pellets

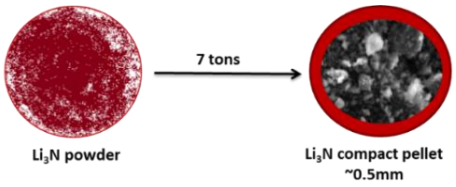


Pellets of lithium nitride were prepared by using pellet die of 10mm. ~3mg of $Li_3N$ (commercial powder) was filled into the cylinder of die cast and 7 tons of pressure under argon atmosphere has been applied, in order to obtain a compact pellet of ~1mm in thickness.

- $Li_3N$ by nitridation technique

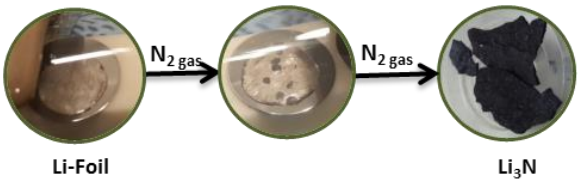


A sealed assembly chamber (Figure 3.3) was designed in order to regulate the conditions for nitridation process.[45] The process starts when $N_2$ gas approaches towards Li-foil, and upon contact the reaction of Li and $N_2$ occurs:

$$6Li + N_2 \rightarrow 2Li_3N$$

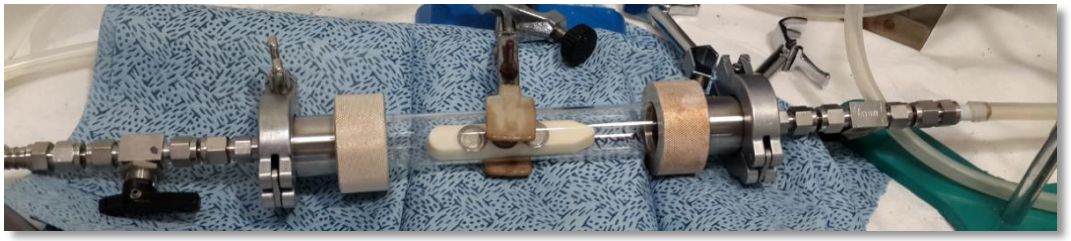

**Figure 3.3: Sealed assembly designed for nitridation.**

In a glovebox under argon atmosphere ($O_2$ and $H_2O$ < 1 ppm), cleaned Li-foil with the thickness of 400 µm was placed in the assembly chamber, it was sealed and taken out of the glovebox. Before starting the reaction, the assembly chamber was flushed with vacuum, following high purity $N_2$ gas flow for 16 h at 25°C. Nitridated Li-foil has been collected as brittle black film of ~300µm. The structure of nitridated Li-foil was confirmed by X-ray diffraction (XRD).

#### 3.4.1.2 $Li_3N$ layer with polymeric binder:

- $Li_3N$/ binder mixed drop coated layers:

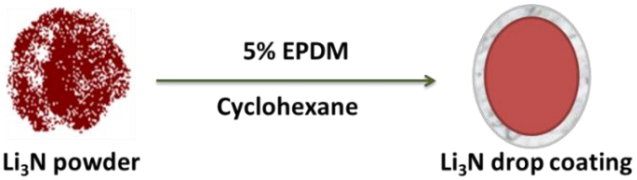


$Li_3N$ was mixed with an EPDM binder by adding a 95:5 wt. % of $Li_3N$: EPDM in 5mL cyclohexane upon stirring. Resulting thick slurry was deposited (thickness~90-150µm) on the surface of cleaned Li-foil by drop-casting method under argon atmosphere inside the glovebox ($O_2$ and $H_2O$ < 1 ppm).

- Nitridated $Li_3N$ pellet:

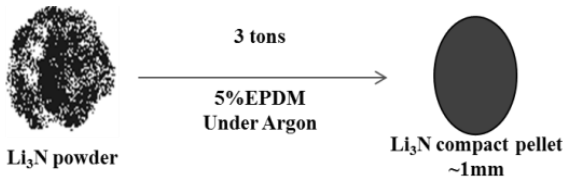

Nitridated $Li_3N$ was grinded and mixed with EPDM binder by adding a 95:5 wt. % in 5mL cyclohexane upon stirring. Resulting slurry was dried inside glovebox under argon and collected powder was compressed into shape of a pellet by using pellet die of 10mm. 7 tons of pressure under argon atmosphere has been applied, the obtained compact pellet was of ~500µm in thickness.

- Nitridated $Li_3N$ deposit:

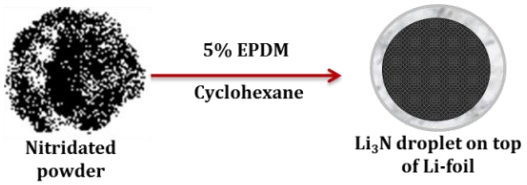


Nitridated $Li_3N$ slurry prepared with EPDM binder as 95:5 wt. % in 5mL cyclohexane was drop-coated on the surface of cleaned Li-foil to obtain the $Li_3N$ layer of ~50-85µm in thickness.

### 3.4.1.3 $Li_3N$ layer formation by additive:

- In-situ $Li_3N$ formation:

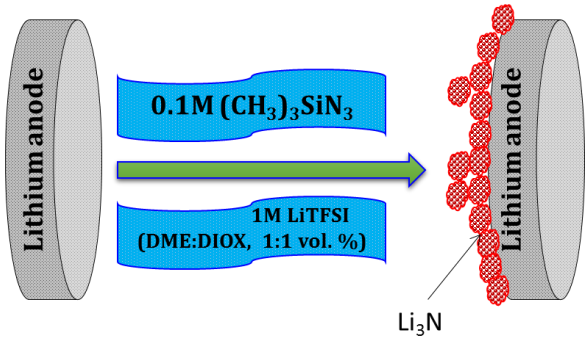


Azido trimethyl silane (sigma Aldrich) was used as an electrolyte additive. Electrolytes with DME: Diox +1M LiTFSI +x moles (x=0.01and 0.1) of additive were prepared. Additional approach was to directly coat Li-foil surface with silane solution for faster reaction. After cleaning the surface of the Li-foil, Azido trimethyl silane was used for the coating method. After covering the sample completely on one side with azide solution, they were allowed to dry inside the glovebox for 10 mins.

### *3.4.2 Cathode preparation, cell assembly, physico-chemical and electrochemical characterization:*

The powder composite cathodes have been used to investigate the role of $Li_3N$ protective layer on the surface of Li-anode. The preparation of cathode composite, information regarding physico-chemical and electrochemical characterization techniques and electrochemical cell assembly can be seen in *Chapter2: Section 2.3.*

## 3.5 Results and discussion:

Different ex-situ techniques were employed to have a protective $Li_3N$ layer on the Li-foil, compressed pellets of $Li_3N$ were directly pressed onto the lithium foil as a physical barrier

whereas in the case of binder mixed $Li_3N$, a uniform layer was casted onto the Li-foil. The nitridated Li-foil was placed on an additional freshly cleaned Li-foil.

### *3.5.1 $Li_3N$ layer without binder:*

- $Li_3N$ pellet

Figure 3.4 shows the comparative discharge capacity of the cells with and without protective layers.

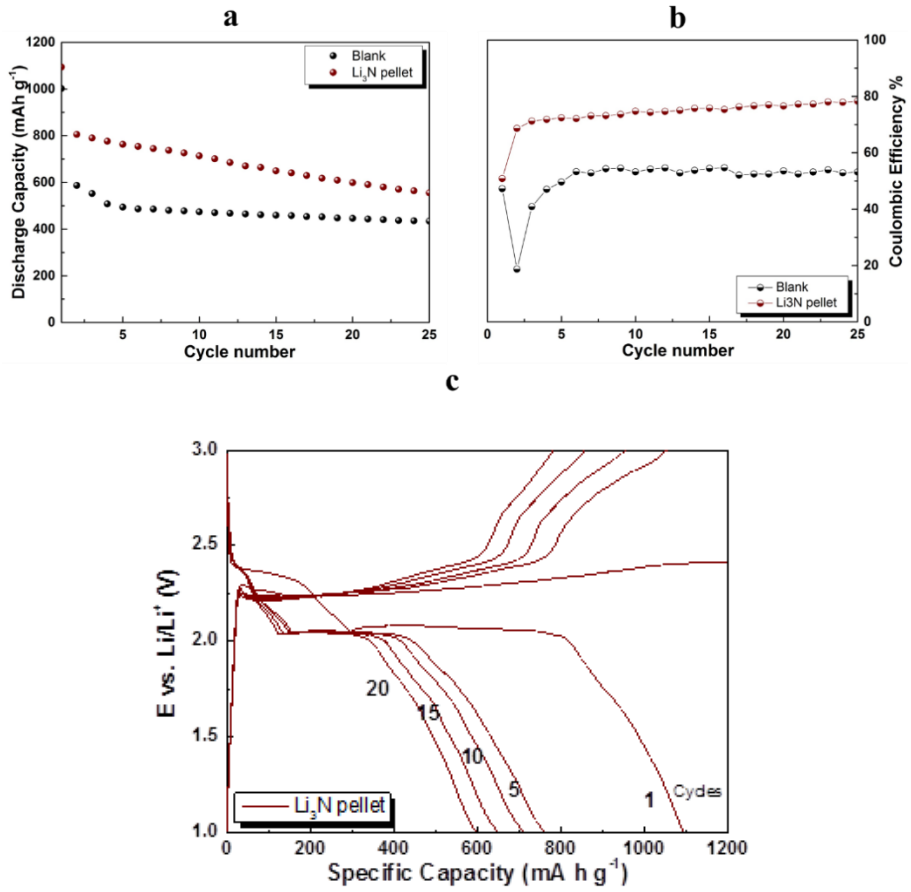


**Figure 3.4: a) Comparative study of galvanostatic cycling with and without $Li_3N$ pellet at C/20, b) Coulombic efficiency %, c) $Li_3N$ pellet discharge/charge voltage profile vs. specific capacity.**

As observed, the $Li_3N$ protective layers in a pellet form showed a higher initial discharge capacity of 1094 mAh $g^{-1}$ compared to the one without protective layer (1004 mAh $g^{-1}$). Capacity degradation was observed before and after 10 cycles, cells with $Li_3N$ protective

layers showed discharge capacity of 716 mAh $g^{-1}$, while the one without protective layer showed 457mAh $g^{-1}$.

However the fade in capacity observed upon cycling with the $Li_3N$ as pellet can be linked to the higher thickness of the pellet. Consequently, the interfacial contacts between protective pellet and Li-foil are weakened, that could contribute to the increased internal resistance of the cell and secondly due to the porosity of the pellet that could also allow the passage of polysulphides towards the Li-anode.

- $Li_3N$ by Nitridation technique

For fabrication of thinner pellets, in order to know the contribution of thickness without a binder was not successful due to the mechanical integrity of the pellets. Hence, in order to obtain pre-formed thinner $Li_3N$ protective layer on the Li-foil surface, ex-situ nitridation was carried out.[43,46] Due to the nitridation taking place on the surface of the Li in an inhomogeneous manner, slightly longer duration had to be maintained to nitridate the entire surface. This resulted in the nitridated layer being formed along the whole depth of the Li foil. Therefore, the Li-foil fully converted into brittle $Li_3N$ film. The XRD pattern of nitridated $Li_3N$ under argon is shown in figure 3.5. The diffraction peaks of XRD pattern can be correlated to pure $Li_3N$ formation when compared to standard JCPDS data.

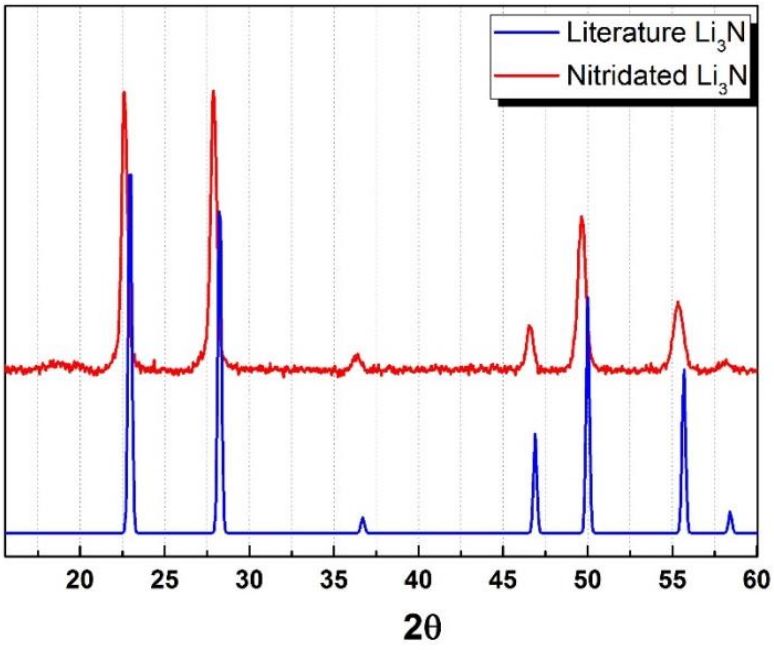


**Figure 3.5: XRD diffractogram of $Li_3N$ formed by nitridation technique compared with standard JCPDS data for $Li_3N$.**[47]

Galvanostatic cycling of nitridated Li-foil alone doesn't show any activity at all. An extra Li-foil has been placed with $Li_3N$ film, which shows an initial discharge capacity of 820 mAh $g^{-1}$ with almost 100% columbic efficiency compared to blank. After 15 cycles, rapid capacity degradation (438 mAh $g^{-1}$) was observed (Figure 3.6), followed by a decrease in the coulombic efficiency (64 %). This was quite expected owing to the brittle nature of the nitridated Li-foil thereby leading to increase in the resistance of the interfacial layer with loss of contacts. The voltage profile clearly indicates the operation of the Li-S cells with its characteristics plateaus at 2.4 and 2.1V and after 15 cycles only slope is observed. Therefore, in order to make the nitridated $Li_3N$ layer more mechanically stable they were ad-mixed with EPDM binder and tested.

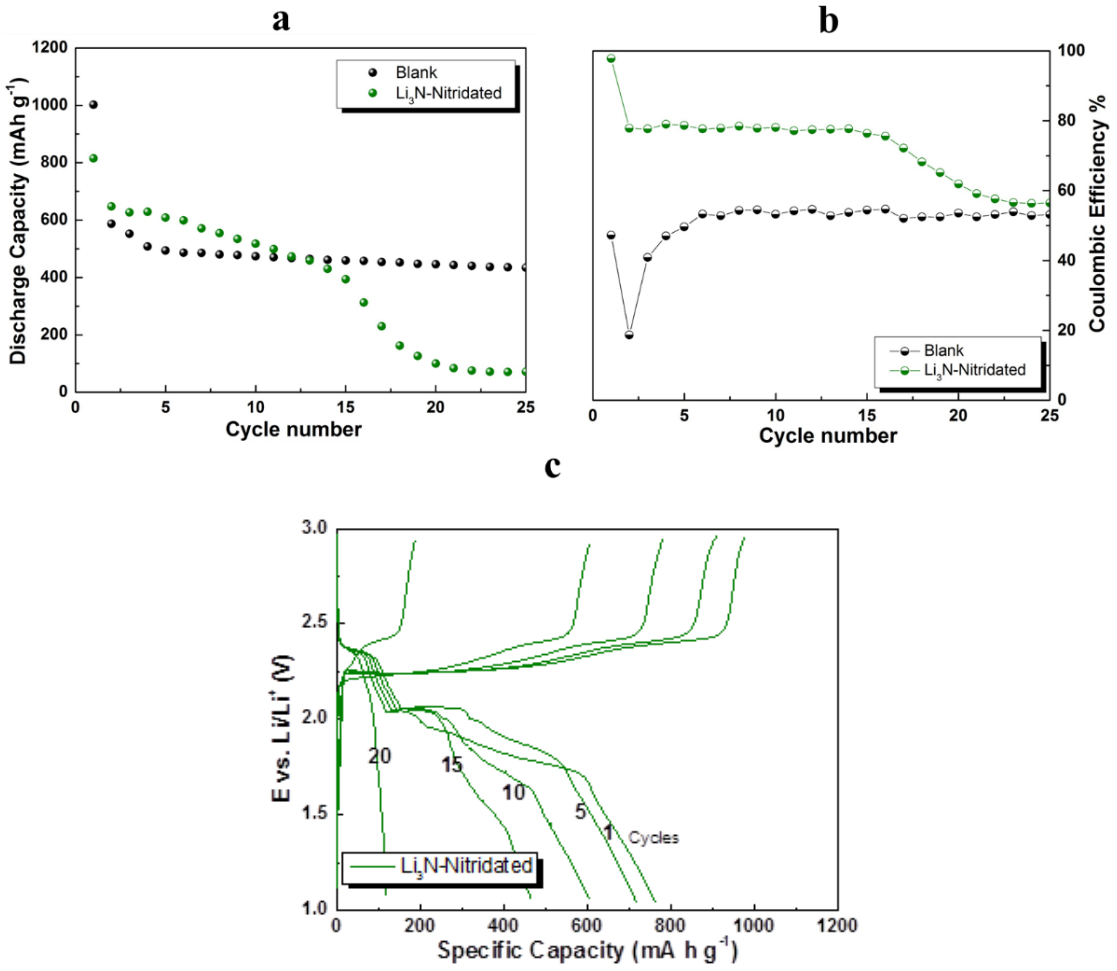


**Figure 3.6: a) Comparative study of galvanostatic cycling with and without nitridated $Li_3N$ at C/20, b) Coulombic efficiency %, c) Nitridated $Li_3N$ discharge/charge voltage profile vs. specific capacity.**

## *3.5.2 $Li_3N$ layer with polymeric binder:*

- $Li_3N$/ binder mixed drop coated layers

Prior results shifted our focus to the EPDM binder coated $Li_3N$ layers, in order to have effective covering of the surface of the Li and also the possibility to achieve thinner layers of $Li_3N$. The SEM analysis has been employed to observe the $Li_3N$ binder mixed coating before cycling (Figure 3.7a). The deposit shows a very good coverage of Li-foil surface. XRD diffraction pattern has been collected to identify the effects of EPDM binder. Comparison with EPDM binder (commercial) and initial $Li_3N$ powder (commercial) is

shown in figure 3.7b, that indicated the absence of any reaction of the EPDM binder on the Li.

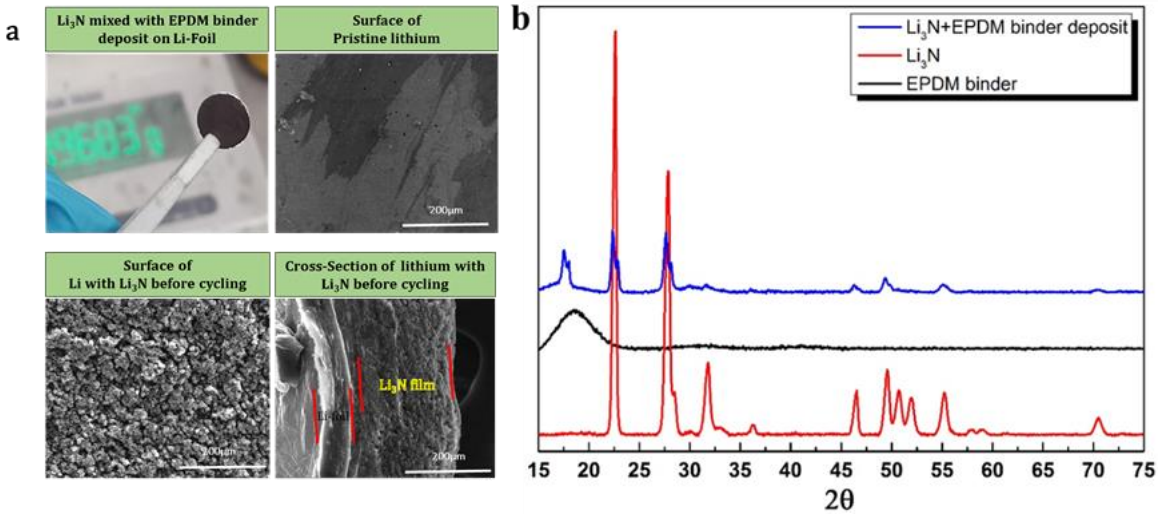


**Figure 3.7: a) Image and SEM morphology is shown for surface of pristine and $Li_3N$ layer, last figure shows the cross section of the layer with Li-foil, b) XRD graph comparing EPDM, $Li_3N$ commercial and $Li_3N$ mixture with EPDM.**

Figure 3.8 represents discharge capacity of the cell with $Li_3N$ protective layer with polymeric binder compared to without protective layers. The $Li_3N$ protective layers showed a stable discharge capacity ~400 mAh $g^{-1}$ when compared to the one without protective layer having a capacity of ~457 mAh $g^{-1}$. Although the discharge capacity was slightly less, the effect of the protective layer was clearly seen with the improvement in the coulombic efficiency to 87% after 25 cycles.

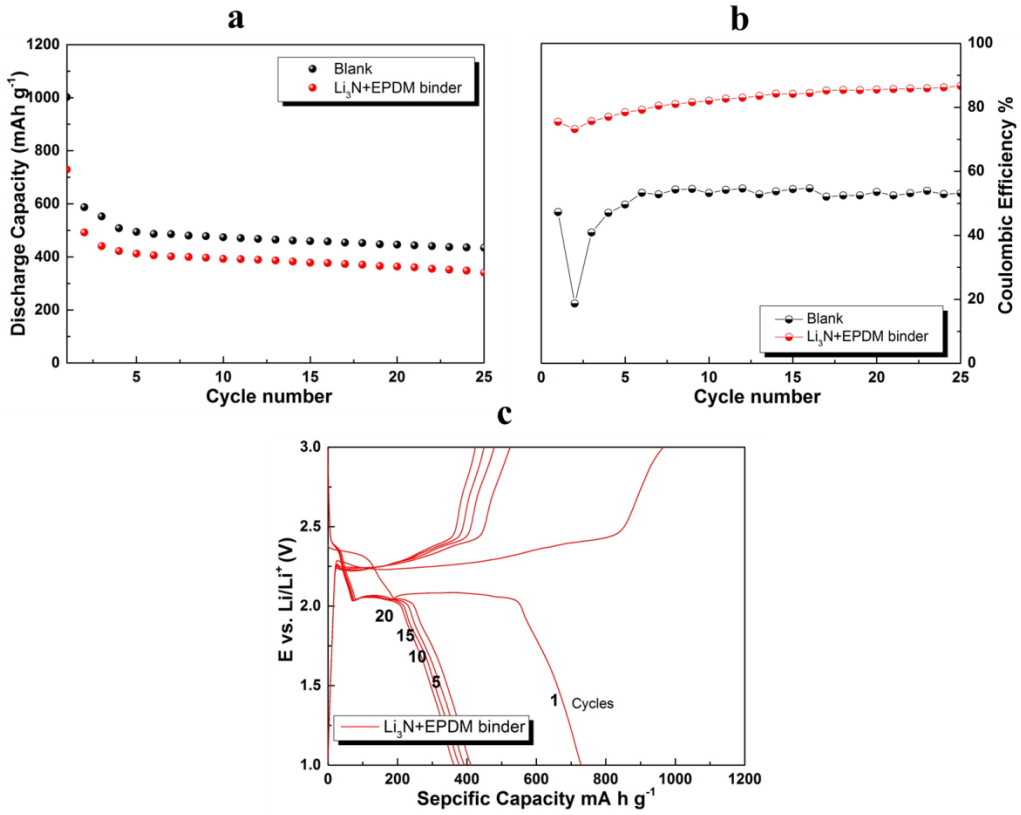


**Figure 3.8: a) Comparative study of galvanostatic cycling with and without $Li_3N$and EPDM binder deposit at C/20, b) Coulombic efficiency %, c) Deposited $Li_3N$ discharge/charge voltage profile vs. specific capacity.**

- Nitridated $Li_3N$ pellet:

Owed to the brittle nature of nitridated film, full protection of Li-anode was not achieved (Figure 3.6) . Thus a composite compact pellet of nitridated powder and EPDM binder was used as a protective layer. Figure 3.9 shows the discharge capacity of nitridated pellet protective layer with binder in comparison to Li without protective layer. A low initial discharge capacity of 723 mAh $g^{-1}$ was observed compared to the cell without protective layer (1004 mAh $g^{-1}$). In comparison to nitridated film without binder, the capacity drop was more stable, this could link to the slightly better interfacial contacts achieved between protective pellet and Li-foil and better masking of Li-anode surface due to the EPDM

binder. Meanwhile noticeable high stable coulombic efficiency of ~88% was achieved in the cell with nitridaed $Li_3N$ protective layer pellets with binders.

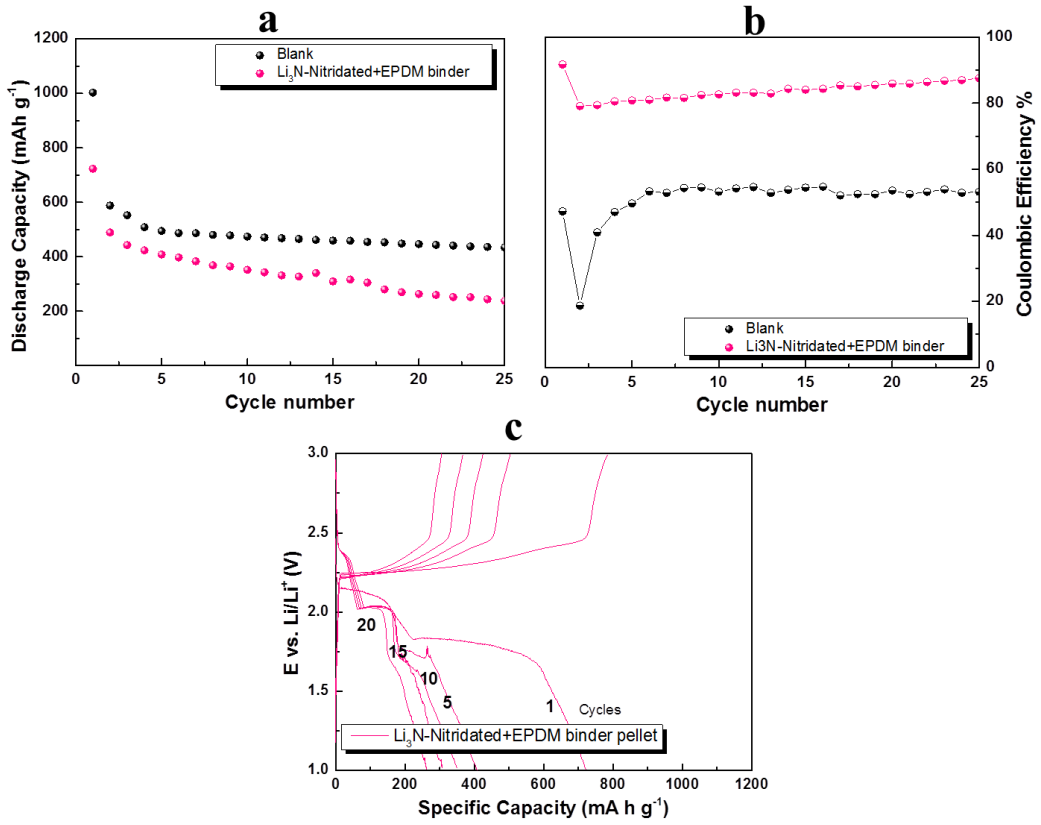


**Figure 3.9: a) Comparative study of galvanostatic cycling with and without nitridated $Li_3N$ with EPDM binder deposit at C/20, b) Coulombic efficiency %, c) nitridated $Li_3N$ deposit discharge/charge voltage profile vs. specific capacity.**

- Nitridated $Li_3N$ deposit by drop coating:

Drop-coating of $Li_3N$ (Nitridated) with EPDM slurry, helps to reduce the thickness of the protective layers (90-150µm) and as well as improve interfacial contacts. Figure 3.10 shows the discharge capacity of 611mAh $g^{-1}$ and coulombic efficiency of ~87.5% for $Li_3N$ protective layer as compared to the one without protective layer (~55%). The protective layer fabricated by using synthetic nitridated $Li_3N$ by nitridation process, edges over the commercial $Li_3N$ mixture, probably by the virtue of higher purity that could be achieved

by using high purity nitrogen gas ($N_2$) during the reaction or due to the morphology of the $Li_3N$ particles formed during nitridation enabling more compactness of the layer. [47,48]

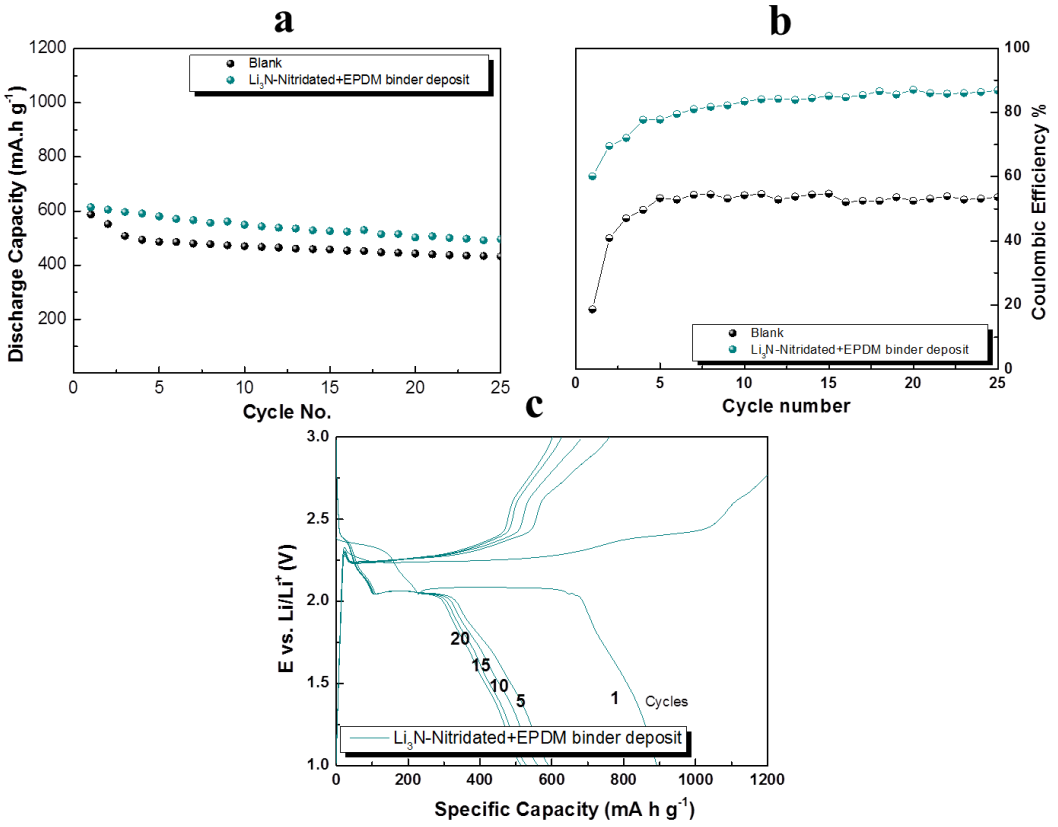


**Figure 3.10: a) Comparative study of galvanostatic cycling with and without $Li_3N$and EPDM binder deposit at C/20, b) Coulombic efficiency %, c) Nitridated $Li_3N$ discharge/charge voltage profile vs. specific capacity.**

Even though, nitridated mixture protective layer shows comparative improvement in results, nevertheless, the process of ex-situ nitridation technique is time consuming and costly. Therefore, further studies in this chapter have been carried out by utilising commercially available $Li_3N$ mixtures.

### *3.5.3 Rate capability:*

In order to understand electrochemical behaviour of $Li_3N$ protective layer within the Li-S systems, the cells usually has been cycled at slower C-rates. Nonetheless, as mentioned

by Linda Nazar et. al[49] , the performance at higher rate is difficult to accomplish due to favoured fast diffusion that lead to huge dissolution of intermediate species into the electrolyte. In this regard, cells with and without $Li_3N$ protective layer have been cycled at a faster rate (C/5) as shown in figure 3.11. In the case of cells without protective layer, the initial discharge capacity was similar at C/20 and C/5 of 1022 mAh $g^{-1}$ and 915 mAh $g^{-1}$, respectively (Figure 3.11a). However upon cycling the cell at C/5 rate shows less capacity degradation with higher discharge capacity. In figure 3.11b, the $Li_3N$ protective pellet however shows better cycling at C/20 (880 mAh $g^{-1}$), meanwhile cycling over C/5, the capacity was almost half (800 mAh $g^{-1}$).

A similar behaviour as $Li_3N$ pellet was observed for $Li_3N$ EPDM deposit at faster C/5, even though the initial discharge capacity was higher (1144 mAh $g^{-1}$) in comparison to C/20 (922 mAh $g^{-1}$), the descent after 3$^{rd}$ cycle shows almost 50% of the capacity degradation(Figure 3.11c).

Surprisingly in figure 3.11d, a similar behaviour of deposited $Li_3N$ (nitridated) protective layer has been observed. Even though, initial discharge capacity was higher at C/5 (1147 mAh $g^{-1}$) but after 5$^{th}$ cycle, the capacity retention was relatively similar.

No dramatic capacity reduction has been seen. This could be attributed to the lower resistance offered by the layers with EPDM binders on the Li anode. The better performance of the nitridated samples could be attributed to the lower grain boundary resistance or due to more compactness between the particles of $Li_3N$ achieved with nitridated samples.

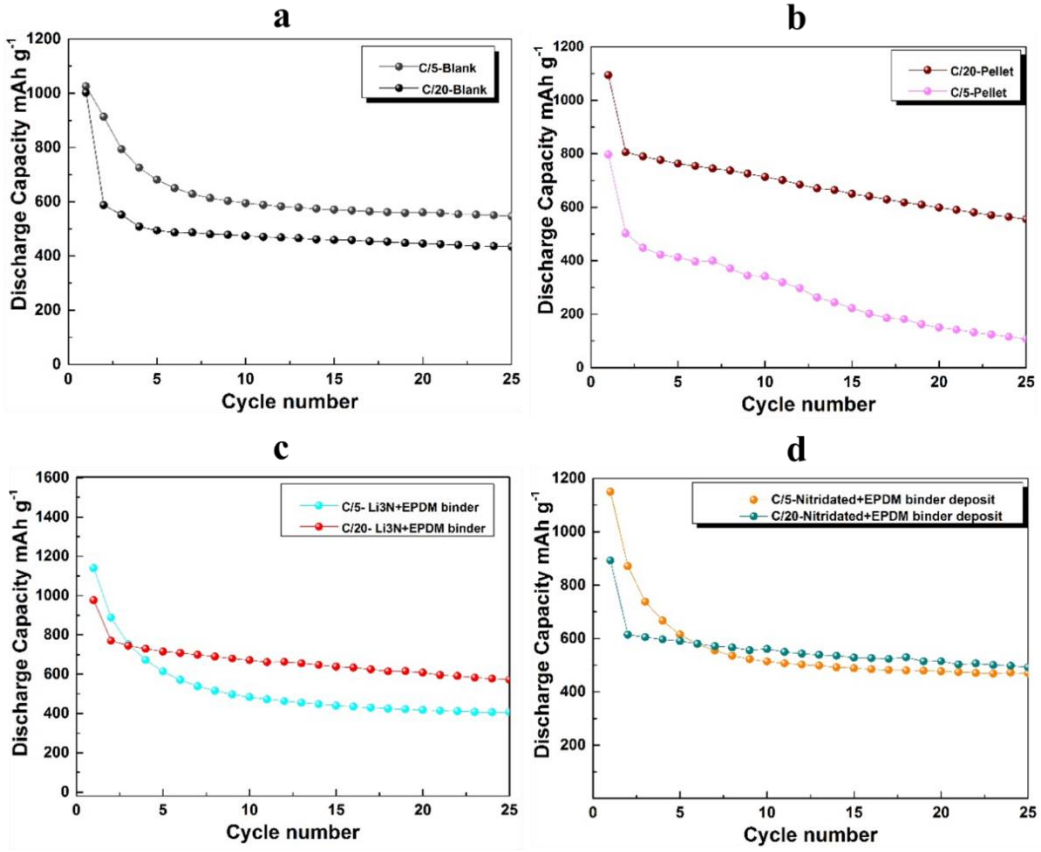


**Figure 3.11: Galvanostatic cycling comparison at similar condition over the C-rate of C/20 and C/5, a) Blank cells, b) $Li_3N$ pellet, c) $Li_3N$ with EPDM binder deposit, d) Nitridated $Li_3N$ with EPDM binder deposit.**

## *3.5.4 CV and Impedance studies: with and without protective layer*

Figure 3.12 (a-c) shows the lithium plating/stripping characteristics of symmetric Li/Li cells with $Li_3N$ pellet, binder mixed and blank cells. As seen from the figure, all three configurations of the cells exhibited good lithium plating and stripping characteristics. Impedance taken before and after Li plating/stripping for 5 cycles indicated low resistance values for the unprotected Li with increased resistance for $Li_3N$ cells whereas the cells with binder mixed protective had an optimum resistance value. After CV cycles a decrease in resistance was observed in the case of unprotected Li and cells with $Li_3N$ binder mixed whereas $Li_3N$ pellets did not show a prominent decrease indicating that

better interfacial contact was achieved with the polymer binder mixed coating on the Li metal anodes than with $Li_3N$ as pellet. Firstly, due to poor interfacial contact between the $Li_3N$ pellet and Li-anode and secondly due to the grain boundary resistance of the $Li_3N$ particles in the pellet.

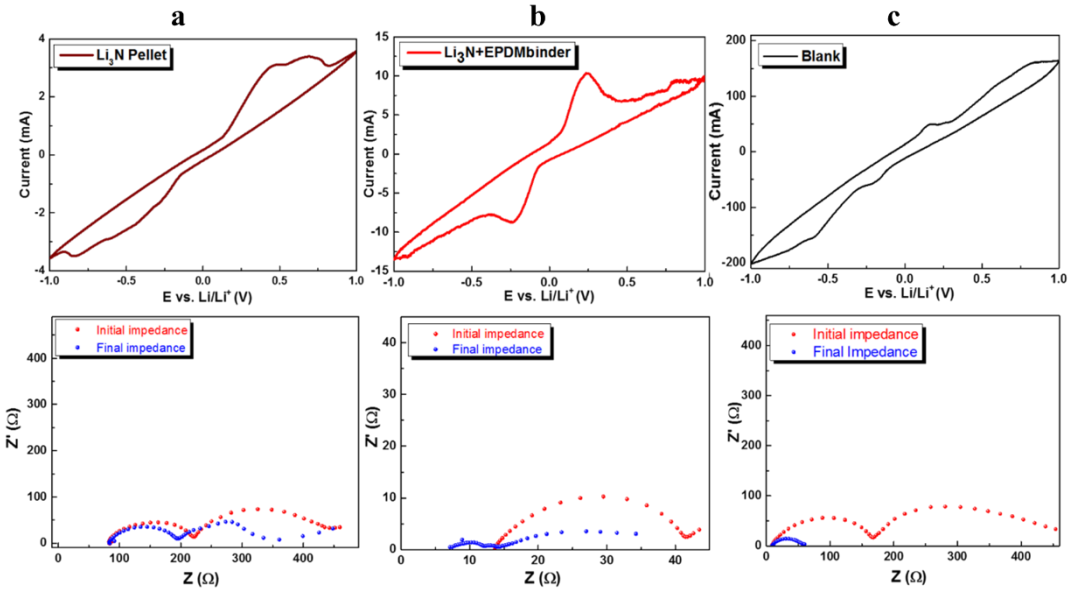


**Figure 3.12: Cyclic voltammetry of the symmetric cell at the scan rate of 0.5mVs$^{-1}$ and EIS measurements before and after CV, a) $Li_3N$ pellet, b) $Li_3N$ with EPDM binder deposit, c) Blank.**

A comparison of cyclic voltammograms of Li/ S cells cycled with binder mixed $Li_3N$ coated layer and a blank cell is shown in figure 3.13. Cells with protective layers showed prominent peaks of the formation of long chain polysulphides during charge and reducing to shorter chain polysulphides during discharge. This shows that incorporating a protective layer does not hinder the reaction taking place in a Li /S cell but instead plays a role in protecting the Li-anode from passivating due to parasitic reactions. The Nyquist plots of a Li-S cell were recorded before and after CV, in order to perceive the deposition/parasitic reactions of Li-polysulphides through cell resistance.

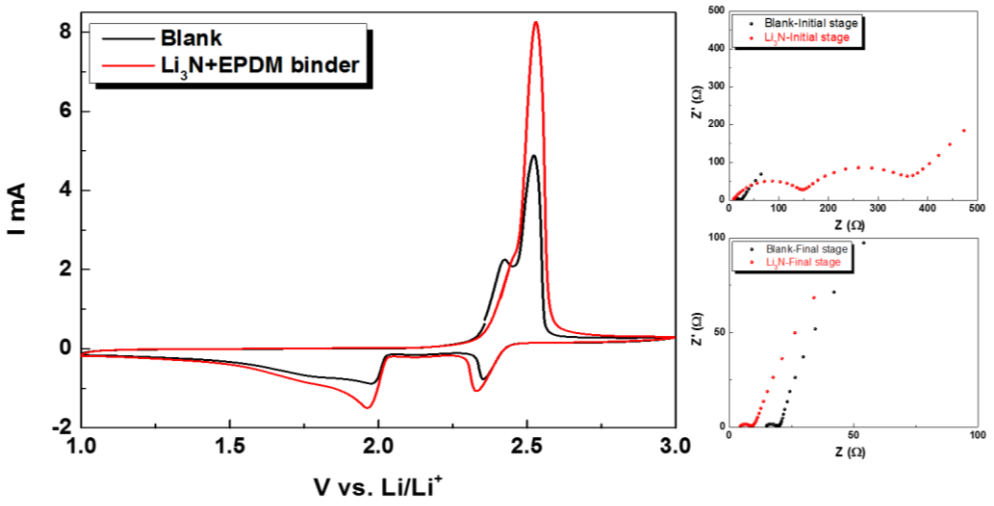


**Figure 3.13: Comparative cyclic voltammetry of the full Li-S cell with (red) and without (black) $Li_3N$ protective layer at the scan rate of 0.5mVs$^{-1}$ and EIS measurements before and after GCPL.**

Before CV cycling, the initial stage Nyquist plot has been measured in the cell with $Li_3N$ protective layer is composed of a semicircle in the HF region (100 kHz–1 kHz), a semicircle in MF region (1 kHz–1 Hz), and a slopping line in the LF region (1 Hz–10 mHz). The Nyquist plot in the cell without protective layer shows a defined small semicircle with another overlapping in HF region with a slopping line in LF region. Since the discharge, insoluble Li-polysulphides wouldn't be generated until the lower voltage plateau,[50–52] the semicircle in HF couldn't be associated to the formation of parasitic film. Meanwhile these HF semicircles could be linked to an extra interphase layer with low interfacial contact within the electrodes in the cell.[53–56] After CV cycling, it can be clearly witnessed that in the cell with protective layer, the two HF and MF semicircle dramatically reduced/ overlapped into one tense semicircle and sharp slopping line, representing the formation of stable solid electrolyte interphase (SEI) or better interfacial contacts with lower cell resistance.[55,57]

## *3.5.5 Post-mortem analysis*

### 3.5.5.1 SEM

Post-mortem SEM analysis was implemented on the series of samples for comparative studies 1) Surface of Li without protective layer 2) Surface of Li with $Li_3N$ coated protective layer with EPDM binder. Reference point was set by pristine metallic Li-foil and the pristine deposited foils. In order to observe the effects and efficiency of protection provided by $Li_3N$ layer, it has been very carefully removed, to observe the Li-foil beneath. Figure 3.14 shows the SEM morphologies of Li-foil before and after cycling (5, 10, and 20 cycles) with and without protective layer.

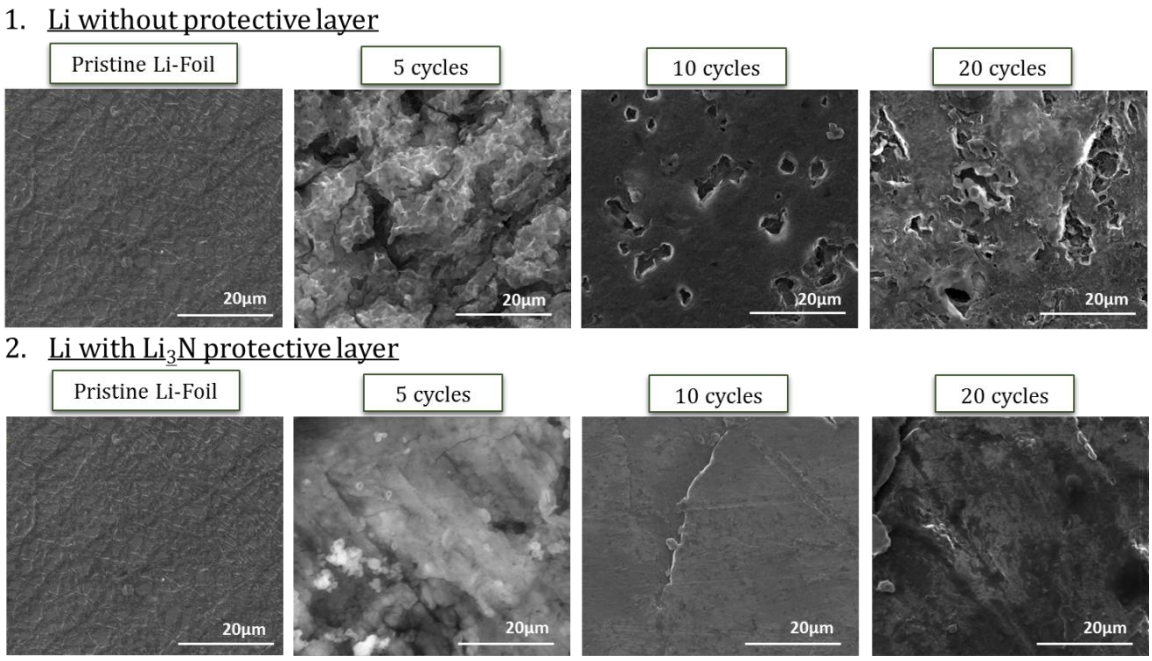


**Figure 3.14: SEM micrograph of the samples 1) Without $Li_3N$ protective layer, 2) With $Li_3N$ protective layer.**

The surface features of Li-foil without protective layer represents an additional film after 5 cycles, After 10 cycles, and visible craters were observed which was more prominent after 20 cycles. The visible craters could be as a result of the decomposition of $(Li_2S_x)_n$ clusters on the Li (111) plane that proceeds further to the subsurface to form $Li_2S$.[58]

In the case of Li surface with the protective layers, after 5 cycles, a surface film was also observed but no change in the surface morphology was observed for further consecutive cycles. EDS analysis (Figure 3.15), shows that the surface film formed after 5 cycles on the Li surface without protective layers has the presence of sulphur species, that could be attributed to the distribution of sulphur (Polysulphides) covering Li-surface.

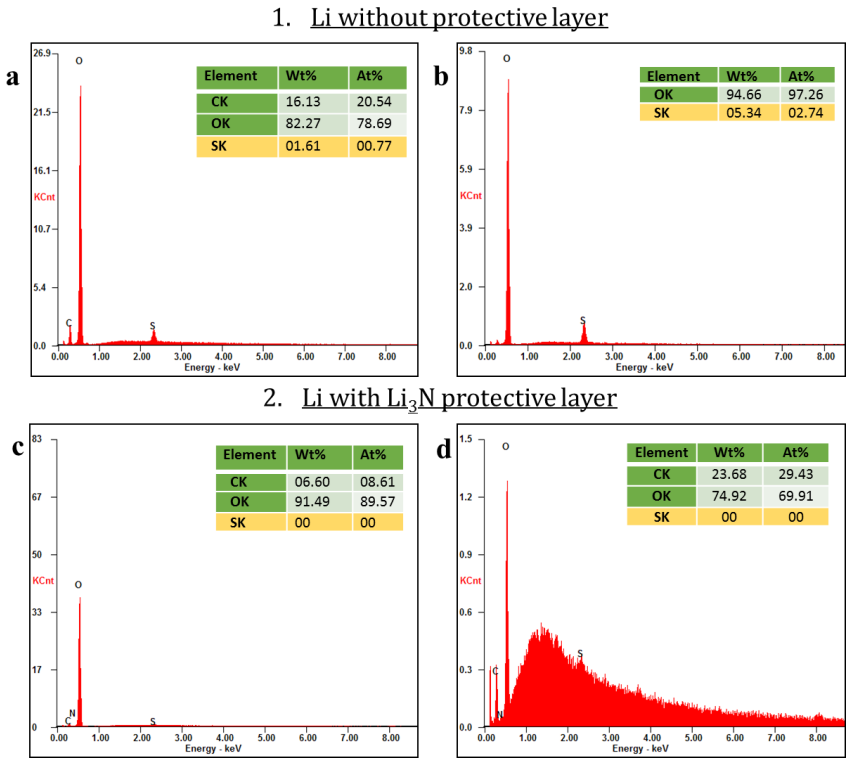


**Figure 3.15: EDS analysis of the SEM micrograph taken for the categories of samples 1) Without $Li_3N$ protective layer (a) After 5 cycles (b)After 10 cycles. 2) With $Li_3N$ protective layer (c) After 5 cycles (d) After 10 cycles.**

In the case of Li surface after 5 cycles the deposit that was observed on the Li could be a probable presence of the EPDM polymer on the surface of the Li as EDS analysis do not show any presence of sulphur species. Moreover even after 20 cycles negligible sulphur presence was observed on the Li surface with the protective layers according to EDF analysis with unchanged Li surface morphology. The SEM and EDF analysis proves the

efficiency and sufficient coverage of the $Li_3N$ protective layer that inhibits deposition and parasitic reactions at the surface of Li-anode with unchanged Li surface morphology.

### 3.5.5.2 XPS

In order to continue more in-depth studies on Li-anode surface, XPS analysis has been conducted using recovered Li-foil, after cycling with and without protective layer. The S 2p spectrum is shown in figure 3.16.[59]

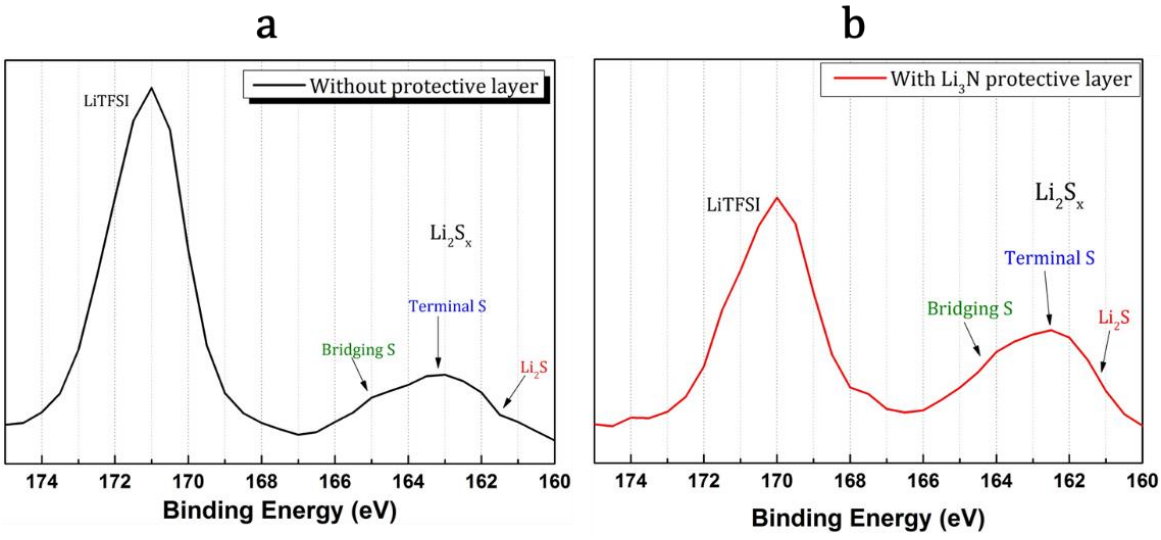


**Figure 3.16: XPS $S_2p$ spectra of: a) Li-foil recovered after 1 cycle without protective layer, (b) Li recovered after 1cycle with $Li_3N$ protective layer in same conditions.**

Taking into account that spin-orbit coupling shows ~1.2 eV difference of binding energy due to split of S 2p peaks denotes as S 2p1/2 and S 2p3/2, therefore the main S 2p3/2 in the vicinity of 169-171 eV is attributed to $TFSI^-$ salt anion.[60] However, the S 2p spectrum of the Li-foil recovered after cycling with $Li_3N$ protective layer is relatively similar to the non-protected one except, the shoulder representing $Li_2S$ at ~161.4 eV, doesn't appear clearly, peak/shoulder for terminal sulphur at ~163 eV is difficult to be seen. One broad peak has been observed, which could represent that the surface chemistry is rather different and its placement at ~162 eV shows the presence of terminal sulphur atoms,

representing probability of the longer chain polysulphide.[36] The presence of these $Li_2S_x$ could be due to the formation of kind of SEI layer. It could be due to reduction of sulphur in the electrolyte, which prohibits further formation of the reduced species such as $Li_2S$ at the Li-anode surface with protective layer. [61]

### *3.5.6 $Li_3N$ layer formation by electrolyte additive:*

- In-situ $Li_3N$ formation:

#### 3.5.6.1 Visual & XPS

Azido trimethyl silane ($(CH_3)_3SiN_3$),[62] expected to form $Li_3N$ layer on contact with fresh Li metal anode was used as an additive in the electrolyte to form an in-situ $Li_3N$ protective layer on Li-anode surface.

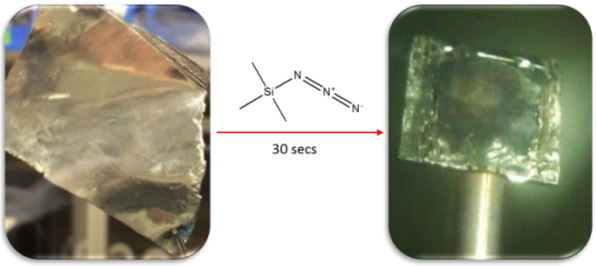


**Figure 3.17: Visual photograph of Lithium foil before and after drop-coating of Trimethyl azide silane.**

In order to better understand the layer/deposit formation of $Li_3N$ on the Li metal anode, azido trimethyl silane [$(CH_3)_3SiN_3$] was directly drop coated on the Li-foil. Figure 3.18 shows the visual effects of $(CH_3)_3SiN_3$ in direct contact with cleaned (cleaned by Ar gun) lithium after 30 seconds by change of colour to dark brown under Ar atmosphere. The XPS Li 1s spectra have been taken for the sample after deposition with comparison to pristine Li-foil.

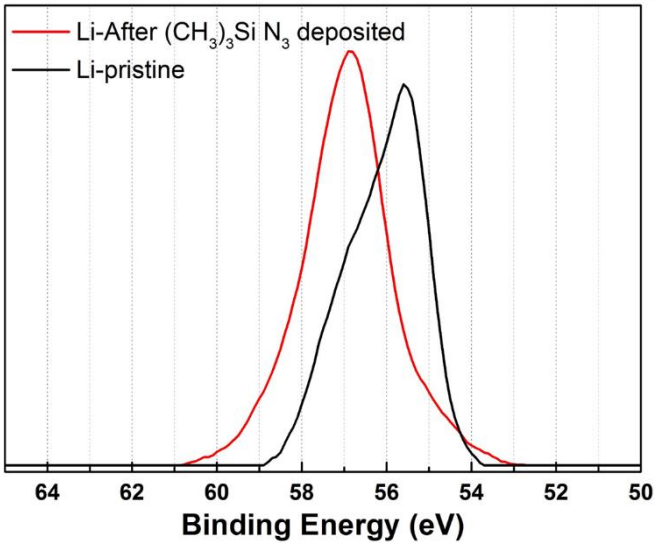


**Figure 3.18 : XPS graph comparing pristine Li-foil and Li-foil coated with $(CH_3)_3SiN_3$.**

Figure 3.18 shows the pristine lithium binding energy peak appears at ~ 55.5 eV, meanwhile after deposition the Li 1s spectra clearly shows the significant peak shift towards higher binding energy i.e. ~ 56.88 denotes the formation of $Li_3N$, in agreement by the Binding Energy difference of ~1.3 eV.

### 3.5.6.2 SEM

To analyse the formation of $Li_3N$ from azide solution, SEM analysis was conducted on the Li-foil after 10 to 15 mins after the drop coat of $(CH_3)_3SiN_3$. Figure 3.19 shows the micrographs of pristine lithium foil before and after deposition of additive on the Li-foil. Clusters were formed on the surface of the Li indicating some reaction taking place and further zoomed in images show the formation of flower shaped cluster deposits as well as singular triangle morphology.

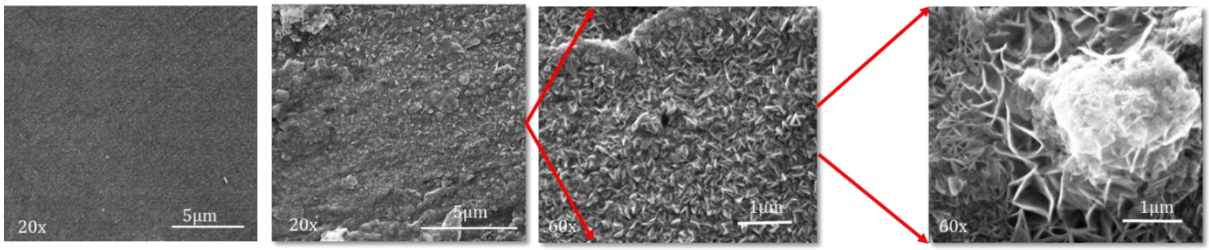


**Figure 3.19: SEM micrograph exhibits evolution of pristine Li-foil and formation of $Li_3N$ when coated with $(CH_3)_3SiN_3$.**

EDS analysis was taken on the pristine and the deposited foils. A closer look at the nitrogen percentage indicates the presence of slightly higher amounts of nitrogen content on the clusters probably due to the formation of $Li_3N$.

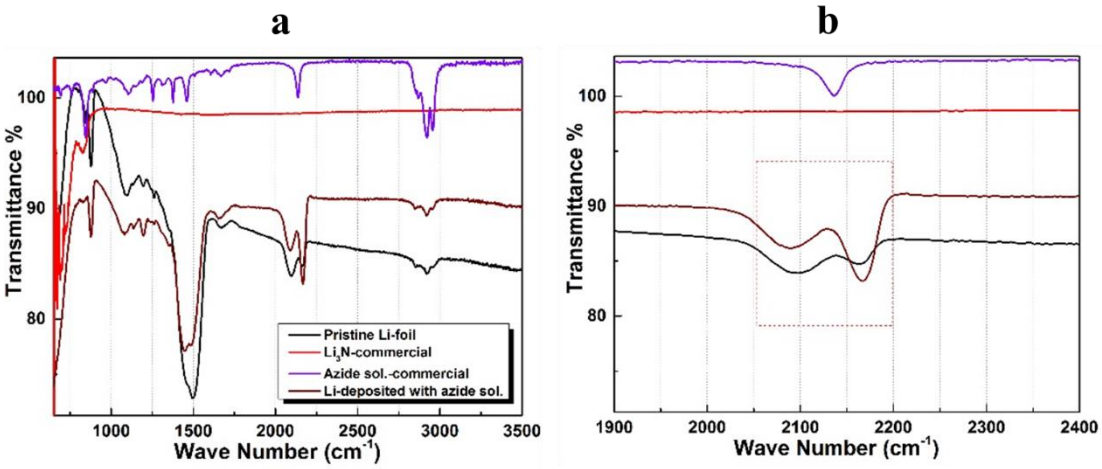


**Figure 3.20: FTIR analysis of pristine Li-foil compared with commercial $Li_3N$, commercial $(CH_3)_3SiN_3$ solvent and coated Li-foil a) Full spectra, b) Enhanced IR range of Azide and Nitride.**

FTIR-ATR results were complicated, and difficult to interpret, though the peak of azide ($^{-}N=^{+}N=^{-}N$) has been noticed on the deposited Li-foil ~ 2096-2124 $cm^{-1}$.[63–65] Meanwhile, it is difficult to see peaks related to N≡N (nitride) group.

### 3.5.6.3 CV studies with and without additive

As show in Figure 3.21, cells assembled with Li as counter electrode, SS counter electrode with the electrolytes with and without additives showed good lithium plating/stripping

properties with no negative effects on the electrochemical stability of the electrolyte. Impedance analysis taken before and after CV cycles indicate a higher impedance with electrolyte containing 0.1M additive showing that there could be a possibility of a surface layer formed on the Li metal with the additive that increase the cell resistance. Upon cycling, the cell impedance reduces and is comparable to the cell without any additives.

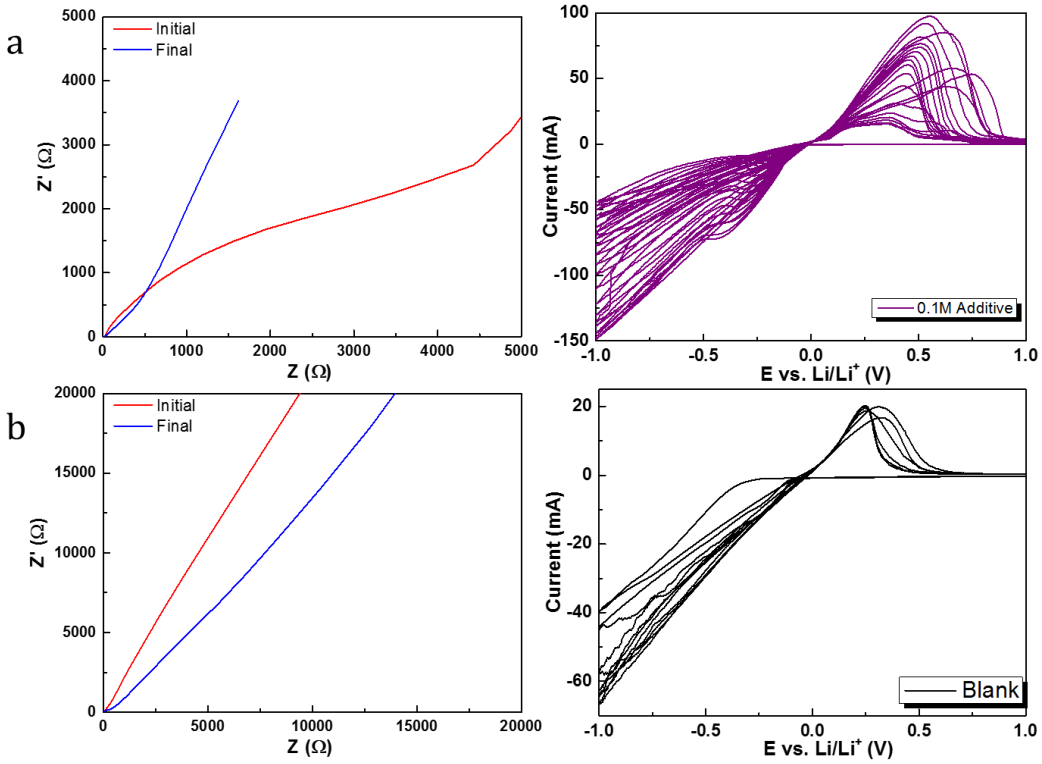


**Figure 3.21: CV plating/stripping experiment of Li-anode vs. stainless steel as $W_E$ with electrolyte a) 0.1M $(CH_3)_3SiN_3$ in 1M LiTFSI (DME: DIOX), b) 1M LiTFSI (DME: DIOX) without any additive.**

Sulphur cells assembled with additive based electrolytes showed prominent sulphur redox properties as shown in figure 3.22.

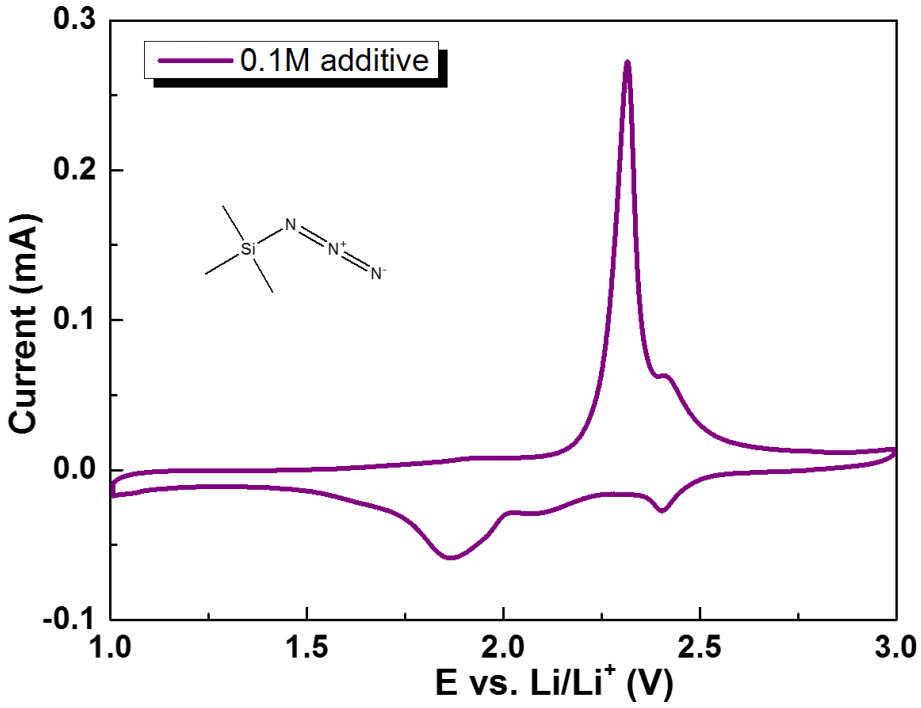


**Figure 3.22: CV of Li-anode vs. sulphur composite cathode as $W_E$ with electrolyte 0.1M $(CH_3)_3SiN_3$ in 1M LiTFSI (DME: DIOX).**

### 3.5.6.4 Galvanostatic cycling

Galvanostatic cycling of Li-S cells prepared with composite powder cathodes are shown in figure 3.23. 0.01M of additive in the electrolyte did not seem to have any effect on the discharge capacity but when the additive content was increased in the electrolyte to 0.1M, there was an increase in discharge capacity (983 mAh $g^{-1}$) for up to 20 cycles and then seems to converge with the discharge capacity of cells without additive.

This behaviour could also be contributed to the non-uniform deposition of $Li_3N$ or maybe in clusters that could be deposited on the Li metal. A prominent difference with the additive was the improvement in coulombic efficiency of the cell with 0.1M additive.

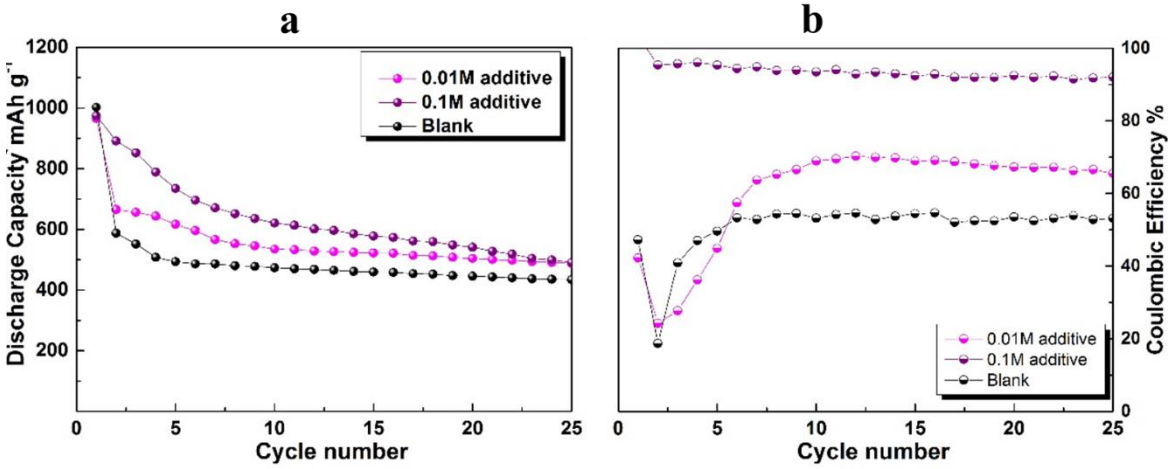


**Figure 3.23: Galvanostatic cycling comparison of a) 0.01M and 0.1M concentration of $(CH_3)_3SiN_3$ in the electrolyte with blank, b) Coulombic efficiency %.**

### 3.5.6.5 Drop coating of $(CH_3)_3SiN_3$ on Li-foil

The discharge capacity after 25$^{th}$ cycle with 0.1M and 0.01M electrolyte additive were about same. Therefore alternative approach of direct drop coating has been employed.

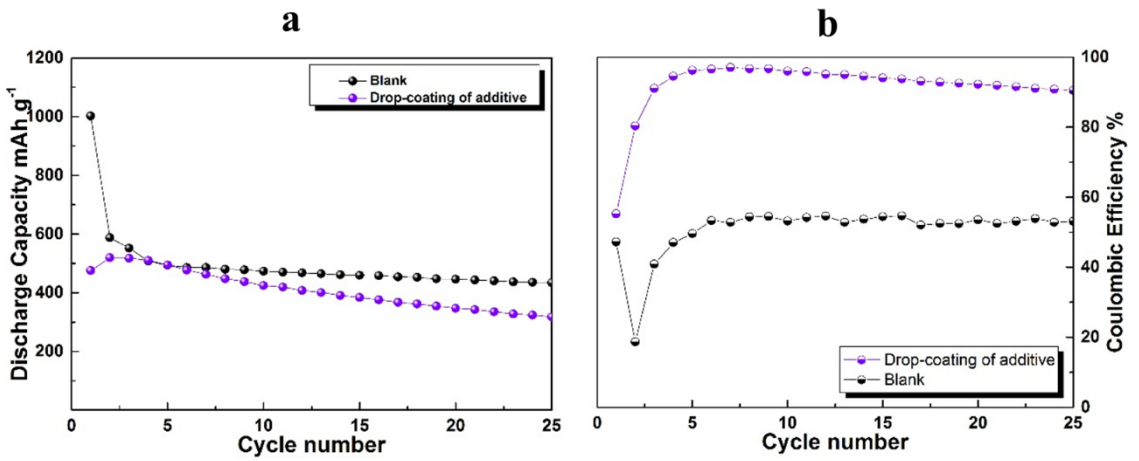


**Figure 3.24: Galvanostatic cycling comparison of a) $(CH_3)_3SiN_3$ drop-coated on Li-anode with blank, b) Coulombic efficiency %.**

Figure 3.24 shows that the discharge capacity slightly decreased when compared to the previous technique but the coulombic efficiency was retained. This might be due to the fact that there is an inhomogeneous deposition of the surface layer ($Li_3N$) due to the additive being dissolved in the electrolyte from the surface of the Li.

## 3.6 Conclusion

$Li_3N$ protective layers on the surface of metallic Li-anode were implemented to cope with the problems of Li-S systems. Different approaches has been used to prepare the best stable Li-ion conductive protective film, to be used as stable SEI, which avoid the surface parasitic reactions of Li-anode with polysulphide species and probability of dendrites growth when in direct contact with electrolyte. The $Li_3N$/Li-anode show improved electrochemical performance compared to non-protected Li-anode. Furthermore, XPS/SEM post-mortem studies have also guided better insights concerning the influence of sulphur deposited on the Li-anode surface without any protection. In-situ formation of $Li_3N$ by utilising Azido trimethyl silane has been achieved and more efforts are underway to optimise the concentration and deposition techniques in order to obtain a uniform layer of $Li_3N$ on the Li-foil using additives in Li-S systems.

## 3.7 References

(1) Kim, H.; Jeong, G.; Kim, Y.-U.; Kim, J.-H.; Park, C.-M.; Sohn, H.-J. Metallic Anodes for next

Generation Secondary Batteries. *Chem. Soc. Rev.* **2013**, *42*, 9011–9034.

(2) Saclay, R. De. Carbon-Based Nanomaterials as an Anode for Lithium Ion Battery Carbon-Based Nanomaterials as an Anode for Lithium Ion Battery.

(3) Urbonaite, S.; Poux, T.; Novák, P. Progress Towards Commercially Viable Li-S Battery Cells. *Adv. Energy Mater.* **2015**, *5*, 1–20.

(4) Mejía, A.; Devaraj, S.; Guzmán, J.; Lopez Del Amo, J. M.; García, N.; Rojo, T.; Armand, M.; Tiemblo, P. Scalable Plasticized Polymer Electrolytes Reinforced with Surface-Modified Sepiolite Fillers - A Feasibility Study in Lithium Metal Polymer Batteries. *J. Power Sources* **2016**, *306*, 772–778.

(5) Goodenough, J. B.; Kim, Y. Challenges for Rechargeable Li Batteries. *Chem. Mater.* **2010**, *22*, 587–603.

(6) Zhang, S. S. A Review on Electrolyte Additives for Lithium-Ion Batteries. *J. Power Sources* **2006**, *162*, 1379–1394.

(7) Verma, P.; Maire, P.; Novák, P. A Review of the Features and Analyses of the Solid Electrolyte Interphase in Li-Ion Batteries. *Electrochim. Acta* **2010**, *55*, 6332–6341.

(8) Lewandowski, A.; Świderska-Mocek, A. Ionic Liquids as Electrolytes for Li-Ion Batteries-An Overview of Electrochemical Studies. *J. Power Sources* **2009**, *194*, 601–609.

(9) Peled, E. The Electrochemical-Behavior of Alkali and Alkaline-Earth Metals in Non-Aqueous Battery Systems - the Solid Electrolyte Interphase Model. *J. Electrochem. Soc.* **1979**, *126*, 2047–2051.

(10) Mikhaylik, Y. V.; Akridge, J. R. Polysulfide Shuttle Study in the Li/S Battery System. *J. Electrochem. Soc.* **2004**, *151*, A1969–A1976.

(11) Aurbach, D.; Pollak, E.; Elazari, R.; Salitra, G.; Kelley, C. S.; Affinito, J. On the Surface Chemical Aspects of Very High Energy Density, Rechargeable Li–Sulfur Batteries. *J. Electrochem. Soc.* **2009**, *156*, A694–A702.

(12) Bauer, I.; Thieme, S.; Brückner, J.; Althues, H.; Kaskel, S. Reduced Polysulfide Shuttle in Lithium–sulfur Batteries Using Nafion-Based Separators. *J. Power Sources* **2014**, *251*, 417–422.

(13) Fu, Y.; Manthiram, A. Enhanced Cyclability of Lithium − Sulfur Batteries by a Polymer Acid-Doped Polypyrrole Mixed Ionic − Electronic Conductor. *Chem. Mater.* **2012**, *24*, 3081–3087.

(14) Zhang, S. S. Liquid Electrolyte Lithium/sulfur Battery: Fundamental Chemistry, Problems, and Solutions. *J. Power Sources* **2013**, *231*, 153–162.

(15) Zheng, J.; Lv, D.; Gu, M.; Wang, C.; Zhang, J.-G.; Liu, J.; Xiao, J. How to Obtain Reproducible Results for Lithium Sulfur Batteries? *J. Electrochem. Soc.* **2013**, *160*, A2288–A2292.

(16) Aurbach, D. Review of Selected Electrode-Solution Interactions Which Determine the Performance of Li and Li Ion Batteries. *J. Power Sources* **2000**, *89*, 206–218.

(17) Bresser, D.; Passerini, S.; Scrosati, B. Recent Progress and Remaining Challenges in Sulfur-Based Lithium Secondary Batteries--a Review. *Chem. Commun. (Camb).* **2013**, *49*, 10545–10562.

(18) Yongguang Zhang, Yan Zhao, Assiya Yermukhambetova, Z. B. and P. C. Ternary sulfur/polyacrylonitrile/Mg0.6Ni0.4O Composite Cathodes for High Performance Lithium/sulfur Batteries. *J. Mater. Chem. A* **2013**, *1*, 295–301.

(19) Zhang, S. S. Role of LiNO3 in Rechargeable Lithium/sulfur Battery. *Electrochim. Acta* **2012**, *70*, 344–348.

(20) Barghamadi, M.; Best, A. S.; Bhatt, A. I.; Hollenkamp, A. F.; Mahon, P. J.; Musameh, M.; Rüther,

T. Effect of LiNO3 Additive and Pyrrolidinium Ionic Liquid on the Solid Electrolyte Interphase in the Lithium–sulfur Battery. *J. Power Sources* **2015**, *295*, 212–220.

(21) Zhang, S. S. A New Finding on the Role of LiNO3 in Lithium-Sulfur Battery. *J. Power Sources* **2016**, *322*, 99–105.

(22) Xiong, S.; Xie, K.; Diao, Y.; Hong, X. Properties of Surface Film on Lithium Anode with LiNO3 as Lithium Salt in Electrolyte Solution for Lithium–sulfur Batteries. *Electrochim. Acta* **2012**, *83*, 78–86.

(23) CHOI, N. Protective Coating of Lithium Metal Electrode for Interfacial Enhancement with Gel Polymer Electrolyte. *Solid State Ionics* **2004**, *172*, 19–24.

(24) Takei, Y.; Takeno, K.; Morimoto, H.; Tobishima, S. I. Effects of Nonaqueous Electrolyte Solutions Mixed with Carbonate-Modified Siloxane on Charge-Discharge Performance of Negative Electrodes for Secondary Lithium Batteries. *J. Power Sources* **2013**, *228*, 32–38.

(25) Mikhaylik, Y. V.; Civanlar, R.; Eleftheriadis, A.; Shapiro, O. United States Patent. **2009**, *1*.

(26) Mikhaylik, Y. V. Electrolytes for Li-S Cells. *United States Pat.* **2008**.

(27) Aurbach, D.; Zinigrad, E.; Cohen, Y.; Teller, H. A Short Review of Failure Mechanisms of Lithium Metal and Lithiaded Graphite Anodes in Liquid Electrolyte Solutions. *Solid State Ionics* **2002**, *148*, 405–416.

(28) Aurbach, D.; Zinigrad, E.; Teller, H.; Dan, P. Factors Which Limit the Cycle Life of Rechargeable Lithium (Metal) Batteries. *J. Electrochem. Soc.* **2000**, *147*, 1274–1279.

(29) Zhang, S. S. Binder Based on Polyelectrolyte for High Capacity Density Lithium/Sulfur Battery. *J. Electrochem. Soc.* **2012**, *159*, A1226–A1229.

(30) Xiong, S.; Kai, X.; Hong, X.; Diao, Y. Effect of LiBOB as Additive on Electrochemical Properties of Lithium-Sulfur Batteries. *Ionics (Kiel).* **2012**, *18*, 249–254.

(31) Xu, K.; Zhang, S.; Jow, T. R. Formation of the Graphite/Electrolyte Interface by Lithium Bis(oxalato)borate. *Electrochem. Solid-State Lett.* **2003**, *6*, A117–A120.

(32) Liu, J.; Chen, Z.; Busking, S.; Belharouak, I.; Amine, K. Effect of Electrolyte Additives in Improving the Cycle and Calendar Life of graphite/Li1.1[Ni1/3Co1/3Mn1/3]0.9O2 Li-Ion Cells. *J. Power Sources* **2007**, *174*, 852–855.

(33) Lin, Z.; Liu, Z.; Fu, W.; Dudney, N. J.; Liang, C. Phosphorous Pentasulfide as a Novel Additive for High-Performance Lithium-Sulfur Batteries. *Adv. Funct. Mater.* **2013**, *23*, 1064–1069.

(34) Ding, F.; Xu, W.; Graff, G. L.; Zhang, J.; Sushko, M. L.; Chen, X.; Shao, Y.; Engelhard, M. H.; Nie, Z.; Xiao, J.; *et al.* Dendrite-Free Lithium Deposition via Self-Healing Electrostatic Shield Mechanism. *J. Am. Chem. Soc.* **2013**, *135*, 4450–4456.

(35) Lee, Y. M.; Choi, N.-S. S.; Park, J.-K. K. H.; Park, J.-K. K. H. Electrochemical Performance of Lithium/sulfur Batteries with Protected Li Anodes. *J. Power Sources* **2003**, *119-121*, 964–972.

(36) Demir-Cakan, R.; Morcrette, M.; Guéguen, A.; Dedryvère, R.; Tarascon, J.-M. Li–S Batteries: Simple Approaches for Superior Performance. *Energy Environ. Sci.* **2013**, *6*, 176–182.

(37) Alpen, U. V.; Rabenau, a.; Talat, G. H. Ionic Conductivity in Li3N Single Crystals. *Appl. Phys. Lett.* **1977**, *30*, 621–623.

(38) Liang, X.; Liu, Y.; Wen, Z.; Huang, L.; Wang, X.; Zhang, H. A Nano-Structured and Highly Ordered Polypyrrole-Sulfur Cathode for Lithium-Sulfur Batteries. *J. Power Sources* **2011**, *196*, 6951–6955.

(39) Yan, Y.; Zhang, J. Y.; Cui, T.; Li, Y.; Ma, Y. M.; Gong, J.; Zong, Z. G.; Zou, G. T. First-Principles

Study of High Pressure Phase Transformations in Li3N. *Eur. Phys. J. B* **2008**, *61*, 397–403.

(40) Abruña, H. D. H. D.; Matsumoto, F.; Cohen, J. L. J. L.; Jin, J.; Roychowdhury, C.; Prochaska, M.; van Dover, R. B. B.; DiSalvo, F. J. F. J.; Kiya, Y.; Henderson, J. C. J. C.; *et al.* Electrochemical Energy Generation and Storage. Fuel Cells and Lithium-Ion Batteries. *Bull. Chem. Soc. Jpn.* **2007**, *80*, 1843–1855.

(41) Ma, G.; Wen, Z.; Wu, M.; Shen, C.; Wang, Q.; Jin, J. Lithium Anode Protection Guided Highly-Stable Lithium- Sulfur Battery. **2014**, *2*, 2–7.

(42) Desjardins C. David, Hossein Sharifian, G. K. M. Lithium-Lithium Nitride Anode. *United States Pat.* **1989**, *4,888,258*.

(43) Wu, M.; Wen, Z.; Liu, Y.; Wang, X.; Huang, L. Electrochemical Behaviors of a Li3N Modified Li Metal Electrode in Secondary Lithium Batteries. *J. Power Sources* **2011**, *196*, 8091–8097.

(44) Kang, Y.; Lee, W.; Suh, D. H.; Lee, C. Solid Polymer Electrolytes Based on Cross-Linked Polysiloxane-G-Oligo(ethylene Oxide): Ionic Conductivity and Electrochemical Properties. *J. Power Sources* **2003**, *119-121*, 448–453.

(45) Zhang, Y. J.; Wang, W.; Tang, H.; Bai, W. Q.; Ge, X.; Wang, X. L.; Gu, C. D.; Tu, J. P. An Ex-Situ Nitridation Route to Synthesize Li 3 N-Modi Fi Ed Li Anodes for Lithium Secondary Batteries. **2015**, *277*, 304–311.

(46) Zhang, Y. J.; Wang, W.; Tang, H.; Bai, W. Q.; Ge, X.; Wang, X. L.; Gu, C. D.; Tu, J. P. An Ex-Situ Nitridation Route to Synthesize Li3N-Modified Li Anodes for Lithium Secondary Batteries. *J. Power Sources* **2015**, *277*, 304–311.

(47) Gregory, D.H.; O'Meara, P.M.; Gordon, A.G.; Hodges, J.P.; Short, S.; Jorgensen, J. . Structure of Lithium Nitride and Transition-Metal-Doped Derivatives, Li3-X-Y Mx N (M = Ni, Cu): A Powder Neutron Diffraction Study. *Chem. Mater.* **2002**, *14*, 2063–2070.

(48) Sigma-Aldrich. Lithium nitride −80 mesh, ≥99: CAS Number 26134-62-3.

(49) He, G.; Ji, X.; Nazar, L. High "C" Rate Li-S Cathodes: Sulfur Imbibed Bimodal Porous Carbons. *Energy Environ. Sci.* **2011**, *4*, 2878-2883.

(50) Pang, Q.; Kundu, D.; Cuisinier, M.; Nazar, L. F. Surface-Enhanced Redox Chemistry of Polysulphides on a Metallic and Polar Host for Lithium-Sulphur Batteries. *Nat Commun* **2014**, *5*, 4759.

(51) Bruce, P. G.; Freunberger, S. A.; Hardwick, L. J.; Tarascon, J.-M. Li-$O_2$ and Li-S Batteries with High Energy Storage. *Nat. Mater.* **2011**, *11*, 19–29.

(52) Barchasz, C.; Mesguich, F.; Dijon, J.; Leprêtre, J. C.; Patoux, S.; Alloin, F. Novel Positive Electrode Architecture for Rechargeable Lithium/sulfur Batteries. *J. Power Sources* **2012**, *211*, 19–26.

(53) Ji, X.; Nazar, L. F. Advances in Li–S Batteries. *J. Mater. Chem.* **2010**, *20*, 9821–9826.

(54) Bruce, P. G.; Freunberger, S. A.; Hardwick, L. J.; Tarascon, J.-M. Li–O2 and Li–S Batteries with High Energy Storage. *Nat. Mater.* **2011**, *11*, 19–29.

(55) Li, Y.; Zhan, H.; Liu, S.; Huang, K.; Zhou, Y. Electrochemical Properties of the Soluble Reduction Products in Rechargeable Li/S Battery. *J. Power Sources* **2010**, *195*, 2945–2949.

(56) Barchasz, C.; Molton, F.; Duboc, C.; Leprêtre, J. C.; Patoux, S.; Alloin, F. Lithium/sulfur Cell Discharge Mechanism: An Original Approach for Intermediate Species Identification. *Anal. Chem.* **2012**, *84*, 3973–3980.

(57) Cheng, X.-B.; Zhang, R.; Zhao, C.-Z.; Wei, F.; Zhang, J.-G.; Zhang, Q. A Review of Solid

Electrolyte Interphases on Lithium Metal Anode. *Adv. Sci.* **2016**, *3*, 1500213(1–20).

(58) Liu, Z.; Bertolini, S.; Balbuena, P. B.; Mukherjee, P. P. Li 2 S Film Formation on Lithium Anode Surface of Li–S Batteries. *ACS Appl. Mater. Interfaces* **2016**, *8*, 4700–4708.

(59) Smart, R. S. C.; Skinner, W. M.; Gerson, A. R. XPS of Sulphide Mineral Surfaces: Metal-Deficient, Polysulphides, Defects and Elemental Sulphur. *Surf. Interface Anal.* **1999**, *28*, 101–105.

(60) Dedryvère, R.; Leroy, S.; Martinez, H.; Blanchard, F.; Lemordant, D.; Gonbeau, D. XPS Valence Characterization of Lithium Salts as a Tool to Study Electrode/Electrolyte Interfaces of Li-Ion Batteries. *J. Phys. Chem. B* **2006**, *110*, 12986–12992.

(61) Vizintin, A.; Lozinšek, M.; Chellappan, R. K.; Foix, D.; Krajnc, A.; Mali, G.; Drazic, G.; Genorio, B.; Dedryvère, R.; Dominko, R. Fluorinated Reduced Graphene Oxide as an Interlayer in Li–S Batteries. *Chem. Mater.* **2015**, *27*, 7070–7081.

(62) Azidotrimethylsilane 95% _ Sigma-Aldrich.

(63) Gai, X. S.; Coutifaris, B. a; Brewer, S. H.; Fenlon, E. E. A Direct Comparison of Azide and Nitrile Vibrational Probes. *Phys. Chem. Chem. Phys.* **2011**, *13*, 5926–5930.

(64) Klump, S. P.; Shechter, H. Conversions of Primary Amines to Azides by N-Butyllithium and Azidotris(diethylamino)phosphonium Bromide. *Tetrahedron Lett.* **2002**, *43*, 8421–8423.

(65) Benkaddour, A.; Jradi, K.; Robert, S.; Daneault, C. Grafting of Polycaprolactone on Oxidized Nanocelluloses by Click Chemistry. *Nanomaterials* **2013**, *3*, 141–157.

# *Chapter4: Novel design of hybrid anode structure.*

# 4 Introduction

The suitable anode material for Li-based batteries depends on the intrinsic properties, such as rapid and high intercalation kinetics of $Li^+$, redox potential versus Li appending adequately the high cell voltage. Structural integrity is a major point for suitable anode material as well, for the better electrical contact over cycling.[1]

Persuasion of developing high energy density materials for Li rechargeable batteries has commenced decades ago, within this chapter, the overview of carbonaceous materials used as an anode material is described briefly.

The implementation of carbonaceous (graphitic) materials as anode depends on their ability of forming intercalated materials with lithium. There is a huge list of possible anode materials studied and available lately.[2,3]

| Anode material | Th.Cap (mAh/g) | Real Cap (mAh/g) | Drawbacks |
|---|---|---|---|
| Tin (Sn) | 994 | 400 | Huge capacity fade and volume expansion per cycle.[4–7] |
| Silicon (Si) | 4200 | 2158 | Huge capacity fade and volume expansion per cycle.[8–11] |
| Metal Oxide Composites (M= Co, Mn, Fe) | 880 | 700 | High volume expansion upon cycling[12,13] |
| Graphite ($LiC_x$) | 372 | 250 | Lower charge capacity[14–19] |
| Graphene (rGO) | 744 | 350 | High voltage hysteresis in cycling profile[20–25] |

Even though these materials look promising due to their higher theoretical capacity when compared to graphite/graphene, the choice of carbonaceous materials can be justified by it being rather inexpensive, they exhibit excellent reversibility of lithium insertion, and safety. Therefore, further overview in this chapter will rather focus on two promising carbonaceous materials i.e. graphite[15,26,27] and graphene[22,28,29].

Due to its excellent properties, flat working potential vs. Li, graphite is the most usuable anode.[30–33] Its low in cost and delivers a decent cycle life In spite of graphite undergoing only 1 Li-ion intercalation with 6 carbon atoms and thus providing a reversible capacity of ~372 mAh $g^{-1}$,

$$C + xLi + xe^{-} \leftrightarrow Li_xC_6$$

Sony commercialised Li-ion battery in 1991,[34] using graphite as an anode material. The chemical diffusion coefficient for lithium in carbon is of the order of $10^{-9}$ $cm^2s^{-1}$. Graphite anode material forms a protective surface film with many electrolyte solutions. This film which is often called SEI (Solid Electrolyte Interface) effectively passivates the graphite surface and prevents further co-interaction decomposition of solvent molecules, allowing only Li ion migration. The term "intercalation" implies the restricting condition that a layered host takes up guests within its interlayer gaps ("galleries"), which may result in volume change perpendicular to layers, but which cause no other structural changes. Even graphite would be not a pure intercalation host, as during Li accommodation the stacking changes by sliding of the graphene layers.

Graphite is a layered compound with hexagonal arrangement of each carbon in the lattice; it can conduct electricity due to the vast electron delocalization within the carbon layers. These valence electrons are free to move, so are able to conduct electricity. However, the electricity is only conducted within the plane of the layers with a surface area of 8.5 $m^2$ $g^{-1}$.

An attempt has been made to use commercial graphite as an anode and in situ formed Li sulphide/microporous carbon ($Li_2S$/MC) as a cathode for the Li-S full cell demonstration.[35] A conventional commercial Li-ion battery electrolyte (1.0 M $LiPF_6$ in EC/DEC (1:1 by volume) could be adopted for such Li-S batteries as it is compatible with a graphite anode. The full cell of $Li_2S$/MC-graphite with a capacity ratio of $Li_2S$/ MC

to graphite of 0.98 ($Li_2S$/MC was the limiting electrode) was discharged/charged at a current density of 168 mA $g^{-1}$. The average discharge voltage of the $Li_2S$/MC-graphite full cell was around 1.6 V, and the full cell showed a stable capacity of around 600 mAh $g^{-1}$ up to 150 cycles with a coulombic efficiency close to 100%. It is seen that even though Li-S battery with a graphite anode offers a relatively lower energy density comparing with that with metallic Li anode, it is still two times higher than a conventional Li-ion battery. A graphite-based all-carbon anode was investigated in a Li-S full cell with an electrolyte consisted of 1 M LiTFSI and 0.25 M $LiNO_3$ in DOL/DME (1:1 v/v).[36]

Extensive studies using several analytical techniques has been dedicated to the reaction mechanism following intercalation/de-intercalation process among Li and graphite.[37,38] In order to discover the anode materials suitable for competitive applications such as EVs or high power portable devices, further advances are mandatory. Hence, to enhance the energy density within Li-based batteries, graphite anode can be a suitable substitute; meanwhile theoretical capacity of intercalated graphite is ~372mAh g-1, only the one-tenth of Li. In addition, the graphite anode has limit up to low power devices i.e. portable computers or mobile phones. Consequently, the carbonaceous materials still shows high capacity,[39,40] therefore the focus of research flex towards other carbonaceous materials i.e. carbon nanotubes (CNTs), porous carbons, nanofibers (NF) and most promising graphene.[40–46] Despite the promising outcomes of the CNT, NF and porous carbon, the open issues regarding expenses, treatment procedures and mass production hinders the fact of their utilisation in practical applications.

Graphene is a carbon single layer with surface area of 492.5 $m^2 g^{-1}$ when compared with the graphite powder which has ~ 8.5 $m^2 g^{-1}$, exhibits numerous interesting intrinsic properties i.e. chemical, mechanical and physical.[47–49] Graphene has been used as an anode material in Li-ion batteries, due to its fascinating nature of acquiring 2s electrons

from lithium stacked between the sheets during the intercalation process. It can be a suitable choice for reversible storage systems such as Li-based batteries, thanks to its great surface-to-volume ratio and high conductivity.

The properties of graphene can be controlled by the route of synthesis applied, Chemical or thermal reduction of graphene results in graphene oxide (GO) compound,[50,51] which is the most popular way of fabricating graphene. An economic and less time consuming process is using graphite as precursor to thermally treat at ~1000°C.[52,53] Exfoliation of graphite can also results in graphene oxide upon mechanical treatments,[47,54] and chemical vapour deposition method.[55–57] As a novel anode material for the lithium-ion batteries, graphene sheets mostly exhibit a higher reversible capacity than graphite.[50,58,59]

Wang et al.[51] used modified Hummer's method[60] to synthesize graphene nano sheets in bulk. The Nano sheets shows good performance, it delivers specific capacity of ~945 mAh $g^{-1}$ in 1$^{st}$ cycle with maintenance of ~460 mAh $g^{-1}$ until 100 cycles.

Graphite powder has been used as a precursor to fabricate high quality graphene by Peichao Lian et al.[50] in nitrogen atmosphere via oxidation and rapid thermal expansion. It shows higher discharge capacity of ~2035 mAh $g^{-1}$ with better reversible capacity, owing to fewer layers favouring more lithium insertion active sites.[61]

Along with the promising theoretical capacity, the problems within Li-anode are grave, such as dendrites growth during cycling, etc. The growth of dendrites favours internal short circuits generating exothermic heat, upon reaching to the melting temperature of lithium (180$^{o}$C), an intensive reaction with cathode will take place. This reaction central the huge amount of heat generation leading to the explosion of battery, if the cathode is in the state of charge.

Recent studies encourages employment of interlayer films to avoid complications within Li-S systems i.e. solid polymer electrolytes[62] or salt in electrolyte.[63] To improve

performance of Li-S systems with least complications of lithium polysulphides, cathode composite of carbon and sulphur has been treated with several methods i.e. sulphur-impregnated carbon nanotubes/ sulphur nanofiller.[64–68] Manthiram et al., introduced a self-standing MWCNT (multiwall carbon nanotubes) interlayer sheet to prevent polysulphide shuttle avoiding the loss of active material and stabilise the cycling performance (Figure 4.1).[69]

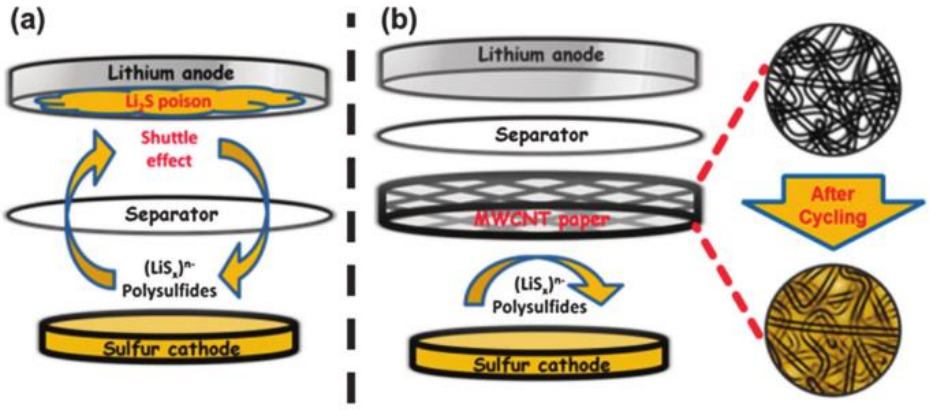


**Figure 4.1: Schematic cell configuration of rechargeable Li–S batteries: (a) traditional configuration with severe shuttle effect and $Li_2S$ poison problems and (b) new configuration with the MWCNT interlayer.**

Reduced graphene oxide (rGO) has been employed through mixing with carbon black (CB) by Wang et al. inhibits a shuttle mechanism in Li–S batteries.[70] However, the drawback of these processes is extra amount of conductive materials i.e. CNT[69], CB[71], and rGO[72] usage, that not only reduce the specific capacity.

As mentioned earlier, in chapter 3 that numerous studies are recently dedicated to avoid Li-anode complications in Li-S batteries i.e. modifications abreast Li-anode surface. Indeed once again, the effective solution is isolation of Li-anode from liquid electrolyte and dissolved polysulphides species. Continuous polysulphide species contamination on the Li anode is the severe cause of shortened lifetime and fiasco cell performance.

However, the unceasing Li-corrosion combined with dissolved polysulphide species lead the continuous growth of unstable SEI.

In this chapter; an approach to protect the Li-anode from any unwanted side surface reaction by constructing a shield over Li-anode made up of graphite/rGO has been employed. It prevents the growth of debilitating interference layer. Rather than utilizing just a protection for Li-anode, novel hybrid anode architecture.

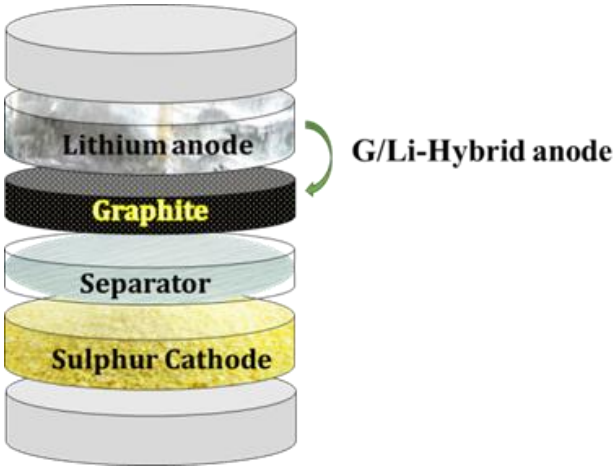


**Figure 4.2: Schematic illustration of the Li-S battery with hybrid anode.**

The hybrid anode system has been introduced by Huang et al.,[14] by using electrically connected graphite in Li-S batteries by using lithiated graphite. In this chapter, we will discuss the utilization of non-lithiated graphite/rGO film or deposit to flex the redox reactions away from Li-anode without any electrical connection.

The schematics of hybrid anode architecture[14] can be seen in figure 4.2. Upon connection of graphite/rGO with lithium in parallel way cause a short circuit of the cell, it allows continuos lithiation into graphite layer, which behave not only just a physical barrier by as well sustains a pseudo-equal potential with the Li-anode. The main function of graphite/rGO is minimizing the direct contact of Li-anode with electrolyte

(polysulphides) by acting as an artificial SEI providing Li-ion for electrochemical reaction.

## 3.8 Experimentation

### *3.8.1 Preparation of Graphite films*

The graphite self-standing films used for hybrid anode testing were prepared by casting suitable consistent slurry onto glass plate with the wet thickness of 300µm. The mixture of slurry contains graphite (SFG6): EPDM binder: Carbon black (Csp) in ratio of 70:20:10 wt. % respectively.

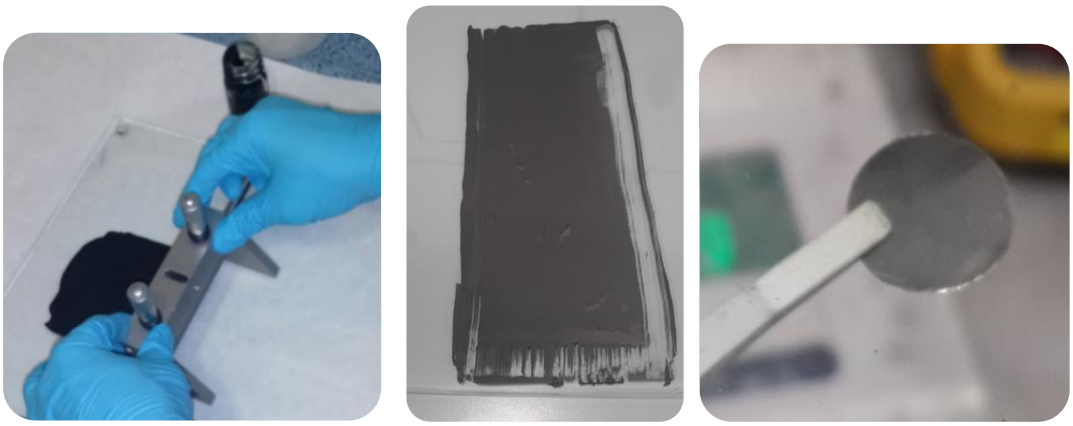

The mixture of Csp and graphite powder was dry hand milled to homogenize to further mix into suspension of EPDM in cyclohexane. The slurry was stirred for 16h until homogenized.

### *3.8.2 Synthesis of reduced-Graphene oxide films*

GO was synthesized in CIC by using graphite as precursor via modified Hummer's method.[60]

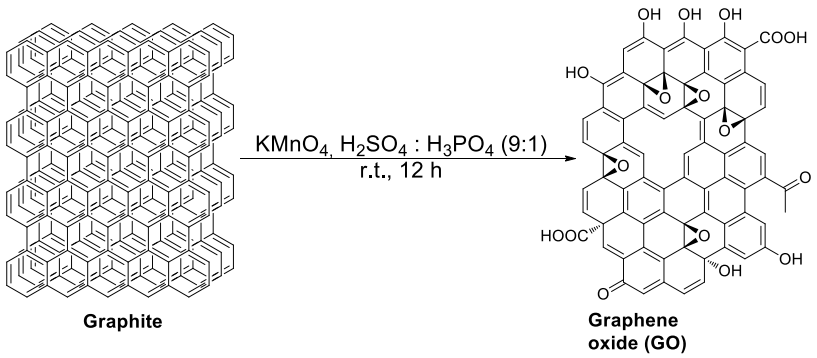


The graphene oxide (GO) was thermally exfoliated and reduced in a tubular furnace under argon flow (100 mL/min) at 900ºC (5ºC/min) to get reduced graphene oxide (rGO).[73]

### *3.8.3 Preparation of rGO deposit*

The suitable slurry was prepared inside the glovebox ($O_2$ and $H_2O$ < 1 ppm). The mixture contains rGO: EPDM binder: Carbon black (Csp) in ratio of 80:10:10 wt. % respectively. The hand grinded mixture of rGO and Csp was added into the suspension of EPDM in 5mL of cyclohexane upon stirring.

Resulting slurry was casted directly on cleaned Li-foil surface by drop-casting method under argon atmosphere inside the glovebox ($O_2$ and $H_2O$ < 1 ppm).

### *3.8.4 Cathode preparation, cell assembly, physico-chemical and electrochemical characterization:*

The powder composite cathodes have been used to investigate the role of hybrid graphite/rGO Li-anode. The preparation of cathode composite, information regarding physico-chemical and electrochemical characterization techniques and electrochemical cell assembly can be seen in *Chapter2: materials and methods* in detail.

## 3.9 Results and Discussion

Herein hybrid anode architecture has been employed; the interfacial redox reaction is shifted from the metallic Li-anode towards graphite/rGO. Graphite/rGO filmwere combined with Li foil as a pseudo-anode.

### *3.9.1 Graphite*

#### 3.9.1.1 Physico-chemical characterization:

#### 3.9.1.1.1 SEM

The morphology of the graphite film has been examined by using electron microscopy, before and after each stage of treatment, i.e. a) fresh film, b) short circuited film, c) cell after 1st discharge ($Li^+$intercalated graphite) by using graphite as cathode versus Li anode separated by GF separator wet with 1M LiTFSI in DME: Diox (1:1 vol. %) and d) after 1st discharge vs sulphur cathode.

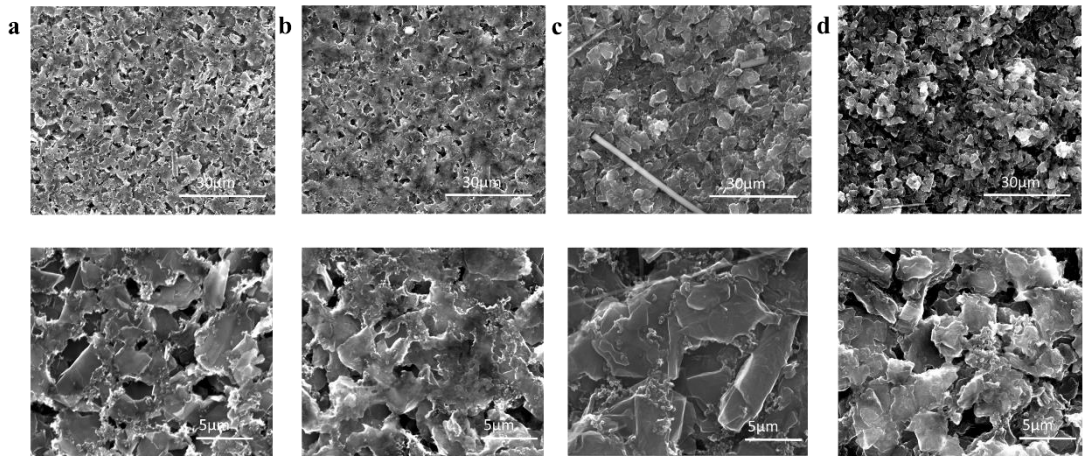


**Figure 4.3: SEM micrographs of graphite film a) fresh b) after short-circuiting in electrolyte c) after discharge vs. Li and d) after discharge vs. sulphur composite cathode.**

The morphology of graphite film from fresh (Figure 4.3a) to short-circuited (Figure 4.3b) in the electrolyte with lithium metal, and after discharging versus Li-anode (Figure 4.3c), remain unchanged. The only difference in figure 4.3c could be the closely packed stacking

of graphite flakes upon each other. However after discharge versus sulphur cathode (Figure 4.3d) the infolding layers changes rather into individual flakes stack upon each other. EDS shows some sulphur trapped within this graphite layer, proving the point of acting as protective layer.

#### 3.9.1.1.2 XRD

XRD analysis were also conducted on the similar series of samples mentioned above, the results shows no obvious change in short circuited film than fresh one (Figure 4.5 a-d). Although after discharging the graphite film as cathode versus Li-anode, the emergence of new peaks at around 27$^{o}$ could be seen, verifying the intercalation process of $Li^{+}$ into graphite. That could also be seen via naked eye, as the colour of the graphite film retrieved (post-mortem analysis) changes from black to marron.

**Figure 4.4: A photograph of coin-cell post-mortem and graphite film displaying colour change from black to marron over discharging with Li-anode in presence of 1M LiTFSI (DME:Diox).**

Nevertheless, after short circuiting within the electrolyte we cannot observe any peak difference in XRD spectra, perhaps due to small extent of lithiation taking place.

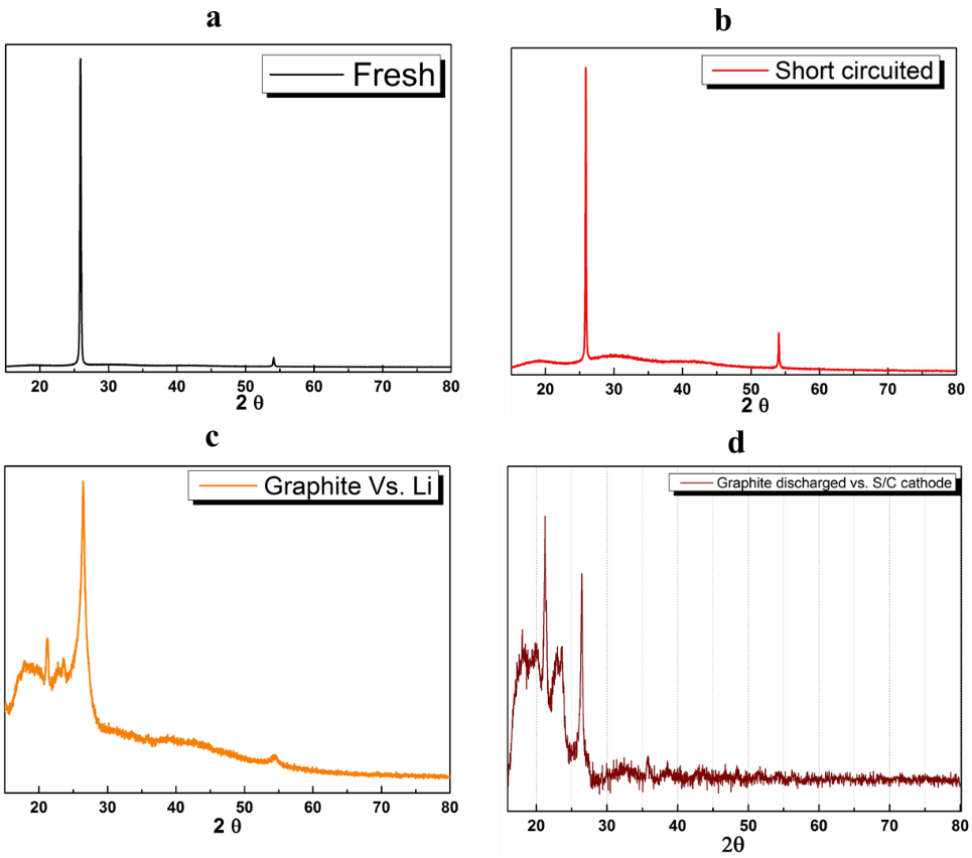


**Figure 4.5: XRD spectra after treating the graphite film in different manners i.e. a) fresh film b) after short-circuiting in electrolyte with Li metal c) after discharge vs. Li and d) after discharge vs. sulphur composite cathode.**

Upon discharge versus sulphur cathode, by utilising the graphite film upon Li-anode as pseudo-anode or as a protective layer, shows no obvious peaks for lithiation of the graphite.

One of the possible reasons could be the formation of a surface film on the graphite as lithiated graphite is quite reactive thereby concealing the peaks. Although, few new peaks were noticed at ~21.24$^{o}$, 23.7$^{o}$, and 26.29$^{o}$, as can be seen in Figure 4.6, those might be indicative slightly shifted peaks of sulphur.

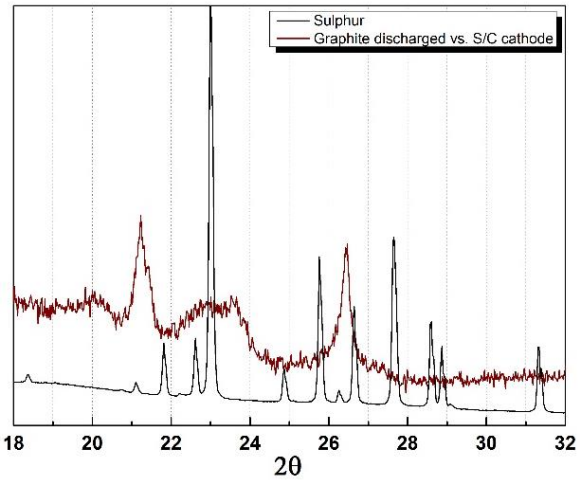


**Figure 4.6: XRD analysis of graphite discharged vs. S/C composite cathode with comparison to elemental sulphur.**

### 3.9.1.1.3 In-situ XRD

Ex-situ studies did not provide clear evidences of the role of the graphite on the Li anode in a Li-S cell and therefore in-situ studies were pursued. The goal was to understand whether the graphite film on the Li anode was acting only as a physical barrier or does it take part in the lithiation/delithiation process acting as a pseudo anode.

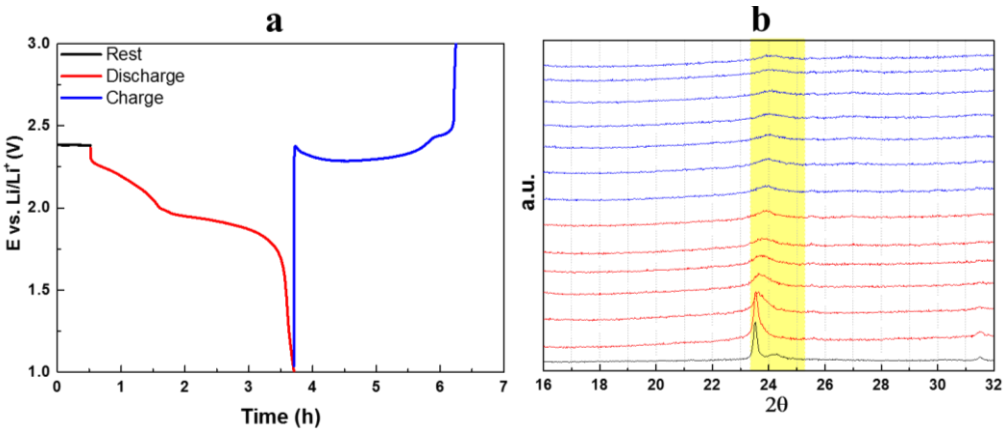


**Figure 4.7: a) Initial rest-discharge-charge voltage profile of graphite film with Li-anode vs. S composite cathode b) in-situ XRD measurement spectra for rest (black), discharge (red) and charge (blue)at C/10 in the range of 1-3V.**

Figure 4.7 shows in-situ XRD measurement data for a Li-S cell with a Li metal and graphite film as anode, The XRD of the graphite film at the initial rest stage of the cell shows peaks at around 23.5°, which at discharge and charge moves towards higher theta values along with peak broadening showing that delithiation of the graphite takes place. Delithiation of the graphite at the initial stage was puzzling. Therefore, the X-ray spectrum of the pure graphite film was compared.

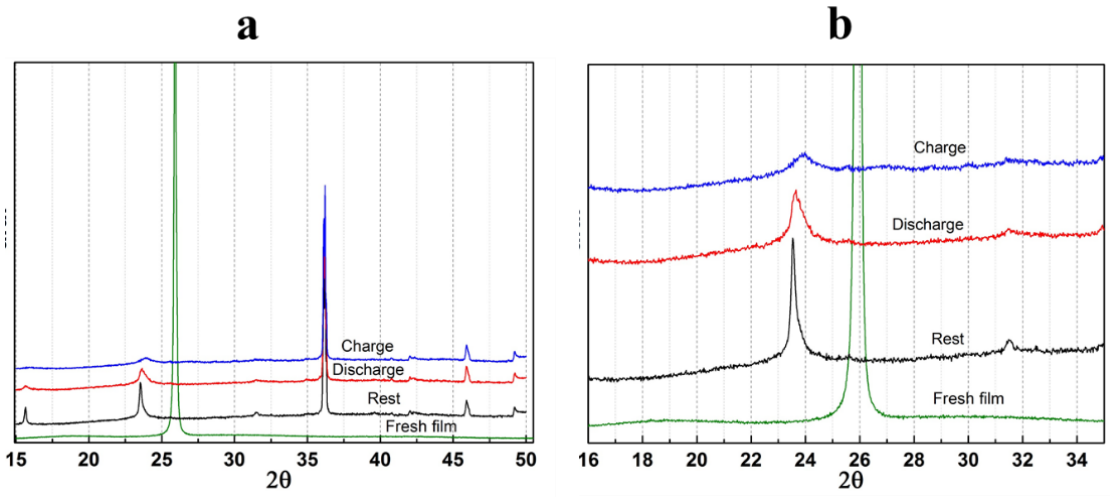


**Figure 4.8: Comparison of XRD spectra of fresh graphite film with spectra taken at rest, discharge and charge state b) the enhance spectra to observe the obvious shift in peaks.**

In Figure 4.8, it clearly shows shift in peaks during the rest stage that indicates the lithiation of the graphite. It also verifies that upon contact with Li-anode even before cycling the lithiation occur, which drive the peak of graphite shift from ~25.9° to ~23.8° During further cycling of the cells delithiation of the graphite occurs.

Even though, the conclusion has been derived via XRD analysis but in order to confirm the lithiation and delithiation of the graphite, ex-situ solid-state $^{7}$Li NMR was used to resolve the role of graphite.

#### 3.9.1.1.4 Solid state NMR

Series of samples have been prepared, as mentioned in the table below:

| No | Anode | Vs. | Electrolyte | C-rate | Status |
|---|---|---|---|---|---|
| 1 | Li | Graphite | LP30 | C/10 | Discharged (0.01V) |
| 2 | Li | Graphite | 1M LiTFSI in DME:Diox | ------ | Short circuited |
| 3 | Li/Graphite | S-cathode | 1M LiTFSI in DME:Diox | C/5 | Discharged (1V) |
| 4 | Li/Graphite | S-cathode | 1M LiTFSI in DME:Diox | C/5 | Discharged-charged (1 -3V) |

Figure 4.9 shows ss-NMR spectra of lithiated graphite using Li metal as anode and 1M $LiPF_6$ in EC: DMC in 1:1wt.% (LP30) as electrolyte at C/10, for intercalation as shown previously by Hahn et al.[74] Two main signals are observed in spectrum 6a resonating at 45 and 17 ppm. Signals marked with asterisks are the satellite transitions of the signals as confirmed by the 2D EXSY spectrum shown in figure 6b. There are different representative peaks for each intercalation step, the intercalation stages showing are $LiC_6$ at 45ppm, and $LiC_x$ (x>12) at 17 ppm.[75,76]

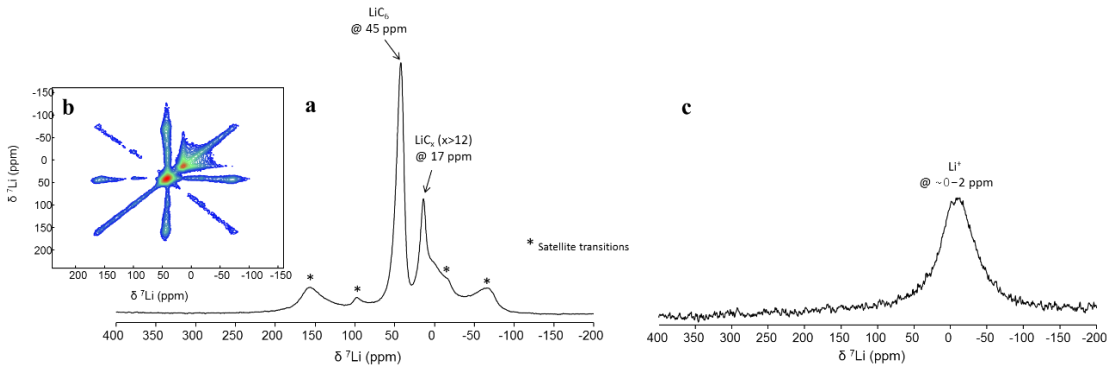


**Figure 4.9: $^7$Li solid –state NMR spectra of the graphite film at the a) discharge with Li-anode in LP30 b) c)short-circuited with Li in 1M LiTFSI in DME: Diox (1:1 vol.%).**

Similarly to the XRD analysis ssNMR confirms that by introducing in electrolyte with lithium doesn't lithiate the graphite. The spectrum shown in figure 4.9c on the other hand only shows a peak at ~ 0 to -2ppm, corresponding to the ionic $Li^+$ present in the electrolyte. Those spectra are in agreement with the results of XRD, though the metal lithium peak at 265 ppm is absent.

Figure 4.10a shows the $^7$Li-NMR of a graphite film on Li-anode after 1 cycle (discharge and charge) vs. sulphur cathode, the peak at -2ppm could signify either the presence of

ionic $Li^+$ via electrolyte or due to formation of the SEI layer. Tang et al., mentioned that it's difficult to distinguish the ionic $^7Li$ NMR signal coming from electrolyte or from the formation of passivation layer. [77] It does shows an intercalation peak, but surprisingly a signal is detected at ~ 17ppm, in agreement with the signal expected for the intercalation of 12 or more carbon atoms.[75,76] The same sample was kept overnight and a spectrum was taken again. The intensity of the signal at 17ppm is clearly decreased. Also, the signal attributed to metallic Li at 265 ppm can be seen in both spectra. The spectra represented in figure 7c corresponds to a difference spectrum obtained subtracting the spectra shown in b. Figure 4.10c shows an obvious peak at 17ppm, confirming the intercalation of >12 carbon atoms and a shoulder at 45ppm, verifying the formation of $LiC_6$.

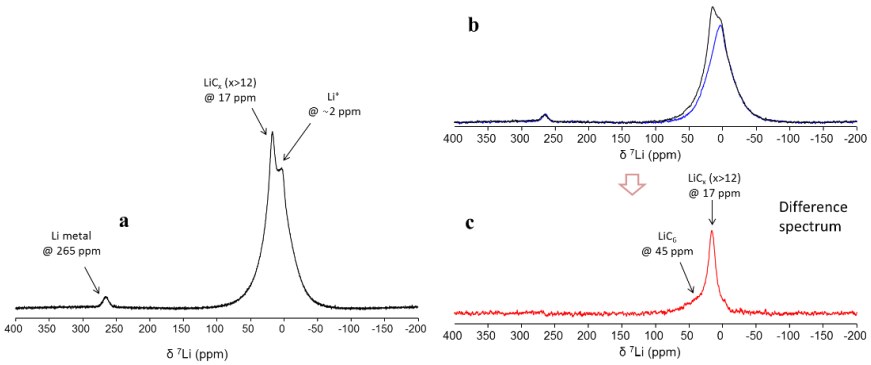


**Figure 4.10: $^7$Li NMR spectra of the graphite film at the a) 1 cycle Vs. sulphur cathode in 1M LiTFSI (DME:Diox) b) spectra taken after resting for 16 h c)difference spectrum of a and b.**

Figure 4.11 shows the spectra of graphite film on Li-anode vs. sulphur cathode but only after discharge, to see the evolution of peaks. The intercalated $Li^+$ in graphite can be reutilised during cycling process.

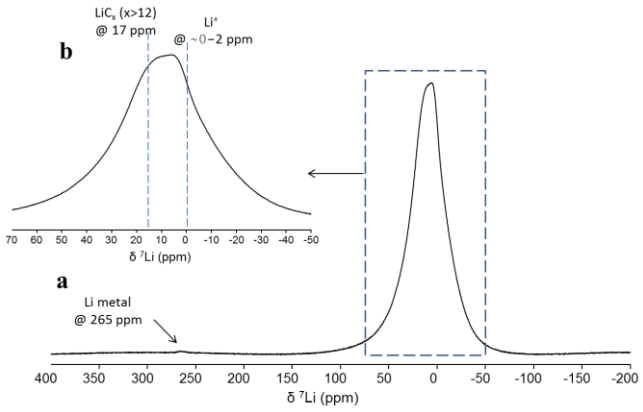


**Figure 4.11: a) $^{7}$Li NMR spectra of the graphite film after discharge vs. sulphur cathode in 1M LiTFSI (DME: Diox) b) enhanced spectra showing a doublet corresponding to ionic Li and LiCx (x>12).**

After 1 discharge a broad peak in the $^{7}$Li NMR spectrum of figure 4.11 is observed, which upon enlarging could be seen as two signals around 0 to-2 ppm and 17ppm an additional signal is also observed at 265ppm corresponding to that are transporting from lithium metal during the 1$^{st}$ discharge. The absence of the peak at 45 ppm in sample 4 can be due to de-intercalation proving the role of graphite as a hybrid anode. For e.g. if graphite is acting as pseudo-anode, which means behaving as self-regulating Li-ion reservoir, it provides the Li-ion for the electrochemical reduction of sulphur upon discharge, leading to the disappearance of the peak at $LiC_6$, while in sample 3, after charge the peak at 45 ppm could be seen, explaining the intercalation or retrieving of the Li-ions back from electrolyte into graphite film.

### 3.9.1.2 Electrochemical characterization:

Galvanostatic cycling was carried out at C/20 by placing a self-standing layer of graphite (75-100µm thickness) over Li-anode vs. composite C/S cathode. The figure 4.12 shows lower 1$^{st}$ discharge capacity (~495 mA h g$^{-1}$) as compared to blank (~1004 mA h g$^{-1}$) with similar coulombic efficiency (~55%) up to 10 cycles. High irreversible capacity of blank during 1$^{st}$ discharge could be due to the unstable SEI layer formation often observed in

the case of Li metal,[78] which could be prevented for the cells at first cycles with additional graphite layer that has a stable SEI layer formation. The faster capacity fade could be correlated to the contact resistance between the self-standing graphite films and the Li metal anode or due to a lesser extent of the lithiation of the graphite as seen from the NMR results.

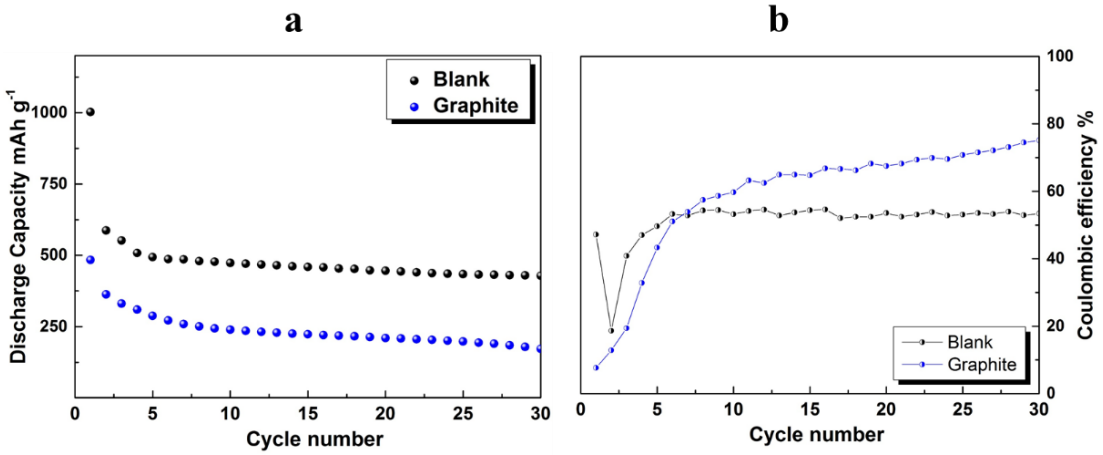


**Figure 4.12: Graphite layer on the surface of Li-anode a) comparative discharge capacities of cell with and without graphite layer. b) Comparative coulombic efficiency graph.**

In order to comprehend the role of graphite as hybrid anode, the 3 electrode Swagelok design was tested with external connection for shortening of the cell. For instance, NMR and XRD studies have proven that graphite plays a role of functional active layer in intercalation and deintercalation rather than just behave as protective layer.

Galvanostatic cycling for externally connected 3-electrode cell carried out at C/20 is shown in figure 4.13; internally the graphite electrode and the Li metal foil anode were separated by a glass fibre separator. The initial discharge capacity deliverance was found to be low (~205 mAh $g^{-1}$).

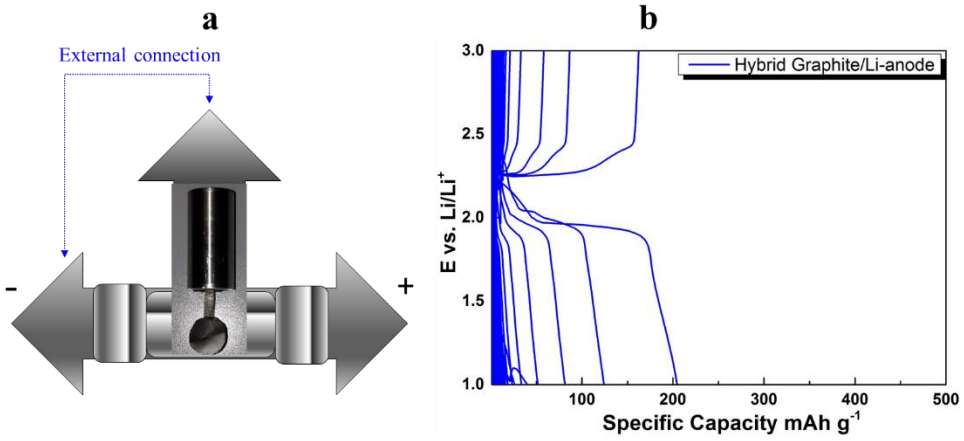


**Figure 4.13: a) 3 electrode design for external short-circuiting of graphite layer with Li metal anode. b) Galvanostatic voltage vs capacity profile.**

Capacity fading with each cycle was around 50%. Meanwhile the distinctive plateaus of Li-S system have been observed at ~2.4 and 2.0 V. The physical reason of lower capacity and fading within cycling that is more rapid than the previous cell configuration could also be a contribution from the cell pressure when compared to CR2032 coin cell configuration.

In order to confirm the effects of cell pressure the hybrid anode structure was carried out in a coin cell CR2032, The graphite film was pressed onto a stainless steel grid and the grid was connected to the Li anode internally as shown in the schematic in figure 11a. The initial discharge capacity at a c rate of C/5 was ~250 mAh $g^{-1}$ (figure 11 b), which increased to 340 mAh $g^{-1}$ on $2^{nd}$ cycle. After the $2^{nd}$ cycle the capacity started to fade with 8% of drop in capacity within each cycle.

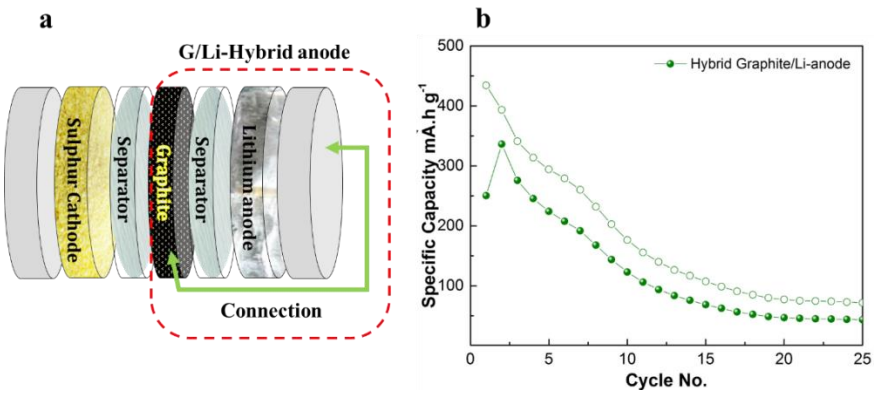


**Figure 4.14: a) Schematic illustration of the hybrid anode containing Li-S battery. b) Galvanostatic discharge/charge capacity graphs showing the huge capacity fade upon 25$^{th}$ cycle, with 8% drop since 2$^{nd}$ cycle.**

The results shown in 13 can prove the working principle of hybrid anode architecture, although it needs to be optimised and revised with improved conditions.

Increasing the C-rate from C/20 to C/5 and testing the cathodes with a lower surface area carbon composite ($62 m^2 g^{-1}$) prepared by DMSO technique, with and without graphite layers on the Li anode is shown in Figure 4.15. The 1$^{st}$ cycle voltage profiles at C/5 show that there is a slight enhancement in capacity when compared to the cell without the graphite layer.

There was no shuttling effect that was observed within Csp/S composite cathode; therefore further experiments were carried out with Csp/S composite electrodes. The capacity fade observed in the cells with graphite layer could be due to interfacial contacts and therefore in order to avoid this direct deposition of graphite slurry on Li-anode using polymeric binder as mentioned in *Chapter 3* was carried out

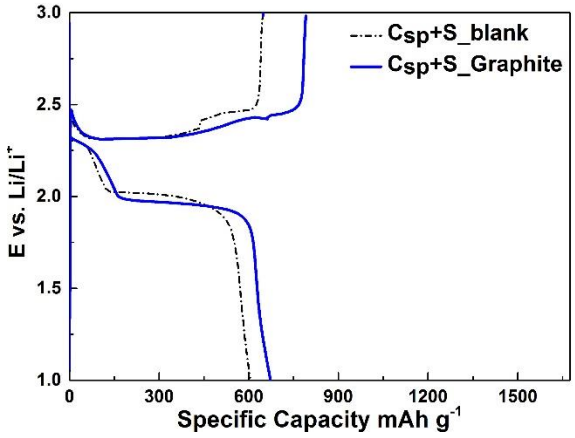


**Figure 4.15: Galvanostatic cycling profile with and without graphite protective layer with Csp/sulphur as composite cathode.**

The discharge capacity observed by direct deposition of graphite on the Li-anode at C/5, were surprisingly low, the initial discharge capacity was ~ 100 mAh $g^{-1}$ as shown in Figure 4.16.

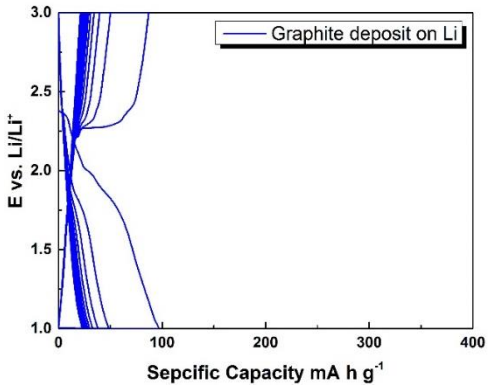


**Figure 4.16: Galvanostatic cycling of graphite deposited Li anode based Li-S cells**

The most probable reason could be due to segregation of the graphite particles during the evaporation process on the Li foil thereby leaving some regions with only the polymer binder which is insulating, on the surface of the lithium thereby make it difficult to access the Li metal.

In the meantime, due to interesting properties of reduced graphene oxide (rGO), we decided to utilise rGO as a protective layer/physical barrier, or as proven by graphite, a pseudo-anode structure by playing a role in lithiation and delithiation.

## *3.9.2 Graphene (rGO)*

### 3.9.2.1 Electrochemical characterization

Three different types of reduced graphene oxide have been used for this study. rGO-1 and rGO-2 has been synthesized by modified hummer's method and after this step, rGO-1 was thermally reduced, while rGO-2 was chemically reduced. rGO-3 was purchased from Graphene-A, which is also chemically reduced graphene oxide.

rGO-1 synthesised at CIC in the form of self-standing membranes (50-100µm) was used as a protective layer on the Li anode and Li-S cells were constructed.

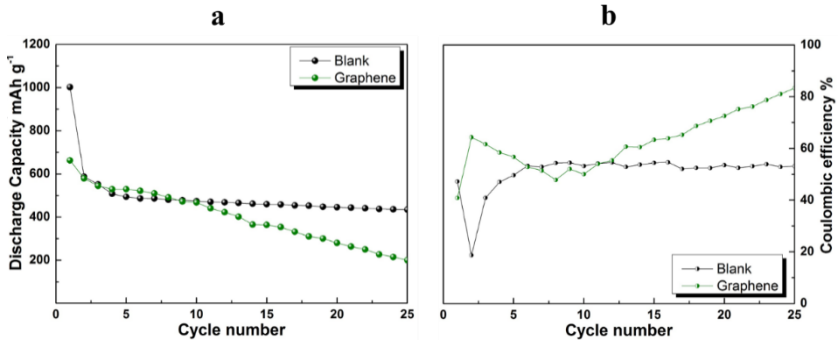


**Figure 4.17: a) Galavanostatic capacity graph by using rGO layer on Li-anode with comparison to blank. b) Coulombic efficiency of cells with and without rGO layer.**

The charge/discharge capacity of the cells with rGO-1 shows a higher initial discharging capacity as shown in Figure 4.17, which is better than the graphite layer, but still capacity fading was observed. Post-mortem analysis of the cells showed cracking of the rGO-1 films on the Li anode since the self-standing membranes were brittle in nature.

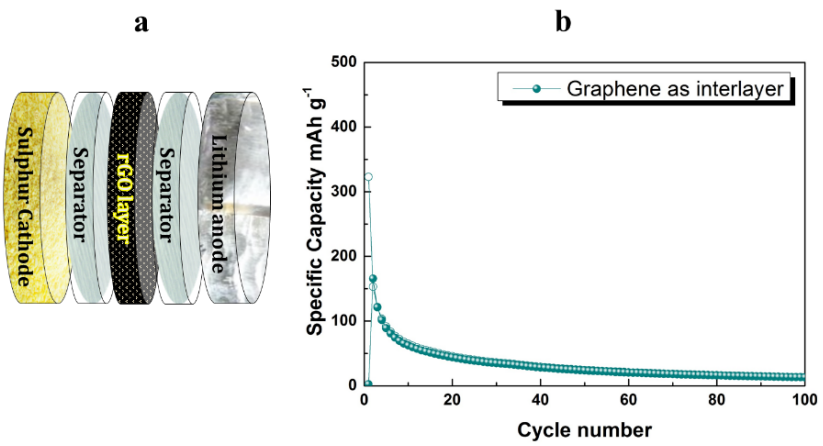


**Figure 4.18: a) Schematic illustration of the hybrid anode structure within a coin cell CR2032. b) Specific capacity curve of graphene used as an interlayer in Li-S systems.**

r-GO1 membranes were placed in between two separators as a physical barrier towards polysulphides. Manthiram et al., [79] demonstrated that by inserting a carbon interlayer in between cathode and separator, full theoretical capacity values can be achieved via redox couple of long-chain polysulphide. The attempt of applying rGO-1 layer doesn't seem to work (Figure 4.18). Upon post-mortem inspection the membranes were found to have some cracks which lead to a conclusion that a flexible non-brittle layer is required for these experiments.

Therefore in order to fabricate a thinner and non-cracking layer on the Li anode, the drop-casting technique was used. 100 µm thick deposit on the Li-anode surface was achieved with all the three reduced graphene oxide namely rGO-1, rGO2 and rGO-3 and the samples were dried overnight inside the glovebox.

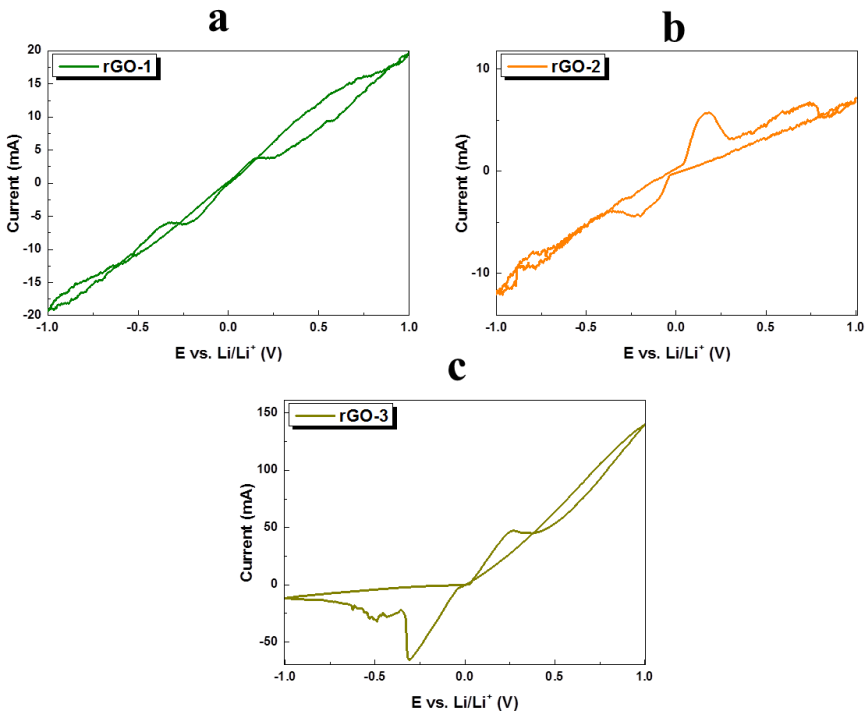


**Figure 4.19: a) rGO-1 (thermally reduced graphene) deposited Li-anode b) rGO-2 (chemically reduced graphene) deposited Li-anode c) rGO-3 (commercial) deposited Li-anode.**

To study the normal stripping/plating behaviour of those casted Li-anodes, symmetrical cells were assembled by using 1M LiTFSI (DME: Diox) as Li-ion conducting electrolyte. The normal Li-stripping/plating behaviour has been observed within all 3 kinds of graphene deposit (Figure 4.19) with a current fluctuation indicating the crucial need for homogenous and uniform deposits

The EIS measurement has been conducted on the symmetric cells (Figure 4.20), before and after performing the CV experiment. rGO-1 shows 2 semicircles in the region of HF and LF, which after CV remains unchanged, the resistance of 1$^{st}$ semicircle stayed unaltered, but the resistance of 2$^{nd}$ semicircle partially increases. The 2$^{nd}$ semicircle might be the contribution from the rGO layer, rGO-2, though shows reduced resistance with only one semi-circle, it can be a proof of having better interfacial contacts between graphene layer and Li-anode.

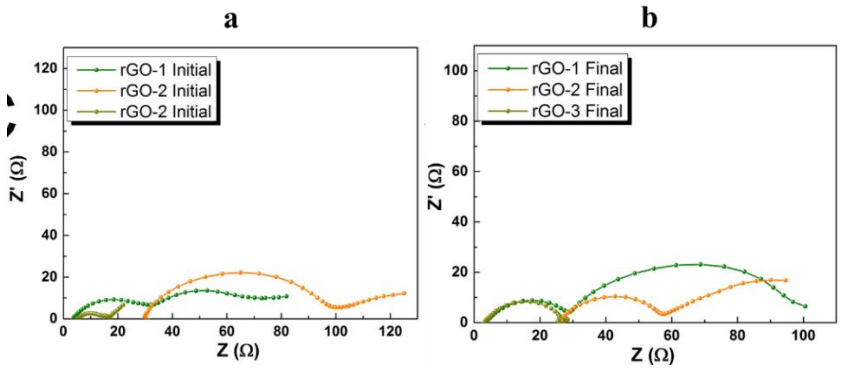


**Figure 4.20: a) EIS measurement graph taken before CV measurements for 3 kinds of rGO. b) EIS measurement graph taken after CV measurements.**

Graphene rGO-3, however had the least resistance in initial stage as well only one semicircle has been observed in initial and final stage, while after the CV the resistance increases slightly.

Lastly the deposited Li-anode with rGO was tested in galvanostatic cycling mode, all three of rGOs were cycled at C/5 in the same conditions. rGO-1 shows reduced initial discharge capacity of ~120 mAh $g^{-1}$, which upon cycling seems to be increasing. In figure 4.21c, the $8^{th}$ cycle shows ~310 mAh $g^{-1}$, which remains quite stable upon further cycling.

The reason could be different nature of SEI layer formation (thinner, thicker, irregular) step in the $1^{st}$ cycle with different rGO's, probably due to the oxygen content present in r-GO cause of synthesizing by different sources or methods.

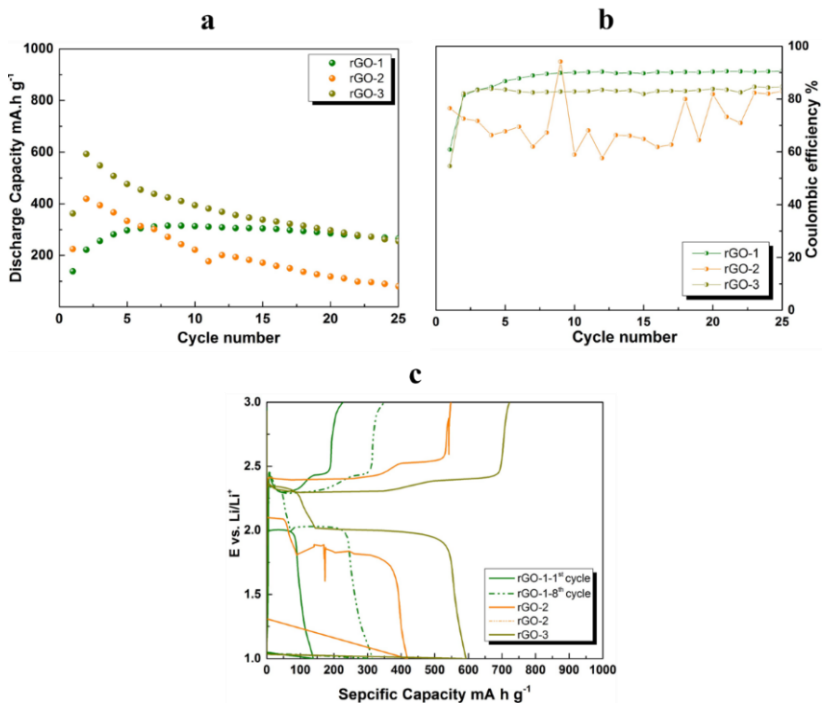


**Figure 4.21: a) Galvanostatic capacity graph comparing the 3 different rGOs b) Coulombic efficiency of all 3 rGOs c) the voltage profile showing 1st and 8th cycle of rGO-1, while 2nd cycle of rGO-2 and rGO-3.**

In rGO-3, 1st cycle shows discharge capacity of ~390 mAh $g^{-1}$, while the 2nd cycle shows discharge capacity of ~600 mAh $g^{-1}$. Out of the three rGO rGO3 was found to having a better performance. Thus the performance of the cells not only depends on the better interfacial contacts with the Li anode but as well depends on the different SEI layer with repect to the property of the rGO's.

## 3.10 Conclusion

Hybrid anode architectural design has been presented by using graphite/reduced graphene oxide with lithium metal. This hybrid anode is used to control undesirable parasitic reactions on the surface of metallic Li-anode, leading to better performance of Li-S batteries. The physico-chemical characterization using *in situ*-XRD, SEM morphology and XRD analysis, solid-state NMR spectroscopy indicates the partial lithiation of the protective layers takes place during the discharge/charge reaction.Electrochemical

characterisation by EIS, CV and galvanostatic cycling measurements in the Li-S cells indicates that although the performance of the cells were not remarkeable with the non lithiated protective graphite/graphene layers, this work paves the feasibility to construct Li-S cells with protective layers with a choice of different graphite/graphene oxides with polymer binders instead of expensive deposition techniques like PLD and sputtering This work also show that the partial lithiation of the protective layer observed in the hybrid configuration will compensate to some extent towards the loss of Li spent in the formation of SEI layer in the Li-S cells and when used with a completed lithiated graphite /graphene layer can act a pseudo anode.

## 3.11References


(1) Shukla, A. K.; Prem Kumar, T. Materials for next-Generation Lithium Batteries. *Curr. Sci.* **2008**, *94*, 314–331.

(2) Tarascon, J. M.; Armand, M. Issues and Challenges Facing Rechargeable Lithium Batteries. *Nature* **2001**, *414*, 359–367.

(3) Goriparti, S.; Miele, E.; De Angelis, F.; Di Fabrizio, E.; Proietti Zaccaria, R.; Capiglia, C. Review on Recent Progress of Nanostructured Anode Materials for Li-Ion Batteries. *J. Power Sources* **2014**, *257*, 421–443.

(4) Kamali, A. R.; Fray, D. J. Tin-Based Materials As Advanced Anode Materials for Lithium Ion Batteries : A Review. *Rev.Adv.Mater.Sci.* **2011**, *27*, 14–24.

(5) Wang, B.; Luo, B.; Li, X.; Zhi, L. The Dimensionality of Sn Anodes in Li-Ion Batteries. *Mater. Today* **2012**, *15*, 544–552.

(6) Pu, W.; He, X.; Ren, J.; Wan, C.; Jiang, C. Electrodeposition of Sn–Cu Alloy Anodes for Lithium Batteries. *Electrochim. Acta* **2005**, *50*, 4140–4145.

(7) Dong, Z.; Zhang, R.; Ji, D.; Chernova, N. A.; Karki, K.; Sallis, S.; Piper, L.; Whittingham, M. S. The Anode Challenge for Lithium-Ion Batteries: A Mechanochemically Synthesized Sn-Fe-C Composite Anode Surpasses Graphitic Carbon. *Adv. Sci.* **2016**, *3*, 1–8.

(8) Teki, R.; Datta, M. K.; Krishnan, R.; Parker, T. C.; Lu, T.-M.; Kumta, P. N.; Koratkar, N. Nanostructured Silicon Anodes for Lithium Ion Rechargeable Batteries. *Small* **2009**, *5*, 2236–2242.

(9) Wen, Z.; Wang, K.; Chen, L.; Xie, J. A New Ternary Composite Lithium Silicon Nitride as Anode Material for Lithium Ion Batteries. *Electrochem. commun.* **2006**, *8*, 1349–1352.

(10) Wu, H.; Chan, G.; Choi, J. W.; Ryu, I.; Yao, Y.; McDowell, M. T.; Lee, S. W.; Jackson, A.; Yang, Y.; Hu, L.; *et al.* Stable Cycling of Double-Walled Silicon Nanotube Battery Anodes through Solid–electrolyte Interphase Control. *Nat. Nanotechnol.* **2012**, *7*, 310–315.

(11) Wu, H.; Chan, G.; Choi, J. W.; Ryu, I.; Yao, Y.; Mcdowell, M. T.; Woo, S.; Jackson, A.; Hu, L.; Cui, Y. Six Thousand Electrochemical Cycles of Double-Walled Silicon Nanotube Anodes for Lithium Ion Batteries. *SLAC Publ.*

(12) Goriparti, S.; Miele, E.; De Angelis, F.; Di Fabrizio, E.; Proietti Zaccaria, R.; Capiglia, C. Review on Recent Progress of Nanostructured Anode Materials for Li-Ion Batteries. *J. Power Sources* **2014**, *257*, 421–443.

(13) Huang, X.; Cui, S.; Chang, J.; Hallac, P. B.; Fell, C. R.; Luo, Y.; Metz, B.; Jiang, J.; Hurley, P. T.; Chen, J. A Hierarchical Tin/carbon Composite as an Anode for Lithium-Ion Batteries with a Long Cycle Life. *Angew. Chemie - Int. Ed.* **2015**, *54*, 1490–1493.

(14) Huang, C.; Xiao, J.; Shao, Y.; Zheng, J.; Bennett, W. D.; Lu, D.; Saraf, L. V; Engelhard, M.; Ji, L.; Zhang, J.; *et al.* Manipulating Surface Reactions in Lithium-Sulphur Batteries Using Hybrid Anode Structures. *Nat. Commun.* **2014**, *5*, 3015.

(15) Aurbach, D.; Zinigrad, E.; Cohen, Y.; Teller, H. A Short Review of Failure Mechanisms of Lithium Metal and Lithiated Graphite Anodes in Liquid Electrolyte Solutions. **2002**, *148*, 405–416.

(16) Shu, Z. X.; Mcmillan, R. S.; Murray, J. J. Electrochemical Intercalation of Lithium into Graphite. *J. Electrochem. Soc.* **1993**, *140*, 922.

(17) Imanishi, N.; Kumai, K.; Kokugan, H.; Takeda, Y.; Yamamoto, O. 7Li-NMR Study of Carbon Fiber and Graphite Anodes for Lithium Ion Batteries. *Solid State Ionics* **1998**, *107*, 135–144.

(18) Arbizzani, C.; Beninati, S.; Lazzari, M.; Soavi, F.; Mastragostino, M.; Babinec, S.; Tang, H.; Talik,

A.; Hughes, S.; Meyers, G.; *et al.* Nanosized Tin Anode Prepared by Laser-Induced Vapor Deposition for Lithium Ion Battery. *J. Power Sources* **2007**, *174*, 643–647.

(19) Hantel, M. M.; Kaspar, T.; Nesper, R.; Wokaun, A.; Koetz, R. Partially Reduced Graphite Oxide as Anode for Li-Capacitors. *Ecs Electrochem. Lett.* **2012**, *1*, A1–A3.

(20) Vizintin, A.; Patel, M. U. M.; Genorio, B.; Dominko, R. Effective Separation of Lithium Anode and Sulfur Cathode in Lithium-Sulfur Batteries. *ChemElectroChem* **2014**, *1*, 1040–1045.

(21) Lin, D.; Liu, Y.; Liang, Z.; Lee, H.-W.; Sun, J.; Wang, H.; Yan, K.; Xie, J.; Cui, Y. Layered Reduced Graphene Oxide with Nanoscale Interlayer Gaps as a Stable Host for Lithium Metal Anodes. *Nat. Nanotechnol.* **2016**, 1–8.

(22) Zhang, Y.; Xia, X.; Wang, D.; Wang, X.; Gu, C.; Tu, J. Integrated Reduced Graphene Oxide multilayer/Li Composite Anode for Rechargeable Lithium Metal Batteries. *RSC Adv.* **2016**, *6*, 11657–11664.

(23) Lee, S. H.; Harding, J. R.; Liu, D. S.; D'Arcy, J. M.; Yang, S. H.; Hammond, P. T. Li-Anode Protective Layers for Li Rechargeable Batteries via Layer-by-Layer Approaches. *Chem. Mater.* **2014**, *26*, 2579–2585.

(24) Hassoun, J.; Bonaccorso, F.; Agostini, M.; Angelucci, M.; Betti, M. G.; Cingolani, R.; Gemmi, M.; Mariani, C.; Panero, S.; Pellegrini, V.; *et al.* An Advanced Lithium-Ion Battery Based on a Graphene Anode and a Lithium Iron Phosphate Cathode. *Nano Lett.* **2014**, *14*, 4901–4906.

(25) Manthiram, A.; Fu, Y.; Chung, S.-H.; Zu, C.; Su, Y.-S. Rechargeable Lithium–Sulfur Batteries. *Chem. Rev.* **2014**, 140715153614001.

(26) Smith, a. J.; Burns, J. C.; Zhao, X.; Xiong, D.; Dahn, J. R. Publisher's Note: A High Precision Coulometry Study of the SEI Growth in Li/Graphite Cells [J. Electrochem. Soc., 158, A447 (2011)]. *J. Electrochem. Soc.* **2011**, *158*, S23.

(27) Li, S.; Xie, M.; Liu, J.; Wang, H.; Yan, H. Layer Structured Sulfur/Expanded Graphite Composite as Cathode for Lithium Battery. *Electrochem. Solid-State Lett.* **2011**, *14*, A105.

(28) Huang, J.-Q.; Zhuang, T.-Z.; Zhang, Q.; Peng, H.-J.; Chen, C.-M.; Wei, F. Permselective Graphene Oxide Membrane for Highly Stable and Anti-Self-Discharge Lithium–Sulfur Batteries. *ACS Nano* **2015**, 150218141233002.

(29) Vizintin, A.; Lozinšek, M.; Chellappan, R. K.; Foix, D.; Krajnc, A.; Mali, G.; Drazic, G.; Genorio, B.; Dedryvère, R.; Dominko, R. Fluorinated Reduced Graphene Oxide as an Interlayer in Li–S Batteries. *Chem. Mater.* **2015**, *27*, 7070–7081.

(30) Scrosati, B.; Garche, J. Lithium Batteries: Status, Prospects and Future. *J. Power Sources* **2010**, *195*, 2419–2430.

(31) Girishkumar, G.; McCloskey, B.; Luntz, A. C.; Swanson, S.; Wilcke, W. Lithium−Air Battery: Promise and Challenges. *J. Phys. Chem. Lett.* **2010**, *1*, 2193–2203.

(32) Kim, H.; Lim, H.-D.; Kim, J.; Kang, K. Graphene for Advanced Li/S and Li/air Batteries. *J. Mater. Chem. A* **2014**, *2*, 33.

(33) Nazri, G. A. *Lithium Batteries: Science and Technology*; 2009; Vol. 34.

(34) Brandt, K. Historical Development of Secondary Lithium Batteries. *Solid State Ionics* **1994**, *69*, 173–183.

(35) Zheng, S.; Chen, Y.; Xu, Y.; Yi, F.; Zhu, Y.; Liu, Y.; Yang, J.; Wang, C. In Situ Formed Lithium Sulfide/Microporous Carbon Cathodes for Lithium-Ion Batteries. *ACS Nano* **2013**, *7*, 10995–11003.

(36) Elazari, R.; Salitra, G.; Gershinsky, G.; Garsuch, A.; Panchenko, A.; Aurbach, D. Rechargeable Lithiated Silicon-Sulfur (SLS) Battery Prototypes. *Electrochem. commun.* **2012**, *14*, 21–24.

(37) Tsubouchi, S.; Domi, Y.; Doi, T.; Ochida, M.; Nakagawa, H.; Yamanaka, T.; Abe, T.; Ogumi, Z. Spectroscopic Analysis of Surface Layers in Close Contact with Edge Plane Graphite Negative-Electrodes. *J. Electrochem. Soc.* **2013**, *160*, A575–A580.

(38) Nakagawa, H.; Domi, Y.; Doi, T.; Ochida, M.; Tsubouchi, S.; Yamanaka, T.; Abe, T.; Ogumi, Z. In Situ Raman Study on the Structural Degradation of a Graphite Composite Negative-Electrode and the Influence of the Salt in the Electrolyte Solution. *J. Power Sources* **2013**, *236*, 138–144.

(39) Zheng, H.; Qu, Q.; Zhang, L.; Liu, G.; Battaglia, V. S. Hard Carbon: A Promising Lithium-Ion Battery Anode for High Temperature Applications with Ionic Electrolyte. *RSC Adv.* **2012**, *2*, 4904–4912.

(40) Li, C.; Li, D.; Qiu, C.; Hou, W. Dendritic Amphiphiles of Carbosilane Dendrimers with Peripheral PEG for Drug Encapsulation. *J. Polym. Res.* **2013**, *20*, 1–6.

(41) F. Orsini, A. du Pasquier, B. Beaudouin, J.M. Tarascon, M. Trentin, N. Langenhuizen, E. de Beer, P. N. In Situ SEM Study of the Interfaces in Plastic Lithium Cells. *J. Power Sources* **1999**, *81–82*, 918–921.

(42) Landi, B. J.; Ganter, M. J.; Cress, C. D.; DiLeo, R. a.; Raffaelle, R. P. Carbon Nanotubes for Lithium Ion Batteries. *Energy Environ. Sci.* **2009**, *2*, 638.

(43) Candelaria, S. L.; Shao, Y.; Zhou, W.; Li, X.; Xiao, J.; Zhang, J.-G.; Wang, Y.; Liu, J.; Li, J.; Cao, G. Nanostructured Carbon for Energy Storage and Conversion. *Nano Energy* **2012**, *1*, 195–220.

(44) Hou, J.; Shao, Y.; Ellis, M. W.; Moore, R. B.; Yi, B. Graphene-Based Electrochemical Energy Conversion and Storage: Fuel Cells, Supercapacitors and Lithium Ion Batteries. *Phys. Chem. Chem. Phys.* **2011**, *13*, 15384–15402.

(45) Cui, G.; Gu, L.; Zhi, L.; Kaskhedikar, N.; van Aken, P. A.; Müllen, K.; Maier, J. A Germanium–Carbon Nanocomposite Material for Lithium Batteries. *Adv. Mater.* **2008**, *20*, 3079–3083.

(46) Kim, C.; Yang, K. S.; Kojima, M.; Yoshida, K.; Kim, Y. J.; Kim, Y. A.; Endo, M. Fabrication of Electrospinning-Derived Carbon Nanofiber Webs for the Anode Material of Lithium-Ion Secondary Batteries. *Adv. Funct. Mater.* **2006**, *16*, 2393–2397.

(47) Novoselov, K. S.; Geim, A. K.; Morozov, S. V; Jiang, D.; Zhang, Y.; Dubonos, S. V; Grigorieva, I. V; Firsov, A. A. Electric Field Effect in Atomically Thin Carbon Films. *Science (80-. ).* **2004**, *306*, 666–669.

(48) Miao, F.; Wijeratne, S.; Zhang, Y.; Coskun, U. C.; Bao, W.; Lau, C. N. Phase-Coherent Transport in Graphene Quantum Billiards. *Science (80-. ).* **2007**, *317*, 1530–1533.

(49) Peres, N. M. R.; Castro Neto, A. H.; Guinea, F. Conductance Quantization in Mesoscopic Graphene. *Phys. Rev. B* **2006**, *73*, 195411.

(50) Lian, P.; Zhu, X.; Liang, S.; Li, Z.; Yang, W.; Wang, H. Large Reversible Capacity of High Quality Graphene Sheets as an Anode Material for Lithium-Ion Batteries. *Electrochim. Acta* **2010**, *55*, 3909–3914.

(51) Wang, G.; Shen, X.; Yao, J.; Park, J. Graphene Nanosheets for Enhanced Lithium Storage in Lithium Ion Batteries. *Carbon N. Y.* **2009**, *47*, 2049–2053.

(52) Li, X.; Wang, X.; Zhang, L.; Lee, S.; Dai, H. Chemically Derived, Ultrasmooth Graphene Nanoribbon Semiconductors. *Science (80-. ).* **2008**, *319*, 1229–1232.

(53) Mcallister, M. J.; Li, J.; Adamson, D. H.; Schniepp, H. C.; Abdala, A. a; Liu, J.; Herrera-alonso, O. M.; Milius, D. L.; Car, R.; Prud, R. K.; *et al.* Single Sheet Functionalized Graphene by Oxidation and Thermal Expansion of Graphite. *Chem. Mater.* **2007**, *19*, 4396–4404.

(54) Lu, J.; Yang, J.; Wang, J.; Lim, A.; Wang, S.; Loh, K. P. One-Pot Synthesis of Fluorescent Carbon Nanoribbons, Nanoparticles, and Graphene by the Exfoliation of Graphite in Ionic Liquids. *ACS Nano* **2009**, *3*, 2367–2375.

(55) Dato, A.; Radmilovic, V.; Lee, Z.; Phillips, J.; Frenklach, M. Substrate-Free Gas-Phase Synthesis of Graphene Sheets. *Nano Lett.* **2008**, *8*, 2012–2016.

(56) Kim, K. S. K. S.; Zhao, Y.; Jang, H.; Lee, S. Y.; Kim, J. M.; Kim, K. S. K. S.; Ahn, J.-H.; Kim, P.; Choi, J.-Y.; Hong, B. H. Large-Scale Pattern Growth of Graphene Films for Stretchable Transparent Electrodes. *Nature* **2009**, *457*, 706–710.

(57) Reina, A.; Jia, X.; Ho, J.; Nezich, D.; Son, H.; Bulovic, V.; Dresselhaus, M. S.; Jing, K. Large Area, Few-Layer Graphene Films on Arbitrary Substrates by Chemical Vapor Deposition. *Nano Lett.* **2009**, *9*, 30–35.

(58) Li, X.; Zhang, G.; Bai, X.; Sun, X.; Wang, X.; Wang, E.; Dai, H. Highly Conducting Graphene Sheets and Langmuir-Blodgett Films. *Nat Nano* **2008**, *3*, 538–542.

(59) Hernandez, Y.; Nicolosi, V.; Lotya, M.; Blighe, F.; Sun, Z.; De, S.; McGovern, I. T.; Holland, B.; Byrne, M.; Gunko, Y.; *et al.* High Yield Production of Graphene by Liquid Phase Exfoliation of Graphite. *Nat. Nanotechnol.* **2008**, *3*, 563–568.

(60) Hummers, W. S.; Offeman, R. E. Preparation of Graphitic Oxide. *J. Am. Chem. Soc.* **1958**, *80*, 1339–1339.

(61) Wu, Y.; Jiang, C.; Wan, C.; Tsuchida, E. Effects of Catalytic Oxidation on the Electrochemical Performance of Common Natural Graphite as an Anode Material for Lithium Ion Batteries. *Electrochem. commun.* **2000**, *2*, 272–275.

(62) Jeong, S. S.; Lim, Y. T.; Choi, Y. J.; Cho, G. B.; Kim, K. W.; Ahn, H. J.; Cho, K. K. Electrochemical Properties of Lithium Sulfur Cells Using PEO Polymer Electrolytes Prepared under Three Different Mixing Conditions. *J. Power Sources* **2007**, *174*, 745–750.

(63) Suo, L.; Hu, Y.-S.; Li, H.; Armand, M.; Chen, L. A New Class of Solvent-in-Salt Electrolyte for High-Energy Rechargeable Metallic Lithium Batteries. *Nat. Commun.* **2013**, *4*, 1481.

(64) Ji, X.; Lee, K. T.; Nazar, L. F. A Highly Ordered Nanostructured Carbon-Sulphur Cathode for Lithium-Sulphur Batteries. *Nat. Mater.* **2009**, *8*, 500–506.

(65) Wang, H.; Yang, Y.; Liang, Y.; Robinson, J. T.; Li, Y.; Jackson, A.; Cui, Y.; Dai, H. Graphene-Wrapped Sulfur Particles as a Rechargeable Lithium-Sulfur Battery Cathode Material with High Capacity and Cycling Stability. *Nano Lett.* **2011**, *11*, 2644–2647.

(66) Yamin, H. 123 Lithium Sulfur Battery. *J. Electrochem. Soc.* **1988**, *135*, 1045.

(67) Wang, J. L.; Yang, J.; Xie, J. Y.; Xu, N. X.; Li, Y. Sulfur-Carbon Nano-Composite as Cathode for Rechargeable Lithium Battery Based on Gel Electrolyte. *Electrochem. commun.* **2002**, *4*, 499–502.

(68) Liang, M.; Zhi, L. Graphene-Based Electrode Materials for Rechargeable Lithium Batteries. *J. Mater. Chem.* **2009**, *19*, 5871.

(69) Su, Y.-S.; Manthiram, A. A New Approach to Improve Cycle Performance of Rechargeable Lithium-Sulfur Batteries by Inserting a Free-Standing MWCNT Interlayer. *Chem. Commun.* **2012**, *48*, 8817–8819.

(70) Wang, B.; Li, K.; Su, D.; Ahn, H.; Wang, G. Superior Electrochemical Performance of Sulfur/Graphene Nanocomposite Material for High-Capacity Lithium–Sulfur Batteries. *Chem. – An Asian J.* **2012**, *7*, 1637–1643.

(71) Yao, H.; Yan, K.; Li, W.; Zheng, G.; Kong, D.; Seh, Z. W.; Narasimhan, V. K.; Liang, Z.; Cui, Y. Improved Lithium–sulfur Batteries with a Conductive Coating on the Separator to Prevent the Accumulation of Inactive S-Related Species at the Cathode–separator Interface. *Energy Environ. Sci.* **2014**, *7*, 3381–3390.

(72) Zhou, G.; Pei, S.; Li, L.; Wang, D.-W.; Wang, S.; Huang, K.; Yin, L.-C.; Li, F.; Cheng, H.-M. A Graphene-Pure-Sulfur Sandwich Structure for Ultrafast, Long-Life Lithium-Sulfur Batteries. *Adv. Mater.* **2014**, *26*, 625–631.

(73) Botas, C.; Álvarez, P.; Blanco, C.; Santamaría, R.; Granda, M.; Ares, P.; Rodríguez-Reinoso, F.; Menéndez, R. The Effect of the Parent Graphite on the Structure of Graphene Oxide. *Carbon N. Y.* **2012**, *50*, 275–282.

(74) Hahn, M.; Buqa, H.; Ruch, P. W.; Goers, D.; Spahr, M. E.; Ufheil, J.; Novák, P.; Kötz, R. A Dilatometric Study of Lithium Intercalation into Powder-Type Graphite Electrodes. *Electrochem. Solid-State Lett.* **2008**, *11*, A151.

(75) Sato, Y.; Tanuma, K.; Takayama, T.; Kobayakawa, K. Li-Nuclear Magnetic Resonance Observations of Lithium Insertion into Coke Carbon Modi ® Ed with Mesophase-Pitch. *J. Power Sources* **2001**, *98*, 165–170.

(76) Chevallier, F.; Letellier, M.; Morcrette, M.; Tarascon, J. M.; Frackowiak, E.; Rouzaud, J. N.; Béguin, F. In Situ 7Li-Nuclear Magnetic Resonance Observation of Reversible Lithium Insertion into Disordered Carbons. *Electrochem. Solid-State Lett.* **2003**, *6*, A225.

(77) Tang, W.; Goh, B.-M.; Hu, M. Y.; Wan, C.; Tian, B.; Deng, X.; Peng, C.; Lin, M.; Hu, J. Z.; Loh, K. P. *In Situ* Raman and Nuclear Magnetic Resonance Study of Trapped Lithium in the Solid Electrolyte Interface of Reduced Graphene Oxide. *J. Phys. Chem. C* **2016**, *120*, 2600–2608.

(78) Cheng, X.-B.; Zhang, R.; Zhao, C.-Z.; Wei, F.; Zhang, J.-G.; Zhang, Q. A Review of Solid Electrolyte Interphases on Lithium Metal Anode. *Adv. Sci.* **2015**, *3*, 1500213(1–20).

(79) Su, Y. S.; Fu, Y.; Guo, B.; Dai, S.; Manthiram, A. Fast, Reversible Lithium Storage with a Sulfur/long-Chain-Polysulfide Redox Couple. *Chem. - A Eur. J.* **2013**, *19*, 8621–8626.

# *Chapter 5: Polymeric ionic liquids as binder in sulphur cathodes.*

# 5 Introduction

Development of suitable cathode architecture with sulphur[1] i.e. porous structured carbons[1–3] or oxide based materials[4,5] has been well studied [6–13]. In addition, consideration has been given to the development of other components of the system i.e. binders [14,15], separators [16–18] electrolytes [19–21] and protective coating for lithium protection. [22–24]

Li-S batteries have been projected by development of electrolyte solvents (organic, aqueous and ionic liquids), salts, states (liquid, solid or polymer) and additives. Most of the work has been done with electrolytes with ether based solvents that are stable towards polysulphides and retain high polysulphide solubility. Their major drawback is a severe shuttling effect [25]. Solid state electrolytes can suppress the shuttling effect, although the rate capability is poor when compared to liquid electrolytes.[26] The study of polymer electrolyte was started in 1973 by Fenton et al.[27]. Subsequently, a large number of polymer electrolytes has been prepared and characterized. For convenience polymers can be categorized into two groups i.e., solid polymer electrolyte (SPE) and gel polymer electrolyte (GPE) are comprises of lithium salts (e.g. $LiClO_4$, $LiBF_4$, $LiPF_6$, $LiCF_3SO_3$, $LiN(CF_3SO_2)_3$) dissolved in polyether matrix of high molecular weight, (e.g., PEO and PPO).[28] Where as GPE is usually prepared by incorporation of high amount of liquid electrolyte into a polymer matrix which forms stable gel polymer host architecture. [29]

Gel polymer electrolytes (GPEs) exhibits several advantages when compared to solid or liquid electrolytes, such as fast charge/discharge, higher energy density without any shape limitations.[26,28,30]

PVdF is the most commonly used polymer used in Li-based batteries, due to its strong electron-withdrawing functional groups (-C-F) and high dielectric constant ($\varepsilon = 8.4$).[31] Cheo et al. demonstrated that electrolyte composed of PVdF-PC-LiTFSI (GPE) can offer 1.74 x $10^{-3}$ S $cm^{-1}$ of ionic conductivity.[32] PVdF have semi-crystalline structure, which

draw Li-ions into the PVdF membrane over contact.[33–37] Hence, GPE have totally open interconnected micropores, helping to enhance the interfacial surface area, Li-ion storage and flexibility of transport.[31,35,38–40] GPE exhibits lower ionic conductivity, which can be solved by introducing ionic liquids or nano-size fillers for improved polymer battery performance.

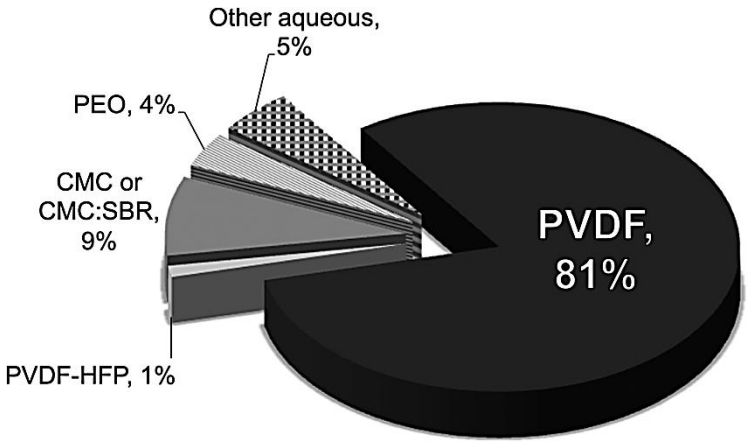


**Figure 5.1: Summary of the most commonly used binders in the Li−S literature according to 79 recent publications where electrodes were prepared from slurry casting techniques. "PVdF" includes grades referred to as only PVdF by the manufacturer or where no grade was specified.**[3]

Typically gel polymer electrolytes can simultaneously act as an electrolyte and a binder, owing to the property of the polymer material present. PVdF [14] as mentioned earlier, is the most commonly used polymer, especially in the form of binder in Li-S batteries. PVdF, normally is processed in *N*-methyl-2-pyrrolidone (NMP), which requires high drying temperatures under vacuum [41] with a risk of losing sulphur by sublimation. Whereas, upon using lower temperatures for drying process leaves a possibility of contamination with remaining NMP solvent in the electrodes [41]. In addition, hydrophobic PVdF, blocks the pores [3] in the composite electrode due to its the morphology limiting the electrolyte access and thereby affects the ionic pathways. Lately, new studies are focussed on the use of alternative binders, such as polyvinyl pyrrolidone (PVP) [42],

polytetrafluoroethylene (PTFE) [43], polyethylene oxide (PEO) [43] and water soluble binders such as carbonyl-β-cyclodextrin (C-β-CD), etc. [15,44,45] for Li-S batteries.

## *5.1 Gel polymer electrolyte (GPE) ionic liquid as a binder*

Moving from liquid to polymer electrolyte systems, safety of the battery enhances owing to reduced probability for internal short-circuiting, absence of combustion reaction products and no electrolyte leakage [25,46–48]. GPE can be a very promising choice for Li-S batteries.[25,49–52]

Incorporating organic electrolyte with ionic liquid was first mentioned by Fernicaola et al., to enhance ionic conductivity and stabilize Li-ion conceded at the surface of polymer (PVdF).[53] 1-n- Butyl-3-methylimidazolium hexafluorophospate ($BMIPF_6$) an aprotic IL was reported by Balducci et al. and was used in hybrid super-capacitor with activated cabon and poly(3-methyl-thiophene) for better cycle life.[54] Egashira *et al*. demonstrated that ion mobility depends on solubility of IL in polymer via GPE-IL.[55]

Additionally, Sakaebe *et al.* compared RTILs having quaternary ammonium cation and imide anion, that these cations could stabilize the reduction of metallic lithium. [56] Generally, these cathions play a role in improving the performance of Li-based batteries.[54,57,58]

The application of a gel polymer electrolyte [59] as a binder in Li-S battery is proposed in this chapter. The GPE (poly(DDA)TFSI-$PYR_{14}$TFSI-LiTFSI) is composed of 58 wt. % polymerionicliquid:poly(diallyldimethylammonium)bis(trifluoromethanesulphonyl)imide (poly (DDA)TFSI), and 1:9 mol ratio of ionic liquid:*N*-butyl-*N*-methylpyrplidinium bis(trifluoromethanesulphonyl)imide ($PYR_{14}$TFSI) with lithium salt: Lithium bis(trifluoromethylsulphonyl)imide (LiTFSI) .

Herein, the properties of the Sulphur cathodes using GPE-PIL as a binder in the composite cathode have been studied with a liquid electrolyte This would lead to simplified electrode

processing by replacement of NMP with acetonitrile or acetone as a solvent for the composite slurry processing.

## 5.2 Experimentation

Gel polymer electrolyte poly (DDA) TFSI-$PYR_{14}$TFSI-LiTFSI (GPE-PIL) was obtained from Solvionic.

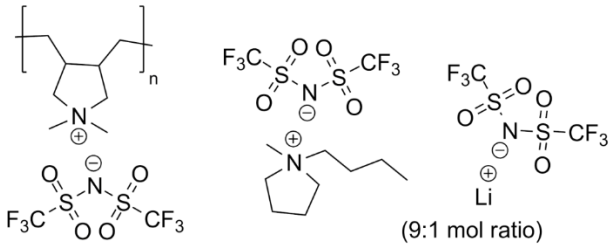


**Figure 5.2: A structural composition of the polymer electrolyte LiTFSI: PYR14TFSI (1:9 mol ratio) with 58 wt. % poly (DDA) TFSI in acetone.**

### *5.2.1 Introduction of GPE-PIL in C/S cathode*

The GPE-PIL solution as received in acetone is hygroscopic; in order to make S/C composite slurry, GPE-PIL was drop casted on Mylar film. Dried coated membranes were collected and used by weight, as a binder.

### *5.2.2 Mixing of sulphur/carbon (ECP600JD) composite with GPE-PIL*

The sulphur/carbon composite was prepared by using DMSO solvent technique. 30 wt. % of carbon black (ECP600JD) and 70 wt. % of sulphur (Sigma-Aldrich, 99.98%) were mixed in DMSO and stirred overnight at 155 °C in a closed vial. The obtained mixture was centrifuged for 45 mins at 400 rpm, the acquired product was dried at 60 °C for 24 h under vacuum.

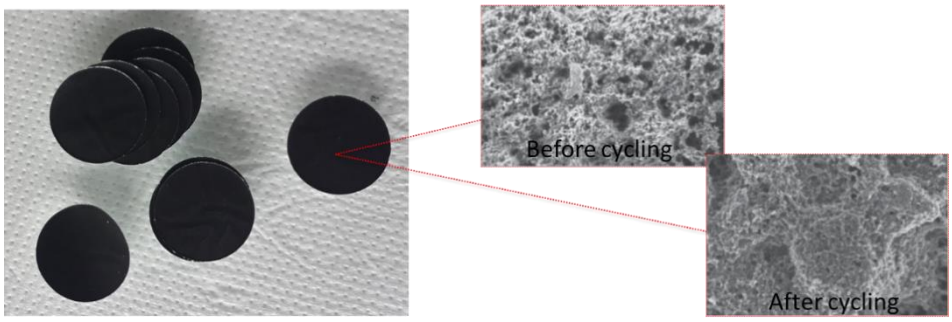


**Figure 5.3: Image of GPE-PIL-S-$C_{ECP600JD}$ cathodes after processing showing the morphology before and after cycling.**

This composite mixture (50 wt. %) was wet ball-milled with 50 wt. % of GPE-PIL for 30 mins in acetonitrile. The slurry was casted on carbon-coated Al-foil substrate and dried overnight at 50 °C under vacuum. Electrodes were punched out as spherical discs of 16 mm diameter (sulphur loading: 1 to 1.5 mg per $cm^{-2}$).

### *5.2.3 Optimization of cathode composites*

Preliminary slurry was made by simple stirring of the mixture of S/C composite with GPE-PIL binder in acetonitrile overnight inside the glovebox. The cathodes were prepared by drop casting inside the glovebox, but the quality was not very suitable for battery testing. Comparative studies have been carried out by using different solvents like acetonitrile, NMP and acetone, in order to obtain homogenous deposits. Difference in atmospheric changes was also take into account by comparing the slurries prepared inside and outside the glovebox (Table.1).

Furthermore, the effect of slurry preparation technique has also been taken into account such as hand milling, stirring or ball milling. Finally to optimize the best lamination quality we optimized the ratio of S/C and binder percentage.

**Table 5.1: Exhibition of different techniques and parameters applied for the optimisation of GPE-PIL-S-$C_{ECP600JD}$ composite cathode.**

| Solvents | Slurry preparation | Binder content (%) | Lamination (Atmosphere) |
|---|---|---|---|
| | Magnetic stirring | 30 | Ar |
| | Magnetic stirring | 50 | Ar |
| Acetonitrile | Hand milling | 50 | Ar |
| | Ball milling | 10 | Air |
| | Ball milling | 25 | Air |
| | Ballmilling | 50 | Air / Ar |
| Acetone | Ball milling | 50 | Air |
| NMP | Ball milling | 50 | Air / Ar |

GPE-PIL cathodes were mainly used in liquid cell configuration, however attempts for all solid-state configuration has been through by using GPE-PIL solid electrolyte.

### *5.2.4 Cell configuration:*

Pouch cell type batteries were assembled in argon filled glove box. Galvanostatic cycling tests of batteries have been carried out on a Maccor 4200 in a 1.5–3 V voltage range at C/20 along with a rate capability test. Detailed cell assembly can be seen in Chapter 2: Materials & methods, section: Battery configurations.

For the comparative evaluation of the electrochemical properties of GPE-PIL-S-$C_{ECP600JD}$ cathodes ordinary cathodes with PVdF binder, PVdF-$C_{ECP600JD}$-S, were prepared. The preparation method can be seen in Chap2: Materials & methods, section 2.3.1.2, sub-section 2. The conditions for galvanostatic cycling tests of the PVdF-S-$C_{ECP600JD}$ cathodes were the same as in the case of GPE-PIL-S-$C_{ECP600JD}$ cathodes.

## 5.3 Results and discussion

### *5.3.1 Physico-chemical characterization*

The morphological changes in the cross section of the electrode containing S-CEcp600JD composite covered with 50 wt. % of the GPE-PIL before and after 100 cycles were checked by using SEM. The morphological changes after 100 cycles are minor, proving the good stability of the electrodes comprising GPE-PIL-based gel type coating (Figure 5.4).

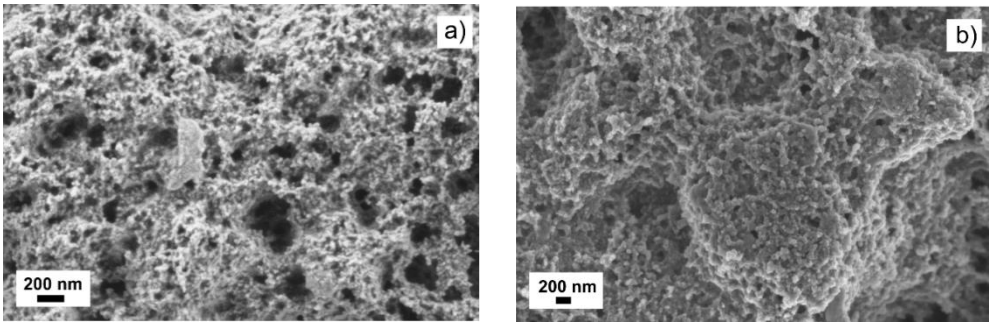


**Figure 5.4: SEM micrographs of the GPE-PIL-CEcp600JD-S: a) before cycling and b) after 100 cycles.**

To figure out the enhanced performance of GPE-PIL binder, the morphology of the composite cathode with different binders (GPE-PIL, PVdF, and PEO) have been observed (Figure 5.5). The electrode contained PVdF and PEO binder shows big sulphur patrticles on the surface. This might be a reason for shuttling as these particles can be rapidly dissolved in the electrolyte thoroughly increasing the concentration of polysulphides in the electrolyte leading to shuttle. Though, in the case of GPE-PIL binder few cracks on the surface have been observed, but the composite coating seemed to be very homogeneous.

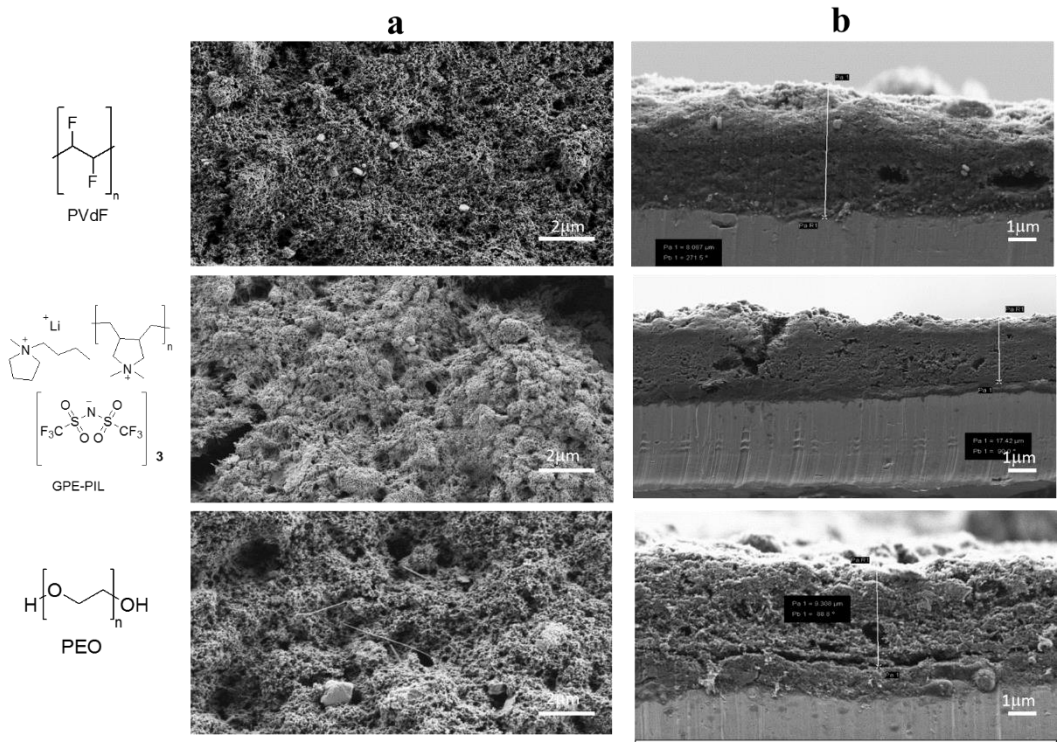


**Figure 5.5: SEM micrographs of the GPE-PIL-S-CEcp600JD cathode with comparison to PVdF-S-CEcp600JD cathode and PEO-S- CEcp600JD cathode, a) Surface view, b) Cross-section view.**

## *5.3.2 In-Situ UV/Vis measurements:*

The diffusion of polysulphides ($Li_2S_x$, $3 \leq x \leq 8$) in the cell with 50 wt. % of GPE-PIL binder has been measured by *in-situ* UV/Vis spectroscopy.[60,61] Metallic lithium used as anode (Ø=16mm) contains a hole (Ø = 13mm) separated by a glassfiber (Ø= 20mm) wetted with 40 µL for per mg of sulphur of 1 M LiTFSI in TEGDME: DIOX in 1:1vol. %. More details about UV/Visible spectroscopy, sample preparation and instrumentation have been given in chapter 2, materials & methods, section: 2.4.2.8. The spectra was recorded each 15 mins within the range of 250-800nm for 1$^{st}$ and 2$^{nd}$ cycle of the battery. It has been demonstrated by Patel et al.[60,61] that the position of the UV/Vis curves can provide quantitative and qualitative information regarding different polysulphides species present in the electrolyte.

In order to investigate the evolution of polysulphide species the deconvolution graph have been prepared.[61]

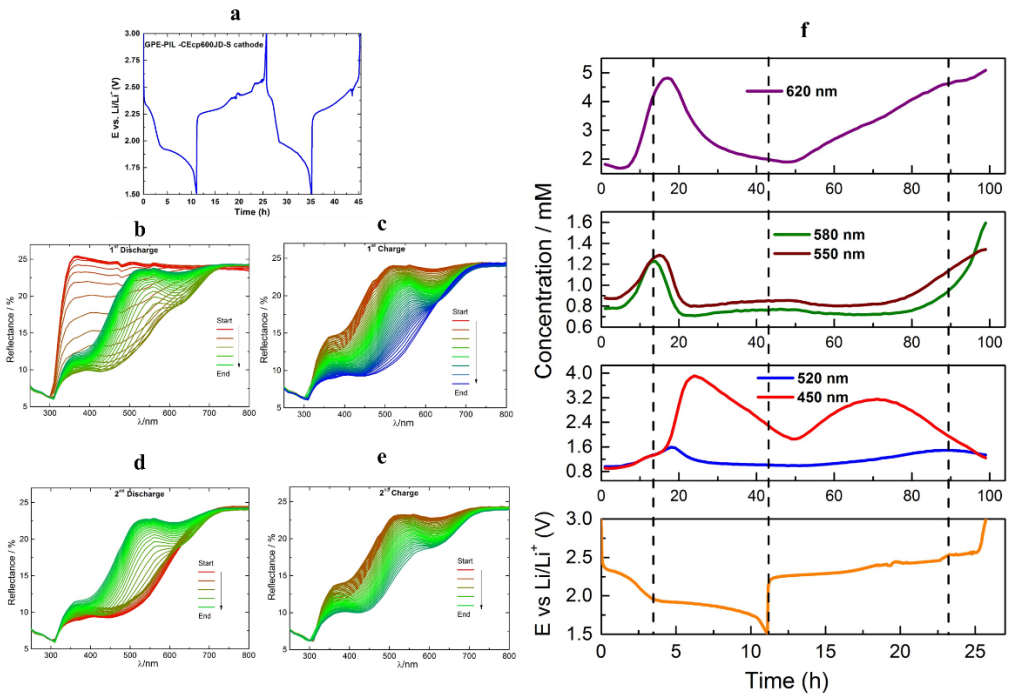


**Figure 5.6: In-situ UV/Vis spectra for the Li-S battery with GPE-PIL-S-CEcp600JD cathode, a). Galvanostatic voltage curve for 1st and 2nd cycle vs. time, UV/Vis spectra measured over, b)1st discharge, c) 1st charge, d) 2nd discharge, e) 2nd charge, f) Deconvolution of the UV/Visible measurements.**

Figure 5.6 shows the in-situ UV/Vis curves for 1st and 2nd cycles with the graph of deconvolution. The association between the normalized reflectance and concentration achieved from the experiment, in a stoichiometric equilibrium is known as deconvolution. At the state of rest the battery doesn't show any presence of polysulphide species. Upon discharge, formation of long-chain polysulphides has been observed between the drop of potential from 2.4 V to 1.9V with a low concentration of short and mid-chain polysulphides.[61] At the end of 1st oxidation, the reduction in long-chain polysulphides could be due to transformation into elemental sulphur, though the amount of short and mid-chain polysulphides remained the same.

The activation of $Li_2S$ can be seen in the mid of 1st charge and the usual polysulphide evolutions classical to Li-S has been observed over the 2nd cycle (discharge/charge).[60,61]

### *5.3.3 Electrochemical characterizations*

Figure 5.7 shows the galvanostatic cycling of cathode impregnated with GPE-PIL in different electrolyte solvents (i.e. DME: Diox, TEGDME: Diox, MeTHF and Sulpholane), it can be seen clearly that the choice of solvents for electrolyte plays an important role in the performance of Li-S batteries. By changing the electrolyte solvent mixture to DME: Diox instead of TEGDME: Diox, the coulombic efficiency of the Li-S cell reaches to > 99% in all 100 cycles. However, TEGDME: Diox shows coulombic efficiency of ~94%.

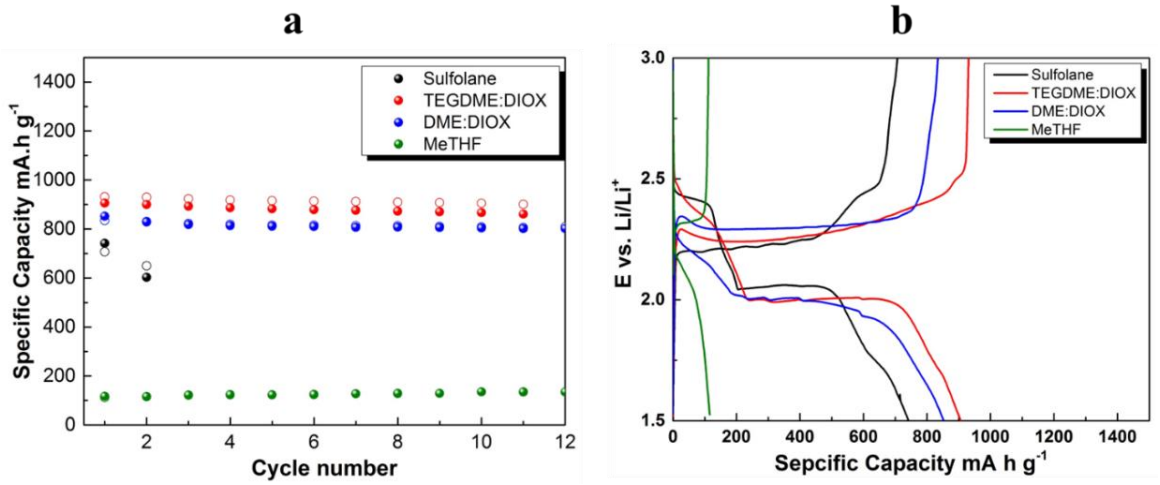


**Figure 5.7: a) Comparitive galvanostatic cycling tests of Li-S battery with GPE-PIL-S-CEcp600JD cathode by using different electrolyte solvents at C/20, b) discharge/ charge voltage profile.**

MeTHF was used, for the fact that PIL might be slightly soluble in mixture of DME (TEGDME): Diox, but the specific capacity observed was lower than 200mAh $g^{-1}$ since 1st cycle, probably due the overall lower conductivity of the electrolyte using MeTHF. In the case of Sulpholane, a well-known electrolyte for Li-based batteries,[62] severe shuttling effect was observed after the 2nd cycle.

Different approaches on the sulphur composite cathode has been employed, in order to determine the best approach for trapping polysulphides using GPE-PIL electrolyte. The cathodes were prepared by embedding the agglomerates of S-CEcp600JD composite in a gel polymer electrolyte without using any additional binder or additional carbon additive.

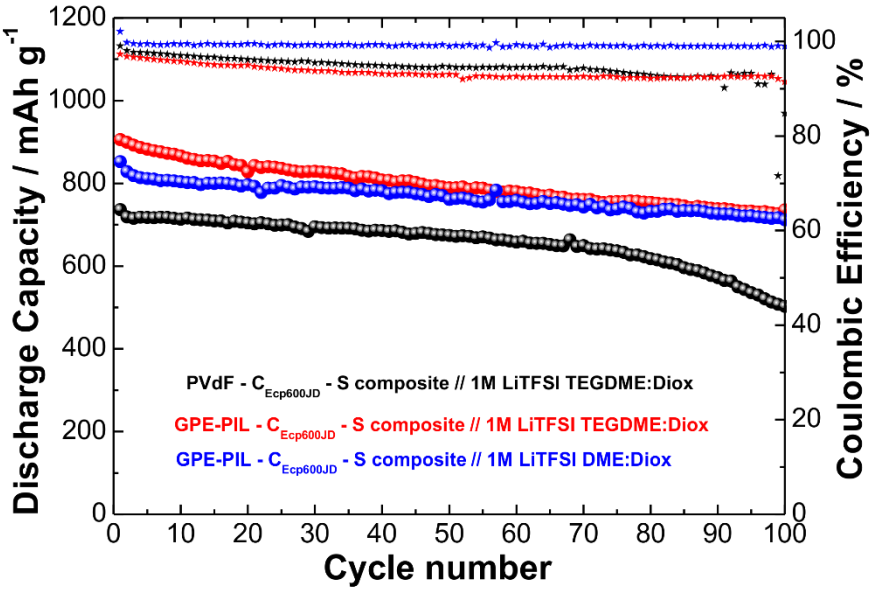


**Figure 5.8: Discharge capacity and coulombic efficiency for Li-S batteries with GPE-PIL-S-CEcp600JDcomposite using different electrolytes and compared with PvdF binder at a c rate of C/20 at RT(25 °C)between 1.5 and 3 V**

TEGDME:Diox was chosen as an electrolyte solvent due to its balance among better coulombic efficiency and specific capacity. Figure 5.8 shows comparative study of gel polymer electrolyte based on PIL binder and PVdF binder. In the formation cycles, about a 20% lower capacity was obtained in the case of PVdF binder using liquid electrolyte (1M LiTFSI TEGDME:Diox), which could be correlated to the hydrophobic nature of PVdF whereby the region of the electrode composite covered with the PVdF are substantially less accessible to $Li^+$ ions from the electrolyte phase.

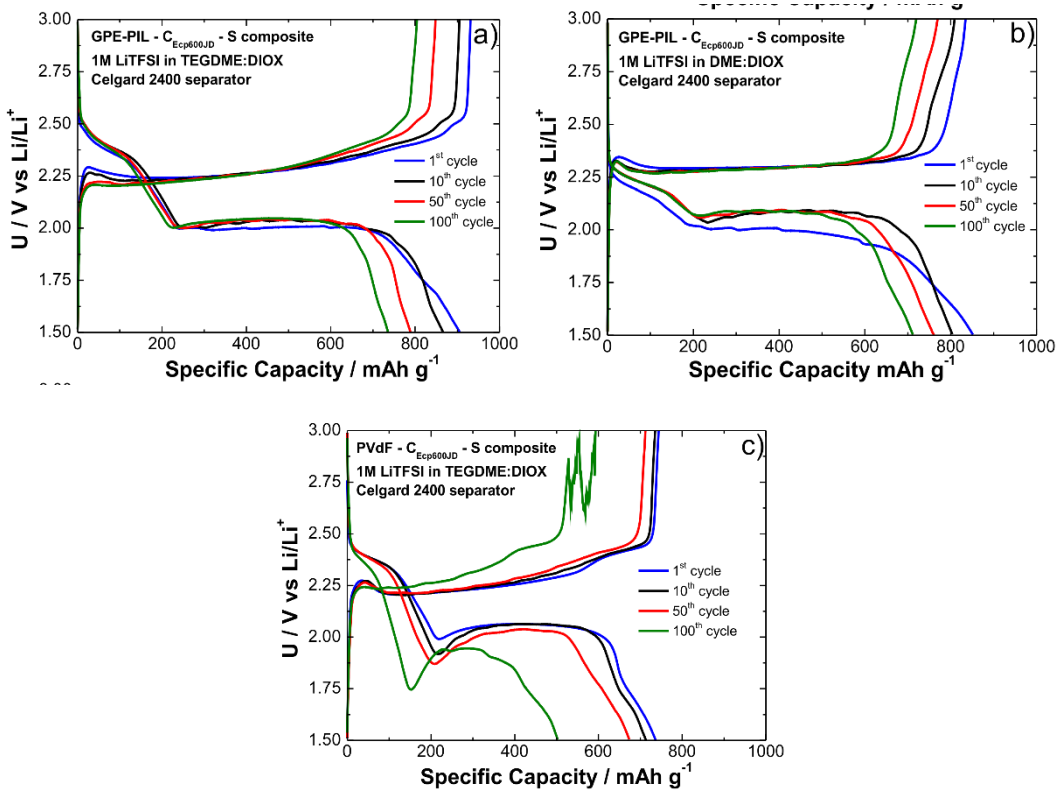


**Figure 5.9:Galvanostatic curves in the 1st, 10th, 50th and 100th cycle measured using C/20 rate for: a) GPE-PIL-S-$C_{Ecp600JD}$ composite with 1M LiTFSI in TEGDME: Diox; b) GPE-PIL-S-$C_{Ecp600JD}$ composite with 1M LiTFSI in DME: Diox and c) PVdF-S-$C_{Ecp600JD}$ composite with 1M LiTFSI in TEGDME: Diox using Celgard 2400 separator.**

Moreover, working with a low amount of electrolyte has an impact on the cycle life. As can be seen in Figure 5.9, the capacity of the cell with the PVdF binder showed increase in degradation (evident after ~$50^{th}$ cycle) while in contrast the cell with the gel polymer electrolyte showed moderate, practically constant degradation of the capacity until 100 cycles.

This observation indicates that the present novel approach in which the binder (PVdF) was replaced with GPE-PIL-based gel demonstrates beneficial properties with enhanced stability of the Li-S electrochemical system. The voltage value of the high voltage plateau in the cell with 1M LiTFSI TEGDME: Diox electrolyte (Figure 5.9a) is approximately

100 mV higher compared to the cell with 1M LiTFSI DME:Diox electrolyte (Figure 5.9b).

After sorting out, the suitable solvent for the electrolyte, the tests have been carried out to discover suitable separator for Li-S systems with GPE-PIL binder. One layer of Celgard 2400 separator was used in the battery assembly. Assuming a 50 vol. % of porosity in the composite cathode, the amount of electrolyte within the cathode and the separator is between 2–3 µL per 1 mg of sulphur. This amount of electrolyte used in our experiment approaches the requirements of achieving a high energy density of the Li-S battery system [10,63]. Nonetheless, by changing from celgard 2400 to glassfiber shows significant difference in capacity values.

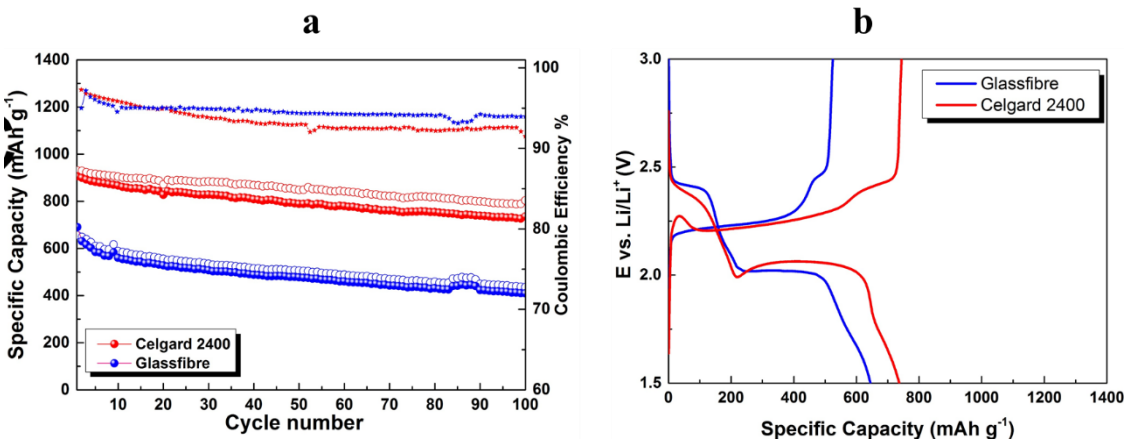


**Figure 5.10: a) Comparative galvanostatic cycling with coulombic efficiency % of GPE-PIL-S-$C_{Ecp600JD}$ cathode with Celgard 2400 and glassfiber separators at C/20, b) Discharge/charge voltage profile.**

Further optimization has been carried out by preparing slurry and cathode outside of the glovebox inert atmosphere. Figure 5.11 shows clearly improved performance with the cathode prepared inside the glovebox, mainly due to hygroscopic nature of GPE-PIL.

Composites with 10 and 25 wt. % of GPE-PIL as binder showed polysulphides shuttling in early cycles while cycling with 50 wt. % of GPE-PIL binder exhibits very stable

cycling, as shown in Figure 5.12. To evaluate the performance of composites containing GPE-PIL, a battery in the conventional configuration using PVdF as a binder within the composite electrode has been cycled for comparison.

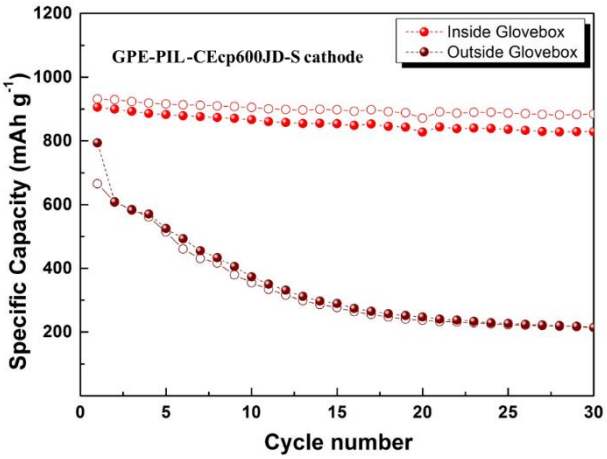


**Figure 5.11: Galvanostatic cycling performance as a function of lamination techniques employed with GPE-PIL-S-C$_{Ecp600JD}$ cathode.**

Preliminary optimization of the composite with a focus to have higher ratio of the sulphur was not successful since with lower amount of GPE-PIL in the composite electrode (25 and 10 wt.%) we observed much faster capacity fading with severe shuttling effect in the early stage of cycling. These results suggest that for the given composition we need a relative high amount of GPE-PIL to achieve stable cycling (Figure 5.12).

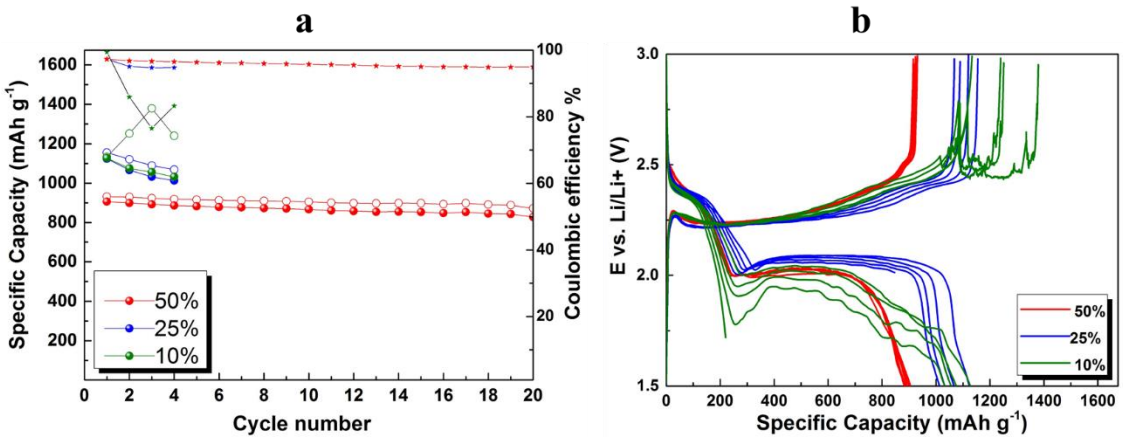


**Figure 5.12: a) Galvanostatic cycling performance as a function of PIL % in the GPE-PIL-S-C$_{Ecp600JD}$ cathode, b) Coulombic efficiency %, c) Discharge/charge voltage profile.**

Namely, to avoid polysulphide shuttle mechanism we need a certain thickness of the GPE-PIL on the particles. On the other hand, such pretreatment allows using lower amount of electrolyte.

In contrast, this work points out the requirement for optimal thickness, where GPE-PIL serves as a barrier for keeping polysulphides close to the surface of the carbon host matrix. The role of the GPE-PIL is then to prevent the fast diffusion of polysulphides out from the cathode and enable their effective conversion in the discharge or the charging process. However, such pre-treatment allows using a lower amount of liquid electrolyte (GPE-PIL is, in fact, a solid electrolyte). In this work, we use only one potential gel electrolyte; however, some other types of gel polymer electrolytes based on the polymer ionic liquids are available for any potential improvements.

Additionally, the GPE-PIL binder was compared with the PEO (LiTFSI, 20:1) as a binder, that is mostly known for usage as binder in solid polymer batteries.[64] Comparison of galvanostatic curves shown in Figure 5.13, demonstrates that the batteries with gel polymer electrolyte in the composite cathode retains stable capacity with ~ 92% of coulombic efficiency, while the cell with PEO shows initial higher capacity, with a decrease of 10% from 1st to 2nd cycle.

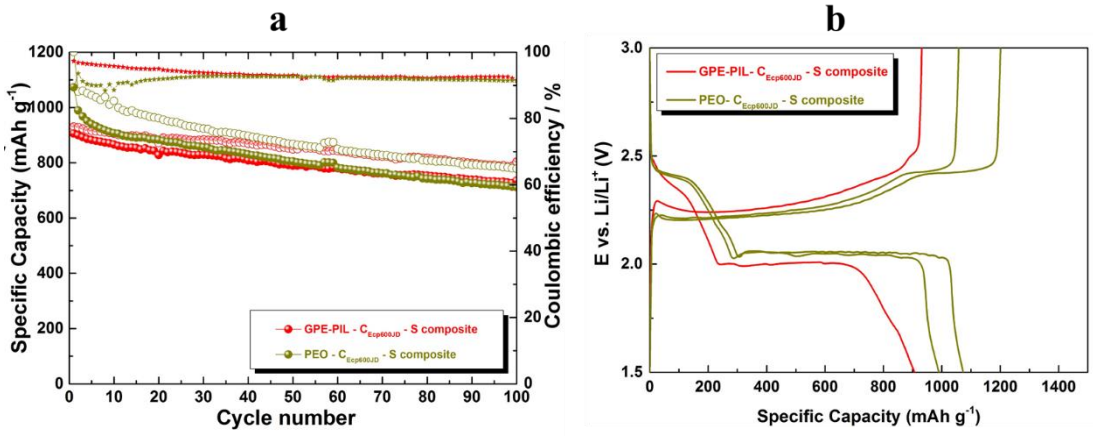


**Figure 5.13: a) Comparative galvanostatic cycling performance of GPE-PIL-S-$C_{Ecp600JD}$ cathode, with different cathode binders, b) Discharge/charge voltage profile.**

The low voltage plateau is relatively flat in both cases, not showing any increase in the polarization during cycling. The discharge curves obtained from the battery with PVdF binder show a pronounced increase of polarization during cycling, particularly at the transition from the high to low voltage plateau, which was observed as distinctive saddle-like appearing local minima in a voltage profile.

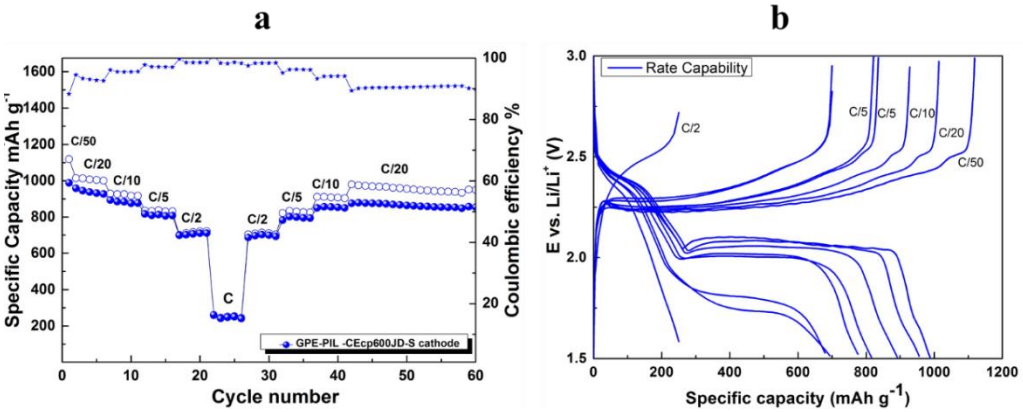


**Figure 5.14: Rate capability of Li-S battery using GPE-PIL-S-$C_{Ecp600JD}$ composite, at various discharge and charge rates from C/20 to 1C and back to C/20.**

The related increase in polarization is due to oversaturation of the electrolyte with polysulphides, and this gradually increases upon cycling. The reasons for the saturation of the electrolyte with polysulphides can be manifold. Among all the possibilities, the most probable is the saturation of the electrolyte with polysulphides due to continuous polysulphide diffusion out from the composite cathode; additionally, we can expect some electrolyte degradation on the fresh surface of Li-anode formed during the stripping and plating of lithium. In addition to increased polarization, the battery with PVdF binder suffered distinct polysulphide shuttle.

Kinetic issues shown in the solid-state configuration compromise the power capability of the battery with the GPE-PIL. However, it is expected that the quantity of the electrolyte in the cell plays very important role in the Li-S battery kinetics. Figure 5.14 shows rate capability of the battery with 50 wt. % of GPE-PIL in the composite cathode at different

current densities corresponding to C/20 to 1C (1.67 mA $mg^{-1}$) and back to C/20. The capacity drop between C/20 and C/2 corresponds to one third of the initial capacity value, and it is recovered at the slower C-rates. Severe capacity drop occurs as the C-rate is increased up to 1C, as the capacity of the lower plateau cannot be utilized anymore in the voltage window used (1.5–3 V).

## 5.4 Conclusions

GPE-PIL has been used as a binder, without using any additional binder. The long-term cycling stability of electrodes containing the GPE-PIL is improved compared to electrodes using PVdF or PEO as a binder. The GPE-PIL composite helps in slow diffusion of polysulphides in liquid electrolyte serving as a buffer which retains them within vicinity of the composite cathode. It offers a system with improved electrochemical stability, further optimization are needed to minimize the quantity of the GPE-PIL in the composite.

## 5.5 References


(1) Ma, Y.; Zhang, H.; Wu, B.; Wang, M.; Li, X.; Zhang, H. Lithium Sulfur Primary Battery with Super High Energy Density: Based on the Cauliflower-like Structured C/S Cathode. *Sci. Rep.* **2015**, *5:14949*, 1–10.

(2) Liang, S.; Liang, C.; Xia, Y.; Xu, H.; Huang, H.; Tao, X.; Gan, Y.; Zhang, W. Facile Synthesis of Porous Li2S@C Composites as Cathode Materials for Lithium–sulfur Batteries. *J. Power Sources* **2016**, *306*, 200–207.

(3) Lacey, M. J.; Jeschull, F.; Edström, K.; Brandell, D. Porosity Blocking in Highly Porous Carbon Black by PVdF Binder and Its Implications for the Li-S System. *J. Phys. Chem. C* **2014**, *118*, 25890–25898.

(4) Vincent, C. A. Lithium Batteries: A 50-Year Perspective, 1959-2009. *Solid State Ionics* **2000**, *134*, 159–167.

(5) Courtney, I. a; Dahn, J. R. Electrochemical and In Situ X-Ray Diffraction Studies of the Reaction of Uthium with Tin Oxide Composites. *J. Electrochem. Soc.* **1997**, *144*, 2045–2052.

(6) Ji, X.; Lee, K. T.; Nazar, L. F. A Highly Ordered Nanostructured Carbon–sulphur Cathode for Lithium–sulphur Batteries. *Nat. Mater.* **2009**, *8*, 500–506.

(7) Yin, Y.-X. X.; Xin, S.; Guo, Y.-G. G.; Wan, L.-J. J. Lithium-Sulfur Batteries: Electrochemistry, Materials, and Prospects. *Angew. Chem. Int. Ed.* **2013**, *52*, 13186–13200.

(8) Evers, S.; Nazar, L. F. New Approaches for High Energy Density Lithium–Sulfur Battery Cathodes. *Acc. Chem. Res.* **2013**, *46*, 1135–1143.

(9) Demir-Cakan, R.; Morcrette, M.; Nouar, F.; Davoisne, C.; Devic, T.; Gonbeau, D.; Dominko, R.; Serre, C.; Férey, G.; Tarascon, J. M. Cathode Composites for Li-S Batteries via the Use of Oxygenated Porous Architectures. *J. Am. Chem. Soc.* **2011**, *133*, 16154–16160.

(10) Pope, M. A.; Aksay, I. A. Structural Design of Cathodes for Li-S Batteries. *Adv. Energy Mater.* **2015**, *5*, 1500124 (1–22).

(11) Evers, S.; Yim, T.; Nazar, L. F. Understanding the Nature of Absorption/adsorption in Nanoporous Polysulfide Sorbents for the Li-S Battery. *J. Phys. Chem. C* **2012**, *116*, 19653–19658.

(12) Yang, Y.; Zheng, G.; Cui, Y. Nanostructured Sulfur Cathodes. *Chem. Soc. Rev.* **2013**, *42*, 3018–3032.

(13) Rosenman, A.; Markevich, E.; Salitra, G.; Aurbach, D.; Garsuch, A.; Chesneau, F. F. Review on Li-Sulfur Battery Systems: An Integral Perspective. *Adv. Energy Mater.* **2015**, *5*, 1500212 (1–21).

(14) Urbonaite, S.; Poux, T.; Novák, P. Progress Towards Commercially Viable Li-S Battery Cells. *Adv. Energy Mater.* **2015**, *5*, 1–20.

(15) Wang, J.; Yao, Z.; Monroe, C. W.; Yang, J.; Nuli, Y. Carbonyl-β-Cyclodextrin as a Novel Binder for Sulfur Composite Cathodes in Rechargeable Lithium Batteries. *Adv. Funct. Mater.* **2013**, *23*, 1194–1201.

(16) Su, Y.-S.; Manthiram, A. A New Approach to Improve Cycle Performance of Rechargeable Lithium-Sulfur Batteries by Inserting a Free-Standing MWCNT Interlayer. *Chem. Commun.* **2012**, *48*, 8817–8819.

(17) Vizintin, A.; Patel, M. U. M.; Genorio, B.; Dominko, R. Effective Separation of Lithium Anode and Sulfur Cathode in Lithium-Sulfur Batteries. *ChemElectroChem* **2014**, *1*, 1040–1045.

(18) Huang, J.-Q.; Zhuang, T.-Z.; Zhang, Q.; Peng, H.-J.; Chen, C.-M.; Wei, F. Permselective Graphene Oxide Membrane for Highly Stable and Anti-Self-Discharge Lithium–Sulfur Batteries. *ACS Nano* **2015**, *9*, 3002–3011.

(19) Scheers, J.; Fantini, S.; Johansson, P. A Review of Electrolytes for Lithium-Sulphur Batteries. *J. Power Sources* **2014**, *255*, 204–218.

(20) Zhang, S. S. Liquid Electrolyte Lithium/sulfur Battery: Fundamental Chemistry, Problems, and Solutions. *J. Power Sources* **2013**, *231*, 153–162.

(21) Demir-Cakan, R.; Morcrette, M.; Guéguen, A.; Dedryvère, R.; Tarascon, J.-M. Li–S Batteries: Simple Approaches for Superior Performance. *Energy Environ. Sci.* **2013**, *6*, 176–182.

(22) Aurbach, D.; Pollak, E.; Elazari, R.; Salitra, G.; Kelley, C. S.; Affinito, J. On the Surface Chemical Aspects of Very High Energy Density, Rechargeable Li–Sulfur Batteries. *J. Electrochem. Soc.* **2009**, *156*, A694–A702.

(23) Lin, Z.; Liu, Z.; Fu, W.; Dudney, N. J.; Liang, C. Phosphorous Pentasulfide as a Novel Additive for High-Performance Lithium-Sulfur Batteries. *Adv. Funct. Mater.* **2013**, *23*, 1064–1069.

(24) Zhang, Y. J.; Wang, W.; Tang, H.; Bai, W. Q.; Ge, X.; Wang, X. L.; Gu, C. D.; Tu, J. P. An Ex-Situ Nitridation Route to Synthesize Li 3 N-Modi Fi Ed Li Anodes for Lithium Secondary Batteries. *J. Power Sources* **2015**, *277*, 304–311.

(25) Zhang, S.; Ueno, K.; Dokko, K.; Watanabe, M. Recent Advances in Electrolytes for Lithium-Sulfur Batteries. *Adv. Energy Mater.* **2015**, *5*, 1500117 (1–28).
(26) Stephan, A. M. Review on Gel Polymer Electrolytes for Lithium Batteries. *Eur. Polym. J.* **2006**, *42*, 21–42.
(27) Fenton, D. E.; Parker, J. M.; Wright, P. V. Complexes of Alkali Metal Ions with Poly(ethylene Oxide). *Polymer (Guildf).* **1973**, *14*, 589–589.
(28) Song, J. Y.; Wang, Y. Y.; Wan, C. C. Review of Gel-Type Polymer Electrolytes for Lithium-Ion Batteries. *J. Power Sources* **1999**, *77*, 183–197.
(29) Zhang, S. S.; Tran, D. T. How a Gel Polymer Electrolyte Affects Performance of Lithium/sulfur Batteries. *Electrochim. Acta* **2013**, *114*, 296–302.
(30) Armand, M.; Tarascon, J.-M. Building Better Batteries. *Nature*, 2008, *451*, 652–657.
(31) Boudin, F.; Andrieu, X.; Jehoulet, C.; Olsen, I. I. Microporous {PVdF} Gel for Lithium-Ion Batteries. *J. Power Sources* **1999**, *81–82*, 804–807.
(32) Choe, H. S.; Giaccai, J.; Alamgir, M.; Abraham, K. M. International Symposium on Polymer Electrolytes Preparation and Characterization of Poly(vinyl Sulfone)- and Poly(vinylidene Fluoride)-Based Electrolytes. *Electrochim. Acta* **1995**, *40*, 2289–2293.
(33) Gentili, V.; Panero, S.; Reale, P.; Scrosati, B. Composite Gel-Type Polymer Electrolytes for Advanced, Rechargeable Lithium Batteries. *J. Power Sources* **2007**, *170*, 185–190.
(34) Salimi, A.; Yousefi, A. A. Analysis Method: {FTIR} Studies of β-Phase Crystal Formation in Stretched {PVDF} Films. *Polym. Test.* **2003**, *22*, 699–704.
(35) Kim, J. R.; Choi, S. W.; Jo, S. M.; Lee, W. S.; Kim, B. C. Electrospun PVdF-Based Fibrous Polymer Electrolytes for Lithium Ion Polymer Batteries. *Electrochim. Acta* **2004**, *50*, 69–75.
(36) Zhang, H. P.; Zhang, P.; Li, Z. H.; Sun, M.; Wu, Y. P.; Wu, H. Q. A Novel Sandwiched Membrane as Polymer Electrolyte for Lithium Ion Battery. *Electrochem. commun.* **2007**, *9*, 1700–1703.
(37) Ji, G.-L.; Zhu, B.-K.; Cui, Z.-Y.; Zhang, C.-F.; Xu, Y.-Y. {PVDF} Porous Matrix with Controlled Microstructure Prepared by {TIPS} Process as Polymer Electrolyte for Lithium Ion Battery. *Polymer (Guildf).* **2007**, *48*, 6415–6425.
(38) Wang, Y.; Travas-Sejdic, J.; Steiner, R. Polymer Gel Electrolyte Supported with Microporous Polyolefin Membranes for Lithium Ion Polymer Battery. *Solid State Ionics* **2002**, *148*, 443–449.
(39) Choi, S. W.; Jo, S. M.; Lee, W. S.; Kim, Y.-R. An Electrospun Poly(vinylidene Fluoride) Nanofibrous Membrane and Its Battery Applications. *Adv. Mater.* **2003**, *15*, 2027–2032.
(40) Montazami, R.; Liu, S.; Liu, Y.; Wang, D.; Zhang, Q.; Heflin, J. R. Thickness Dependence of Curvature, Strain, and Response Time in Ionic Electroactive Polymer Actuators Fabricated via Layer-by-Layer Assembly. *J. Appl. Phys.* **2011**, *109*, 1–5.
(41) Schneider, H.; Garsuch, A.; Panchenko, A.; Gronwald, O.; Janssen, N.; Novák, P. Influence of Different Electrode Compositions and Binder Materials on the Performance of Lithium–sulfur Batteries. *J. Power Sources* **2012**, *205*, 420–425.
(42) Seh, Z. W.; Zhang, Q.; Li, W.; Zheng, G.; Yao, H.; Cui, Y. Stable Cycling of Lithium Sulfide Cathodes through Strong Affinity with a Bifunctional Binder. *Chem. Sci.* **2013**, *4*, 3673–3677.
(43) Urbonaite, S.; Novák, P. Importance of "Unimportant" Experimental Parameters in Li-S Battery Development. *J. Power Sources* **2014**, *249*, 497–502.
(44) Lacey, M. J.; Jeschull, F.; Edström, K.; Brandell, D. Functional, Water-Soluble Binders for Improved Capacity and Stability of Lithium–sulfur Batteries. *J. Power Sources* **2014**, *264*, 8–14.
(45) Wang, Q.; Wang, W.; Huang, Y.; Wang, F.; Zhang, H.; Yu, Z.; Wang, A.; Yuan, K. Improve Rate Capability of the Sulfur Cathode Using a Gelatin Binder. *J. Electrochem. Soc.* **2011**, *158*, A775–A779.
(46) Armand, M. The History of Polymer Electrolytes. *Solid State Ionics* **1994**, *69*, 309–319.
(47) Bruce, P. G.; Vincent, C. A. Polymer Electrolytes. *J. Chem. Soc. Faraday Trans.* **1993**, *89*, 3187–3203.
(48) Baril, D.; Michot, C.; Armand, M. Electrochemistry of Liquids vs. Solids: Polymer Electrolytes. *Solid State Ionics* **1997**, *94*, 35–47.
(49) Jin, J.; Wen, Z.; Liang, X.; Cui, Y.; Wu, X. Gel Polymer Electrolyte with Ionic Liquid for High Performance Lithium Sulfur Battery. *Solid State Ionics* **2012**, *225*, 604–607.
(50) Jeddi, K.; Ghaznavi, M.; Chen, P. A Novel Polymer Electrolyte to Improve the Cycle Life of High Performance Lithium–sulfur Batteries. *J. Mater. Chem. A* **2013**, *1*, 2769–2772.
(51) Zhang, S. S.; Tran, D. T. A Simple Approach for Superior Performance of Lithium/sulphur Batteries Modified with a Gel Polymer Electrolyte. *J. Mater. Chem. A* **2014**, *2*, 7383–7388.
(52) Wang, J.; Liu, L.; Ling, Z.; Yang, J.; Wan, C.; Jiang, C. Polymer Lithium Cells with Sulfur Composites as Cathode Materials. *Electrochim. Acta* **2003**, *48*, 1861–1867.
(53) Fernicola, A.; Scrosati, B.; Ohno, H. Potentialities of Ionic Liquids as New Electrolyte Media in

Advanced Electrochemical Devices. *Ionics (Kiel).* **2006**, *12*, 95–102.

(54) Balducci, A.; Soavi, F.; Mastragostino, M. The Use of Ionic Liquids as Solvent-Free Green Electrolytes for Hybrid Supercapacitors. *Appl. Phys. A* **2006**, *82*, 627–632.

(55) Egashira, M.; Todo, H.; Yoshimoto, N.; Morita, M.; Yamaki, J. I. Functionalized Imidazolium Ionic Liquids as Electrolyte Components of Lithium Batteries. *J. Power Sources* **2007**, *174*, 560–564.

(56) Sakaebe, H.; Matsumoto, H. N-Methyl-N-Propylpiperidinium Bis(trifluoromethanesulfonyl)imide (PP13–TFSI) – Novel Electrolyte Base for Li Battery. *Electrochem. commun.* **2003**, *5*, 594–598.

(57) Fuller, J.; Carlin, R. T.; Osteryoung, R. A. The Room Temperature Ionic Liquid 1-Ethyl-3-methylimidazolium Tetrafluoroborate: Electrochemical Couples and Physical Properties. *J. Electrochem. Soc.* **1997**, *144* , 3881–3886.

(58) Fung, Y. S.; Zhou, R. Q. Room Temperature Molten Salt as Medium for Lithium Battery. *J. Power Sources* **1999**, *81–82*, 891–895.

(59) Appetecchi, G. B.; Kim, G.-T.; Montanino, M.; Carewska, M.; Marcilla, R.; Mecerreyes, D.; De Meatza, I. Ternary Polymer Electrolytes Containing Pyrrolidinium-Based Polymeric Ionic Liquids for Lithium Batteries. *J. Power Sources* **2010**, *195*, 3668–3675.

(60) Patel, M. U. M.; Demir-Cakan, R.; Morcrette, M.; Tarascon, J. M.; Gaberscek, M.; Dominko, R. Li-S Battery Analyzed by UV/vis in Operando Mode. *ChemSusChem* **2013**, *6*, 1177–1181.

(61) Patel, M. U. M.; Dominko, R. Application of In Operando UV/Vis Spectroscopy in Lithium – Sulfur Batteries. *ChemSusChem* **2014**, *7*, 2167–2175.

(62) Liang, C.; Wang, F.; Xu, Y.; Chen, J.; Liu, D.; Luo, Z. A Stable Electrolyte Makes a Nonaqueous Li–O 2 Battery Truly Rechargeable As a Result of Their Ultra-High Specific Energy and Potential Use in Electric Vehicles and Grid Energy. *New J. Chem. New J. Chem* **2568**, *37*, 2568–2572.

(63) Hagen, M.; Hanselmann, D.; Ahlbrecht, K.; Maça, R.; Gerber, D.; Tübke, J. Lithium-Sulfur Cells: The Gap between the State-of-the-Art and the Requirements for High Energy Battery Cells. *Adv. Energy Mater.* **2015**, *5*, 1401986 (1–11).

(64) Jeong, S. S.; Lim, Y. T.; Choi, Y. J.; Cho, G. B.; Kim, K. W.; Ahn, H. J.; Cho, K. K. Electrochemical Properties of Lithium Sulfur Cells Using PEO Polymer Electrolytes Prepared under Three Different Mixing Conditions. *J. Power Sources* **2007**, *174*, 745–750.

# *Chapter 6: Organosulphur polymers as cathodesin Li-S batteries.*

# 6 Introduction

Organic compounds as cathode materials offers several advantages i.e. high theoretical capacities , recyclability and potential low cost over inorganic ones.[1] Since decades the improvement of organic cathode materials, including free radical compounds, organosulphur, and carbonyls, has been under specific consideration (***Figure 6.1***).

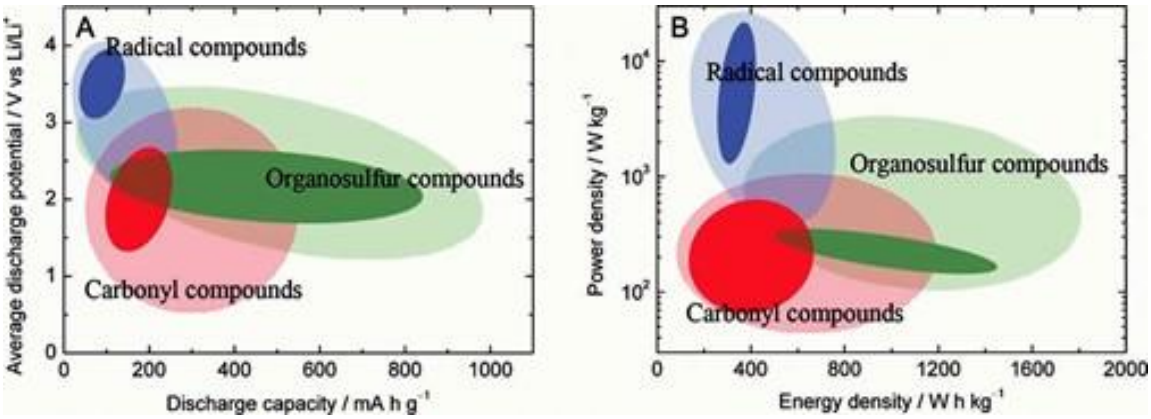


**Figure 6.1: Assessment of the cell performance in radical compounds (blue), organosulphur (green), and carbonyl (red) by mean of (A) discharge potential vs discharge capacity (B) power density vs energy density.**

Visco and DeJonghe,[2,3] firstly projected dimeric organosulphur named Tetraethylthiuram disulphide (TETD) to be used as cathode material in high temperature Na-batteries. Liu et al.[4–6] then investigated deeply the kinetic behaviour and reaction mechanism of different organodisulphur and thiolate redox couplesbut due to the eminent solubility of thiolates in electrolyte, they suffer from poor cycle life, slow reaction kinetics and self-discharge in lithium rechargeable batteries, leading to a possible option of testing those organosulphur compounds mainly with solid electrolytes at high-temperature (typically 80–130 °C).

Cleavage and formation of S-S bonds in organosulphur compounds is well known,[2,7] the reaction involving 2 electrons resulting in lithium-thiolate, potentially offer high capacity and high discharge voltage.[3,4] Aneconomical access, different from conventional Li-ion batteries:

$$RSSR + 2e^{-} + 2Li^{+} \Leftrightarrow 2LiSR$$

R represents the organic moiety. Disulphide bond in RSSR undergoes cleavage during discharge and generate monomeric anions, which could afterwards oxidise back into principal disulphide bond upon charge. These materials faced the same dissolution problem of the generated thiolate ions during the reduction reaction, leading to capacity fading.

Visco et *al.*[3] however faced the same dissolution problem of the generated thiolate ions during the reduction reaction, leading to capacity fading. Thus, side-chain organosulphur polymers were investigated as second generation materials overcoming the dissolution. The cleavage/formation in these types of organosulphur does not occur in the main chain and no low molecular weight materials are released or dissolved in the electrolyte. However, most of the reported materials suffered from a rapid capacity drop during discharge/charge cycling.[1]

Poly (2, 2'-dithiodianiline) (PDTDA) was the first side-chain organosulphur implemented in rechargeable lithium-based batteries.[1] These electrodes materials showed a capacity of 270 mA h $g^{-1}$ when cycled with a gel electrolyte and a smooth discharge plateau was seen at ~2.5 V vs $Li/Li^{+}$.[8] Mimicking the same concept, several polymers were synthesised successfully where every repeating unit bears a disulphide bond in the side chain.[9,10] All these materials showed a combination synergy between the disulphide side chain bonds and the polyaniline (PAn) main chain, but suffered from a rapid capacity drop during

discharge/charge cycling.[1] Additionally, polyacene and polyphenyl main chain polymers and the side chain containing disulphide moieties were presented.[5,11–14] Among all these polymers, the material obtained by heat treatment of the polyacrylonitrile and elemental sulphur at 450°C was evaluated as active cathode materials in lithium batteries. [14] It was highlighted that the existence of π-conjugation and the disulphide bond improves the redox rates and cyclability at room temperature. [14] The attractiveness of this material is the stable discharge capacity maintained at 480 mA h $g^{-1}$ and capacity retention at ca. 92% after about 240 cycles. It is not clear however if only S-S bonds attached to the condensed pyridine are present or if $S–S_x–S$ polysulphides are present to explain the very high capacity.

Oyama *et al.* demonstrated 2, 5-demercapto-1, 3, 4-thiadiazole (DMcT, theoretical capacity 362 Ah $kg^{-1}$) as a new composite cathode.[15] At a current density of 0.1mA $cm^{-2}$, it shows an energy density of 303 Wh $kg^{-1}$ Vs. $Li/Li^+$ with a voltage of 3V. Organosulphur bearing DMcT gained ample attention within other organosulphurs as cathode materials in rechargeable lithium-based batteries due to their high theoretical capacity.[16–22] Nevertheless, the kinetics are slow when compared to other redox reactions as well as a deprived rate capability. The thiolate based composite cathode, i.e. DMcT with a conducting polymer, reduction products of disulphide polymer dissolves in organic electrolyte leading to poor cycle life.[17,20,23] Consequently, DMcT in electrode is partially reactive and the intrinsic dissolution along with slower kinetics makes it, the least favourite for application in lithium-based batteries. Meanwhile, the investigation for cathode material endures with the synthesis of organosulphur based on dimercaptothiophene and its derivatives, it includes diverse functional groups with the $e^-$-donating/$e^-$-withdrawing properties.[17,24]

Organosulphur side-chain-type polymers are basically comprised from main chain conducting polymer and side chain disulphide (S-S) or polysulphides $[(\text{-S-S-})]_n$. During cleavage of S-S bond upon charge/discharge, side-chain-type polymers inhibit the breaking of backbone moiety offering improved cycling stability compared to main-chain-type polymers. Conducting polymers containing side chain linkers (S–S bonds) to connect two moieties of aniline were primarily established by Naoi et al.[24,25] Centred on this concept, interconnected S-S bond based polymers achieve great fame for energy storage applications in rechargeable lithium-based batteries.[26,27]

Numerous studies of sulphur bearing conductive polymer matrixes[28–30] have been reported as possible cathode for rechargeable batteries. They could be defined as the legitimate substitute of sulphur, which have showed 1 electron transfer with electrochemistry based on the mimic of the cleavage/formation mechanism between S-S bonds during discharge/charge.[1]

The use of organosulphur polymers instead of elemental sulphur is under study in order to avoid the transport of polysulphides from cathode to anode and the corresponding capacity fading.[1] Organosulphur polymers, despite having lower theoretical capacity than elemental sulphur, have higher voltage (~50% higher) resulting in similar overall energy densities.

In this Chapter, novel approach has been described regarding synthesis of new cathode materials based on redox organosulphur polymers and examined in rechargeable Li-S batteries as a proof of concept study. These cathodes give good chemical activity on the basis of cleavage/formation of the designated bonds. Herein, we describe cleavage/formation of N-S bond attached to a conjugated polyazomethine backbone and cleavage/formation of S-S bonds (***Scheme 6.1***) with an aliphatic polyamine backbone upon

discharge/charge.[23] It also offers the non-soluble system to avoid parasitic reactions of polysulphides.

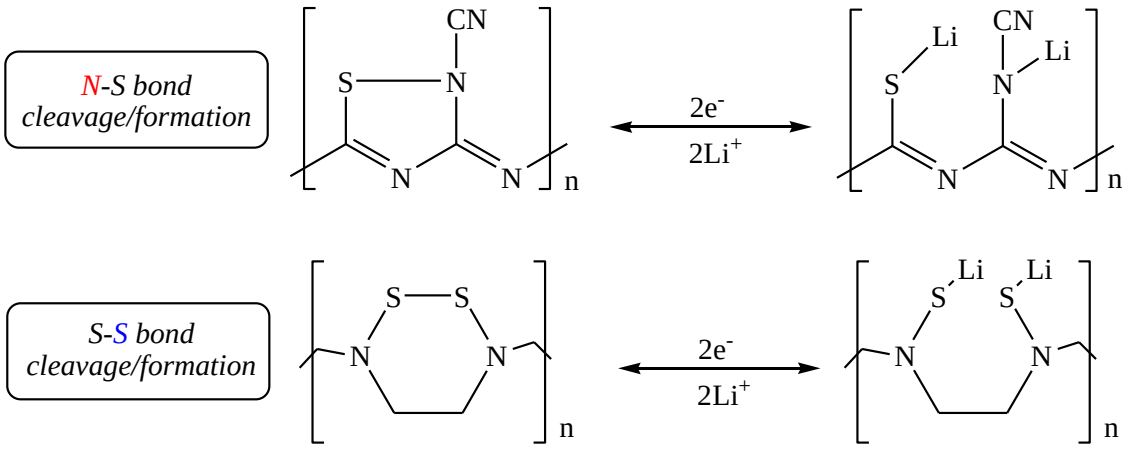


**Scheme 6.1: Reaction showing cleavage/formation of N-S and S-S bonds during discharge/charge.**

Higher voltage is expected from the attachment to electron-withdrawing group (N, C=N) and the rate capabilities reflect fast kinetics and diffusion. During cleavage of S-S bond, the direct attachment with polyamine backbone avoids the loss of depolymerized (cleaved) compound in organic electrolyte upon discharge[31] improving cycling performance. Synthesized organosulphur polymer bear side-chain N–S bond, leading to high voltage,[32] and possible presence of S-radical leads towards faster kinetics of reaction.[33]

# 6.1 Synthesis

## *6.1.1 Part 1: N-S bond cleavage/formation*

**Poly (Z)-N-(cyanamido (methylamino) methylene) ethanethioamide (NS)**

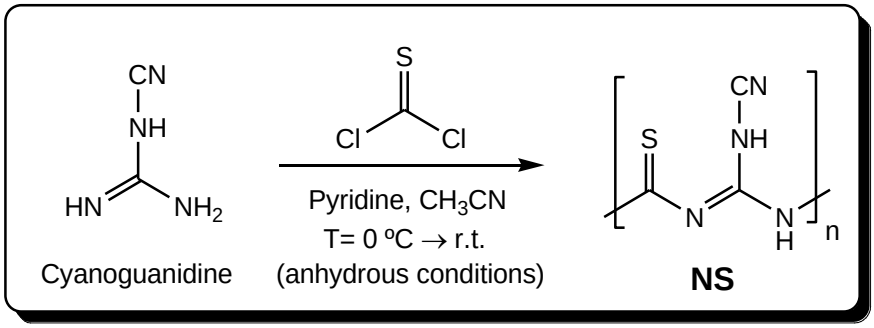


Cyanoguanidine and thiophosgene was reacted with pyridine as HCl trap in anhydrous acetonitrile under argon flow for 16h. Temperature of the reaction has been maintained at 0°C due to exothermic and high volatile nature of thiophosgene.[34] The black precipitated solid obtained in the first step, was washed extensively with acetone/ethanol and dried at 100°C under vacuum.

**Poly (Z)-5-methyl-3-(methylimino)-1, 2, 4-thiadiazole-2(3H)-carbonitrile (NS-1)**

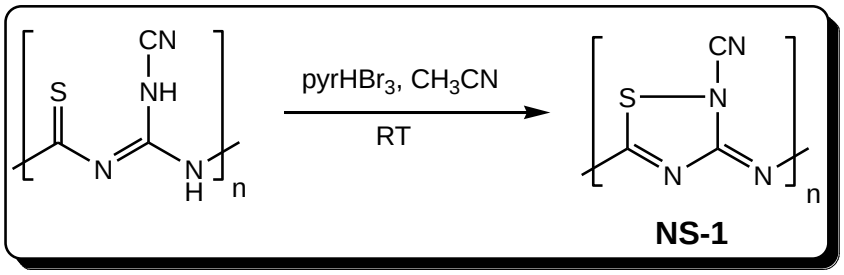


The dried solid was reacted with pyridinium hydro-tribromide in anhydrous acetonitrile under argon flow at RT for 16h. Subsequently, the obtained solid (NS-1) was washed and dried at 60°C under vacuum.

The NS and NS-1 organosulphur polymers were characterized via FTIR spectroscopy using a Perkin Elmer Spectrum 400 FTIR spectrometer with ex situ, external reflectance

mode in potassium bromide (KBr) pellets. To analyse the thermal stability, thermal gravimetric analysis (TGA) in the temperature range from 50 to 500 °C with a heating rate of 10 °C/min on a Netzsch STA under continuous argon flow were performed.

### *6.1.2 Part 2: S-S bond cleavage/formation*

**Poly $N^1$, $N^2$-diethylethane-1, 2-diamine (PA)**

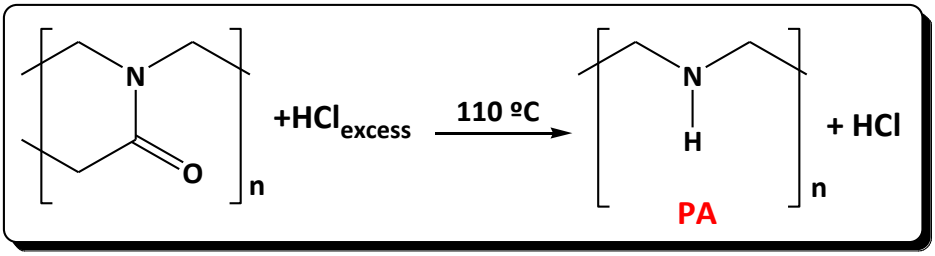


Poly (2-ethyl-2-oxazoline) was introduced in a round bottom flask and dissolved in 20% HCl (in excess) solution. The reaction mixture was stirred at 110 ºC with condenser for 72 h. The resulting precipitate (polyethylene-imine-HCl) was washed with MeOH, dried and followed by dissolving in water, White solid precipitate appeared upon addition of diluted solution of NaOH (0.25M). The precipitate, polyamine (PA), were filtered and washed with water until neutral, and dried at 80ºC under vacuum (85% yield).

**Poly (3, 6-diethyl-1, 2, 3, 6-dithiadiazinane) (NS-2)**

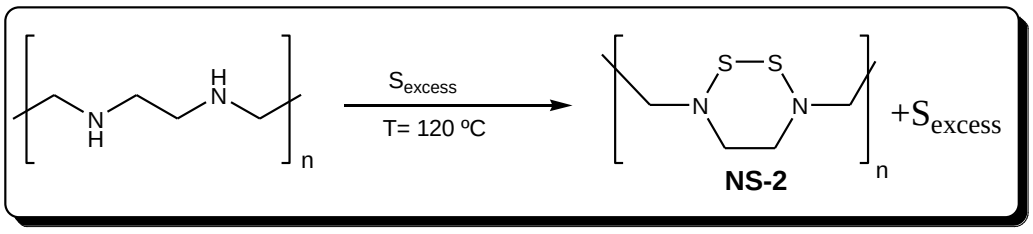


The dried precipitate of Polyamine (PA) was reacted with sulphur (in excess) after blending for 5 mins in a speed mixer at 800 rpm (***Figure 6.2***a). The reaction was solvent-free at 120 ºC for 24h with a trap for $H_2S$. The mixture was then purified with $CS_2$ in

order to remove excess sulphur impurities. The remaining orange powder (NS-2) was dried at 60ºC under vacuum (28.7% yield).

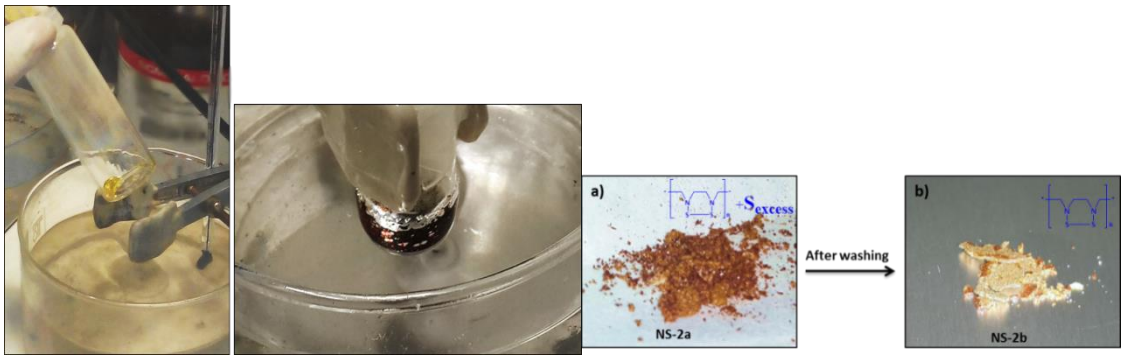


**Figure 6.2: a) The picture shows state of mixture during reaction at 120ºC b) Product after the reaction and after washing with $CS_2$.**

### *6.1.3 Physico-chemical characterization*

The compositions of the obtained solids were determined via FTIR spectroscopy.[35] Further confirmation of the S-S and N-S bonds has been followed by Raman[26,36] via Nanonics & Renishaw-Nanonics Multiview 2000 Ters with Raman Spectrometer and XRD via D8 discover by Bruker, due to uncertainty about presence of excess sulphur/ longer chain S-S bonds for dithiadiazinane organosulphur polymer.

Thermal gravimetric analysis (TGA) was conducted in the temperature range from 50 to 500 °C with a heating rate of 10 °C/min.

### ***6.1.4 Preparation of the carbon (Ckj-600) -organosulphur cathode:***

The obtained NS-1 organosulphur was dried and ball milled with carbon (Ckj-600) in a 70: 30 % ratio in 8000M mixer/mill (© SPEX Sample Prep) for 5 min. The composite powder was dried at 60 ºC under vacuum prior use for electrochemical tests.

NS-2 organosulphur has been tested as a powder cathode in an electrochemical cell by using composite of NS-2 70 wt. % dry ball milled with 30 wt. % of carbon (kj-600) for 5 mins.

The composite slurry for lamination was prepared with mixture of 70 wt. % of organosulphur (NS-2) powder, 20 wt. % of $Carbon_{KJ600}$ and 10 wt. % of EPDM binder in cyclohexane. Conventional wet ball milling technique for 5 mins was used. Electrodes used were with diameter of 13mm (active mass loading, 1 $mg/cm^2$) after being dried at $60^oC$ under vacuum for 15h.

### *6.1.5 Electrochemical characterization*

Galvanostatic cycling was performed in CR2032 coin cell type batteries, cathode wetted with ether based electrolyte 2wt. % $LiNO_3$ in 1M LiTFSI in DME/DIOX (v: v = 1:1), separated by Celgard 2400 with Li-foil as an anode at room temperature (NS-1 cathode was tested in similar conditions with 1M LiTFSI in DME/DIOX without $LiNO_3$).

## 6.2 Results and discussion

### *6.2.1 Part 1: N-S bond cleavage/formation*

During the first reaction step a very dark brown insoluble powder was collected (NS), which was reacted in a second step to obtain the final black powder product (NS-1). After repeated washing with ethanol/acetone, all excess reactive chemicals and short chains oligomers were removed. Thiophosgene is well known as a very reactive chemical with a wide range of chemical functional groups,[32] that makes the selection of suitable solvents for the targeted reaction delicate. The obtained redox conjugated polymers (NS and NS-1) are insoluble in all usual solvents, which make them difficult to characterize.

On cyanoguanidine chromophore (commercial), the vibration bands attributed to the nitrile group (C≡N) analysed by IR spectroscopy shows a doublet at 2166 $cm^{-1}$ and 2211 $cm^{-1}$. This doublet is an indication of the presence of two tautomer with different structures as mentioned in the literature.[37]

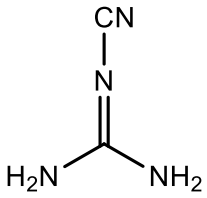


Type 1

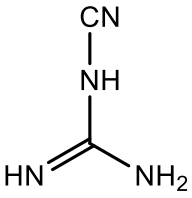


Type 2

In NS-1, the nitrile group (C≡N) shows vibration bands at around 2188 $cm^{-1}$ attributing to the presence of only one compound. It indicates that the nitrile group was not affected either by the nucleophilic substitution during 1st step reaction or by the oxidation (cyclization) reaction in 2nd step (Figure 6.3a). The final C–N organosulphur was elucidated by the appearance of peak at 1170 $cm^{-1}$, which was assigned to the C–N stretching vibration of the tertiary amines.[38] The imine C=N elongation has been seen ~ 1640-1690 $cm^{-1}$.[39]

The first substitution was revealed by the disappearance of the multiple peaks in the 3350-3500 $cm^{-1}$ of N–H stretching of primary amines.[40–42]

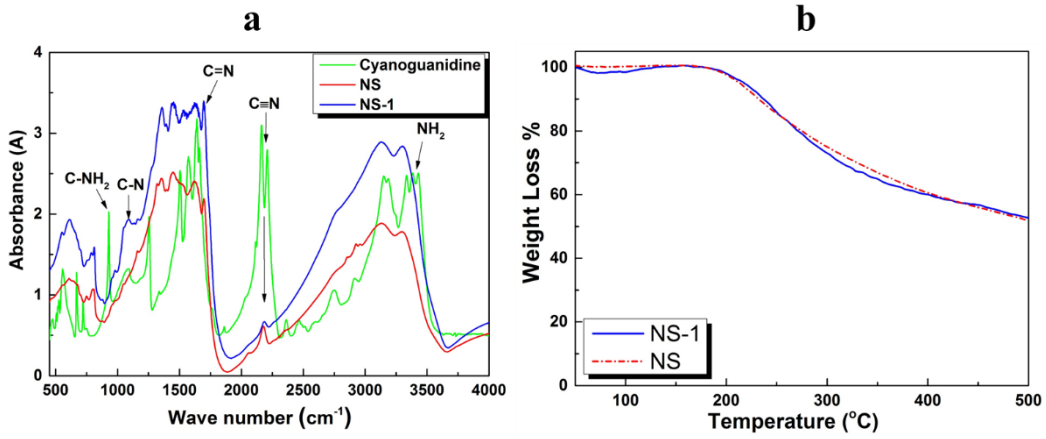

**Figure 6.3: a) FTIR spectra of cyanoguanidine and the organosulphur polymers NS and NS-1 obtained in step 1 and step 2, b) TGA thermogram of organosulphur polymers NS and NS-1.**

Characterization of both products NS and NS-1 by TGA under continuous argon flow shows no degradation up to a temperature of 210°C (Figure 6.3b).

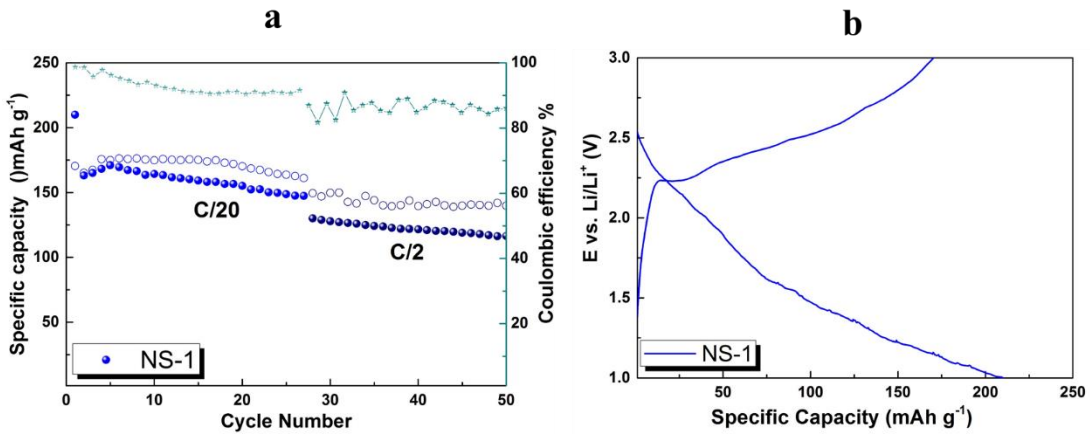


**Figure 6.4: a) Gavanostatic cycling of organosulphur cathode at C/20 formation cycles and C/2. b) Discharge/charge profile of first cycle at C/20.**

The charge/discharge profiles of NS-1 organosulphur as powder cathode by galvanostatic cycling between 1-3 V at the C-rate of C/20 and C/2 (theoretical capacity = 426 mA.h g-1) were obtained. A first discharge capacity of 213 mA h $g^{-1}$ was obtained which is almost half of its theoretical capacity (Figure 6.4a). Meanwhile 10% of capacity loss was observed when the C-rate was increased from C/20 to C/2. After 50 cycles a capacity of 130 mAh $g^{-1}$ at C/2 was obtained. Only a single voltage plateau (Figure 6.4b) at ~2.2 V was observed during discharge/ charge process, indicating the reduction processes of S–N bonds .[23]

The assumed bond cleavage/formation occurring in the S–N bonds of organosulphur (NS-1) is not detrimental, since the main azomethine chain remains intact. The cyclic voltammetry was carried out at a scan rate of 0.5 mV $s^{-1}$, showing its redox behaviour and revealing its electrochemical reversibility. In the first sweep of the potential from 1-3.5V one broad oxidative peak is observed at a potential of 2.3 V with a shoulder peak at 2.43

V indicating that the oxidation reaction has occurred. In the reduction process two peaks at potential of 2.2 V and 2.4 V were observed. In the 5th cycle, however, the oxidation and the reduction potentials were slightly shifted to 2.5 V and 2.05V, respectively and no shoulder peak in the anodic scan was observed (Figure 6.5).

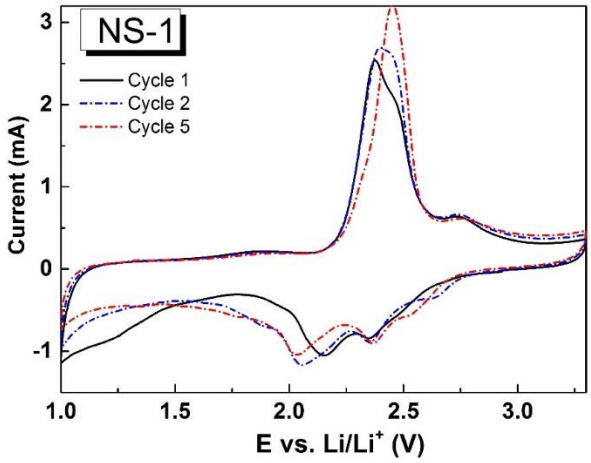


**Figure 6.5: Cyclic voltammogramm with organosulphur cathode separated by GF separator wet with 1M LiTFSI in DME: DIOX (1: 1 wt. %) in a coin Cell CR2032 at a scan-rate of 0.5 mV $s^{-1}$.**

Meanwhile the difference in cycle 1, 2 and 5, can be explained by the sequencing selection of monomer units in the polymer. Upon electrochemical reaction, the reduction took place on the alternative (even or odd) monomer units in the monomer sequence distribution based on their neighbouring group interactions and the vicinity of reduction reaction. For e.g. there could be 1$^{st}$ and the 3$^{rd}$ replacement or 1$^{st}$ and the 4$^{th}$ unit replacement, during the process each monomer molecules which adds is so polarized that an effective negative charge is located on terminating atoms which might be a reason for no reduction taking place on the near neighbouring monomer unit.[43]

No further changes were observed for further cycles, which suggest the S–N bond cleavage (reduction) and formation (oxidation) are reversible. The S–N cleavage/formation rate capability may be attributed to the conjugated backbone of the polymer and the cyanoguanidine chromophore formed with the nitrile group.

Furthermore, the observed reversibility can be attributed to the fact that the S–N bonds are bonded chemically within the same polymer chain as side functional groups. In fact, the functional groups in α and β positions adjacent to the N-S bond have a direct effect on the standard rate constant of the redox reaction.[9,12,44]

### *6.2.2 Part 2: S-S bond cleavage/formation*

The FTIR spectra of NS-2 organosulphur polymer reveal two main characteristic peaks attributed to the S-S[23,26,35,45] and N-S[26,28] bonding vibration at around 500 and 1100 $cm^{-1}$ respectively (Figure 6.6a). The peaks attributed to C–N stretching[46] and bending vibrations are at 1330 and 1484 $cm^{-1}$ respectively, normally for stretching modes of the C-N bond the region from 1150−1300 $cm^{-1}$ are allocated.[38] The stretching vibration of N-H bond of primary amines can be seen in PA sample ~3250-3500 $cm^{-1}$ but in NS-2, the slope has been observed. This slope might be an indication of unsubstituted N-H bonds remaining. The stretching of the backbone C-H bond could be seen in both compound in the region of 2800-3000 $cm^{-1}$.[47]

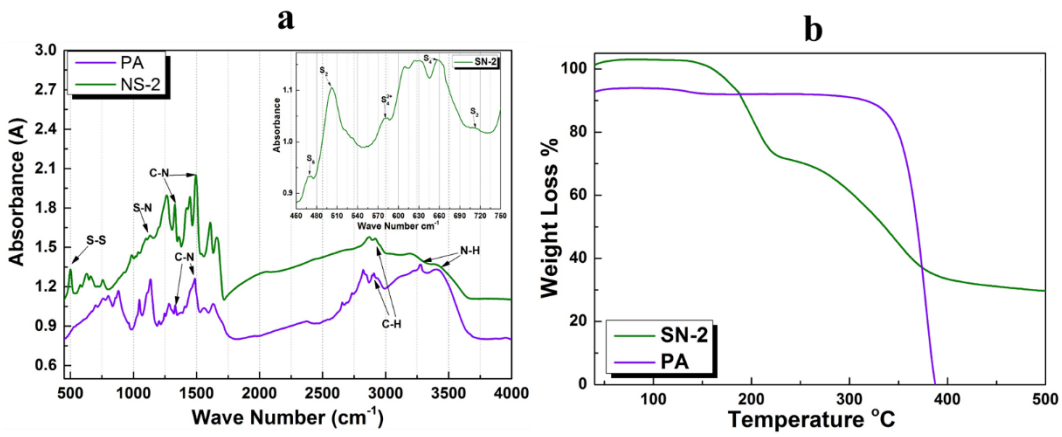


**Figure 6.6: a) FTIR spectra of Poly (diethylamine) and the organosulphur polymers NS-3a obtained after washing with $CS_2$. b) TGA thermogram representing the NS-2 product after washing with $CS_2$ comparing with initial polyamine reactant used for reaction.**

This justifies the suggested structure, but also few weak signals has been observed (enhanced spectra in figure 6.6a) which according to Beat Meyer[48], correlates with the allotropes of sulphur. This can be linked either to S inaccessible to $CS_2$ washing, or to more than 2 S in the rings formed with the polymer, to 7 or 8 members.

TGA thermogram of NS-2 organosulphur polymer has not shown any visible degradation of the compound up to 200 °C (Figure 6.6b). A significant weight loss in the range from 200 to 400 °C was observed that might correspond to the organosulphur polymer.

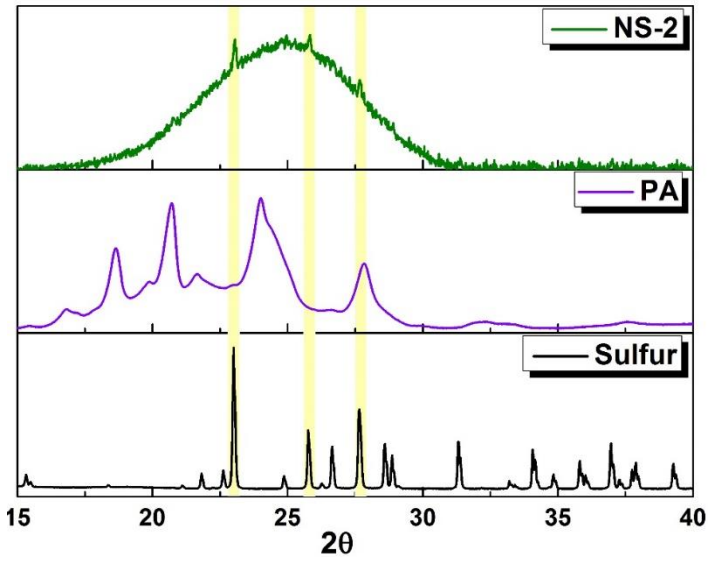


**Figure 6.7: XRD comparison of organosulphur polymer (NS-2) with polyamine compound (PA) and elemental sulphur (S) at RT.**

Due to uncertainty of some peaks present in FTIR, further characterisation has been carried out by X-Ray diffraction (XRD) and Raman spectroscopy measurements. Unlike NS-1, this organosulphur polymer (NS-2) was like glassy powder, which makes it easier to handle.

X-ray diffractogram (Figure 6.7) shows a broad peak at 24.9° along with small peaks at 23°, 25° and 27°, correlating to sulphur/polysulpide impurities.

The purpose for Raman analysis was to find conformational peaks of N-S and S-S bonds. [26,35,49,50] Due to weak band intensity only broad bands have been observed (Figure 6.8). The medium intensity band at 465cm$^{-1}$ corresponds to S-S bonding[36,51] and the weak band at 614 cm$^{-1}$ might as well correlates with S-S stretching. Bands corresponding to N-S bonds normally appears between 900-1090cm$^{-1}$ [52] and in this case was observed at 948 cm$^{-1}$.

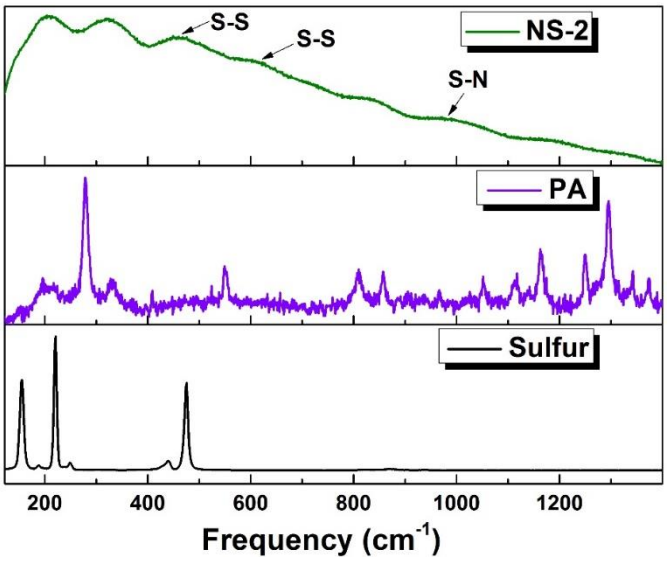


**Figure 6.8: Raman measurements of organosulphur polymer (NS-2) with polyamine compound (PA) and elemental sulphur (S) at RT.**

Figure 6.9 shows the comparison of organosulphur (NS-2) powder before and after washing with $CS_2$. Two batches have been prepared, 1. Before washing, and 2. After washing, both of them were mixed with carbon (KJ600) by dry ball milling technique. The cells were cycled at C/10 by using same cell assembly conditions. For the cells without washing, higher specific capacity than theoretical capacity has been observed.

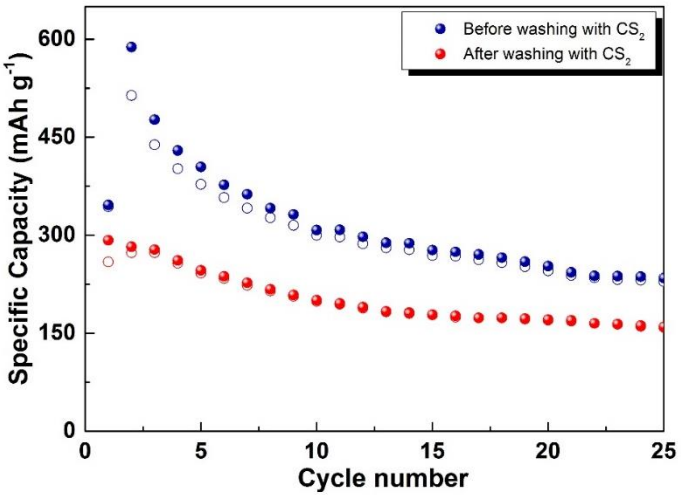


**Figure 6.9: Galvanostatic cycling of cells with NS-2 powder cathode before (blue dots) and after (red dots) washing with $CS_2$ at C/10.**

The elevated capacity can be the influence of excess amount of sulphur present, which allows free $S_8$ mobility in the electrolyte to form Li-polysulphides ($Li_2S_x$). Upon washing off those sulphur impurities with $CS_2$, no obvious contribution attributed to free $S_8$ has been observed.[46] Thus, the specific capacity achieved in the cell cycles with washed organosulphur cathode, could be attributed to the electrochemical activity from only the organosulphur cathodes material.

Therefore, NS-2 powder washed several times with $CS_2$ have been tested by galvanostatic cycling at C/10 and C/4 by using 1M LiTFSI in DME:DIOX (1:1, V:V%) with 2 wt. % $LiNO_3$ against metallic Li-anode. A capacity of 300 mAh $g^{-1}$ at C/10 was observed, which drops down with each cycle and show some polarization after 90$^{th}$ cycle. The final capacity observed at 100$^{th}$ cycle was around 120mAh $g^{-1}$. Meanwhile, the cell at C/2 exhibits initial capacity of 200 mAh $g^{-1}$ dropping down to ~150 mAh $g^{-1}$ (Figure 6.10a). Two voltage plateaus were observed in discharge voltage profile at ~2.4 and ~2.1 V.

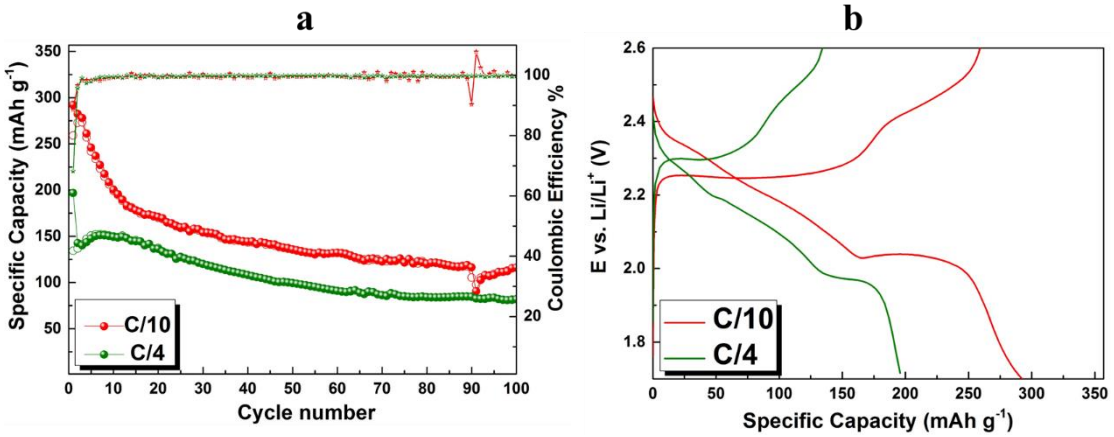


**Figure 6.10: Galvanostatic cycling of cells with NS-2 powder cathode: (a) Specific capacity at C/10 and C/2 with Coulombic efficiency. (b) 1st discharge/charge profile at C/10 and C/4.**

Cathode laminates of NS-2 were prepared using the procedure as described above. The cells displayed an initial discharge capacity of 300 mAh $g^{-1}$ and 250 mAh $g^{-1}$ at C/5 and C/2 respectively, which decreases to 150 mAh $g^{-1}$ over 100 cycles (Figure 6.11a).

The discharge capacity difference and low polarisation at different C-rate demonstrates the relatively faster kinetics due to the intermediary of sulphur radicals.[32,53] Although the voltage profile displays two discharge plateaus at about ~2.4 and ~2.1 V, probably due to the presence of longer S-S chain than expected, such as tri or tetrasulphide.[24] The first discharge plateau corresponds to cleavage of longer S-S tri or tetra bond and 2nd plateau reciprocates the breakage of disulphide bond (Figure 6.11b).

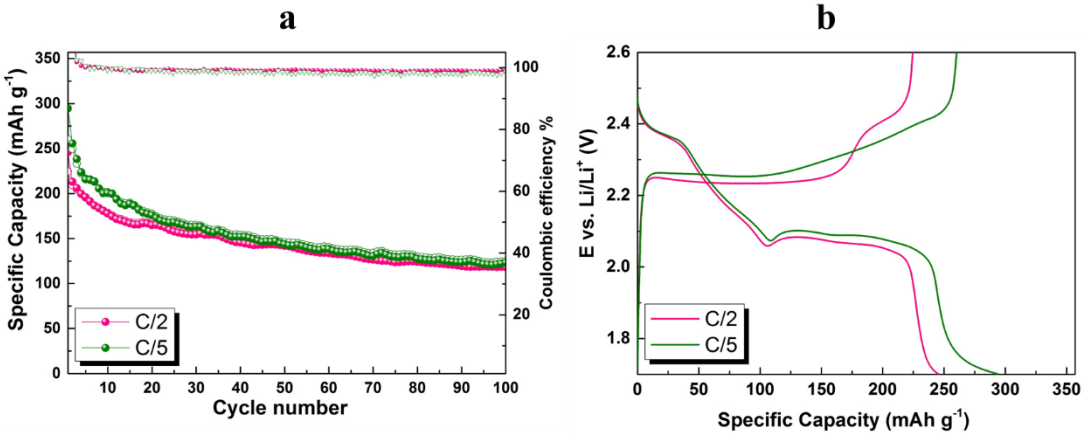


**Figure 6.11: Galvanostatic cycling with NS-2 cathode: (a) Discharge capacity with Coulombic efficiency. (b) 1st discharge/charge profile at C/2 and C/5.**

Cyclic voltammogram of NS-2 is shown in figure 6.12, assumingly the presence of N-S bond, due to nitrogen electronegativity provides an advantage of faster reduction of sulphur at higher voltage compared to sulphur cathodes.

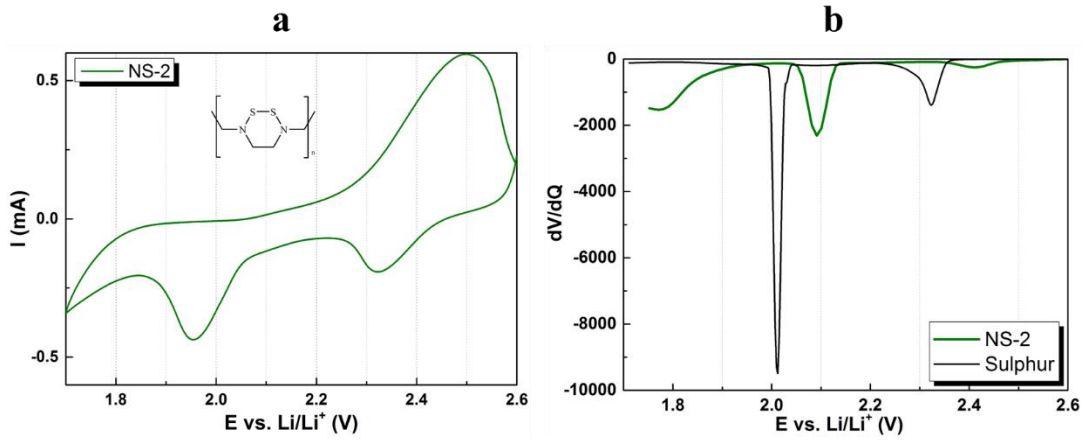


**Figure 6.12: a). Cyclic voltammogramm of NS-2 organosulphur at 0.1 mV $s^{-1}$. b). DQ/dV vs. V curves of first discharge of the cell composed with NS-2/C composite cathode (green line) and elemental S/C composite cathode (black line) at C/20.**

The derivative curve (dQ/dV vs. V, at a slow rate C/20) was plotted (Figure 6.12b). The first discharge between 1.7-2.6 V vs. $Li^+/Li$ shows reduction peaks of NS-2 at 2.41 V and 2.09 V, both slightly higher than those of elemental sulphur/sulphides. The presence of

N-S is favourable for the faster reduction of sulphur within S-S bond, owing to high electronegativity of nitrogen bond.

## 6.3 Conclusion

Novel concepts of redox organosulphur polymers have been proposed. In the first approach, an electronically conducting azomethine backbone has been used to anchor neighbouring S and N (CN) groups, which are linked together in the oxidized state of the material. In the second, elemental sulphur was used as an electrophile to create N-S bonds in a non-conjugated backbone, but facilitating the redox reaction through N-S$^{\bullet}$ radicals

Though no effort has been made in terms of optimization of the electrodes always difficult with polymeric materials, both approaches appear to be successful conceptually, as redox activities have been observed with fast kinetics (> classical Li-S) and ending at potentials slightly higher than that of the Li-$S_8$ couple, indicating the role of the electronegativity of the backbone on the redox couple position. The insolubility of both electrode materials either in the reduced or oxidized state is demonstrated with high D/C during cycling. We hope that these examples will be an inspiration for the design of similar environmentally sulphur-based electrode materials.

## 6.4 References


(1) Liang, Y.; Tao, Z.; Chen, J. Organic Electrode Materials for Rechargeable Lithium Batteries. *Adv. Energy Mater.* **2012**, *2*, 742–769.

(2) Visco, S. J. Ionic Conductivity of Organosulfur Melts for Advanced Storage Electrodes. *J. Electrochem. Soc.* **1988**, *135*, 2905.

(3) Visco, S. J. A Novel Class of Organosulfur Electrodes for Energy Storage. *J. Electrochem. Soc.* **1989**, *136*, 661.

(4) Liu, M. Electrode Kinetics of Organodisulfide Cathodes for Storage Batteries. *J. Electrochem. Soc.* **1990**, *137*, 750.

(5) Liu, M. Novel Solid Redox Polymerization Electrodes. *J. Electrochem. Soc.* **1991**, *138*, 1896.

(6) I, R. N. Cation Radicals of Organosulphur Compounds. **1995**, *25*, 637–651.

(7) Lippincott, E. R.; Tobin, M. C. The Vibrational Spectra and Structure of Nitrogen Tetrasulfide. *J. Chem. Phys.* **1953**, *21*, 1559.

(8) Li, J.; Zhan, H.; Zhou, L.; Deng, S.; Li, Z.; Zhou, Y. Aniline-Based Polyorganodisulfide Redox System of High Energy for Secondary Lithium Batteries. *Electrochem. commun.* **2004**, *6*, 515–519.

(9) Amaike, M.; Iihama, T. Chemical Polymerization of Pyrrole with Disulfide Structure and the Application to Lithium Secondary Batteries. *Synth. Met.* **2006**, *156*, 239–243.

(10) Deng, S. R.; Kong, L. B.; Hu, G. Q.; Wu, T.; Li, D.; Zhou, Y. H.; Li, Z. Y. Benzene-Based Polyorganodisulfide Cathode Materials for Secondary Lithium Batteries. *Electrochim. Acta* **2006**, *51*, 2589–2593.

(11) Uemachi, H.; Iwasa, Y.; Mitani, T. Preparation and Charge–Discharge Properties of a Novel Organosulfur Polymer, Poly (P-Phenylene Thiuret), for Battery Applications. *Chem. Lett.* **2000**, *29*, 946–947.

(12) Yu, X. G.; Xie, J. Y.; Yang, J.; Huang, H. jiang; Wang, K.; Wen, Z. S. Lithium Storage in Conductive Sulfur-Containing Polymers. *J. Electroanal. Chem.* **2004**, *573*, 121–128.

(13) Krishnan, P.; Park, J.-S.; Yang, T.-H.; Lee, W.-Y.; Kim, C.-S. Sulfonated Poly(ether Ether Ketone)-Based Composite Membrane for Polymer Electrolyte Membrane Fuel Cells. *J. Power Sources* **2006**, *163*, 2–8.

(14) Sotomura, T.; Uemachi, H.; Takeyama, K.; Naoi, K.; Oyama, N. New Organodisulfide-Polyaniline Composite Cathode for Secondary Lithium Battery. *Electrochim. Acta* **1992**, *37*, 1851–1854.

(15) Oyama, N.; Tatsuma, T.; Sato, T.; Sotomura, T. Dimercaptan-Polyaniline Composite Electrodes for Lithium Batteries With High-Energy Density. *Nature*, 1995, *373*, 598–600.

(16) Oyama, N. Effects of Adding Copper(II) Salt to Organosulfur Cathodes for Rechargeable Lithium Batteries. *J. Electrochem. Soc.* **1997**, *144*, L47.

(17) Kiya, Y.; Iwata, A.; Sarukawa, T.; Henderson, J. C.; Abru??a, H. D. Poly[dithio-2,5-(1,3,4-Thiadiazole)] (PDMcT)-poly(3,4-Ethylenedioxythiophene) (PEDOT) Composite Cathode for High-Energy Lithium/lithium-Ion Rechargeable Batteries. *J. Power Sources* **2007**, *173*, 522–530.

(18) NuLi, Y.; Guo, Z.; Liu, H.; Yang, J. A New Class of Cathode Materials for Rechargeable Magnesium Batteries: Organosulfur Compounds Based on Sulfur-Sulfur Bonds. *Electrochem. commun.* **2007**, *9*, 1913–1917.

(19) Kiya, Y.; Hutchison, G. R.; Henderson, J. C.; Sarukawa, T.; Hatozaki, O.; Oyama, N.; Abruña, H. D. Elucidation of the Redox Behavior of 2,5-Dimercapto-1,3,4-Thiadiazole Electrodes and

Application of the DMcT-PEDOT Composite Cathodes to Lithium/Lithium Ion Batteries. *Langmuir* **2006**, *22*, 10554–10563.

(20) Canobre, S. C.; Davoglio, R. A.; Biaggio, S. R.; Rocha-Filho, R. C.; Bocchi, N. Performance of a polyaniline(DMcT)/carbon Fiber Composite as Cathode for Rechargeable Lithium Batteries. *J. Power Sources* **2006**, *154*, 281–286.

(21) Kiya, Y.; Henderson, J. C.; Hutchison, G. R.; Abruna, H. D. Synthesis, Computational and Electrochemical Characterization of a Family of Functionalized Dimercaptothiophenes for Potential Use as High-Energy Cathode Materials for Lithium/lithium-Ion Batteries. *J. Mater. Chem.* **2007**, *17*, 4366–4376.

(22) Gao, J.; Lowe, M. A.; Conte, S.; Burkhardt, S. E.; Abruña, H. D. Poly(2,5-Dimercapto-1,3,4-Thiadiazole) as a Cathode for Rechargeable Lithium Batteries with Dramatically Improved Performance. *Chem. - A Eur. J.* **2012**, *18*, 8521–8526.

(23) NuLi, Y.; Guo, Z.; Liu, H.; Yang, J. A New Class of Cathode Materials for Rechargeable Magnesium Batteries: Organosulfur Compounds Based on Sulfur-Sulfur Bonds. *Electrochem. commun.* **2007**, *9*, 1913–1917.

(24) Naoi, K.; Kawase, K.; Mori, M.; Komiyama, M. Electrochemistry of poly(2,2'-dithiodianiline): A New Class of High Energy Conducting Polymer Interconnected with S-S Bonds. *J. Electrochem. Soc.* **1997**, *144*, L173–L175.

(25) Naoi, K.; Kawase, K.; Inoue, Y. A New Energy Storage Material: Organosulfur Compounds Based on Multiple Sulfur-Sulfur Bonds. *J. Electrochem. Soc.* **1997**, *144* , L170–L172.

(26) Hiromu Sugeta, Akikatsu Go, and T. M. Vibrational Spectra and Molecular Conformations of Dialkyl Disulfides. *Bull. Chem. Soc. Jpn.* **1973**, *46*, 3407–3411.

(27) Su, Y. Z.; Niu, Y. P.; Xiao, Y. Z.; Xiao, M.; Liang, Z. X.; Gong, K. C. Novel Conducting Polymer Poly[bis(phenylamino)disulfide]: Synthesis, Characterization, and Properties. *J. Polym. Sci. Part A Polym. Chem.* **2004**, *42*, 2329–2339.

(28) Schotte, L. Some Sulphur Compounds Related to Pimelic Acid. *Acta Chim. Scand* **1954**, *8*, 131–133.

(29) Hwang, T. H.; Jung, D. S.; Kim, J.; Kim, B. G.; Choi, J. W. Rechargeable Batteries Operating at Room Temperature. **2013**.

(30) Wang, L.; He, X.; Sun, W.; Li, J.; Gao, J.; Tian, G.; Wang, J.; Fan, S. Organic Polymer Material with a Multi-Electron Process Redox Reaction: Towards Ultra-High Reversible Lithium Storage Capacity. *Rsc Adv.* **2013**, *3*, 3227–3231.

(31) Tsutsumi, H.; Oyari, Y.; Onimura, K.; Oishi, T. Electrochemical Behavior of Polyamides with Cyclic Disulfide Structure and Their Application to Positive Active Material for Lithium Secondary Battery. *J. Power Sources* **2001**, *92*, 228–233.

(32) Liu, M.; Visco, S. J.; De Jonghe, L. C. Electrochemical Properties of Organic Disulfde/thiolate Redox Couples. *J. Electrochem. Soc.* **1989**, *136*, 2570–2575.

(33) Glass, R. S. *Sulfur Radical Cations*; 1999.

(34) Thiophosgene in Organic Synthesis.pdf.

(35) Trofimov, B. A.; Sinegovskaya, L. M.; Gusarova, N. K. Vibrations of the S-S Bond in Elemental Sulfur and Organic Polysulfides: A Structural Guide. *J. Sulfur Chem.* **2009**, *30*, 518–554.

(36) Van Wartz, H. E.; Scheraga, H. a. Raman Spectra of Strained Disulfides. Effect of Rotation about Sulfur-Sulfur Bonds on Sulfur-Sulfur Stretching Frequencies. *J. Phys. Chem.* **1976**, *80*, 1823–1832.

(37) Kozhevina, L. I. Experimental and Theoretical Study of Monosubstituted Guanidines by Vibrational Spectroscopy. **1997**, *9*, 1357–1360.

(38) Guo, J.; Yang, Z.; Yu, Y.; Abruña, H. D.; Archer, L. a. Lithium-Sulfur Battery Cathode Enabled by Lithium-Nitrile Interaction. *J. Am. Chem. Soc.* **2013**, *135*, 763–767.

(39) Peter Larkin. Infrared and Raman Spectroscopy Principles and Spectral Interpretation. *Copyright © 2011 Elsevier Inc. All rights reserved.*, 2011, 117–133.

(40) Division, C. Electrical Conductivity of Heteroaromatic Ladder Polymers. 3. Phenothiazine and the Structurally Related Ladder Polymers. **1986**, *23*, 137–139.

(41) Lee, Y. S.; Kim, O. Electronic Structures of Heterocyclic Ladder Polymers; Polyphenothiazine, Polyphenoxazine, and Polyphenoquinoxaline. **1992**, 378–383.

(42) andreani1991.pdf.

(43) Edited by N. KHARASCH. Organic Sulfur Compounds. **1961**, *1*, 1–625.

(44) Sharma, S. The Chemistry of Thiophosgene. *Sulfur reports* **1986**, *5*, 1–87.

(45) Sugeta, H.; Go, A.; Miyazawa, T. S–S and C–S Stretching Vibrations and Molecular Conformations of Dialkyl Disulfides and Cystine. *Chem. Lett.* **1972**, 83–86.

(46) Xiao, L.; Cao, Y.; Xiao, J.; Schwenzer, B.; Engelhard, M. H.; Saraf, L. V; Nie, Z.; Exarhos, G. J.; Liu, J. Molecular Structures of Polymer/sulfur Composites for Lithium-Sulfur Batteries with Long Cycle Life. *J. Mater. Chem. A* **2013**, *1*, 9517–9526.

(47) Richardson, J. Table of Characteristic IR Absorptions. *Univ. Color. Boulder, Chem. Biochem. Dep.* **2011**, *3610*, 1.

(48) Meyer, B. Elemental Sulfur. *Chem. Rev.* **1976**, *76*, 367–387.

(49) Biswas, N.; Waring, A. J.; Walther, F. J.; Dluhy, R. A. Structure and Conformation of the Disulfide Bond in Dimeric Lung Surfactant Peptides SP-B1-25 and SP-B8-25. *Biochim. Biophys. Acta - Biomembr.* **2007**, *1768*, 1070–1082.

(50) Van Wart, H. E.; Lewis, a; Scheraga, H. a; Saeva, F. D. Disulfide Bond Dihedral Angles from Raman Spectroscopy. *Proc. Natl. Acad. Sci. U. S. A.* **1973**, *70*, 2619–2623.

(51) Duan, B.; Wang, W.; Wang, A.; Yu, Z.; Zhao, H.; Yang, Y. A New Lithium Secondary Battery System: The Sulfur/lithium-Ion Battery. *J. Mater. Chem. A* **2014**, *2*, 308–314.

(52) Yukiko Tanaka and Yoshimasa Tanaka. Infrared Absorption Spectra of Organic Sulfur Compounds. *Chem. Pharm Bull.* **1965**, *13*, 858–861.

(53) Cuisinier, M.; Hart, C.; Balasubramanian, M.; Garsuch, A.; Nazar, L. F. Radical or Not Radical: Revisiting Lithium-Sulfur Electrochemistry in Nonaqueous Electrolytes. *Adv. Energy Mater.* **2015**, *5*, 1–6.

# *Final Conclusions & perspectives*

This thesis work aimed at finding solutions for complex issues related to Li-anode in Li-S batteries concentrated on four different strategies namely protective layers, hybrid anode architecture, alternative binders and alternative cathode materials. The conclusions can be described as follows:

## 7.1 Conclusions:

- ✓ $Li_3N$ protective layers on the surface of metallic Li-anode via multiple approaches to inhibit direct contact of Li-anode with electrolyte have been successfully implemented.
- ✓ The $Li_3N$/Li-anode exhibits improved electrochemical performance with efficient protection of lithium metal morphology as compared to non-protected Li showing that $Li_3N$ could be a material of choice for Li-anodes in Li-S batteries.
- ✓ In-situ $Li_3N$ deposition proved to be an alternative technique for protective of Li metal anode.
- ✓ The graphite/rGO protective layer for lithium metal and as hybrid anode indicates the feasibility of hybrid architecture as suitable anodes for Li-S batteries.
- ✓ Completely lithiated graphite/rGO layer can act as pseudo-anode in Li-S cells.
- ✓ *In-situ* XRD and solid state NMR have been shown as suitable techniques to study the Li metal anode/graphite hybrid anode architecture.
- ✓ Partial lithiation of the graphite/rGO layer in the hybrid configuration has been proved to compensate the loss of Li spent in the formation of SEI layer in Li-S cells.
- ✓ The graphite/rGO layer paves the way to construct Li-S cells with protective layers only with polymer binders instead of using expensive deposition techniques like PLD and sputtering.

- ✓ GPE-PIL has been identified as an alternative binder for sulphur cathodes showing improved long-term cycling stability as well strategy to retain polysulphides within cathode.
- ✓ The GPE-PIL composite helps in slow diffusion of polysulphides in liquid electrolytes serving as a buffer, which retains them within the composite cathode.
- ✓ GPE-PIL can be used successfully as polymer electrolyte in Li-S cells.
- ✓ Redox organosulphur polymers with conjugated backbone with N-S bond were projected as alternative cathode material for Li-S battery system.
- ✓ Slightly higher redox potential was achieved due to N-S bond and S-S chain attached directly to the polyamine backbone providing a trap for polysulphides; inhibiting one of the prime challenges of the classical Li-S battery.

## 7.2 Perspectives

- ➢ Optimization of $Li_3N$ deposition using binders could be a next step forward to obtain homogenous thin coating of protective layers on Li metal anodes.
- ➢ *In-situ* deposition technique has been identified as a possible solution for protective coating on Li-anode. Probing different materials capable of forming thin layers on the Li metal anodes can lead to interesting performance enhancement.
- ➢ In depth interfacial studies of Li-anode with graphite/rGO protective layer (hybrid architecture) can complement to significant improvement for the Li-S system.
- ➢ Optimisation studies on minimizing GPE-PIL quantity in the cathode composite with efficient composite mixing techniques followed by screening different PIL for use as binders could provide routes to employ binders as a binding agent as well as a polysulphide trap.

- Optimization of the organosulphur electrodes to understand the redox reaction mechanism and electrode kinetics will be of great interest.
- As a future work, studies on the use of organosulphur redox polymers in all solid-state batteries can be a significant asset.

# *Appendix*

# Glossary

**Active mass** is the material that generates electrical current by means of chemical reaction within the battery.

**Allotrope**: Two or more forms of the same element in the same physical state (solid, liquid, gas) that differ from each other in physical and sometimes chemical properties.

**Ampere-hours:** Symbol Ah is a unit of charge. Example: Drawing a current of one ampere (1A) from a battery for one hour (1h) equates in one ampere-hour (1Ah).

**Battery cycle:** Charge followed by a discharge and recharge. No standard exists as to level of charge and discharge to constitute a cycle.

**Button cell**: Miniaturized battery also known as coin cell. Most are non-rechargeable.

**Capacity**: Electrical energy of a battery in ampere-hours (Ah). The stored energy is measured by observing the elapsed time while discharging at a constant current to the end-of-discharge voltage. The capacity is the leading health indicator of a battery.

**Charge:** Replenishing electrical charge to a cell or battery. **Charging** is the operation in which the battery is restored to its original charged condition by reversal of the current flow.

**Coulombic efficiency,** also called faradaic efficiency or current efficiency describes the charge efficiency by which electrons are transferred in a batteries.

**Coffee bag cell:** Packaged into a flexible, heat-sealable foil pouch similar to wrapping food products.

**C-rate**: Unit by which charge and discharge times are scaled. At 1C, the battery charges and discharges at a current that is at par with the marked Ah. (See BU-402)

**Cycle:** Charge/discharge/charge. No standard exists as to what constitutes a cycle.

**Cycle life:** Number of cycles a battery can deliver. (End of-battery-life for portable devices is commonly set to 80 %.)

**Cylindrical cell:** Positive and negative plates are rolled up and placed into a cylindrical container.

**Discharging** is the operation in which the battery delivers electrical energy to an external load.

**Electrode:** Conductor or plate in a cell in which an electrochemical reaction occurs.

**Electrolyte:** Liquid conductor of electricity and ion movement between positive and negative electrodes of a battery.

**Energy:** Work measures over time. Multiplying voltage x current x time = Watt-hours (Wh). Energy is also given in joules (J); 1,000 joules are 0.277Wh.

**Energy density:** Also known as volumetric energy density; specifies the amount of energy a cell can hold in volume (Wh/l). Energy density is synonymous with the runtime of a battery.

**Farad (f):** Charge in coulombs necessary to change the potential between the plates of a capacitor by 1V. (1 Farad = 1 Coulomb per Volt)

**Frequency:** Number of events in a given time. Indicates how often the AC voltage changes from positive to negative per second, or how many times a battery is cycled.

**Graphene:** Allotrope of carbon in a two-dimensional hexagonal lattice in which one atom forms each vertex; establishes the basic structural element of graphite, charcoal diamonds and more.

**Graphite:** A form of carbon with hexagonally crystallized allotrope, used in lead pencils, lubricants, batteries and the anode of most Li-ion.

**Gravimetric energy density:** Also known as specific energy; indicates the amount of energy a cell holds in weight (Wh/kg); synonymous with battery runtime.

**Hertz (Hz):** Unit of frequency; 1Hz constitutes one full cycle per second.

**Hysteresis charge:** Charger turns off at full charge and resumes after a time to compensate for parasitic loads and self-discharge.

**Impedance:** Combination of capacitive, inductive and ohmic resistance; measured in ohms (R); frequency dependent. **Internal resistance** or impedance is the resistance or impedance that a battery or a cell offers to current flow.

**Internal resistance:** Electrical resistance of a battery pack in milliohms (m□). A good battery has low resistance; corrosion raises it.

**Ion:** Atom or molecule with unequal number of electrons and protons; provides a positive or negative electrical charge.

**Lithium (Li):** Soft, silver-white metal belonging to the alkali metal group; lightest and least dense metal in the element family; discovered by Johan August Arfwedson in 1817; metal is named after the Greek word "lithos" meaning "stone."

**Milliampere-hour (mAh):** Specifies battery capacity or rating; 1000mAh equals 1Ah.

**Millihertz:** Unit of frequency. Example: 1 Hertz = 1 cycle/second; 1mHz = 1,000 seconds.

**Nyquist plots:** Invented by Harry Nyquist (1889–1996) while working at Bell Laboratories; provides the frequency response of a linear system that displays both amplitude and phase angle on a single plot using frequency as parameter.

**Open-circuit voltage** is the voltage across the terminals of a cell or battery when no external current flows. It is usually close to the thermodynamic voltage for the system.

**Passivation layer:** Resistive layer that forms on some batteries after prolonged storage. Applying a brief load breaks the layer and enables current flow.

**Polymer:** Electrical insulator that passes ions.

**Prismatic cell:** A battery in which the positive and negative plates are stacked instead of rolled.

**Ragone chart:** Plots battery performance on specific energy versus specific power

**Resistance:** Restriction to current flow; high resistance generates voltage drop and heat.

**Self-discharge:** Capacity loss due to internal leakage.

**Separator:** A physical barrier between the positive and negative electrodes to avoid electrical shorting. Separators must be permeable to the ions and inert in the battery environment.

**Solid electrolyte interface (SEI):** A film composed of lithium oxide and lithium carbonate forms on the surface of the Li-ion anode. The SEI layer grows with cycling and can form a barrier to obstruct ion flow.

**Spectroscopy:** Analysis of a compound or a battery when scanned with a frequency.

**Voltage (V):** Electric energy potential per unit charge. 1V = 1J/Coulomb. (1,000 joules = 0.277Wh).

**Volumetric energy density:** Also known as energy density; specifies energy storage in volume (Wh/l).

**Watt (W):** Unit of power; ampere (A) times volt (V) equals watts (W).

**Watt-hour (Wh):** Unit of electrical energy equivalent to a power consumption of one watt for one hour (One watt-hour = 3600 Joules). Multiplying a battery voltage (V) by the rated capacity (Ah) gives the battery energy in Wh. Example: 14.4V x 2.5 Ah = 36 Wh.

# Abbreviations

In alphabetical order:

| | |
|---|---|
| AM | Active Mass |
| CICE | Centro Investigacion Corporativas EnergiGUNE |
| CV | Cyclic Voltammetry |
| CC | Specific charge during Li-ion extraction (mAh $g^{-1}$) |
| CD | Specific charge during Li-ion insertion (mAh g-1) |
| C-rate | Specific current proportional to theoretical amount of specific charge in a given material (mA $g^{-1}$) |
| Coul.eff. | Coulombic efficiency |
| DSC | Thermogravimetric Analysis |
| dQ/dV | Differential (incremental) capacity analysis as a function of cell potential. |
| EIS | Electrochemical Impedance Spectroscopy |
| F=NAe | Faraday's constant (9.64853 · 105 C mol-1) |
| F | Frequency ($s^{-1}$) |
| g/mol | Grams per mole |
| GB | Glove Box |
| GCPL | Galvanostatic Cycling with Potential Limitation |
| GPE | Gel Polymer Electrolyte |
| I | Current (mA) |
| LiB | Lithium-Ion Battery |
| Li-S | Lithium-Sulphur Battery |
| $Li_2S_x$ | Lithium polysulphides |
| $Li_2S$ | Lithium sulphide |
| mA | Mili Amperes |
| mA h $g^{-1}$ | Mili ampere hour per gram |
| NMR | Nuclear Magnetic Resonance spectroscopy |
| $N_A$ | Avogadro's constant (6.02214 ·1023 mol-1) |
| PIL | Polymeric ionic liquid |

| | |
|---|---|
| OCV/ $V_O$ | Open Circuit Voltage |
| R | Resistance (Ω) |
| SEM | Scanning Electron Microscopy |
| SOA | State-of the-Art |
| t (s) (hrs) | Time (seconds) (hours) |
| Temp. ($^oC$, $^oK$) | Temperature (Degree Celsius, Degree Kelvin) |
| TGA | Thermogravimetric Analysis |
| UPV | Universidad del País Vasco |
| UV/Vis | Ultraviolet/Visible spectroscopy |
| V | Voltage |
| Wt. % | Weight Percentage |
| XPS | X-ray Photoelectron Spectroscopy |
| XRD | X-ray Diffraction |

# List of Figures

**Figure 1.1: Prognosis of the energy requirements up to year 2050 within whole world.** ..... 1
**Figure 1.2: Timeline of battery evolution, starting from 1748 when Benjamin Franklin first devised the word "Battery".** ..... 3
**Figure 1.3: Commercially available different types of batteries .i.e. (right to left) CR2032 & LR44 coin cells, 9-Volt box battery, 23A, AAAA, AAA, AA, C, D, 4.5-volt.** ..... 5
**Figure 1.4: Pyramid of different battery systems according to their energy densities (Wh kg$^{-1}$) and EV driving force (km).** ..... 7
**Figure 1.5: Graphical drawing of a typical Li-ion battery with graphite anode and $Li_xFePO_4$ cathode immersed in $Li^+$ conducting organic electrolyte.** ..... 8
**Figure 1.6: Theoretical and experimental gravimetric energy density (Wh kg$^{-1}$) of Li-based systems. Practical estimated values denote to the cell level.** ..... 9
**Figure 1.7: Diagram of a classic Li-air system using Li-based anode and porous carbon as cathode with organic $Li^+$ conducting electrolyte.** ..... 10
**Figure 1.8: schematic diagram showing evolution of energy density in Li-based batteries.**[1] ..... 11
**Figure 1.9: Schematic diagram of a Li−S cell with its charge/discharge operations.** ..... 12
**Figure 1.10: A typical voltage vs. capacity plot for a Li-S cell explaining the evolutions of polysulphide species.** ..... 14
**Figure 1.11: Discharge/charge voltage vs. capacity profile of a typical Li-S battery.** ..... 14
**Figure 1.12. a) CMK-3, a channel of mesoporous carbon with sulphur encapsulation using vapour phase infusion. b) Comparison of CMK-3/S with PEG (black) vs. CMK-3/S without PEG (red).** ..... 16
**Figure 1.13: Representation of electrochemical reaction of polysulphides within the organic electrolyte.** ..... 18
**Figure 1.14: Commonly used cathode in LIBs. a) Layered pattern of $LiCoO_2$, Theoretical capacity: 140 mAh g$^{-1}$(b) Cubic $LiMn_2O_4$ (LMO) spinel, Theoretical capacity: 100-120 mAh g$^{-1}$ (c) $LiFePO_4$ (LFP) with olivine structure, Theoretical capacity: 150-170 mAh g$^{-1}$.** ..... 19
**Figure 1.15: Summary of the effects of polysulphide dissolution, Shuttle phenomenon, effect on the cathode, insoluble products upon charge and discharge.** ..... 20
**Figure 2.1: schematic diagram of the composite mixing by using DMSO solvent technique.** ..... 29
**Figure 2.2: Showing casting on current collector by using Dr. Blade technique; prepared laminate and the punched spherical disc cathodes.** ..... 30
**Figure 2.3: The homogenous slurry of PEO: LiTFSI in dry acetonitrile after stirring for 24hrs and the structural diagram of PEO: LiTFSI.** ..... 31
**Figure 2.4: PTFE disc for casting of PEO: LiTFSI mixture.** ..... 32
**Figure 2.5: Casted and punched membrane of PIL-EM005 (200um) and structure of EM005-PIL comprised of 3 cations ($PIL^+$, $IL^+$, $Li^+$) and 1 anion ($TFSI^-$).** ..... 33
**Figure 2.6: Image of metallic Li before and after cleaning for battery testing.** ..... 33
**Figure 2.7: a) schematic diagram of CR2032 coin type cell configuration. b) Photograph of coin cell within the holder.** ..... 34
**Figure 2.8: a) Photograph of a Li-S coffee bag cell. b) Schematic presentation of the liquid Li-S battery configuration.** ..... 35

**Figure 2.9: Image of battery component to be tested in in-situ experiment before assembly, and assembled coffee bag cell with a glass window for the in-situ UV/Visible measurements.** ..... 36
**Figure 2.10: a) Image of in-situ XRD cell with beryllium window and PTFE body, b) Schematic diagram of the configuration of cell, c) The perforated Li-anode, with 10mm hole used for in-situ measurements.** ..... 36
**Figure 2.11: a) SEM equipment used for SEM measurements, b) Sample holder showing the preparation of samples by adhesion on carbon tape.** ..... 39
**Figure 2.12: Schematics of the XPS equipment used for sample measurements.** ..... 41
**Figure 2.13: Raman spectrometer used to collect data.** ..... 43
**Figure 2.14: a) Bruker advance D8 diffractometer used for testing samples, b) sample holder cover with capton for air-sensitive samples.** ..... 44
**Figure 2.15: The image of Bruker instrument for in-situ XRD.** ..... 45
**Figure 2.16: Solid state NMR 500 MHz instrument used for analysis of NMR and the Image of sample holder prepared inside the glovebox under argon atmosphere.** ..... 46
**Figure 2.17: UV/Visible equipment used for in-situ measurements.** ..... 47
**Figure 2.18: The TG-DSC instrument used for measurements.** ..... 48
**Figure 3.1: Schematic explanation of the self-healing electrostatic shield mechanism of the Li deposition process.** ..... 55
**Figure 3.2: Schemtaic diagram of Li-S cell (a) without the protective layer (b) with $Li_3N$ protective layer.** ..... 57
**Figure 3.3: Sealed assembly designed for nitridation.** ..... 59
**Figure 3.4: a) Comparative study of galvanostatic cycling with and without $Li_3N$ pellet at C/20, b) Coulombic efficiency %, c) $Li_3N$ pellet discharge/charge voltage profile vs. specific capacity.** ..... 63
**Figure 3.5: XRD diffractogram of $Li_3N$ formed by nitridation technique compared with standard JCPDS data for $Li_3N$.** ..... 65
**Figure 3.6: a) Comparative study of galvanostatic cycling with and without nitridated $Li_3N$ at C/20, b) Coulombic efficiency %, c) Nitridated $Li_3N$ discharge/charge voltage profile vs. specific capacity.** ..... 66
**Figure 3.7: a) Image and SEM morphology is shown for surface of pristine and $Li_3N$ layer, last figure shows the cross section of the layer with Li-foil, b) XRD graph comparing EPDM, $Li_3N$ commercial and $Li_3N$ mixture with EPDM.** ..... 67
**Figure 3.8: a) Comparative study of galvanostatic cycling with and without $Li_3N$and EPDM binder deposit at C/20, b) Coulombic efficiency %, c) Deposited $Li_3N$ discharge/charge voltage profile vs. specific capacity.** ..... 68
**Figure 3.9: a) Comparative study of galvanostatic cycling with and without nitridated $Li_3N$ with EPDM binder deposit at C/20, b) Coulombic efficiency %, c) nitridated $Li_3N$ deposit discharge/charge voltage profile vs. specific capacity.** ..... 69
**Figure 3.10: a) Comparative study of galvanostatic cycling with and without $Li_3N$and EPDM binder deposit at C/20, b) Coulombic efficiency %, c) Nitridated $Li_3N$ discharge/charge voltage profile vs. specific capacity.** ..... 70
**Figure 3.11: Galvanostatic cycling comparison at similar condition over the C-rate of C/20 and C/5, a) Blank cells, b) $Li_3N$ pellet, c) $Li_3N$ with EPDM binder deposit, d) Nitridated $Li_3N$ with EPDM binder deposit.** ..... 72
**Figure 3.12: Cyclic voltammetry of the symmetric cell at the scan rate of 0.5mV$s^{-1}$ and EIS measurements before and after CV, a) $Li_3N$ pellet, b) $Li_3N$ with EPDM binder deposit, c) Blank.** ..... 73

**Figure 3.13: Comparative cyclic voltammetry of the full Li-S cell with (red) and without (black) $Li_3N$ protective layer at the scan rate of 0.5mVs$^{-1}$ and EIS measurements before and after GCPL.** ..... 74
**Figure 3.14: SEM micrograph of the samples 1) Without $Li_3N$ protective layer, 2) With $Li_3N$ protective layer.** ..... 75
**Figure 3.15: EDS analysis of the SEM micrograph taken for the categories of samples 1) Without $Li_3N$ protective layer (a) After 5 cycles (b)After 10 cycles. 2) With $Li_3N$ protective layer (c) After 5 cycles (d) After 10 cycles.** ..... 76
**Figure 3.16: XPS $S_2p$ spectra of: a) Li-foil recovered after 1 cycle without protective layer, (b) Li recovered after 1cycle with $Li_3N$ protective layer in same conditions.** ..... 77
**Figure 3.17: Visual photograph of Lithium foil before and after drop-coating of Trimethyl azide silane.** ..... 78
**Figure 3.18 : XPS graph comparing pristine Li-foil and Li-foil coated with $(CH_3)_3SiN_3$.** .. 79
**Figure 3.19: SEM micrograph exhibits evolution of pristine Li-foil and formation of $Li_3N$ when coated with $(CH_3)_3SiN_3$.** ..... 80
**Figure 3.20: FTIR analysis of pristine Li-foil compared with commercial $Li_3N$, commercial $(CH_3)_3SiN_3$ solvent and coated Li-foil a) Full spectra, b) Enhanced IR range of Azide and Nitride.** ..... 80
**Figure 3.21: CV plating/stripping experiment of Li-anode vs. stainless steel as $W_E$ with electrolyte a) 0.1M $(CH_3)_3SiN_3$ in 1M LiTFSI (DME: DIOX), b) 1M LiTFSI (DME: DIOX) without any additive.** ..... 81
**Figure 3.22: CV of Li-anode vs. sulphur composite cathode as $W_E$ with electrolyte 0.1M $(CH_3)_3SiN_3$ in 1M LiTFSI (DME: DIOX).** ..... 82
**Figure 3.23: Galvanostatic cycling comparison of a) 0.01M and 0.1M concentration of $(CH_3)_3SiN_3$ in the electrolyte with blank, b) Coulombic efficiency %.** ..... 83
**Figure 3.24: Galvanostatic cycling comparison of a) $(CH_3)_3SiN_3$ drop-coated on Li-anode with blank, b) Coulombic efficiency %.** ..... 83
**Figure 4.1: Schematic cell configuration of rechargeable Li–S batteries: (a) traditional configuration with severe shuttle effect and Li2Spoison problems and (b) new configuration with the MWCNT interlayer.** ..... 94
**Figure 4.2: Schematic illustration of the Li-S battery with hybrid anode.** ..... 95
**Figure 4.3: SEM micrographs of graphite film a) fresh b) after short-circuiting in electrolyte c) after discharge vs. Li and d) after discharge vs. sulphur composite cathode.** ..... 98
**Figure 4.4: A photograph of coin-cell post-mortem and graphite film displaying colour change from black to marron over discharging with Li-anode in presence of 1M LiTFSI (DME:Diox).** ..... 99
**Figure 4.5: XRD spectra after treating the graphite film in different manners i.e. a) fresh film b) after short-circuiting in electrolyte with Li metal c) after discharge vs. Li and d) after discharge vs. sulphur composite cathode.** ..... 100
**Figure 4.6: XRD analysis of graphite discharged vs. S/C composite cathode with comparison to elemental sulphur.** ..... 101
**Figure 4.7: a) Initial rest-discharge-charge voltage profile of graphite film with Li-anode vs. S composite cathode b) in-situ XRD measurement spectra for rest (black), discharge (red) and charge (blue)at C/10 in the range of 1-3V.** ..... 101
**Figure 4.8: Comparison of XRD spectra of fresh graphite film with spectra taken at rest, discharge and charge state b) the enhance spectra to observe the obvious shift in peaks.** 102
**Figure 4.9: $^7$Li solid –state NMR spectra of the graphite film at the a) discharge with Li-anode in LP30 b) c)short-circuited with Li in 1M LiTFSI in DME: Diox (1:1 vol.%).** . 103

**Figure 4.10: $^{7}$Li NMR spectra of the graphite film at the a) 1 cycle Vs. sulphur cathode in 1M LiTFSI (DME:Diox) b) spectra taken after resting for 16 h c)difference spectrum of a and b.** ..... 104
**Figure 4.11: a) $^{7}$Li NMR spectra of the graphite film after discharge vs. sulphur cathode in 1M LiTFSI (DME: Diox) b) enhanced spectra showing a doublet corresponding to ionic Li and LiCx (x>12).** ..... 105
**Figure 4.12: Graphite layer on the surface of Li-anode a) comparative discharge capacities of cell with and without graphite layer. b) Comparative coulombic efficiency graph.** ..... 106
**Figure 4.13: a) 3 electrode design for external short-circuiting of graphite layer with Li metal anode. b) Galvanostatic voltage vs capacity profile.** ..... 107
**Figure 4.14: a) Schematic illustration of the hybrid anode containing Li-S battery. b) Galvanostatic discharge/charge capacity graphs showing the huge capacity fade upon 25$^{th}$ cycle, with 8% drop since 2$^{nd}$ cycle.** ..... 108
**Figure 4.15: Galvanostatic cycling profile with and without graphite protective layer with Csp/sulphur as composite cathode.** ..... 109
**Figure 4.16: Galvanostatic cycling of graphite deposited Li anode based Li-S cells**..... 109
**Figure 4.17: a) Galavanostatic capacity graph by using rGO layer on Li-anode with comparison to blank. b) Coulombic efficiency of cells with and without rGO layer.** ..... 110
**Figure 4.18: a) Schematic illustration of the hybrid anode structure within a coin cell CR2032. b) Specific capacity curve of graphene used as an interlayer in Li-S systems.** .. 111
**Figure 4.19: a) rGO-1 (thermally reduced graphene) deposited Li-anode b) rGO-2 (chemically reduced graphene) deposited Li-anode c) rGO-3 (commercial) deposited Li-anode.** ..... 112
**Figure 4.20: a) EIS measurement graph taken before CV measurements for 3 kinds of rGO. b) EIS measurement graph taken after CV measurements.** ..... 113
**Figure 4.21: a) Galvanostatic capacity graph comparing the 3 different rGOs b) Coulombic efficiency of all 3 rGOs c) the voltage profile showing 1$^{st}$ and 8$^{th}$ cycle of rGO-1, while 2$^{nd}$ cycle of rGO-2 and rGO-3.** ..... 114
**Figure 5.1: Summary of the most commonly used binders in the Li−S literature according to 79 recent publications where electrodes were prepared from slurry casting techniques. "PVdF" includes grades referred to as only PVdF by the manufacturer or where no grade was specified.** ..... 123
**Figure 5.2: A structural composition of the polymer electrolyte LiTFSI: PYR14TFSI (1:9 mol ratio) with 58 wt. % poly (DDA) TFSI in acetone.** ..... 125
**Figure 5.3: Image of GPE-PIL-S-$C_{ECP600JD}$ cathodes after processing showing the morphology before and after cycling.** ..... 126
**Figure 5.4: SEM micrographs of the GPE-PIL-CEcp600JD-S: a) before cycling and b) after 100 cycles.** ..... 128
**Figure 5.5: SEM micrographs of the GPE-PIL-S-CEcp600JD cathode with comparison to PVdF-S- CEcp600JD cathode and PEO-S- CEcp600JD cathode, a) Surface view, b) Cross-section view.** ..... 129
**Figure 5.6: In-situ UV/Vis spectra for the Li-S battery with GPE-PIL-S-CEcp600JD cathode, a). Galvanostatic voltage curve for 1$^{st}$ and 2$^{nd}$ cycle vs. time, UV/Vis spectra measured over, b)1$^{st}$ discharge, c) 1$^{st}$ charge, d) 2$^{nd}$ discharge, e) 2$^{nd}$ charge, f) Deconvolution of the UV/Visible measurements.** ..... 130
**Figure 5.7: a) Comparitive galvanostatic cycling tests of Li-S battery with GPE-PIL-S-CEcp600JD cathode by using different electrolyte solvents at C/20, b) discharge/ charge voltage profile.** ..... 131

**Figure 5.8: Discharge capacity and coulombic efficiency for Li-S batteries with GPE-PIL-S-CEcp600JDcomposite using different electrolytes and compared with PvdF binder at a c rate of C/20 at RT(25 °C)between 1.5 and 3 V** ..... 132
**Figure 5.9:Galvanostatic curves in the 1st, 10th, 50th and 100th cycle measured using C/20 rate for: a) GPE-PIL-S-$C_{Ecp600JD}$ composite with 1M LiTFSI in TEGDME: Diox; b) GPE-PIL-S-$C_{Ecp600JD}$ composite with 1M LiTFSI in DME: Diox and c) PVdF-S-$C_{Ecp600JD}$ composite with 1M LiTFSI in TEGDME: Diox using Celgard 2400 separator.** ..... 133
**Figure 5.10: a) Comparative galvanostatic cycling with coulombic efficiency % of GPE-PIL-S-$C_{Ecp600JD}$ cathode with Celgard 2400 and glassfiber separators at C/20, b) Discharge/charge voltage profile.**..... 134
**Figure 5.11: Galvanostatic cycling performance as a function of lamination techniques employed with GPE-PIL-S-$C_{Ecp600JD}$ cathode.**..... 135
**Figure 5.12: a) Galvanostatic cycling performance as a function of PIL % in the GPE-PIL-S-$C_{Ecp600JD}$ cathode, b) Coulombic efficiency %, c) Discharge/charge voltage profile.**..... 135
**Figure 5.13: a) Comparative galvanostatic cycling performance of GPE-PIL-S-$C_{Ecp600JD}$ cathode, with different cathode binders, b) Discharge/charge voltage profile.** ..... 136
**Figure 5.14: Rate capability of Li-S battery using GPE-PIL-S-$C_{Ecp600JD}$ composite, at various discharge and charge rates from C/20 to 1C and back to C/20.**..... 137
**Figure 6.1: Assessment of the cell performance in radical compounds (blue), organosulphur (green), and carbonyl (red) by mean of (A) discharge potential vs discharge capacity (B) power density vs energy density.**..... 143
**Figure 6.2: a) The picture shows state of mixture during reaction at 120°C b) Product after the reaction and after washing with $CS_2$.** ..... 150
**Figure 6.3: a) FTIR spectra of cyanoguanidine and the organosulphur polymers NS and NS-1 obtained in step 1 and step 2, b) TGA thermogram of organosulphur polymers NS and NS-1.** ..... 153
**Figure 6.4: a) Gavanostatic cycling of organosulphur cathode at C/20 formation cycles and C/2. b) Discharge/charge profile of first cycle at C/20.** ..... 153
**Figure 6.5: Cyclic voltammogramm with organosulphur cathode separated by GF separator wet with 1M LiTFSI in DME: DIOX (1: 1 wt. %) in a coin Cell CR2032 at a scan-rate of 0.5 mV $s^{-1}$.**..... 154
**Figure 6.6: a) FTIR spectra of Poly (diethylamine) and the organosulphur polymers NS-3a obtained after washing with $CS_2$. b) TGA thermogram representing the NS-2 product after washing with $CS_2$ comparing with initial polyamine reactant used for reaction.** ..... 155
**Figure 6.7: XRD comparison of organosulphur polymer (NS-2) with polyamine compound (PA) and elemental sulphur (S) at RT.**..... 156
**Figure 6.8: Raman measurements of organosulphur polymer (NS-2) with polyamine compound (PA) and elemental sulphur (S) at RT.**..... 157
**Figure 6.9: Galvanostatic cycling of cells with NS-2 powder cathode before (blue dots) and after (red dots) washing with $CS_2$ at C/10.** ..... 158
**Figure 6.10: Galvanostatic cycling of cells with NS-2 powder cathode: (a) Specific capacity at C/10 and C/2 with Coulombic efficiency. (b) 1st discharge/charge profile at C/10 and C/4.** ..... 159
**Figure 6.11: Galvanostatic cycling with NS-2 cathode: (a) Discharge capacity with Coulombic efficiency. (b) 1st discharge/charge profile at C/2 and C/5.** ..... 160
**Figure 6.12: a). Cyclic voltammogramm of NS-2 organosulphur at 0.1 mV $s^{-1}$. b). DQ/dV vs. V curves of first discharge of the cell composed with NS-2/C composite cathode (green line) and elemental S/C composite cathode (black line) at C/20.**..... 160

# List of tables

**Table 1.1: Different systems of primary batteries, denoting their major characteristics and applications. ..... 4**
**Table 1.2: Characteristics and applications of the secondary (rechargeable) battery systems ..... 6**
**Table 1.3: Demonstration shows theoretical voltages and capacities of few lithium based batteries. Values mentioned are denoted to the cathode and anode. ..... 9**
**Table 5.1: Exhibition of different techniques and parameters applied for the optimisation of GPE-PIL-S-$C_{ECP600JD}$ composite cathode. ..... 127**

# List of Publications

Part of the work presented in this thesis have been submitted/ to be submitted for publication. The following is a list of citations for these publications:

1. **Marya Baloch**, Alen Vizintin, Jože Moškon, Devaraj Shanmukaraj, Teofilo Rojo, Robert Dominko "Application of the gel polymer electrolytes based on ionic liquids in the Li-S batteries"- Submitted to Journal of the Electrochem. Soc. (2016).
2. **Marya Baloch**, Oleksandr Bondarchuk, Emilie Bekaert, Teofilo Rojo, Michel Armand, Devaraj Shanmukaraj "Electrochemical Studies of Lithium Nitride as Protective Layer for Metallic Lithium Anode in Lithium Sulphur Batteries"- Submitted to Journal of Power Sources (2016).
3. **Marya Baloch**, Hicham Ben youcef , Chunmei Li, Oihane Garcia-Calvo, Devaraj Shanmukaraj, Teofilo Rojo, Michel Armand "New Redox material based on reversible cleavage of S–N bonds as cathode material" -Dalton Transactions (2016)- To be Submitted.
4. **Marya Baloch**, Juan Miguel López Del Amo, Teofilo Rojo, Michel Armand, Devaraj Shanmukaraj, "Role of Graphite/rGO as Protective Layer /Hybrid-Anode In Lithium Sulphur Batteries " Chem Electro Chem (2016) –To be submitted.

# Papers presented in national/international conferences

Poster presentation on "Interfacial and surface analysis of Li-anode with $Li_3N$ protective layer for lithium-sulphur batteries" in ABAA8 conference, 30Sep-2Oct 2015, Bilbao, Basque country, Spain.

Poster Presentation on "Electrochemical studies of lithium nitride as protective layer for metallic Lithium anode in lithium-Sulfur batteries" in 3rd Li-S batteries workshop, 12-13 November 2014, Dresden, Germany.

# Marya BALOCH

Av. Naciones Unidas 16, 01015, Vitoria-Gasteiz, Spain

maryabaloch1@gmail.com

+34-692 447 724


## *ACADEMIC QUALIFICATIONS:*

| | |
|---|---|
| **2014-2016** | PhD studies on "Strategies towards performance enhancement in Lithium-Sulphur batteries". |
| **2015** | 3 months of PhD research stay on "Application of ionic liquids in the Li-S batteries" in NIC, Ljubljana, Slovenia. |
| **2013-2014** | PhD research experience on "Regime-selected morphological patterns during the Electrodeposition of catalytic nanoparticles." |
| **2012** | Enrolled in master of French language courses, University of Rennes2, Rennes, France. |
| **2012** | GAT (Graduate Recorded Examination-General) Test, Pakistan. |
| **2011-2012** | Internship in Palladium catalysis on C-H activation and functionalization at University of Rennes 1, Rennes, France. |
| **2009-2011** | International Master of Catalysis, Molecules, and Green Chemistry from University of Rennes 1, Rennes, France. |
| **2004-2007** | B.S (4 years, equivalent to masters) Analytical Chemistry, in 1st Class from Institute of Chemistry, University of Sind, Pakistan. |

## *PROFESSIONAL EXPERIENCES*

| | |
|---|---|
| **2014-2016** | PhD research experience on "Strategies towards performance enhancement in Lithium-Sulphur batteries" including studies to improve Lithium anode and sulphur cathodes for Li-S batteries, Under direction of Devaraj Shanmukaraj and Teofilo Rojo.<br><br>Contact:dshanmukaraj@cicenergigune.com, trojo@cicenergigune.com |
| **2015** | 3 months of PhD research stay on "Application of ionic liquids in the Li-S batteries" including use of polymeric ionic liquids as binder in Sulphur compiste cathodes, under direction of Robert Dominko.<br><br>Contact: robert.dominko@ki.si |

| | |
|---|---|
| **2013-2014** | PhD research experience on "Regime-selected morphological pattern during the electrodeposition of catalytic nanoparticles" including catalytical electrochemical deposition combined with chemical vapor deposition techniques to grow nanocarbon electrodes for Li-based batteries under direction of Carmen M. López. Contact: padmanirv@gmail.com |
| **2011-2012** | Internship in Catalysis on catalyzed arylation by palladium complexes by C-H activation under the direction of Dr. Henri Doucet.<br><br>Contact: henri.doucet@univ-rennes1.fr |
| **2009-2010** | Experimental work experience of Masters (2years) on "Synthesis and characterization of Organometallic Chromophores applied to Two Photon Absorption "in Group of Organometallics & Molecular Materials, UMR 6226, University of Rennes I, France under the direction of Dr.Jean-Luc Fillaut and Dr. Huriye Akdas Killig. Contact: Jean-luc.fillaut@univ-rennes1.fr |
| **2007** | 6 months research on "Experimental Studies on Variations of Enzyme Activity (CPK, AKP, LDH, S-GPT and S-GOT) and metal content (Fe, Cu, Mg, and Zn) in serum Of Patients with Hepatic Encephalopathy" in Laboratory of Analytical Chemistry, University of Sindh, under the supervision of Prof. S. A. Memon and Prof. G.A.Qureshi. Contact: sikandermemon48@yahoo.com |

## *TECHNICAL SKILLS:*

**NMR**

$^{1}H$ (Hydrogen) , $^{31}P$ (Phosphorus) , $^{13}C$ (Carbon)

**UV/Visible and fluorescence Spectrophotometry**

Absorption/Reflectance spectroscopy in the ultraviolet-visible region.

**IR, FTIR, ATR Spectrophotometry**

Surface Analysis in infrared region.

**Atomic Absorption Spectroscopy (AAS)**

Investigation of Metals (Fe, Cu, Zn, and Mg) from Blood Serum Samples.

**Microlab (300)**

Investigation of Enzymes (SGPT, SGOT, LDH, CPK and AKP) from Blood serum samples.

**Optical microscopy**

Magnified imaging of micro sized samples.

**GC, GCMS, HPLC & Capillary Electrophoresis**

Liquid and gas chromatography by HPLC, GC and separation/analysis of macromolecules (DNA, RNA and proteins) and their fragments by Electrophoresis.

**COD**,**BOD** & **DOD Analysis**

Analysis of Water samples.

**Standard schlenk line technique**

Moisture and air sensitive reagents/reactions.

**Glove Box**

Inert atmosphere research.

**VSP (Potentiostat & Galvanostat)**

For Electrochemical Deposition (ECD), Electrochemical Impedance Spectroscopy (EIS), Cyclic Voltammetry (CV) and Battery testing.

**Electrochemical deposition (ECD)**

Growth of Catalytical nanoparticles.

**Chemical Vapor Deposition (CVD)**

Growth of Nano Carbons.

**Cell Assembly**

Li-Ion, and Li-S batteries (Swagelok and Coincell 2032 & 2015)

**Maccor**

Battery & Cell Testing Equipment

**Scanning electron microscopy (SEM)**

Secondary electrons (SE), Back-scattered electrons (BSE), Characteristic X-rays (EDX)

**TGA/DSC**

Thermogravimetric analysis/ Differential Scanning Calorimetry

## *COMPLIMENTARY SKILLS:*

| | |
|---|---|
| **Languages** | English (Fluent), Sindhi (Native/Fluent), Urdu (National/Fluent), French (Intermediate), Spanish (Intermediate). |
| **Extra Knowledge** | Operate and Trouble shoot computer, Handling of MS-Office & Internet, Scientific programmes like, ChemDraw, Scifinder, Kaleidagraph, OriginLab, Mestrec(NMR), Difrraceva(XRD), web of knowledge. |

## *ACHIEVEMENTS:*

* Poster presentation on “Interfacial and surface analysis of Li-anode with Li3N protective layer for lithium-sulfur batteries” in ABAA8 conference, 30Sep-2Oct 2015, Bilbao, Basque country, Spain.
* Poster Presentation on “Electrochemical studies of lithium nitride as protective layer for metallic Lithium anode in lithium-Sulfur batteries” in 3rd Li-S batteries workshop, 12-13 November 2014, Dresden, Germany.

* Poster Presentation on “Production of novel Fe-nanoparticle-Nano carbon composite electrodes using ECD and CVD techniques as an anode in Li-Ion batteries” in Power our Future (POF), 2-4 April 2014, Vitoria, Spain.
* Oral Presentation on “"Iron based Nanoparticle-Nano carbons as Electrodes for Li-based batteries" in International conference on Nanotechnology, Nanomaterial and Thin films for Energy applications, 19-21 February 2014 at London, UK.
* Poster Presentation on "Pulsed-Electrochemical Deposition of Fe-based nanoparticles from non-aqueous media: effect of different additives on morphology development" in Trends in Nanoapplications in ImagineNano 23-26 April 2013 at Bilbao, Spain.
* Participation in organizing and attending the International Green Catalysis Symposium & Advanced Spring School on Green Catalysis (IGCS) 2012 held in Rennes, France.
* Participation in organizing and attending the 19th International Symposium on Metathesis (ISOM XIX) 2011 held in Rennes, France, benefiting from the congregation of a large number of experts and Noble Laureates.
* Received Master degree (2009-2011) from the hands of honorable Noble Laureates Yves-Chauvin, Richard Schrock, Robert H. Grubbs (Noble Laureate for Metathesis in chemistry, 2005) and Jean-Marie Lehn (Noble Laureate for synthesis of cryptands in chemistry, 1987).

## *PUBLICATIONS:*

1. **Marya Baloch**, Alen Vizintin, Jože Moškon, Devaraj Shanmukaraj, Teofilo Rojo, Robert Dominko “Application of the gel polymer electrolytes based on ionic liquids in the Li-S batteries”- Submitted to Journal of the Electrochem. Soc. (2016).
2. **Marya Baloch**, Oleksandr Bondarchuk, Emilie Bekaert, Teofilo Rojo, Michel Armand, Devaraj Shanmukaraj “Electrochemical Studies of Lithium Nitride as Protective Layer for Metallic Lithium Anode in Lithium Sulphur Batteries”- Submitted to Journal of Power Sources (2016).
3. **Marya Baloch**, Hicham Ben youcef , Chunmei Li, Oihane Garcia-Calvo, Devaraj Shanmukaraj, Teofilo Rojo, Michel Armand “New Redox material based on reversible cleavage of S–N bonds as cathode material" -Dalton Transactions (2016)- To be Submitted.
4. **Marya Baloch**, Juan Miguel López Del Amo, Teofilo Rojo, Michel Armand, Devaraj Shanmukaraj, “Role of Graphite/rGO as Protective Layer /Hybrid-Anode In Lithium Sulphur Batteries ” Chem Electro Chem (2016) –To be submitted.
5. **Marya Baloch**, Carmen M. López “Effect of Additives on the Pulsed-Galvanostatic Electrodeposition of Iron Nanoparticles from Formamide Media” Chemelectro chem, online 2016, DOI: 10.1002/celc.201600039.
6. **Marya Baloch**, David Roy, Souhilla Bensaid, Véronique Guerchais, Henri Doucet “Sequential Palladium-Catalysed Direct Arylation followed by Suzuki Coupling of Bromo-2-chloropyridines: Simple access to a variety of 2-Arylpyridines” Eur. JIC, 2012; 28, 4454–4462.
7. S. Baloch, G. S. Gachal, S. A. Memon, **M. Baloch** “Determination of Glucose, Urea, and Albumin in Blood Serum of Malarial Patients” Sindh Univ. Res. Jour. (Sci. Ser.) 2012; 44 (2) 195-196.
8. **Marya Baloch**, Reny Jacob Roy, David Roy, Kassem Beydoun, Henri Doucet “Palladium Catalysed Direct Polyheteroarylation of Di- or Tribromobenzene derivatives: A One Step Synthesis of Conjugated Poly (hetero) aromatics” RSC Advances, 2011; 1, 1527–1536.
9. Saira Baloch, S. A. Memon, G. S. Gachal, **Marya Baloch**. "Determination of trace metals abnormalities in patients with malaria.” Iranian J Parasitol: 2011; 6(2) 54-59.
10. Saira Baloch, G. S. Gachal, S. A. Memon, **Marya Baloch.** “Enzyme activity of AKP, CPK, LDH and SGOT in Blood Serum of Malarial Patients." Sindh Univ. Res. Jour. (Sci. Ser.) 2011; 43(1) 33-36.
11. Saira Baloch, G. S. Gachal, S. A. Memon, **Marya Baloch.** “Electrolyte Concentration in Malarial Patients by Flame Photometer." J Bacteriol Parasitol. 2011, 2(7).

12. S Baloch, G. S. Gachal, S. A. Memon, **M Baloch.** “Serum Copper Concentration in Malarial Patients by Atomic Absorption Spectroscopy." Sindh Univ. Res. Jour. (Sci. Ser.) 2011; 43(2) 147-148.
13. S. Baloch, G. S. Gachal, S. A. Memon, G. A. Qureshi, and **M. Baloch** “Determination of zinc content in blood serum of malarial patients" Sindh Univ. Res. Jour. (Sci. Ser.) 2008; 40(1) 41-44.
14. Mohammad Ali Pir, Bikha Ram Devrajani, Saira Baloch, and **Marya Baloch.** “Serum enzyme activities in patients with vivax malaria and falciparum malaria." International Journal of Multidisciplinary Sciences and Engineering. 2012; 3(6) 31-34.
15. Saira Baloch, Bikha Ram Devrajani, **Marya Baloch** and Mohsin Ali Baloch. “Trace Metals concentration in patients with falciparum Malaria by Atomic Absorption Spectroscopy." Nature and Science 2013; 11(4) 65-67.